University of Hertfordhire

Improved Aerosol Deposition Profiles from Dry Powder Inhalers

Submitted to the University of Hertfordshire in partial fulfilment of the requirements of the degree of Doctor of Philosophy

Irene Parisini

November 2014

To my family

Acknowledgments

I would like to thank my family and friends for their support in this long and hard journey. I would like to thank the technicians at the University of Hertfordshire for the assistance, support and training especially Mr James Stanley. I would like to thank the members of staff for helping me understand the science beyond the inhalation field especially Dr Jim Collett. Mainly I would like to thank Sean Cheng and Digby Symons for the help in manufacturing the Cyclone-spacers involved in the current study. I would like to thank the undergraduate students for their help during my project particularly Soumaya Hakim. The clinical research was carried out thanks to the precious help of Dr Omar Usmani and Ms Sally Meah, without whom the recruitment of the patients would have not happened. I would like to thank societies that financially supported my PhD: the Aerosol Society, the SEMT and the RSC. I would like to heartily thank Vanessa and Mubinah for supporting me during my many moments of vent and for the amazing week we spent in Italy! Last but not the least; I would like to thank my supervisory team: Dr Darragh Murnane and Dr Andy Kostrzewski.

My deepest gratitude goes to Dr Darragh Murnane for the constant support during my PhD. Not only as a supervisor and a mentor, from whom I have learnt a lot and more than I would ever have imagined, but also as a friend. His help in putting together this work was priceless. Without his precious effort it could have not been possible. I would also like to thank him for his support in grant applications and his trust in my work that helped me in building my confidence. I also would like to thank him for introducing me to the key people involved in my current career.

.

Abstract

Lung diseases such as asthma and chronic obstructive pulmonary disease (COPD) are major health burdens on the global population. To treat diseases of the lung, topical therapies using dry powder inhalers (DPIs) have been employed. However, a relatively small amount of dose (5.5 – 28 %) reaches the lung during DPI therapy leading to high inter-patient variability in therapy response and oropharyngeal deposition. Strategies were assessed to take patient variability in inhalation performance into account when developing devices to reduce throat deposition and to mitigate flow rate dependency of the emitted aerosol. A cyclone-spacer was manufactured and evaluated with marketed and in-house manufactured formulations. An in vivo study showed that a high resistance inhaler would produce longer inhalation times in lung disease patients and that a spacer with high resistance may prove a suitable approach to address inter-patient variability. Two spacer prototypes were evaluated with cohesively- and adhesively-balanced particle blends. The data suggested that the throat deposition dramatically decreased for the emitted particles when the spacers were used with the inhalers (e.g. 18.44 ± 2.79% for salbutamol sulphate, SS 4 kPa) due to high retention of the formulation within the spacer (87.61 ± 2.96%). Moreover, variation in fine particle fraction and dose was mitigated when increasing the flow rate (82.75 ± 7.34 %, 92.2 ± 7.7 % % and 77.0 ± 10.1 % at 30, 45 and 60 $Lmin^{-1}$, respectively). The latter was an improvement over previous proposed DPI spacers, where variability in emitted dose due to airflow rate was a major issue. Due to the different physicochemical properties of the active pharmaceutical ingredients used in the formulation, throat deposition and respirable fraction for adhesively-balanced particles (e.g. SS) were double that of the cohesively- balanced particles (salmeterol xinafoate, SX) (e.g. 65.83 ± 8.99 % vs. 45.83 ± 5.04 % for SS:Coarse Lactose (CL) and SX:CL, respectively). Scanning electron microscopy revealed that surface-bound agglomerates were more freely removed from the carrier, but subject to decreased impaction-type deagglomeration forces in the spacer than for carrier-bound drug. An ex vivo study using breath profiles from healthy volunteers identified the minimization of differences between adhesively- and cohesively-balanced blends when full breath profiles were studied compared to square-wave airflow. Therefore the use of constant flow for in vitro testing should not be the sole flow regime to study aerosolization when developing new inhalation devices and formulations.

Parts of this PhD thesis have been already published or submitted for publication as follows:

I Parisini, SJ Cheng, DD Symons and D Murnane (2014).A combined computational fluid dynamic (CFD) and Compendial testing approach to study miniaturized cyclone spacers for commercial inhalers. Respiratory Drug Delivery, Fajardo, Puerto Rico

I Parisini, J. L. Collett, and D Murnane, Optimized mathematical approach for understanding deagglomeration behaviour of powder in formulation with coarse carrier. Respiratory Drug Delivery, Fajardo, Puerto Rico

I Parisini, SJ Cheng, DD Symons and D Murnane (2013), Reverse flow cyclone spacers with improved in vitro dry powder delivery, Pharmaceutical Research, Pharm Res. 2014 May; 31(5):1133-45.

I Parisini, S Hakim and D Murnane (2013), Iterative mathematical approach for understanding deagglomeration behaviour of micronized cohesive powder in formulations, DDL24, Edinburgh, UK.

I Parisini, S Hakim, SJ Cheng, DD Symons and D Murnane (2013), Studying deagglomeration process for dry powder inhaler formulations in reverse flow cyclone device, APS PharmSci, Edinburgh, UK.

I Parisini, SJ Cheng, DD Symons, MB Brown, A Kostrzewski, D Murnane (2012), Can a cyclone spacer reduce the flow rate dependence of dry powder inhalation?, AASC, Bristol, UK.

I Parisini, SJ Cheng, DD Symons. A Kostrzewski and D Murnane (2012). A generic dry powder spacer: Proving the principal for commercial carrier-based dry powder inhalers, DDL23, Edinburgh, UK.

I Parisini, SJ Cheng, DD Symons, MB Brown, A Kostrzewski, D Murnane (2011), Assessment of a cyclone-type spacer device for use in dry powder inhalation, DDL22, Edinburgh, UK.

List of Figures

List of Tables

Chapter 1: Introduction

1. The respiratory system

The human respiratory system permits us to inhale and exhale air. It is divided in two main regions: the conduction and the respiratory zone. The first is represented by the airways that deliver air to the second region, where the gas exchange with blood occurs. The conduction zone is divided in 2 sections: the upper respiratory tract comprised of the nose and sinuses, the pharynges and part of the oral cavity; and the lower respiratory tract comprised of the larynx, trachea, bronchi and bronchioles. The respiratory zone is represented by the alveoli where the gas exchange occurs, providing the oxygen to the systemic circulation. The respiratory route maximizes the pharmacological effects of inhaled medication while minimizing side-effects. Compared to the oral route, the respiratory system has been used widely for the delivery of bronchodilators, anti-asthmatic drugs, and antiviral agents [1]. The human lung possesses a large surface area of 126 m^2 for drug absorption, low metabolic activity compared to the gastrointestinal tract, high permeability of alveolar epithelium and a rich blood supply [2]. As the respiratory tract is one of the main exposure routes of our body, many drug products have been delveloped for the treatment of several diseases [3]. The following sections will discuss in more detail the conduction and respiratory airways.

1.1. Anatomy of the lung

The air is warmed and humidified when inhaled through the nose, due to the nasal epithelium that also removes particulate material. It then passes through the conduction airways, which epithelium is composed of ciliated cubic or columnar epithelium with goblet cells. The air reaches the trachea that divides into the right and left bronchi that branch through the chest into 16 generations of bronchioles as proposed by Weibel [4]. All of the branches of the airways have different size and diameters. The bronchi have large walls 1 mm in thickness, which are reinforced with cartilage, whilst bronchioles do not possess such thickened walls [3]. In the manoeuvre of respiration, inspiration occurs more commonly at the right main bronchus because of the gentler angle to the trachea compared the left bronchus. The lung occupies the thoracic cavity that is a space bounded by the chest wall and the diaphragm. This space is lubricated by the fluid present in the pleura (double-layer membrane of the lung). The lungs connect the internal environment with the pulmonary artery, pulmonary vein, lymphatic and vagus nerves [5]. The major

functions of the lungs are gaseous exchange, systemic circulation, homeostatic maintenance of blood pH, vocal expression. The right lung is further subdivided into upper, middle and lower lobes which each connect with the bronchus. The left lung is subdivided only into two lobes: the upper and lower. The shape of the lung is pyramidal and the height is about 20 cm where the density, when it is fully inflated, is 0.2 kg dm^{-3}. Approximately, the lungs weigh between 500 g and 600 g in a young healthy person [6].

The bronchi become terminal bronchioles approximately at generation 16, where after they are classified as respiratory bronchioles that eventually join with the alveolar sacs of the lung. Here the layer of the epithelial cells becomes the lining of the alveoli. Macrophages, neutrophilis and eosinophilis can be found and, at the level of alveoli, type I epithelial cells allow the gas exchange and form the thin air-blood barrier which is 0.5 µm wide. Type II pneumocytes produce a surfactant that is stored in the form of lamellar bodies in the cells. Approximately 300 million pneumocytes are assembled together among the blood capillaries to create an air – blood interface and a surface area of 126 m^2. Each acinus has a size of 0.072 cm^2 [3]. In the alveoli capillaries are present and they are connected to a network of arteries and veins. The pulmonary artery and its branches deliver blood rich in carbon dioxide (CO_2, and lacking in oxygen) to the capillaries that surround the air sacs. Inside the air sacs, carbon dioxide moves from the blood into the air. At the same time, oxygen moves from the air into the blood in the capillaries. The oxygen-rich blood then travels to the heart through the pulmonary vein and its branches. The heart pumps the oxygen-rich blood out to the body [6].

For breathing, muscles including the diaphragm, intercostals and abdominal muscles and muscles in the neck and collarbone area are required. The diaphragm, the main muscle, is located below the lungs and it separates the chest cavity from the abdominal cavity. The intercostal muscles are located between the ribs that create the thoracic cavity. Abdominal muscles are located below the diaphragm. They help to breathe out when fast breathing occurs, for example during physical activity [6]. Muscles located in the neck and collarbone area are involved when the muscles mentioned above do not work well or when lung disease impairs breathing.

1.2. Physiology of the lung

The three main physiological functions of the respiratory zone are ventilation, diffusion and perfusion [3]. The ventilation (inspiration and expiration) brings the air from the external environment to the alveoli and vice versa. The elasticity of the lungs permits the inspiration and expiration due to a pressure differential. The positive internal pressure is made by airways and alveoli, while the negative external pressure is made by the thoracic cavity (within the interstitial liquid). LaPlace's law and tension explain how the alveoli work. When inhalation occurs, the thoracic cavity pressure decreases and the alveoli become filled with air. LaPlace's law (Equation 1) describes how the pressure changes with regards to the surface tension and radius of the alveoli, necessary to create the positive pressure [5].

$$P = \frac{2T}{r} \quad (1)$$

Where P = pressure, T=surface tension and r= radius.

During inhalation the radius of the alveoli increases from about 0.05 mm to 0.1 mm with surface tension of 50 dynes/cm. Therefore, the pressure shifts from 15 to 7.5 mmHg. However, the surfactant present in the alveoli reduces the surface tension by a factor of 15 in order to maintain the normal respiratory pressure difference of 1 mmHg [5]. According to LaPlace's law, the pressure created by the surface tension would be greater in the smaller alveoli than in the big ones. If the surfactant was not present, the small alveoli would empty the air into the bigger ones and would therefore collapse. However, the presence of surfactant avoids the latter occurrence by reducing surface tension. The surfactant is a mixture containing phospholipids and proteins and, therefore, it positions itself between water molecules reducing hydrogen bonds (the main feature of aqueous surface tension).

The diffusion (gas exchange) is measured by diffusion capacity for CO_2 which tests how well the gas can cross the wall of alveoli and enter the capillary. Diffusion occurs in the lungs and in the cells. CO_2 diffuses out of the cell and into the blood whereas oxygen diffuses into the cell from the blood. Smokers or patients affected by asthma show high values of CO_2 [5].

The final function of the respiratory tract is perfusion. Each division of the respiratory tract has its own blood supply. The pulmonary artery capillaries that surround the alveoli transport the oxygen and other gases into the blood and CO_2 from the blood back to the lung to be expelled [3].

Several terms have been developed to describe the various physiological capacities of the respiratory tract. Total lung capacity (TLC) is the volume of gas in the lungs following maximal inspiration, while the functional residual capacity (FRC) is the volume of the gas in the lungs at the end of normal expiration and it is comprised of the expiratory reserve volume (ERV, the amount of air expelled with maximal expiratory effort, approximately 1.2 L in an average weight male) and the residual volume (RV, volume of air after maximal expiration, approximately 3.1 L in an average weight male). Lung compliance (C_L) is also very important to assess the stiffness of the lungs (Equation 2) [5]:

$$C_L = \frac{\Delta V}{\Delta P} \quad (2)$$

Where ΔV = volume of air in the lung and ΔP = the difference between alveolar pressure and intrapleural pressure. In a young male, the C_L is about 1.5-2.0 L kPa^{-1}.

1.3. Mechanics of inhalation and airflow

When breathing, the diaphragm muscles contract, pulling the diaphragm downwards. The lung volume increases and the inta-alveolar pressure decreases causing air to flow into the lungs. During exhalation, the diaphragm relaxes and rises decreasing the lung volume. The pressure within the alveoli rises and the air is pushed out. Lung function testing measures the ability of the lung to work properly. The test gives an instant idea of any breathing problem such as shortness of breath [5].

1.3.1. Lung function testing

Lung function tests measure the lung capacity (e.g. how much air can be taken into the lung and the amount of air that can be exhaled). Doctors use lung function tests to help diagnose conditions such as asthma, pulmonary fibrosis (scarring of the lung tissue), and COPD (chronic obstructive pulmonary disease). Also, these tests might be used to check how well treatments, such as asthma medicines, are

working. The breathing tests commonly used are: body plethysmography, spirometry and lung diffusion capacity.

The term ‘‘lung volume’’ usually refers to the volume of gas within the lungs, as measured by body plethysmography. It assesses the FRC (Functional Residual Capacity), the specific airways resistance (sRaw), RV and TLC [7]. FRC is the volume of gas present in the lung at end expiration during tidal breathing. The ERV is the volume of gas that can be maximally exhaled from the end-expiratory level during tidal breathing (i.e. from the FRC). The maximum volume of gas that can be inspired from FRC is the inspiratory capacity (IC). The inspiratory reserve volume (IRV) is the maximum volume of gas that can be inhaled from the end-inspiratory level during tidal breathing. RV refers to the volume of gas remaining in the lungs after maximal exhalation (regardless of the lung volume at which exhalation was started). IVC is the inspiratory vital capacity that is the inhaled volume from the point of maximum expiration. VC (volume capacity) is the volume change at the mouth between the positions of full inspiration and complete expiration [7, 8].

Spirometry is the assessment of the pulmonary function and measures the inhalation and exhalation volumes of air as a function of time [9]. Lung function markers, such as Peak Expiratory Flow (PEF), FEV_1 (forced expiratory volume in 1 sec) and Forced Vital Capacity (FVC), are assessed by spirometry. The ratio between FEV_1 and FVC predicts the severity of lung obstruction [10, 11]. FEV_1 is effort independent and highly repeatable for patients affected of mild asthma [11]. A reduced FEV_1/FVC below the 5^{th} percentile of the predicted value shows narrowed airways (obstruction) during exhalation. In fact, a ratio < 0.7 typically occurs in those subjects affected with asthma [1]. When % FEV_1 predicted is used as marker, 5 classes of degree severity of airways obstruction can be distinguished [11]:

- Mild >70 %
- Moderate 60–69 %
- Moderately severe 50–59 %
- Severe 35–49 %
- Very severe <35 %

The graph below represents the normal volume - time dependent curve to show the FEV_1 (Figure 1.1).

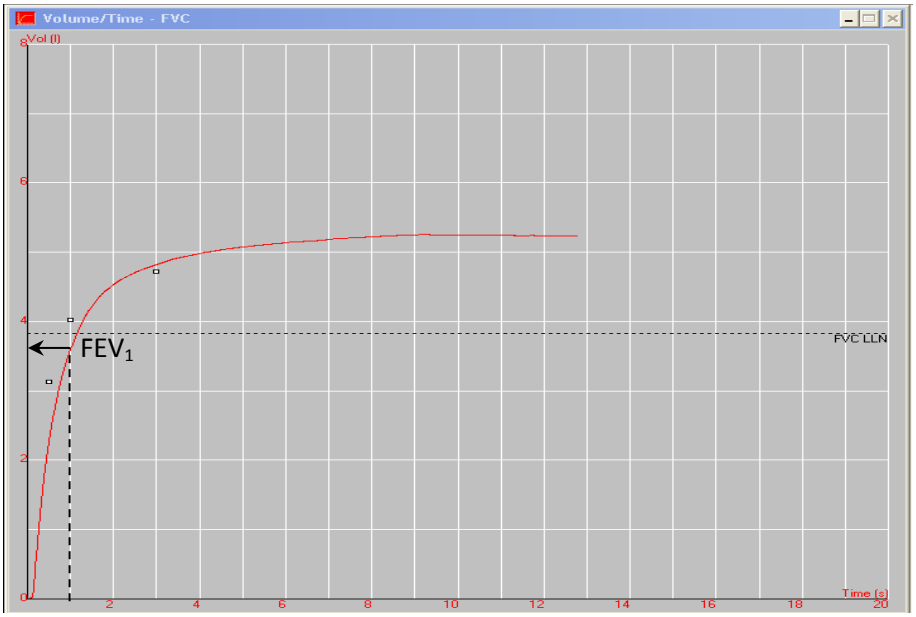

Figure 1.1. Volume-time loop of a healthy male showing the FEV_1 (forced expiratory volume in 1 sec).

Peak expiratory flow (PEF) is another marker used to monitor asthma and define the severity of obstruction. It is also, used as a reference value for monitoring the effects in changing the treatments. PEF is the highest flow achieved from a maximum forced expiratory manoeuvre and it is effort dependent. PEF (expressed as % of the predicted value) is usually compared to patients' own previous best measurements when they used their own peak flow meter [10]. If the PEF is between 50-75%, the obstruction is moderate [11]. On the other hand, if PEF is between 33-50%, then the obstruction is severe.

Another marker for asthma is the peak inspiratory flow (PIF) as it depends upon the patient's ability to draw air into their lungs (e.g. through inhalers) [12]. It measures the highest flow that a patient is able to perform when s/he inhales. The PIF can be measured using the In-Check® system. [12, 13].

1.3.2. Inspiratory flow loop

Using the spirometer to assess lung function, a flow-volume loop can be drawn (Figure 1.2). It is generated by plotting the inspiratory (negative values) and expiratory flow (positive values) against the volume of air. It can predict early stages of obstructions and one advantage is that it shows whether the airflow is appropriate for a particular lung volume [14]. The flow-volume loop graph starts with a curve that

reaches a peak (PEF). After PEF is reached, the curve decreases (flow decreases) and more air is expired. After 25% of the total expired volume, FEF_{25} is reached. At half way FEF_{50} is calculated (FEF at 50% of FVC). At 75%, FEF_{75} is achieved. The mean flow between FEF_{25} and FEF_{75} is called FEF_{25-75}. After the expiratory manoeuvre the patient has to make a complete and forced inspiration to close the flow volume loop [9].

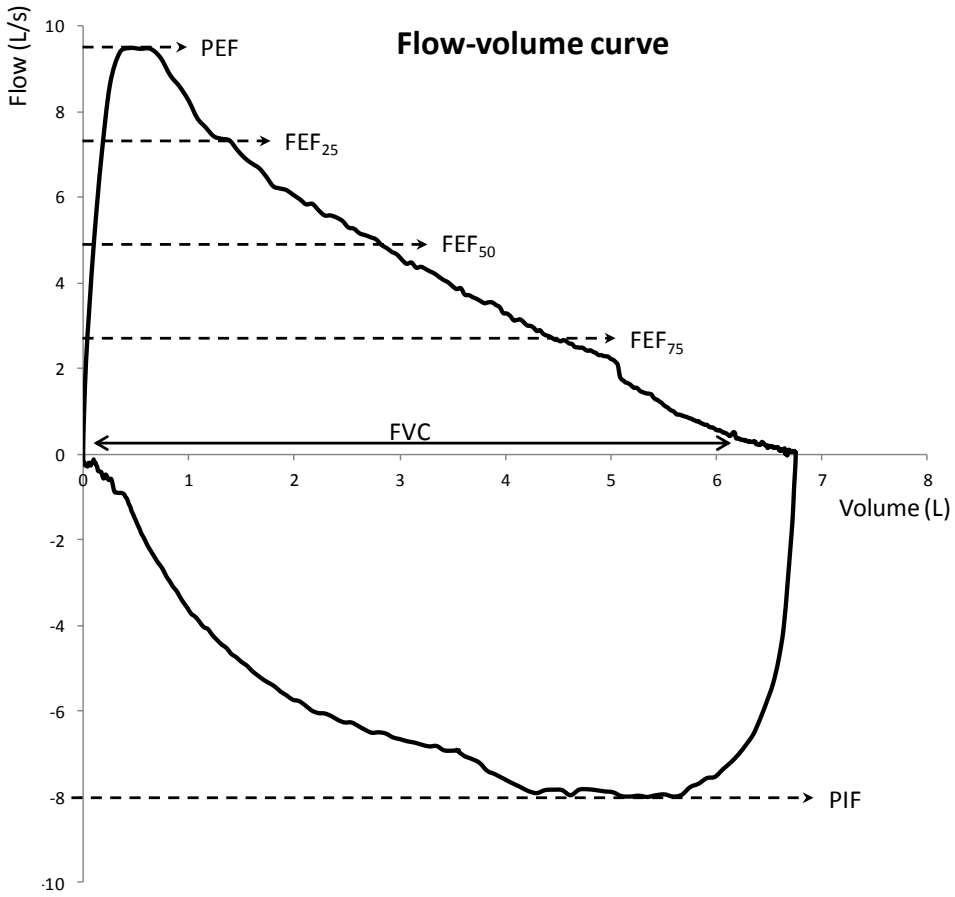

Figure 1.2. Flow-volume curve. On the x-axis volume of air is represented. On the y-axis inspiratory (negative values) and expiratory (positive values) is reported.

The shape of the loop depends on the mechanical properties of the lung and different diagnoses can be made:

- Normal - on exhalation the maximal expiratory flow is rapidly reached followed by a linear decline until exhalation is complete (as per Figure 1.2).
- Asthma - typically the curve is a smooth concave shape as airway obstruction is relatively constant throughout expiration [9].

In patients with obstructive lung disease such as COPD, the small airways are partially obstructed. A patient with obstructive lung disease typically has a concave flow-volume loop (Figure 1.3) [9].

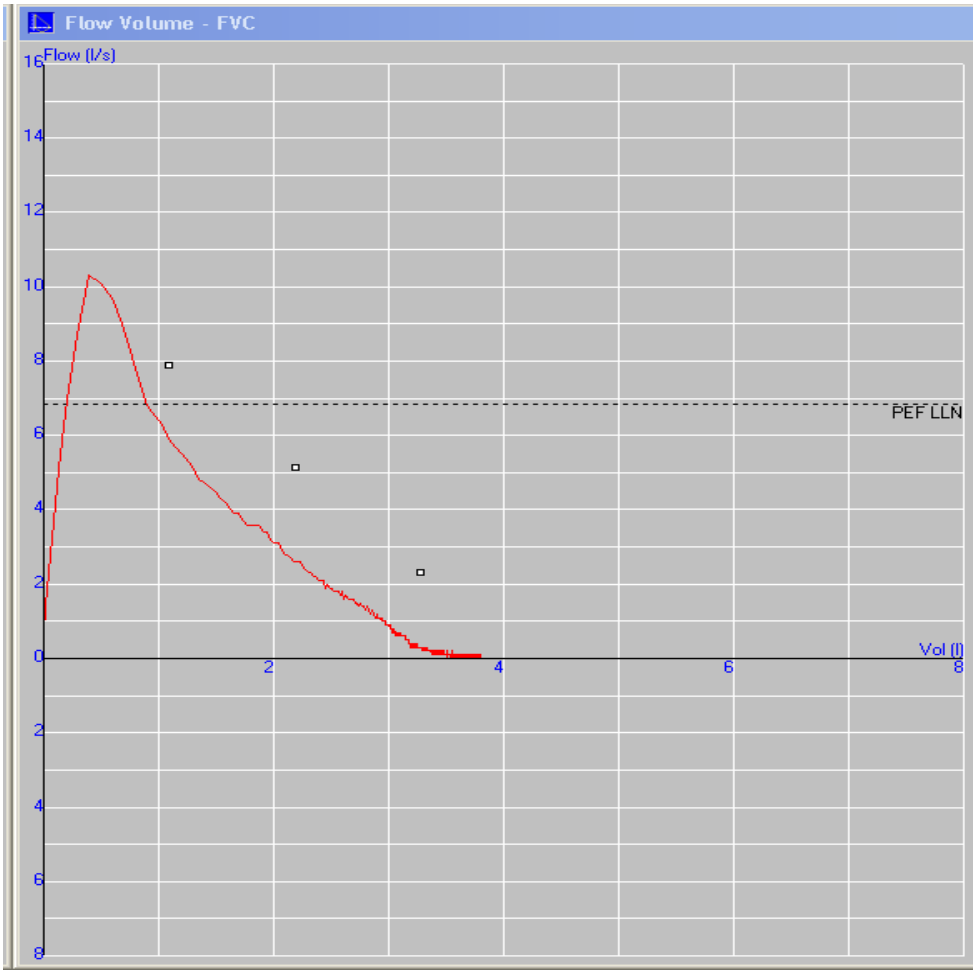

Figure 1.3. Flow-volume in obstructive lung disease.

The air in the large airways can be exhaled without problems, so the PEF will be normal. However, when the lung is obstructed the small airways are partially blocked, so the air will escape more slowly. This will result in a lower flow and a sharp fall in the flow-volume. FEV_1 and FEF_{25-75} will be low compared to healthy subjects. Typically the patient will have a normal FVC [14].

Restrictive lung disease means that the total lung volume is too low (Figure 1.4). Since the airways are normal, the flow volume loop will have a normal shape: the curve will descend in a straight line from the PEF to the X-axis.

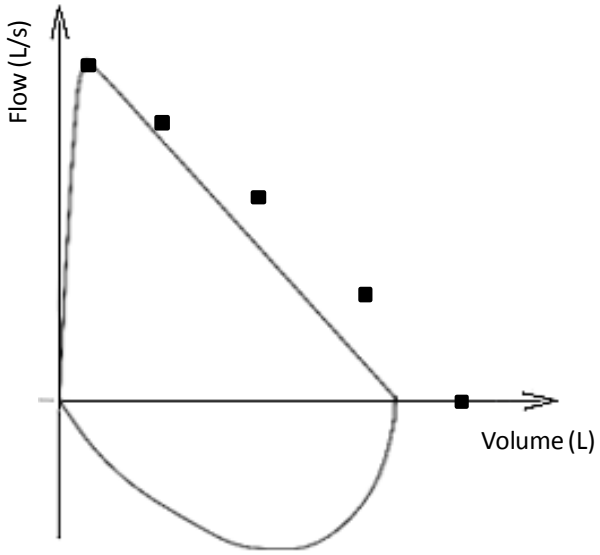

Figure 1.4. Flow-volume in restrictive lung disease: shape normal with low FVC.

Often patients will show signs of both obstructive and restrictive lung disease showing a flow-volume loop with characteristics of both syndromes (Figure 1.5) [14].

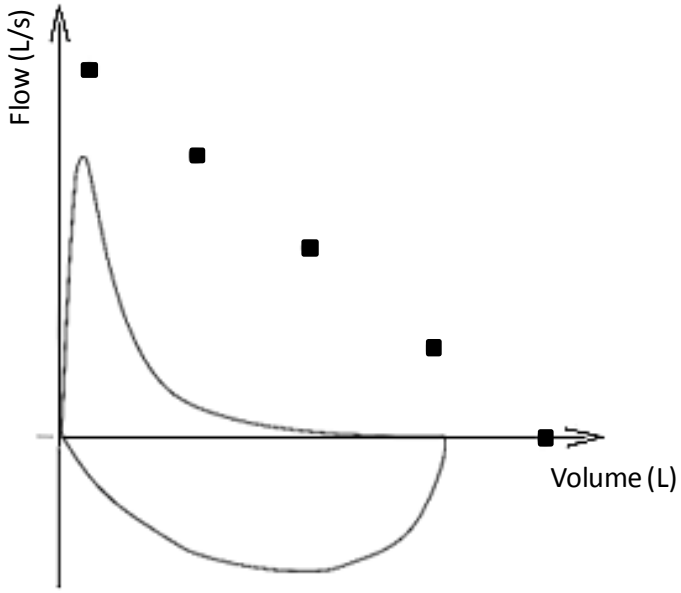

Figure 1.5. Volume-time curve in mixed lung disease: FVC, FEV_1 and FEF_{25-75} are too low.

1.4. Pathophysiology of lung disease

Diseases that affect lung function can cause obstructive or restrictive dysfunction. Obstructive diseases are characterised by a reduction in airflow and airflow limitation such as asthma, chronic bronchitis, COPD and emphysema.

Restrictive lung diseases are characterised by a reduction in lung size or an increase in lung stiffness resulting in a decrease in the maximum volume of air can be breathed (e.g. pulmonary fibrosis, asbestosis). Airway obstruction may be due to obstruction inside the airway lumen (e.g. secretion of mucus in chronic bronchitis), obstruction in the wall of the airway (e.g. inflammation in asthma), and obstruction outside the airways in the per bronchial region (e.g. destruction of the lung parenchyma in emphysema or tumour) [15].

1.4.1. Asthma and chronic obstructive pulmonary diseases

Asthma and COPD are a major disease burden worldwide. In developing countries between 6.5 to 7.7 % of the population suffers from chronic bronchitis due to open-fire cooking with high child mortality [16]. In the United States, more than 22 million people are known to have asthma and nearly 6 million of these people are children. The diseases are a major burden also in the UK with 7 million people suffering from asthma and 800,000 from COPD and with more than 1,200 deaths per year [11]. There is no a standard definition for asthma, however, it is characterised by inflammation and narrowing of the airways that lead to breathlessness, coughing and wheezing [11]. The inflammation is due to increased airway hyperresponsiveness to various stimuli and manifests by widespread narrowing of the airways that changes in severity either spontaneously or a result of treatment. Symptoms of asthma are commonly encountered in childhood but the disease can occur at any age. A variety of "triggers" may initiate or worsen an asthma attack (e.g. antigen, pollen, animal fur or tobacco smoke) [17]. It has been found that also the enzyme tryptase (found in mast cells, a type of white blood cell important for fighting infection) may cause asthma and other inflammation disorders. Progression of asthma needs to be controlled because exacerbation (during which symptoms worsen over-and-above the baseline respiratory function decline of the disease, typically requiring a change in therapy [11]) leads to poor quality of life characterized by reduced physical activity, increased mortality and morbidity, increased health costs and hospitalization rates [18]. Exacerbations can also have a significant impact on the patient’s long-term condition; it has been reported that repeated episodes result in faster decline in lung function, thereby contributing to disease progression.The exacerbations can have different classification of severity:

- mild, which involves an increase in respiratory symptoms that can be controlled by the patient with an increase in the usual medication;
- moderate, which requires treatment with systemic steroids and/or antibiotics;
- severe, which describes exacerbations that require hospitalization [19].

Similar effects of this disease are present in COPD a disease of the lungs most frequently associated with smoking (9 out of 10 COPD-related deaths) [20]. People with COPD suffer shortness of breath, they sometimes have spasms of airways of the lung (especially of bronchial branches), and suffer with cough and wheeze. Symptoms and lung damage slowly deteriorate over time and the lung function rapidly declines [21]. Cardiovascular diseases are often associated with COPD and are the causes of mortality in COPD [22]. Donaldson et al [23] analysed 25,857 patients with COPD over a 2 year time period. They correlated the risk of cardiovascular disease with episodes of COPD exacerbation. Risk of myocardial infarction or stroke 1-5 days and 1-49 days after an exacerbation episode were reported, respectively [23]. The mechanisms linking COPD and heart disease are still unclear but systemic inflammation might be an explanation of the increased risk of vascular events [24, 25].

1.4.2. Pulmonary remodelling

Chronic inflammation and airway hyperresponsiveness damage the epithelium of the lung, leading to smooth muscle and mucus gland hypertrophy (an increase in size of airway smooth muscle cells) and hyperplasia (an increase in the number of airway smooth muscle cells) [26]. The thickening of the airway wall causes irreversible airflow limitation as the tract will be narrowed and, therefore, increasing airway resistance [27]. This would lead to difficulties in breathing for the patient and a rescue therapy of bronchodilators is needed. The remodelling is also driven by inflammatory mediators such as interleukins, histamine, eosinophils, mast cells, metallo-proteases that have destructive, restorative and chemiotaxic properties [19, 28, 29]. All the structures of the bronchi are involved in asthma and inflammation. The separation of the mucosal cells in bronchial epithelium could be observed, leaving an intact basal cell layer. Ebina et al [30] preformed 3-D morphometry of airway muscle cells on serial sections of autopsied lungs from 10 asthmatic patients. In some cases the thickened muscles were found only in the central and larger

bronchi without hypertrophy, while there were some cases where thickened muscles were found everywhere in the tract and hyperplasia was mild and localized only in the bronchi. Moreover, airway macrophages were found in increased numbers in asthmatic bronchi. They appear to be in an activated state and release enzymes, mediators that cause bronchoconstriction and mucus secretion, eicosanoids, platelet-activating factor (PAF), oxygen free radicals and cytokines, including tumour necrosis factor (TNF) that might be deleterious to the bronchi. Macrophages can also synthesize and secrete elastase and a group of metallo-proteases having the capacity to degrade various extracellular macromolecules such as elastin [26]. Moreover, macrophages in addition to fibroblasts are responsible for the production of collagen, leading to fibrosis [26, 31].

1.4.3. Changes in the airflow anatomy

It has been shown that airway remodelling is an important mechanism that leads to fixed airflow obstruction in asthma [27]. This is due to the inability to reach the predicted lung function levels after bronchodilator therapy. The airways structure in asthma is altered due to the thickening of the walls of the conducting airways. Moreover, the lumen narrows and excessive mucus is produced. This narrows the airways further, leading to a high resistance to airflow [32]. Studies have found that increased airway inflammation was strongly correlated with destruction of alveolar attachment, suggesting a role for leukocyte-derived proteases in alveolar disruption [33, 34]. The obstruction in the small airways is caused by epithelial changes (e.g. goblet cell hyperplasia and squamous cell metaplasia), and fibrosis [15]. Airway inflammation increased with the severity of airflow limitation, and was correlated to increased numbers of macrophages, neutrophils, B and T lymphocytes and lymphoid follicles [15]. Therefore, small airways are major contribution to airflow limitation in asthma and COPD [35].

1.4.4. Ventilation, mucus and lung function test changes

Studies reported that asthmatic patients with recurrent exacerbations and with stable condition had increased closing volume and closing capacity (CC) in the same manner, even after bronchodilator therapy [36]. Therefore, narrowing of the small airways is a risk in severe asthmatic patients with frequent exacerbation episodes. The lumen mucus is secreted in large quantities by cells and mucus-secreting

submucosal glands. Goblet cell hyperplasia is a feature of the large airways in both asthma [37] and chronic bronchitis [38].

It has been reported that asthma and COPD are associated with a rapid decline in FEV_1 [21]. The ratio of FEV_1 and FVC is a criterion of the presence of airflow limitation and should be the primary guide for distinguish obstructive from non-obstructive patterns [31]. It was shown that [32] the wall area internal to the muscle was significantly thickened over the entire range of cartilaginous airways measured and that this was associated with a reduction in FEV_1/FVC ratio.

1.5. Particle - lung interactions

Understanding the deposition of particles is important to improve the efficiency in drug delivery for inhalation therapies, but also to understand risks of inhalation toxicology [39]. Deposition is the process by which an inhaled particle separates from the airflow stream and contacts the respiratory surface from which there is no re-suspension [40].

1.5.1. Mechanisms of deposition of the particles

Deposition is a very complicated process and it is divided in five mechanisms, depending on particulate structure, size, chemistry, shape, physiological factors of the environment. The five different mechanisms are: impaction, sedimentation, diffusion, interception and electrostatic precipitation.

Inertial impaction occurs when a particle that has a specific momentum cannot follow the airstream and thus deviates from the airflow during inhalation and impacts on any anatomical structures in its path [40]. The probability of a deposition of a particle by impaction is a function of Stokes number (Equation 3) [40], which is a dimensionless number that describes the behavior of particles in a suspension and it is defined as the ratio of the stopping distance of a particle to a characteristic dimension of the obstacle:

$$Stk = \frac{\rho C V D_p^2}{9 \mu D_j} \quad (3)$$

Where Stk is Stokes number; ρ is the particle density (g/cm^3); C is the Cunningham slip correction factor; V is the velocity (cm/sec); D_p is the particle diameter (cm), μ is the fluid viscosity (Pa sec); D_j is the jet diameter (cm) [40]. The higher is Stokes number, the more readily the particle will impact. When air is inhaled, large particles with high momentum will deposit in the upper airways where impaction commonly occurs [40].

Sedimentation is a time-dependent process where particles travel under gravitational force and it is dominant in the smaller airways (i.e. the bronchiolar region where the flow velocity is low and airway diameter is small). Stokes Law determines the velocity of sedimentation (Equation 4) [40]:

$$V=\frac{2}{9}\frac{(\rho_p-\rho_f)}{\mu}gR^2 \quad (4)$$

Where V is the velocity of sedimentation, ρ_p is the density of the particle, ρ_f is the density of the air, g is the gravital acceleration, μ is the dynamic viscosity, R is the radius of the particle.

For particles of smaller size (< 1 μm), the motion becomes random and diffusion, or Brownian motion, occurs. This motion increases as the particle size is reduced and it occurs in the deepest part of the lung.

Interception takes place when the centre of gravity of a particle is in the gas phase while one of its ends comes in contact with the airway or alveolar wall. Deposition by interception is important when the dimension of the airways is comparable with one of the particles' dimensions. For similar volume, elongated particles are likely to deposit by this mechanism [40].

A charged particle may induce an image charge of opposite sign on the surface of the airways that are electrically conducting and then deposit by electrostatic precipitation [40]. This mechanism contributes less that 10% of overall deposition [41]. Thus, the deposition due to charge is usually small compared to deposition by the previously mentioned mechanisms [42] (Figure 1.6).

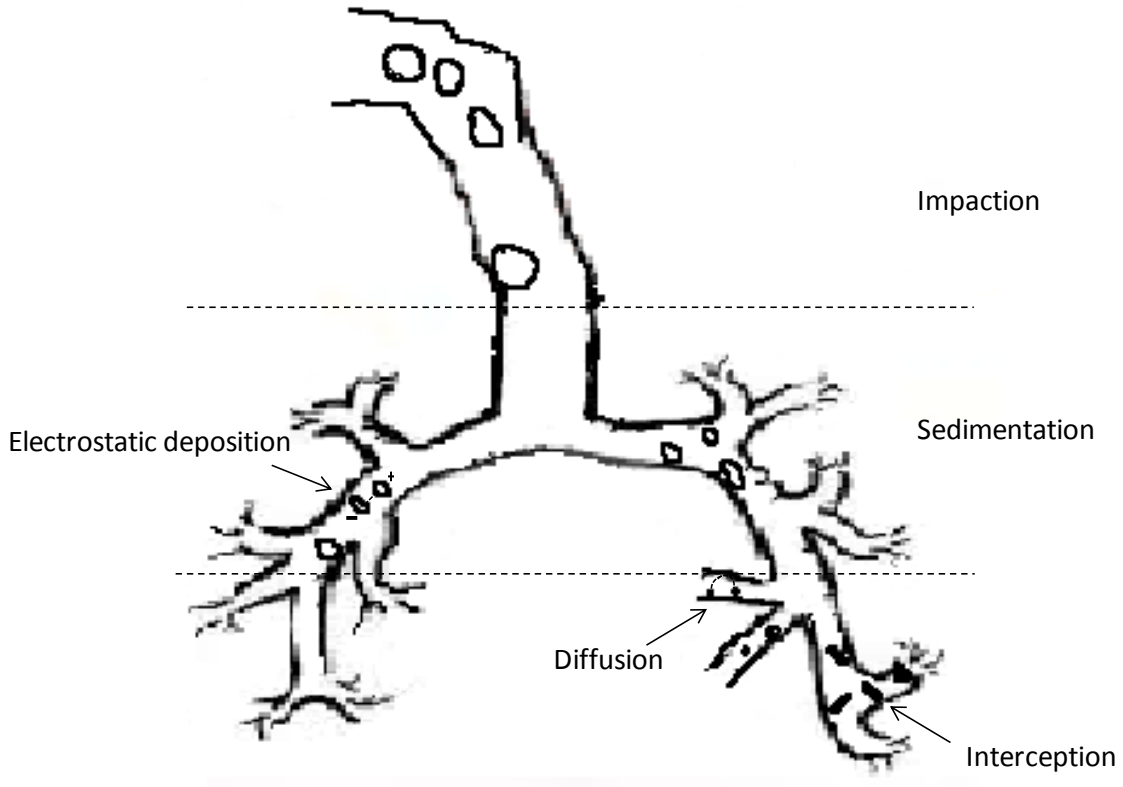

Figure 1.6. Diagram of the mechanisms of deposition of the particles: impaction, sedimentation and diffusion, interception and electrostatic deposition.

From a toxicological point of view, all particles smaller than 10 µm in geometric diameter have the potential of being biologically active in susceptible individuals [43]. Deposition is dependent on particle size so it would be useful to predict where the particles may deposit in the respiratory tract considering their size. Particles larger than 10 µm in diameter are likely to deposit in the mouth and throat [40].

Pharmaceutical inhalation technology suggests that particles smaller than 5 µm deposit in the lower airways (bronchiolar-alveolar level) therefore, pharmaceutical powders are required to be of this size [40, 44, 45]. In fact, particles with size range of 1-5 µm will deposit in bronchi and bronchioles by impaction, whilst particles with size range of 1.0-2.5 µm will deposit in alveoli and bronchioles by sedimentation [46]. Particles with a diameter below 1 µm deposit by diffusion and the one with 0.5 µm size are exhaled as they do not have enough mass and momentum to deposit by impaction and sedimentation [40].

The target of inhaled drugs for treatment of asthma and COPD is the lower areas of the respiratory tract, in particular the bronchioles and the alveolar region. The target region for deposition of the active agents is related to the location of the receptor sites. For example, β-adreno receptors are located in lower respiratory tract in small conducting airways [47], whereas the cholinergic receptors (e.g. M_3 muscarinic receptors) are located on the airway smooth muscle [48]. Thus, in order to have a better local effect, β-agonists should be deposited in peripheral as well as central airways of the lower regions of the lung [46-48].

1.5.2. Physicochemical properties: aerodynamic diameter and particle size distribution

Although particle size is probably the major factor affecting particle deposition in the lung, several other factors affect the total and the regional deposition of particles. These factors can be particle characteristics (e.g. particle density), physiological factors, lung anatomy, and environmental factors. Also the shape can have an important effect on the aerodynamic behaviour of the particles and therefore on deposition efficiency. The airways have a particle-size selective system as a function of the aerodynamic diameter of the particles. Aerodynamic diameter is the diameter of a hypothetical spherical particle of unit density that settles in air at the same falling velocity as the physical particle (Equation 5) [49].

$$d_{ae} = d_g \sqrt{\frac{\rho}{\chi}} \tag{5}$$

where d_{ae}= aerodynamic diameter, d_g= geometric diameter, ρ= particle density and χ= shape factor.

Thus, it is important to measure the particle size and density in order to predict the deposition of the released particles from an inhaler as an indicator of the efficacy of the device. The term "aerodynamic diameter" has been developed in order to provide a simple means of categorizing the sizes of particles having different shapes and densities with a single dimension. Also, aerodynamic diameter is suitable to describe the deposition behavior for non-spherical particles [46]. The aerodynamic diameter is useful for:

- Predicting the behavior of particle in air
- Determining site of deposition in lung
- Optimizing air sampling characteristics

In Figure 1.7 a representation of particle deposition in the respiratory tract based on the aerodynamic diameter is reported.

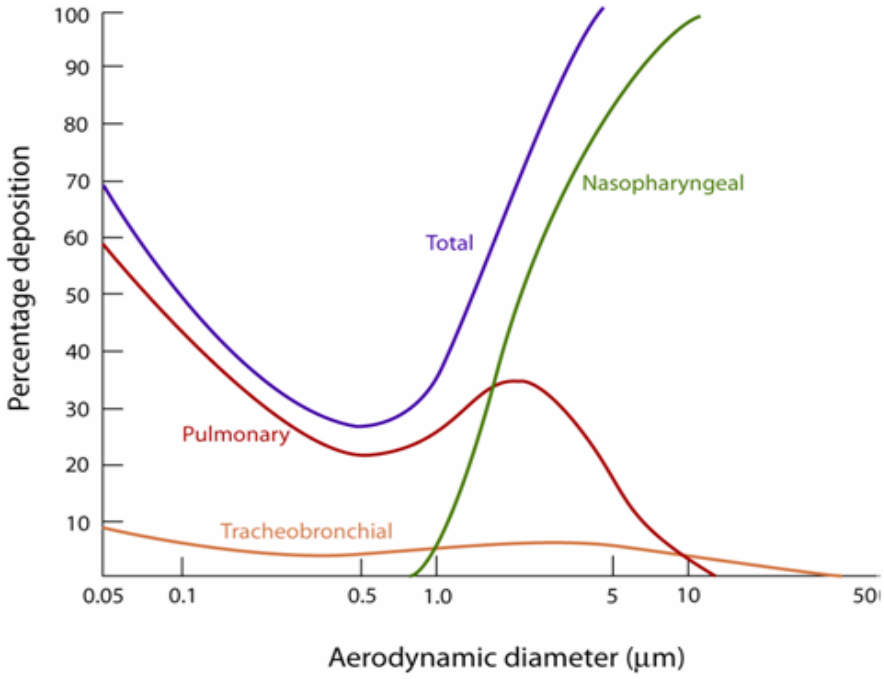

Figure 1.7. Deposition of particles according to the aerodynamic diameter [50].

Aerodynamic size is important when porous particles are used for aerosol medication [51]. The density of porous particles is lower than for non-porous ones. Therefore, according to the definition, if the density of a particle is reduced the aerodynamic particle size would decrease. For appropriate porous particle delivery, the correct size should be created and the relationship between geometric diameter, aerodynamic diameter and particle density has to be taken into consideration. To deliver large particles, the density can be reduced, i.e. increasing its porosity [51]. The porous structure permits deep lung delivery of relatively large diameter therapeutic aerosols, for example greater than 5 µm [52]. Because of their rough surface, particle agglomeration can be reduced and a powder with high dispersibility can be provided, which is ideal for aerosolization via DPIs (dry powder inhalers), leading to lower deposition in the mouth and throat. One of the problems with porous

particles is that they are more likely to be deformable than non-porous particles during powder processing and also, due to a high specific surface area, they can uptake water vapour and so increase their density and aerodynamic diameter, thereby, decreasing their dispersibility [40].

The aerodynamic diameter is important for predicting lung deposition and bioavailability, formulation of inhaled medication, flow and packing properties. Therefore, particle size analysis has been developed to obtain quantitative data on the mean size, particle size distribution (PSD) and shape of the particles to be used in pharmaceutical formulation to assure the quality of the final dosage forms and drug delivery systems. The PSD is the particle frequency distribution that shows the percentage of particles found in each size range [53]. The PSD can be related to: the number-weighted, surface-weighted and volume (or mass)-weighted. However, the volume (mass)-weighted PSD is the most appropriate description for pharmaceutical materials. The number-weighted PSD is useful for determining the size of primary particles in agglomerated systems as well as the tightness of a PSD. The closer the number weighted and volume weighted PSDs, the greater the monodispersity of the particle size [53]. Accordingly to the definition of PSD, frequency or cumulative distribution can be plotted (on the Y-axis) by number count, surface area, or mass/volume and the graph showed in Figure 1.8 will be obtained.

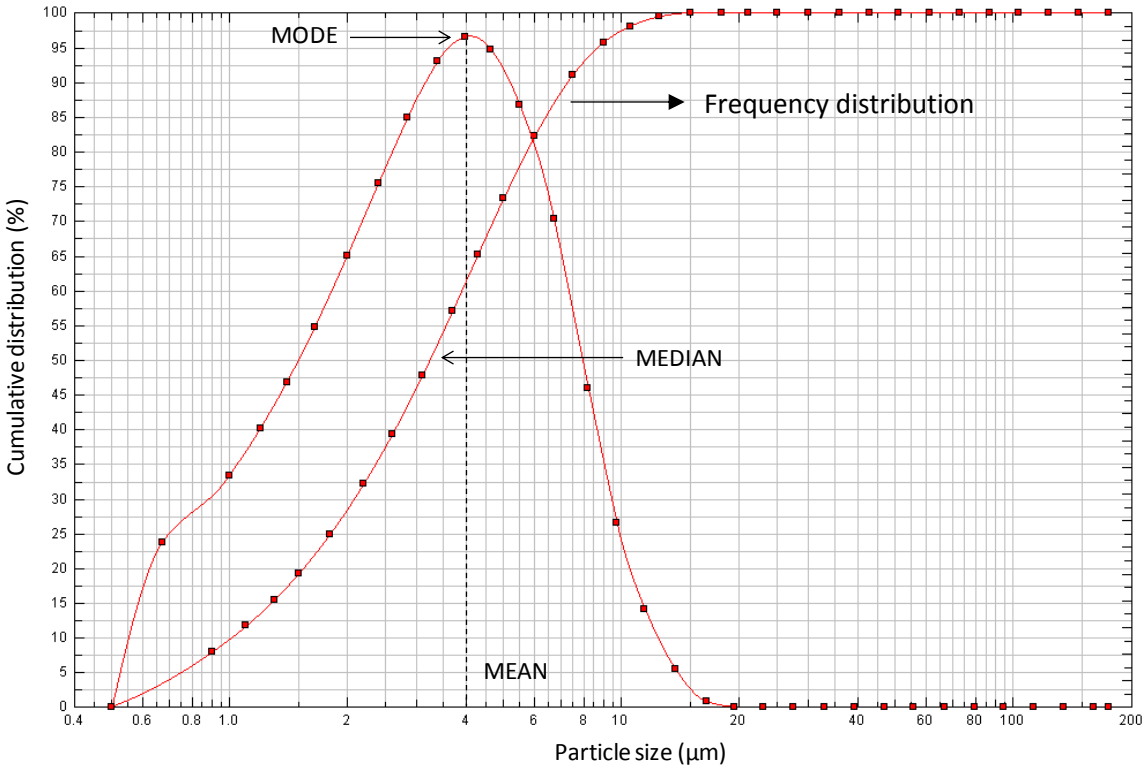

Figure 1.8. Particle size distribution of fine lactose (LH 300) at 5 bar using the laser diffraction instrument (Rodos, Sympatec GmbH).

The mode (value that occurs most frequently in a distribution) diameter corresponds to the peak of the distribution and for a symmetric distribution is equivalent to the mean and median diameter. The median diameter represents 50% (particle diameter that divides the frequency distribution in half, DV50) of the particle population. The width of the PSD (or span) is calculated from lower and upper fractions of the cumulative PSD as Equation (6) [54]:

$$\text{span} = \frac{\text{Dv}_{90} - \text{Dv}_{10}}{\text{Dv}_{50}} \quad (6)$$

Most aerosols are polydisperse and have a wide range of diameters. Therefore, it can be said that most particles in a powder sample with a narrow distribution have a similar particle size, while a sample with a wide distribution may possess the same median diameter as the narrow sample but possess a wider range of particle sizes [53]. Aerosol size distribution (for dry powder inhalers (DPIs) and metered dose inhalers (MDIs)) is better described by a log normal distribution. Therefore, when the

fraction of particles (of a particle size) is plotted against the logarithm of the particle diameter, a Gaussian distribution will result (Figure 1.8) [55].

1.6. Pulmonary drug delivery

Orally-inhaled products (OIPs) are used for local treatment lung diseases due to the large surface area and the lack of hepatic first - pass effect. Moreover, delivery of drugs for inhalation can also lead to a systemic delivery (e.g. insulin). Small molecules can be delivered with very rapid action, low metabolism and high bioavailability; and macromolecules can be delivered without injections, as highlighted by the first inhaled insulin product [56].

1.6.1. Medications to treat asthma

The principal medications used in asthma are corticosteroids and bronchodilators. Corticosteroids can suppress inflammation of the airways, even in very low doses. However, they have poor clinical effect for COPD as they treat inflammation that is often absent in obstructed lungs. In both asthma and COPD, corticosteroids are commonly given as combination inhalers with long acting β2-agonists (LABA, such as salmeterol xinafoate and formoterol fumarate) [57]. At a cellular level inhaled corticosteroids reduce the numbers of inflammatory cells in asthmatic airways, including eosinophils, T-lymphocytes, mast cells and dendritic cells [58]. Corticosteroids include budesonide, fluticasone propionate, becometasone dipropionate and they exhibit similar chemical structures as they are derivatives of cortisone. Patients with mild asthma treated with a low dose of corticosteroids (budesonide 400 μg daily) showed fewer symptoms and a progressive improvement in lung function [59] with fewer episodes of exacerbation [60]. Combination of corticosteroids and LABA (becomethlasone propionate 200 μg and salmeterol 50 μg) led to an improvement of the lung function in asthmatics [61]. Therefore, adding a LABA is more effective than increasing the dose of corticosteroids [11] in terms of improving asthma control and reducing exacerbations [62].

1.6.2. Difficulties in delivering pulmonary medications

The conduction zone of the respiratory tract is composed of bronchi and bronchioles. The bronchiolar diameter decreases further down towards the

respiratory zone whereas the number of airways for each generation increases at a much higher rate. Moreover, in the upper airways the air stream is subject to a sharp change in direction and deposition by impaction may occur [3]. Furthermore, the tracheo-bronchial region ciliated cells are present which facilitates mucociliary clearance of any deposited particles [29]. Delivery of inhaled drug, therefore, might be difficult [41, 63]. In the alveoli, the columnar epithelial cells are replaced primarily by Type I cells alongside their progenitor Type II cells that also produce lung surfactant. In this region the alveolar macrophages and proteases are found too [3]. They are one of the most important mechanisms of defence presents into the lung when particles of 1-6 μm size are inhaled. They can dispose of particles either by transporting them along the alveolar surface to the mucociliary escalator, or by translocation to tracheo–bronchial lymph or by internal enzymatic degradation (for protein and peptide drugs) [64]. Lombry et al [65] demonstrated that alveolar macrophages comprise one of the major barriers to the transport of macromolecules from the lungs into the bloodstream, particularly for moderate-sized to large proteins. Therefore, strategies to increase systemic absorption of macromolecules over the last decade have been developed: chemical or physical alternatives for minimizing alveolar macrophages; inhibition of endocytosis using physiological modulators; co-administration of ligands competing with proteins for binding on membranes of macrophages; and the preparation of large porous particles combined with various excipients to enhance absorption and/or retain the drug at the site of deposition.

1.6.3. Inhalation therapies

MDIs (metered dose inhalers) and DPIs (dry powder inhalers) have been used widely with historical improvements in the delivered dose. Inhaler use is common in Europe with MDIs comprising 75% of all sales in the UK [66]. Nevertheless, the NHS bulletins show an increase in hospitalization of asthmatic and COPD patients. For example, between 2009-2010 there were more than 100,000 emergency admissions to hospital in England for exacerbations of COPD [67]. This is due to multiple causes such as poor patient concordance, compliance and competence. Many patients display poor inhalation technique, having received inappropriate training from the medical staff and the prescription of unsuitable inhalers [11, 68, 69]. Constant design and formulation changes are made to improve the aerosolization of the particles from inhalers. GlaxoSmithKline (GSK) manufactured the Gemini® DPI, that has a similar

design to the Diskus™, but instead of having a single strip of blisters, there are two stripes of blisters containing one a corticosteroids and one a LABA. At actuation, the two strips come in contact with each other for a better aerosolization of the drug. Moreover, GSK together with Theravance, manufactured the Relvar® to deliver vilanterol and fluticasone. Acton Pharmaceuticals also developed a new pMDI (Aerospan®) to deliver flunisolide [70, 71].

1.7. Dry Powder Inhalers

The first dry powder inhaler for treatment of lung disease was the Abbot/Spinhaler® developed in 1970. Seven years later the Rotahaler® (a single dose DPI) was used with salbutamol. Subsequently, the Turbuhaler® and Diskhaler®, the first multidose DPIs were employed, followed by GlaxoSmithKline's Diskus™ [72]. DPI doses can be loaded with a single capsule (Cyclohaler®), or multi single unit dose (Diskus™) or as reservoir device (Turbuhaler®) [73]. DPIs have been designed to be able to deliver a dose in the range of inhalation flow rate between 30 and 90 $Lmin^{-1}$ [74]. There are differences between MDIs and DPIs. DPIs are propellant free (in comparison to MDIs); can deliver a high dose of drug particles and are breath-actuated so they avoid the hand-lung coordination required for MDIs [75]. Thorsson et al. [76] and Borgstrom et al. [77] showed that twice the dose is delivered to the lungs when emitted from the Turbuhaler® than from a MDI [76]. However, the efficiency of delivery of medicaments to the target regions of the lung is typically low and variable for DPIs. Less than 15 % of the emitted budesonide reached the lung in healthy volunteers (n=10) [78] and when the inhalation rate increased, aclidinium bromide emitted from Genuair® DPI showed 34 % of lung deposition [79]. The same trend was previously shown for MDIs with only 5.5 – 28 % of a dose depositing in the lung [80]. Patients with obstructive lung disease are unable to generate an aerosol cloud effectively from DPIs [81]. In particular a high fraction of the emitted dose deposits in the oropharynx, and the latter fraction cannot be therapeutically active and contributes to side-effects [82]. Borgstrom et al. [77] showed that the lung deposition from a Turbuhaler of terbutaline sulphate (nominal dose of 0.25 mg) in thirteen asthmatic patients was 20.8 %. When a MDI was used for the same drug, the lung deposition was only 4.8 % for 0.25 mg. Therefore, in this study, an improved lung deposition has been shown and that the use of a DPI has greater potential. DPIs, therefore, are overtaking the MDI market [66].

DPIs are termed passive inhalers because they employ the patient's own inhalation for the aerosolization of the drug product [83]. The design of the DPI helps the deagglomeration of the formulation within the device. The design of each DPI is optimised to emit the formulation as a respirable dose during inhalation. However, each DPI has different resistance due to a different design and this plays a major role on the magnitude and properties of the delivered dose. For example, the size of the internal diameter of the device mouthpiece might affect the turbulence to air flow through each device [84]. Rotahaler®, Spinhaler® have low resistance, Diskus™ and Cyclohaler® have medium resistance, and Easyhaler™ and Turbuhaler® have high resistance [85]. Al-Showair et al. [81] showed that the higher the internal resistance of DPI, the lower is the flow rate generated for a given pressure drop. Therefore, it has been suggested that patients with obstructed lungs require a low to medium resistance inhaler, to be able to generate sufficient airflow rate foe effective aerosolization.

Single-unit dose inhalers such as the Cyclohaler® consist of a capsule that must be replaced after each actuation. The patient presses the buttons on the side of the inhaler that are connected with pins that pierce the capsule (Figure 1.9, A). Upon inhalation the velocity of the particles increases and more collisions occur between the drug and the grid which also creates more energetic turbulence [86]. A multiunit-dose inhaler such as the Accuhaler™, contains prepared unit dose drug powder in sealed blisters, which are pealed open by lifting the mouthpiece lid and the powder is dispersed by the turbulent shear upon inhalation (Figure 1.9, B) [87]. Multi-dose reservoir inhalers (e.g. Easyhaler™) have been designed to minimize the flow dependency between patients. The Easyhaler™ consists of a bulk supply of drug from which individual doses are metered with each actuation (Figure 1.9, C) [88]. In this way, up to 200 doses can be delivered. The Easyhaler™ has a protective case and the hopper is designed so that is impossible for the patients to blow inside the inhaler.

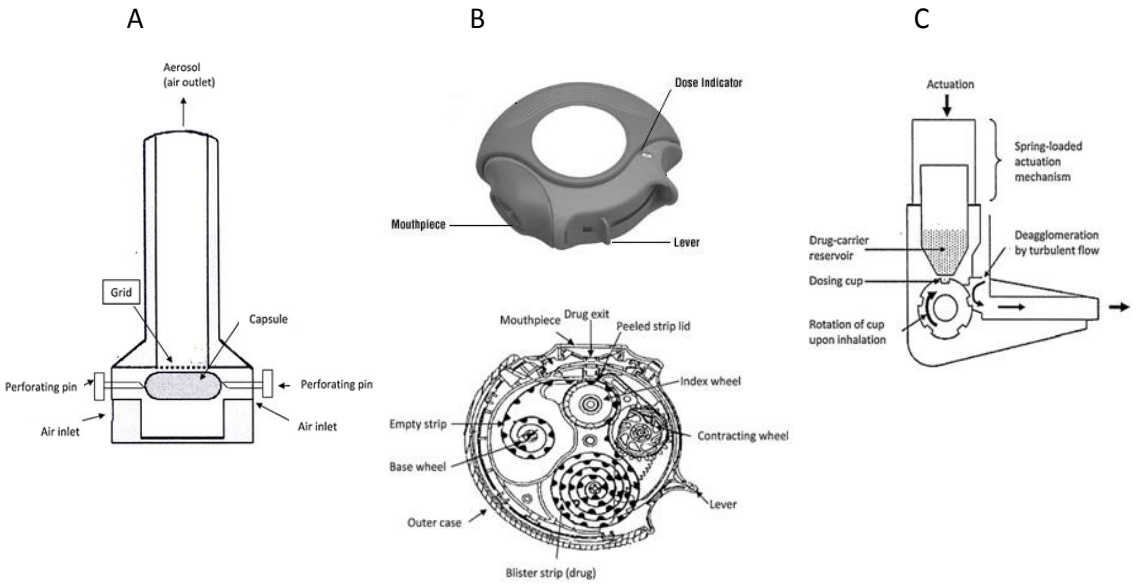

Figure 1.9. Design of three different dry powder inhalers: Cyclohaler® (A), Accuhaler™ (B) and Easyhaler™ (C).

The change in dimension of the airflow path between DPIs maximizes the particle separation. As a result, the fine particle fraction (FPF), and the lung deposition ratio of drug particles are enhanced [86]. The literature [89] highlights that dose emission from an Easyhaler™ is fairly consistent irrespective of the flow rates compared to other DPIs (Figure 1.10). Easyhaler™ also is easy to use therefore, more suitable for patients [90].

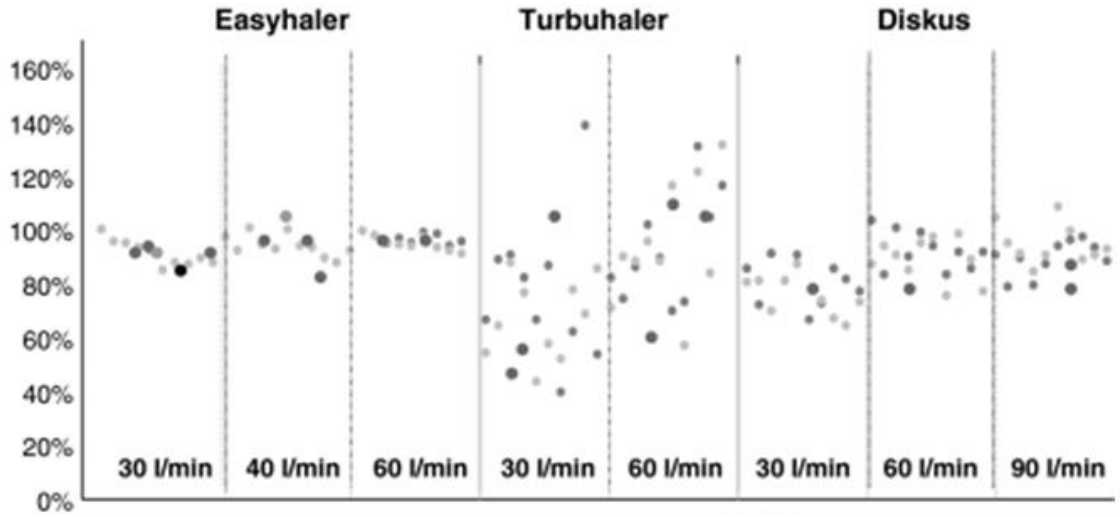

Figure 1.10. Dose delivery (% of the nominal labelled dose) from three salbutamol-containing multi-dose powder inhalers at different flow rates in asthmatic patients: Buventol Easyhaler (200 µg/dose), Inspiryl Turbuhaler (100 µg/dose) and Ventolin Diskus (200 µg/dose) [89].

The design of the DPIs has been improved over 40 years, and a modern device has been developed and marketed (the Conix™) that shows a greater delivery of the dose compared to the Accuhaler™ [91] because it contains a miniature reverse flow cyclone that helps the deagglomeration of the particles. Another DPI with a cyclone system has been developed: the AirMax™ (Figure 1.11).

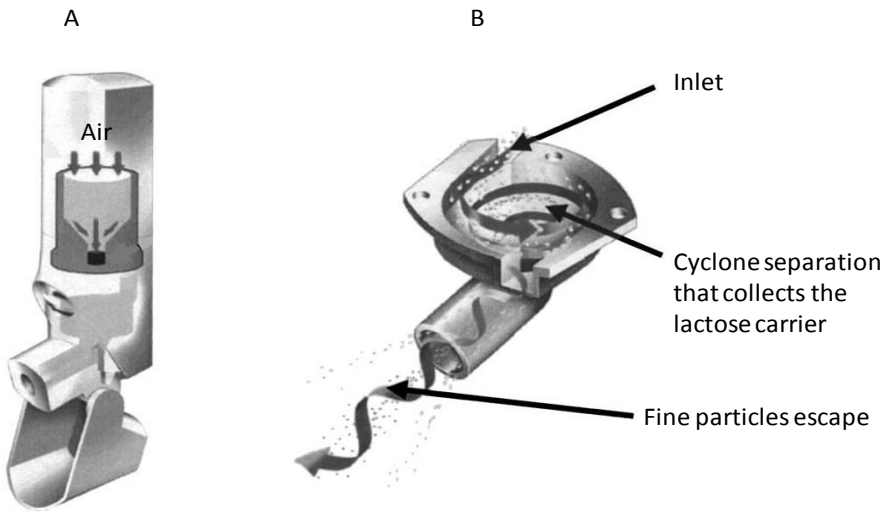

Figure 1.11. Design of the novel dry powder inhalers AirMax™ (A) with the cyclone system (B) [92].

The design of the AirMax™ is similar to a pMDI for patients' convenience. Tests using either budesonide or salbutamol on the FPF (fine particle fraction) and total emitted dose from the AirMax™ demonstrated significant improvement compared to that of the Turbuhaler® and more constant dose delivered regardless of the inhalation flow rates used [93] .

1.7.1. Fluidisation of inhalation powders

Most DPI formulations are composed of micronized drug and coarse carrier, which is typically lactose monohydrate (size of 63-90 μm), that improves the flowability of cohesive particles and therefore, minimizes the interparticulate forces caused by their micronized size. It is also necessary as a bulking agent as the dose of the drug is typically small [75]. The patient's inhalation airflow causes fluidisation within the device and creates turbulence that should be sufficient to de-aggregate drug/carrier mixture [75, 85] into fine particles with the potential to deposit in the lung (i.e. the respirable dose). The principal forces leading to powder de-agglomeration in inhalers can be divided into frictional forces, drag and lift forces, and internal forces

[94]. The deagglomeration of drug particles to form a fine, respirable aerosol cloud is caused by particle interaction with shear flow and turbulence, particle-device and particle-particle impaction [95]. In the formulation sometimes, ternary agent (e.g. fine lactose) is added to enhance dispersion of the active pharmaceutical ingredient (API).

There are two theories that explain the attachment of the API to the carrier: the active site theory and the agglomeration theory (Figure 1.12). It has been suggested that due to the rough surface of the carrier, there are sites with high energy to which the API is likely to be attached. Therefore, the presence of fine carrier particles is required to compete with the API. Thus, when the dose is delivered, the API is dislodges easily [75, 96]. Other studies suggested that the API with the fine particle carrier creates agglomerates on the surface of the coarse lactose and, upon aerosolization, the agglomerates are released from the carrier, therefore the drug is liberated from the fine carrier particles [83].

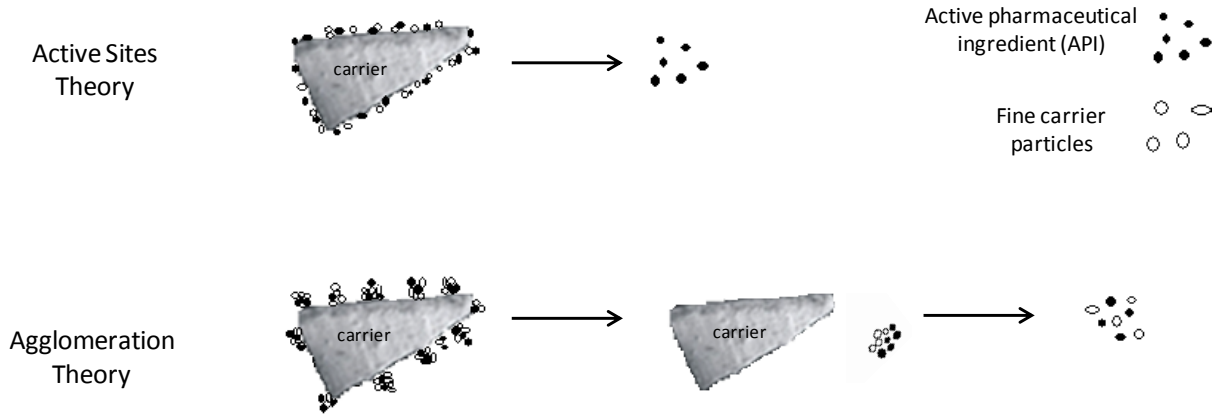

Figure 1.12. Diagram of active site and agglomeration theories for the attachment of the drug to the carrier

In order to deliver the dose to the lung, passive inhalers employ patients' inspiratory flow that creates turbulence that should be sufficient enough to allow the transition of the powder bed from a static to a suspended state in the airstream, and to deaggregate the fluidised particles into smaller ones due also to impaction of particles on the device components (e.g. capsules, walls and outlet). This process is called fluidisation [75].

1.7.2. Powder and blend structure of the formulation

The micronized drug particles required for pulmonary delivery (1-5 μm) show cohesive behaviour, and dispersion upon inhalation can be difficult [97]. To overcome this issue, lactose monohydrate or other type of carrier (with size between 63-90 μm) is added to the formulation, and improve the flowability of micronized drug. Marketed formulations often contain carrier with the drug (Ventolin™ and Seretide/Accuhaler™, Easyhaler™). In vitro studies have shown also that different types and % of lactose might affect the aerosolization of the formulation [98-101].

A small carrier size has been demonstrated to increase the fine particle fraction of budesonide from 26.36 ± 0.79% to 37.46 ± 0.15% when carrier size decreased from 120-180 μm to 32 μm [102]. Moreover, increasing the API dose load on the carrier surface increased the emitted dose with a linear relationship [96].

It has also been shown that the aerosolization of the drug and coarse lactose is improved when a fine ternary agent is added. Zeng et al [103] showed that adding fine lactose to the formulation of salbutamol sulphate/lactose monohydrate decreased the pre-separator deposition from 55.6 % for blends without micronized lactose to 36.1 % for blends with the ternary agent. Adi et al [104] showed that adding fine lactose to the formulation of salmeterol xinafoate/coarse lactose increased almost three-fold the FPF of the drug than when fine lactose was absent (11.7% and 4.0%, respectively). Therefore, it seems that the introduction of a small amount of micronized lactose to the formulation improves drug detachment from the carrier particles and consequently, improves the FPF of the API. In fact, as per the theory described in Section 1.7.1, adding micronized lactose particles may reduce the drug/carrier interactions as the fine lactose competes with the API and occupies possible drug binding sites on the carrier lactose particle surface. Some studies suggested that the presence of fine lactose is sufficient to enhance the respirable fraction most probably due to the fact that the API, not adhering to the coarse lactose surface, is more available for dispersion. Srichana et al. [105] showed an improvement in the fine particle fraction of SS when micronized lactose was added to the drug rather than when only coarse lactose was used (44.29 ± 1.30 % vs. 29.76 ± 0.69 %).

There is an increasing interest in formulations that do not need the coarse carrier to aid the flowability of micronized drug. The Turbuhaler®, for example, consists of a carrier-free formulation. Here, micronized drug particles are loosely agglomerated into larger particles with improved flowability such that the agglomerates can flow from the drug reservoirs into metering chambers of the inhaler [106]. During the patient's inspiratory action, shear and collision forces provided by the turbulent air stream generated within the device disperse the agglomerates and break them up into smaller particles that can penetrate into the lung.

1.7.3. Physicochemical proprieties affecting formulation performance

When a formulation is manufactured, particle size, shape, morphology and chemistry need to be taken in consideration. Also the surface rugosity of the carrier plays an important role. The high energy areas on the carrier surface provide sites to which drug particles adhere leading to poor dispersion. On the other hand, when the surface of the carrier is smoother, the particles are more exposed. It has been demonstrated that smooth carrier particles facilitate higher respirable fractions [107]. Moreover, irregular drug particle shape can also reduce the ease of dispersion as it increases the area of inter-particle contact. Furthermore, very big carrier size affects the drug dispersion: larger particles are subject to greater aerodynamic drag forces and can enhance the drug dispersion from the surface [103].

1.7.3.1. Cohesive and adhesive behaviours

The surface electrostatic forces associated particles in the inhalable size range overcome gravitational force, resulting in the development of cohesive powders (drug-drug interaction) with poor flow [40]. Therefore, micronized particle behave as agglomerates. However, when carrier is added, micronized particles may exhibit two different behaviours: they evenly spread on its surface (e.g. salbutamol sulphate, SS), leading to an adhesive behaviour (drug-carrier interaction) [108, 109] or create agglomerates (e.g. salmeterol xinafoate, SX [98, 104]) as a result of a more cohesive behaviour. The drug particles are bound by physical forces to active sites on the surface of the carrier particles [73]. The interaction between lactose and drug molecules provides a degree of resistance to segregation, but must not be so great as to prevent the deaggregation of the drug from the carrier during drug delivery. Any

drug still adhering to the lactose after the aerosol has been generated will be deposited in the oropharyngeal region, which has the potential to cause local side-effects, as in the case of inhaled corticosteroids [82].

1.7.3.2. The nature of interparticulate forces driving cohesive and adhesive formulations

The degree of drug dispersion depends upon the forces of interaction within the powder formulation and the mechanical forces of dispersion from the device and patient's inspiration. The adhesion forces between drug and carrier consist mainly of Van der Waals forces but also Columbic forces and capillary forces [40]. Studies demonstrated that strong adhesion of the drug to coarse carrier reduced the extent of dispersion of the micronized particle [99, 110]. Factors affecting interparticulate forces within the powder formulation include the drug and carrier properties, drug-carrier ratio, ternary components, mixing process conditions, presence of electrostatic charges, moisture content, carrier surface rugosity and storage conditions [111, 112]. Adi et al. [99] showed that adding fine lactose improved the dispersion process of the salmeterol xinafoate from the coarse carrier, because the interaction between the fine lactose and the SX produced mixed agglomerates with enhanced dispersion efficiency, and more easily broken up during inhalation.

The adhesion of fine particles to the carrier varies when the roughness of the carrier varies. Increasing the surface roughness of lactose particles improves delivery efficiency. Kawashima et al. [110] showed that increasing the surface rugosity of the carrier increased the emitted dose of the drug as the lactose can carry more drug particles, but it decreases the respirable fraction. However, mixing fine lactose particles improved deaggregation, as well as the fine particle fraction. Smaller particles have a lower degree of surface roughness and smaller interparticulate contact area than big particles. Therefore, the liberation of the drug from the surface of fine lactose can occur with more efficiency than from the coarse carrier [101]. Thus, the respirable fraction is enhanced when fine lactose is present, while the flowability of the powder is maintained by the coarse lactose. Other studies showed that the presence of coarse carrier is not necessary [113]. Behara et al. [113] showed that SS and fine lactose mixtures with increased lactose content (1:4 to 1:8) improved powder aerosolisation. However, at high flow rates, a negative

effect on SS aerosolization was found. The deagglomeration of the mixture was greater than for individual powders, indicating that adhesive interactions overcome forces that otherwise reduced deagglomeration.

1.8. In vitro formulation performance analysis

In order to predict deposition in the lungs, impaction studies have been widely proposed [114-116]. DPIs and MDIs are meant to aerosolize drug particles and the deposition of the latter inside the pulmonary regions is a function of the aerodynamic diameter. Laser diffraction analysis has been proposed to assess the particle size distribution based on the number or volume of particles. However, many studies have used monodisperse aerosol to study deposition mechanisms [117, 118] and therefore, a generator that can create monodipserse aerosol has been proposed. Moreover, it is essential to validate, device and impactor stage cut-off diameters and monodisperse aerosol are necessary to achieve this.

1.8.1. Monodisperse aerosol generator

Several studies [117, 118] have used monodisperse aerosol in order to deliver a specific sized particle to a particular lung region. The monodisperse aerosol generator uses a liquid jet to create the particles. Therefore, the solid has to be dispersed and diluted in an appropriate solvent before coagulation occurs. The vibrating orifice aerosol generator (VOAG, model 3540) used in the current project was composed of four major parts (Figure 1.13):

- the liquid feed system
- the droplet generator
- the droplet dispersion system
- the aerosol flow system

The liquid feed system consists of a syringe pump that feeds the droplet generator with liquid at a constant flow rate. The droplet generator consists of a stainless steel cup, an orifice disc placed inside the bottom of the cup, a Teflon O-ring on top of the orifice disc and a stainless steel cap placed onto the O-ring to hold the orifice disc in place. There is also a ring-shaped piezoelectric ceramic that vibrated when the aerosol is generated. The liquid, from the liquid feed system, is fed through the cap into the cup and is then sprayed through the orifice. A voltage is applied to the

piezoelectric ceramic which vibrates the cup and create a single liquid jet at a constant frequency. The frequency helps to create a uniform jet leading to emission of monodisperse aerosol [119]. When the frequency is either too high or too low, the jet splits in two leading to more than one size of droplet (called “satellites”) [120]. The droplet stream enters the dispersion system. The droplet dispersion system consists of a Perspex steel holder and cover for the droplet generator, a pressure regulator, a flow meter, and an absolute filter. The cover has a dispersion orifice through which both the droplet stream and a turbulent air jet pass. When the droplet stream reaches the turbulence of this air jet, it is dispersed into a conical shape. The dispersed droplets (aerosol) then enter the aerosol flow system.

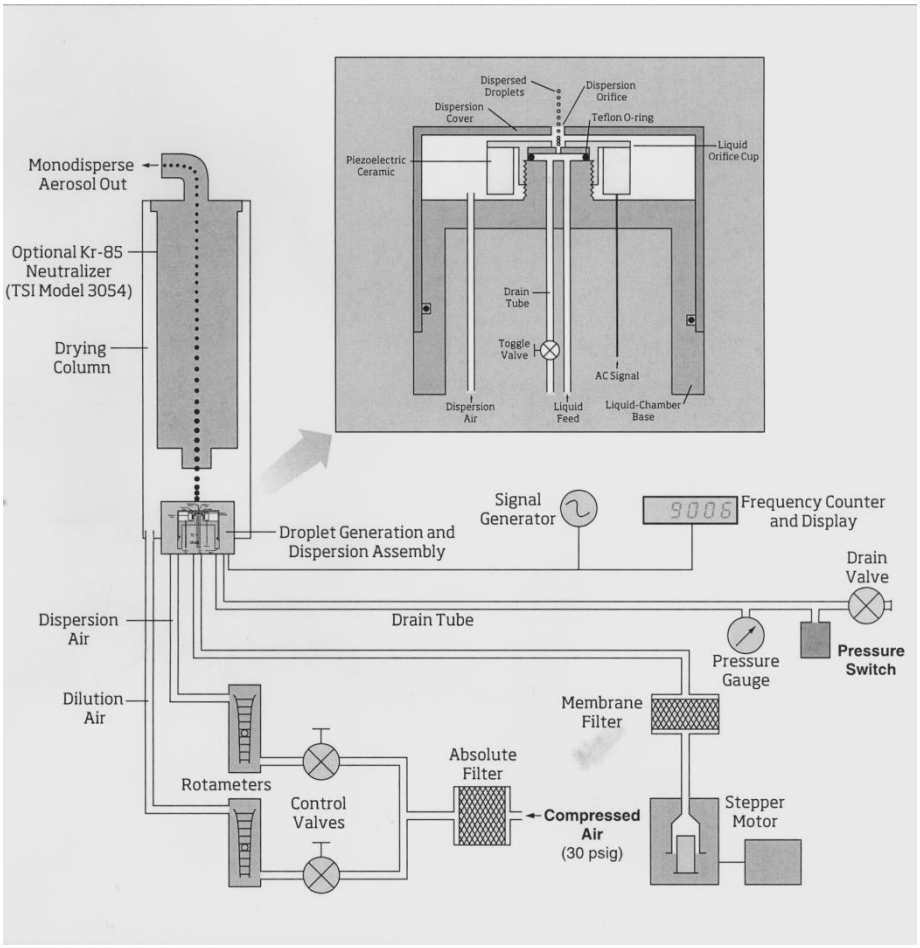

Figure 1.13. Diagram of a monodisperse aerosol generator.

The aerosol flow system consists of a blower and flow meter for the main dilution air, an absolute filter, a perforated plate which supports the droplet generator assembly, and a vertical plastic tube for diluting and drying the volatile liquid droplets. Air from the blower passes through the absolute filter, through the perforated plate, and then

mixes with the dispersed droplets. This clean air dilutes and transports the aerosol, and, in the case of a non-volatile solute in a volatile solvent, the clean air also evaporates the volatile solvent. The monodisperse aerosol then leaves at the top of the plastic tube [119].

1.8.2. Impaction analysis of aerosol particle size

Cascade impactor is the technique based on inertial impaction of particles and is used to measure the particle distribution based on the aerodynamic size [115]. Cascade impactors group together Multi Stage Impinger, Andersen Cascade Impactor (ACI) and Next Generation Impactor (NGI). Cascade impaction is based on a simple principle: when the airflow changes direction, particles in the airstream are subjected to two forces. The first one is the momentum derived when the particles travel along the streamline; the second one is the hydrodynamic force (i.e. friction) with the surrounding air stream as the particle changes direction. The momentum keeps the particle in its original flow trajectory, whilst the friction created between the particle and the air makes the particle accelerate in a new direction in the air. Therefore, until the particle loses the inertia, it will keep travelling in the original direction. Then it will change direction within a characteristic time. The latter determines whether or not a particle will deposit in a specific collection surface [40]. The technique is used widely because the emitted dose from the inhaler is divided into aerodynamic size classes that characterize the potential region for deposition in the respiratory tract [121]. The aerosol is guided by the air stream at a defined flow rate through a model mouth, throat and to the next stages where the particles are deposited depending on their size; therefore each stage represents a specific particle size range [115]. The whole system is described by the flow rate of the air and the geometry of the nozzles in each stage and these parameters are used for calculating the size cut-off of a stage [116, 122]. In an impactor, the particle is drawn through the nozzle, which accelerates the air and the particle to high speed. The surface of the impaction plate deflects the air which makes a sharp turn. The particles with sufficient inertia continue their movement to the collection surface and impact into it [115]. At each stage if the nozzle diameter or the number of nozzles is decreased, then the air velocity will increase as a consequence in order to keep the volumetric flow constant and thus the inertia of the particles is increased progressively. If a small particle does not have sufficient inertia to deposit in one

stage, it will deposit onto a later stage due to increased inertia at that stage. Thus, each stage collects particles that have diameter larger than its cut off size. The cutoff point is defined as the point of 50% collection efficiency [115].

1.8.3. Laser diffraction analysis of aerosol particle size

The difference between laser diffraction analysis (LDA) and impaction techniques is that LDA provides information of the geometric particles size, whereas impaction gives information on the aerodynamic particle size of aerosolized particles. Therefore, the impaction technique is widely accepted as an in vitro prediction of how particles will deposited in the lungs based on their aerodynamic size.

Along with cascade impaction, laser diffraction analysis (LDA) has been evaluated to investigate aerosol particle distributions [116]. LDA measures the particle size that corresponds closely to the volume equivalent diameter for a near spherical powder [116, 123]. In the LDA, a monochromatic laser beam hits the aerosol cloud that scatters the light into a Fourier lens. This lens focuses the scattered light into a multi-element detector and, using an inversion algorithm, a particle size distribution is calculated from the collected diffracted light intensity data [44]. Therefore, the particle size is a function of the angle of the diffracted light and thus, the particle volume. LDA uses an optical model to interpret the scattering data and hence calculate a particle size distribution and the Dv_{10}, Dv50 and Dv_{90} that correspond to the particle diameter (by volume) below which 10%, 50% and 90% of the particles exist [123]. There are two optical methods that convert the light energy diffraction pattern into a size distribution: the Fraunhofer approximation and the more rigorous Lorenz - Mie theory [124]. The first is simpler and describes diffractions of light at the contour of the particles. It does not require knowledge of the optical proprieties (such as refractive index including light absorption coefficient) of the particles and it works well with uni-modal size distribution and for particles that are bigger that 5 µm. Therefore the assumption is that particles of all the dimensions scatter the light with the same efficiency. It assumes that particles being measured are opaque and scatter light at narrow angles. This is why it is only applicable for large particles. The Mie theory is more rigorous and predicts scattering intensities for all particles (small, large, transparent and opaque). It assumes a homogeneous and optically linear material irradiated by an infinitely extending plane wave. It assumes

that the scattering of the light by particles approaching the wavelength of incident radiation is a function of the angles of scattering, the wavelength of the incident light, differences in refractive indices, and the diameter of a sphere [40]. It takes into consideration the refractive index between particles and dispersion medium and the theory is recommended when the refractive index of the particles is close to that of the supporting medium and for particles smaller than 5 µm.

1.8.4. Inhalation simulation

Cascade impactor analysis uses a constant flow rate. However, it has been shown that in patients a constant flow is not achievable [125]. In fact, previous studies showed that acceleration of flow influences the peak inspiratory flow rate and the time when it is reached [12, 126]. Many in vitro studies have now started to utilize real inhalation profiles for a better comparison with in vivo results. The electronic lung device (ELD), the inhalation manager and the breath simulator in combination with the NGI (Next Generation Impactor) are few examples of cascade impactor techniques with real inhalation profiles. The dispersion of the aerosol will be generated by the inhalation profiles and not by an unrealistic constant flow rate. The electronic lung device is an inhalation simulator and it separates the dose dispersion system for the particle size process. The dose dispersion occurs during the simulation of the patient inhalation, whilst the particle size process occurs thanks to an additional constant flow rate [127].

1.9. Clinical efficacy and adherence studies

Inhalation therapy plays a major role in asthma and COPD. However, it has been established that there is poor adherence by the patients. Around 60% of COPD patients [128, 129] and between 30 to 70 % of asthmatics [130] do not adhere to their therapy. The main reason of the poor adherence is the patients' fear of the side effects caused by inhaled corticosteroids. Moreover, they reported that there was lack of information from the medical staff and the increasing cost of the medications became a burden [131]. However, lack of communication, poor adherence and incorrect inhalation techniques lead to a progression and poor management of the disease [132].

1.9.1. Poor management of asthma

Achieving and maintaining the control of asthma are the aims of asthma management. However, many patients show poor asthma control and this increases the cost of management [133, 134]. “Control of asthma” is defined as the fluctuations or lack of symptoms and lung function over a period of time [132]. Minimal or no symptoms of asthma during day and night, absence of asthma attack, no hospitalization or no requirement for rescue therapies (such as bronchodilators) are the targets for a good control and management of the disease [68]. However, many patients require a change in the medication due to a poor response to corticosteroids as the inflammation may persist [69]. In Table 1.1 the main factors that cause inadequate control of asthma are listed and how they can be avoided [74, 132, 135].

Table 1.1. List of causes of poor asthma control and possible solutions.

Cause of poor control asthma	Possible solutions
Exposure for prolonged time to triggers of asthma	Avoid unnecessary exposure to triggers
Underestimated symptoms	Correct diagnosis
Lack of adherence of the patients to the therapy	Awareness of patients of the early stage of the disease
Incorrect usage of the inhalers	Adequate training in use of inhalers
Inadequate dose reached the peripheral lungs	Change of the medication

In order to identify poor management, alongside clinical measurements such as lung function, peak expiratory flow (PEF) and forced expiratory volume in 1 second (FEV_1), inflammatory markers are widely used [68, 136]. Many studies have been performed using hyperreactivity to methacholine or histamine, markers in sputum such as the number of eosinophils and nitric oxide (NO) [137-140]. Remodelling of the airways (hypersensitiveness of the airway where the constriction of the muscles in the airways is accentuated) and increase in neutrophils are good markers to identify poor response to glucocorticosteroid therapy, and therefore, to poor asthma control [69]. Variability in clinical markers represents a poor control of the disease, but a distinction needs to be made between poor control and severity of asthma. These two definitions do not replace each other, but the severity of the disease might be a consequence of the poor management. Whilst poor control reflects the inadequacy of treatment, severity reflects the disease process and the irregularity in the pathology [141].

1.9.2. Progression of asthma

Poor management of asthma can lead to a progression of the disease. To identify disease progression, persistent symptoms, impaired lung function, high bronchodilator use, unscheduled consultations, hospitalisations, and rescue therapy are the markers that need to be taken in consideration [132]. Progression of asthma needs to be controlled because exacerbation, during which symptoms worsen over-and-above the baseline respiratory function that shows decline of the disease leading to a change in therapy [142]. This leads to poor quality of life characterized by reduced physical activity, increasing mortality and morbidity, increasing in the health cost and hospitalization. Prevention of exacerbation and disease progression are, therefore, the key components of management's strategy for asthma [11, 68].

1.9.3. Clinical inhaler use issues

Studies have been reported that patients don't feel the need to talk about their lung diseases as they underestimate the symptoms [131]. This is because most of the patients do not take the medications and they have incorrect inhalation technique. Constant improvement to the inhaler design has been made helping the patient to achieve a better inhalation technique. MDIs contain propellant that complicates effective inhaler use by paediatric patients and the elderly. The impact of the aerosol on the throat leads the patient to stop breathing. Moreover, patients find it difficult to coordinate the actuation of the device and the inhalation of the aerosol or they breathe too rapidly. Spacers have been used widely to overcome this issue [143]. Clement Clarke International has manufactured a training device that can teach the patients the correct inhalation technique. The Flo-Tone is attached to the MDI and, on inhalation, it will make a sound that informs the patient when to actuate the inhaler [144].

Some patients are prescribed with DPIs which lack the requirement of hand-lung coordination. However, it is their inhalation strength that aerosolizes the formulation. Studies reported that there is a high inter-patient variability in the flow rate [77, 85] and the medication is inhaled before the peak inspiratory flow is reached [12, 125, 126]. The inter-patient variability leads to a variable and low emitted dose of the medication and high dependency on the flow rate. Moreover, their lungs are obstructed therefore, the inhalation strength is low and the medication

impacts on the throat. As seen for the Flo-Tone, with DPIs the pharmaceutical companies provided some design features to help the patient to achieve the appropriate technique. The Novolizer® for example has multiple feedback signals which inform the patient that sufficient drug has been delivered to the lungs [145]. Some of the signals are: colour change in a control window, ‘‘click’’ sound when the inhalation is performed correctly. Moreover, the Novolizer® also prevents patients from inadvertently overdosing with the preparation because the device cannot be reloaded until the previously loaded dose has been correctly inhaled. A similar feature is present in the Easyhaler™ that has a hopper so that is impossible for the patients to blow inside the inhaler [88].

Better technology has been recently used to manufacture novel devices: cyclone technology has been used for the Airmax® [92, 93] that has a design similar to MDI and a miniature reverse cyclone has been added to the Conix® [91, 146]. This technology increases the respirable fraction and capture in the device the big particle carrier that otherwise would impact on the throat. However, these are only two DPIs with different formulations. Therefore, a generic spacer for DPI that achieves the specific benefits of the latter design features is required

1.10. Aims and scope of the thesis

It is reported that patients struggle with their inhalers and some show progression of asthma and COPD diseases despite constant improvement in the marketing of novel DPI technologies. The main issues are lack of adherence of the patients to the therapy and the inappropriate choice of inhaler prescription based solely on the peak inspiratory flow, rather than a full inhalation profile. This is despite knowledge that a full profile gives a better understanding on the mechanism of aerosolization of the particles based on the device resistance. It has been suggested that the ex-vivo studies with either reproduced human inhaler profiles or real patient profiles produce more parameters to be considered to predict aerosol deposition, such as flow acceleration, time to reach the peak inspiratory flow (PIF), inhalation volume and deceleration. Studies have reported that the dose is delivered prior reaching the PIF. The primary aim of this thesis is to develop a diagnostic tool to guide DPI choice for clinicians based on the ability of inspiration of the patients, and therefore on their inhalation profiles through multiple marketed DPIs. Moreover,

differences in the flow achievable through a given inhaler by patients leads to variability in the flow rates and, therefore, also of the emitted dose and its particle size distribution. In many cases this is associated with high throat deposition of the emitted aerosol. Therefore, the second aim of the thesis is to investigate strategies to decrease throat deposition of the emitted dose and to mitigate the flow dependency of the aerosol emitted from DPIs using novel inhaler technologies.

1.10.1. Objectives of the thesis

I. To design a new test system to collect patients' inhalation profiles though a wide range of marketed inhalers
II. To estimate the flow rate variability with commercial inhalers.
III. To test new technologies to mitigate the flow rate dependency of the emitted dose
IV. To assess the difference in aerosol deposition when employing the standard metric of square wave peak inhalation flow compared to a full inhalation profile.

Chapter 2: Development and characterization of reverse – flow cyclones for pulmonary delivery

2.1. Development and characterization of reverse – flow cyclones for pulmonary delivery

2.1.1 Defining the performance of dry powder inhalers

The use of dry powder inhalers (DPIs) to deliver aerosol formulations for pulmonary delivery has been increasing over the last 25 years [66]. Most DPI formulations are composed of micronized drug with a coarse carrier, typically lactose monohydrate with a size of 63-90 μm that improves the flowability of cohesive particles and therefore, minimizes the cohesive interparticulate forces of micronized drugs [83]. The patient's inhalation airflow causes fluidisation within the device and creates turbulence that should be sufficient to de-aggregate the drug/carrier mixture [83, 85] into fine particles. The deagglomeration of drug particles to form a fine respirable fraction aerosol cloud is caused by interactions of powder and particles with shear flow and turbulence, particle – device and particle – particle impaction [95].

Impaction analysis is the pharmacopoeial test to assess the particle size distribution of a formulation based on the aerodynamic particle size [147]. Cascade impactor techniques such as Twin Stage Impinger (TSI), Andersen Cascade Impactor (ACI) and Next Generation Impactor (NGI) require a constant flow to predict the particle size of an emitted particle for potential pulmonary delivery [115]. Fine particle mass (FPM), fine particle dose (FPD) and mass median aerodynamic diameters (MMADs) are parameters to quantify and asses the aerosolization efficiency and particle size in impaction studies [148, 149]. However, they do not provide information about induction port deposition in a cascade impactor.

In vitro testing requires a constant flow rate as per FDA (Food and Drug Administration) recommendation [150].The British Pharmacopoeia prescribes testing of inhalers at 4 kPa pressure drop [147], but in real inhalation manoeuvres the flow rate accelerates [12]. In humans a constant PIF is generally achieved only with a high resistance device, but patients would find it uncomfortable to maintain the highest PIFs during aerosolisation [125]. The PIF has been correlated with the force available for de-aggregation of DPI blends [85] into fine particles that can potentially deposit in the lung (i.e. the respirable dose). However, many patients with

obstructive lung disease are unable to generate sufficient force for efficacious delivery of medicaments [80, 151].

2.1.2 Pulmonary and oropharyngeal deposition: the impact of flow rate

The performance of DPIs depends on the inhalation strength of the patient leading to variable and low deposition in the lungs. The force of the patient's inhalation flow through the DPI creates turbulence leading to high deposition through impaction of the emitted particles in the extra thoracic region leading to side effects [82]. A study on the lung deposition of budesonide emitted from the Turbuhaler® in healthy volunteers reported that only 14.8 % of the dose deposited in the lung and 66.6 % in the oropharynx region at 35 L min^{-1} [78]. A more recent study [79] showed that at high flow rates (80 L min^{-1}), lung deposition of aclidinium bromide emitted from the Genuair® DPI was 34.0 % of the delivered dose but the oropharyngeal deposition was still substantial, being 61.9 % of the delivered dose.

Lung deposition depends on aerosolization of the formulation to an appropriate aerosol size distribution, a process depending on the inhalation strength of the patient for passive DPIs. Both in vitro and in vivo studies have shown that the higher is the flow rate, the greater is the resultant fine particle fraction produced (i.e. the respirable fraction the patient would inhale) [125, 149, 152, 153]. A wide range of commercial DPIs have been tested and impaction studies have shown that the fine particle fraction (FPF) almost doubled from 30 to 90 L min^{-1} for low resistance devices [153]. Munzel at al. [154] showed a similar correlation between variability of fine particle dose (FPD) and flow rates in healthy subjects through in vitro impaction studies of budesonide emitted from the Novolizer® and the Turbuhaler®. In vivo lung deposition showed that between 45 and 90 L min^{-1} the fraction of budesonide deposited increased from 19.9% to 32.0 % for the Novolizer®, whereas the Turbuhaler® showed only 21.4 % at 60 L min^{-1}. However, one study [155] showed that at slow (30 L min^{-1}) and fast (60 L min^{-1}) inhalation rates the lung deposition of salbutamol (radiolabelled with 99mTc), in healthy volunteers (42.2 µg vs. 52.8 µg) for the MAGhaler device did not differ significantly.

2.1.3 Cyclone technology for improvement delivery of drug from dry powder inhaler

In recent years, miniature reverse airflow cyclone technology has been suggested and used for DPIs to capture the particles with high momentum in order to liberate only the fine particles to achieve higher pulmonary delivery. The Airmax™ device design resembles a pMDI (pressured metered dose inhaler) and the FPF and total emitted dose from the AirMax™ for both budesonide and salbutamol demonstrated significant improvement compared with that of the Turbuhaler®. This included greater consistency of delivered dose regardless the flow rates used [93]. The Conix™ was developed by Cambridge Consultants Ltd. [156] and licensed by 3M Drug Delivery Systems (3M Ltd). 3M Ltd showed [91] a greater amount of potentially respirable particles from the Conix™ than for the Accuhaler™ due to the retention of large agglomerates inside the device. $FPD_{3\mu m}$ (fine particle dose below 3 μm) of fluticasone propionate and salmeterol xinafoate delivered from the Conix™ was 41.8 % and 40%, respectively, compared to 14% and 12.3% when the Advair Diskus® was used [146]. Plasma concentration data showed that the Conix™ increased pulmonary deposition compared to the Diskus for both drugs. Considering the FEV_1 of the asthmatic subjects in the study, the Conix® showed comparable in vivo results although the delivered dose was one-third compared to the Advair® [146]. The Conix® was tested also with salbutamol sulphate and the device retained 80% of the drug [91]; which would reduce the mouth and throat deposition in the patients [146]. Moreover, the Conix™ almost halved the mass median aerodynamic diameter for the drugs compared to the Accuhaler™, thereby promoting a more specific pulmonary delivery (1.99 μm for salbutamol sulphate delivered from Accuhaler™ compared to 0.99 μm for the Conix™) [91].

2.1.4 Principles of cyclone separation

Reverse airflow cyclone technology has been widely employed. The Dekati® Cyclone has been used in many applications [157] to remove large particles from sampled environmental air. Another example is the Dyson vacuum cleaner that uses cyclonic separation to remove dust and other particles from an air stream. Cyclone separation is based on centrifugal sedimentation, where particles sediment out of a

helical gas or liquid stream. With a reverse flow cyclone, when a patient inhales, the air is drawn into the cyclone chamber (cone section in Figure 2.1) where an axially downward-flowing vortex occurs.

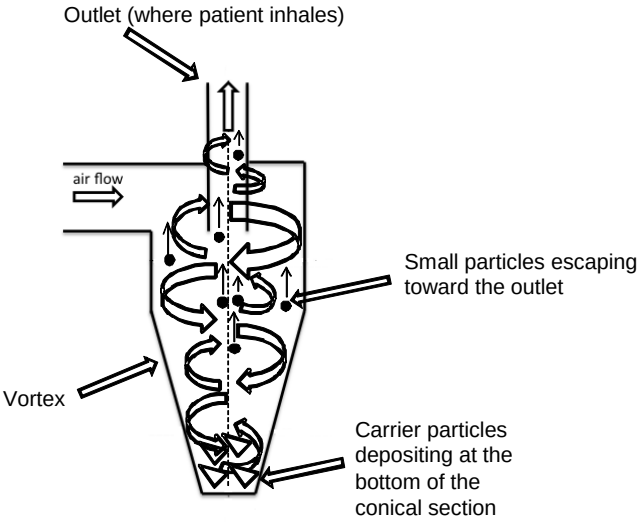

Figure 2.1. The reverse flow cyclone principle.

As the diameter of the cyclone body decreases towards the closed bottom, the downward flow is radially forced towards the centre, where it reverses direction and directs upwards. The core of the cyclone thus forms a second vortex with axially upward flow towards the exit orifice. The inhalation creates a vortex field with high velocities and energy which is favourable for the process of de-agglomeration. Collisions between particles and the cone wall as well as other particles occur as a result of the cyclonic flow field [146]. In this way, particles with large mass and size (e.g. lactose carrier) will deposit in the bottom of the cone and only the finest particle (e.g. 5 µm salbutamol sulphate) will escape the cyclone [91]. Therefore, drug that remains adhered to the lactose is retained within the device instead of being released into the respiratory tract. This would decrease the deposition in the throat that occurs in the traditional DPI, reducing subsequent side effects. However, it has been suggested that the efficiency still depends on the patient's inhalation flow rate [93].

2.2. Aims

Little information has been reported into the operation of miniature reverse-flow cyclones or the formulation factors determining their suitability for inhaled drug delivery. Previous work has involved computational fluid dynamic investigations of particle behaviour in miniature cyclones [158, 159]. The investigations identified the potential of reverse-flow cyclones to restrict particle output to sizes within the respirable range, and therefore identified the potential for a generic applicability to lung drug delivery. The aim of the current work was to investigate the potential of a cyclone spacer to improve in vitro drug delivery for a typical DPI (Cyclohaler®) and reduce throat deposition of the emitted particles.

The objectives of the project were:

- to manufacture a prototype cyclone spacer (hereafter called Cheng 1);
- to assess the in vitro throat deposition of Ventolin/Accuhaler™ formulation composed of SS (salbutamol sulphate) and coarse lactose when the Cheng 1 was used with the Cyclohaler®
- to compare particle size distribution of the emitted dose of SS from Cyclohaler® with and without Cheng 1.

2.3. Materials and methods

2.3.1. Materials

Micronized salbutamol sulphate (SS, batch number B027798) was obtained from GlaxoSmithKline Research and Development (Ware, UK). Lactose monohydrate, chromatography grade methanol, hydrochloric acid solution (HCl) 5M, sodium hydroxide and n-Hexane were purchased from FisherScientific (Loughborough, UK). Hipersolv® grade ammonium acetate was purchased from Lab3 Ltd (Northampton, UK). A Luna 3 µm C18 column (150 mm x 4.6 mm x 3 µm) was obtained from Phenomenex (Macclesfield, UK). Silicone oil - Dow Corning Corporation 200® fluid was obtained from Sigma-Aldrich (Gillingham, UK). Fluorescein disodium salt and oleic acid were purchased from Acros organics (Geel, Belgium). The DPIs tested were Ventolin/Accuhaler™ 200 µg/dose (purchased from Allen & Hanburys, Uxbridge, Middlesex, UK) and a Pulmicort/Turbuhaler® 400 µg/dose purchased form

AstraZeneca. A Cyclohaler® device was obtained from AAH Hospital Supplies (Coventry, UK). Size 4 hard gelatine capsules were obtained from Meadow Laboratories Ltd. (Romford, UK). The cyclone spacer (Cheng 1) was manufactured in-house (University of Cambridge, UK) from a Perspex block (Engineering & Design Plastics Ltd, Cambridge, UK); the exit duct was cut and polished from stock brass tubing (Engineering Department Storeroom, University of Cambridge, UK). The flow meter (model number DFM2), next generation impactor (NGI) and a model HCP5 vacuum pump were all purchased from Copley Scientific Ltd (Nottingham, UK).

2.3.2. Cyclone manufacture

A miniature reverse-flow cyclone (Cheng 1) was manufactured using empirical models [157] from Department of Engineering at Cambridge University to have a theoretical particle cut-off diameter below 5 μm for flow rates between 30 and 120 $Lmin^{-1}$. The Cheng 1 was machined from Perspex with a circular inlet orifice of diameter 4.14 mm to facilitate relatively high inlet velocities with high pressure drops. For dimensional accuracy, easy sample collection and interchangability, the Cheng 1 was manufactured in three separate sections – exit duct (top), inlet and cylinder body (mid) and cone (bottom); the bottom of the cone section had a through-hole for sample collection, which was sealed during experiment. In Figure 2.2 the dimensions of the cyclone are reported. An inlet adapter was also manufactured out of Perspex to enable connectivity with the Cyclohaler® (Figure 2.2).

	Cheng 1
D	20
D_e	5.9
a^1	4.1
b^1	4.1
H	57.9
h	24.7
S	17.3
B	6.2

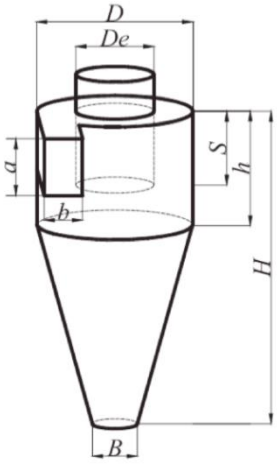

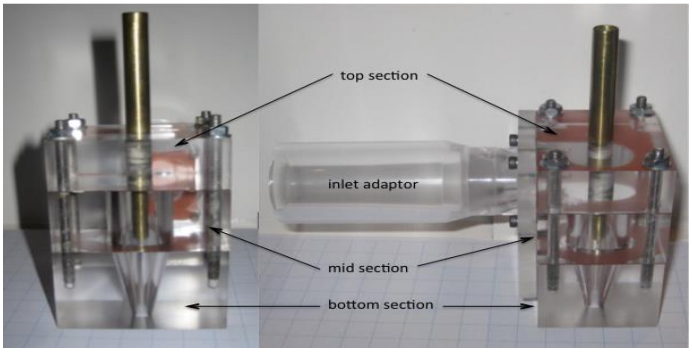

Figure 2.2. Dimensions of simulated cyclone geometries (units in mm) and photograph of reverse flow cyclone spacer

[1]Cheng 1 was manufactured with a circular inlet orifice, diameter 4.1mm.

2.3.3. High performance liquid chromatographic assay validation of salbutamol sulphate

Salbutamol sulphate (SS) was analysed using high performance liquid chromatographic (HPLC) assay. A stock solution was prepared by weighing accurately approximately 0.0025 g of the drug on a weighing scale (Mettler Toledo, UK), transferring it into 50 ml volumetric flask and bringing the solution to volume with an 80:20 (v/v) mixture of 0.6% (w/v) aqueous ammonium acetate: methanol (solution pH adjusted to 4.5 with HCl 1M). The stock solution was used in order to prepare a calibration series by pipetting the volumes shown in Table 2.1 and the set of calibration standards were run using HPLC (Agilent 1050 Series, Agilent Technologies UK Ltd., Edinburgh, UK) with a Luna 3 µm C18 column (150 mm x 4.6 mm x 3 µm) at 1 ml min^{-1}. The column temperature was 50 °C and injection volume was 50 µl. SS was detected by UV at 272 nm.

Table 2.1. Volume of stock solution (ml) required to prepare a calibration series in the concentration range of 0.05-50 µg ml^{-1}.

Theoretical concentration ($\mu g ml^{-1}$)	Volume of stock solution (ml)	Final volume (ml)
25	10	20
10	5	25
5	1	10
1	1	50

2.3.4. Data analysis of high performance liquid chromatography

2.3.4.1. Assay linearity, precision and reproducibility

The linear regression analysis was performed using the LINEST function of Microsoft Excel to establish the relationship between peak area and concentration. Three injections were made for each standard and the raw data for each day (n=3) were used. The mean peak area response and the relative standard deviation (RSD) at each concentration level were determined to assess intra-day variation. To assess inter-day variation, the peak area responses of the calibration standards were normalized to unit concentration to account for slight variation in the drug

concentration from the nominal value. The mean normalized peak area response and RSD for each concentration level was considered.

2.3.4.2. Limits of detection (LOD) and limits of quantification (LOQ)

The LOD and LOQ were calculated to determinate the sensitivity of HPLC of analysis using Equation (2.1) and (2.2).

$$LOD = 3Sy/m \quad (2.1)$$

$$LOQ = 10Sy/m \quad (2.2)$$

Where “Sy” is the standard deviation of the y-intercept from the linear regression analysis and “m” is the linear regression coefficient (gradient).

2.3.4.3. Accuracy determination

Two sets of five standard solutions were prepared; the first set was prepared with 0.002 g of SS dissolved into 20 ml of mobile phase and making a 1:10 dilution in order to obtain a 10 $\mu g ml^{-1}$ solution. The second set was prepared with 0.002 g of the API and 0.048 g of lactose monohydrate dissolved into 50 ml of mobile phase and 1:4 dilutions were performed to obtain the same concentration mentioned above. The peak area response of the standards when analyzed by HPLC according to the assay in Section 2.3.2 was determined. The amount of SS recovered was calculated using the calibration curve and the percentage recovery of the drug was calculated using Equation (2.3).

$$\% \text{ recovery} = \frac{\text{calculated concentration } (\mu g ml^{-1})}{\text{theoretical concentration } (\mu g ml^{-1})} \quad (2.3)$$

2.3.5. Spectrofluorimetric assay for fluorescein disodium salt

Fluorescein disodium salt (uranine) was tested using a spectrofluorimetric assay. A stock solution (100 μM) [160] was prepared by weighing accurately approximately 0.004 g of uranine, transferring it into 100 ml volumetric flask and bringing the solution to volume with NaOH 0.1 M. The stock solution was used in order to prepare a series of calibration standards (1-0.025 μM). The range of

calibration standards between 0.5-0.025 μM was analyzed using spectrofluorimetry (fluorescence spectrometer, PerkinElmer, LS 55) at 513 nm for emission wavelength and 489 nm for absorption wavelength.

2.3.6. Dose content assay

2.3.6.1. Dose content for mixture of salbutamol sulphate and lactose recovered from Ventolin/Accuhaler™ 200 μg/dose

The mixture of micronized SS and lactose was removed from marketed Ventolin/Accuhaler™ products. A set of six solutions was prepared by weighing accurately approximately 0.0125 g of the blend and dissolving into 10 ml of mobile phase. The concentration of SS was determined by HPLC assay. The dose content for SS was calculated using Equation (2.4) in order to identify the amount of drug contained in each dose (μg/dose).

$$\text{Dose content} = \frac{\text{mass of the drug determined byHPLC (μg)}}{\text{mass of the mixture (mg)}} \quad (2.4)$$

2.3.7. Resistance of Cheng 1

The resistance of Cheng 1 was measured across the spacer and Cyclohaler® in series using a dose uniformity sampling apparatus (DUSA, Copley Scientific Ltd., Nottingham, UK). The DUSA was connected to a critical flow controller TPK (Copley Scientific Ltd., Nottingham, UK) to adjust the flow rate. Once the flow rate was set through the DUSA, the Cheng 1 with the Cyclohaler® was attached to the DUSA to record the pressure drop of the two devices in series. The range of flow rates tested was between 17-70 L min^{-1}. The pressure drops obtained were then plotted against the corresponding flow rates and the resistance calculated using the equation (2.5):

$$R = \frac{\sqrt{\Delta P}}{Q} \quad (2.5)$$

Where “R” is the resistance ($kPa^{1/2} L^{-1}min$), “ΔP” is the pressure drop (kPa) and “Q” is the flow rate ($L\ min^{-1}$).

2.3.8. Impaction studies

2.3.8.1. Impactor plate coating

In order to have 1% w/v solution for coating the NGI plates, 1 g of silicon oil was accurately weighed and dissolved into 100 ml of n-Hexane. Approximately 15 ml of the solution was added into the first stage and the stage rotated, excess solution transferred into the second stage and so on until the last stage was covered. The plates were left under the fume hood in order to allow the hexane to evaporate leaving a thin layer of silicon oil as coating.

2.3.8.2. Cyclohaler® capsule filling

The mixture of micronized SS and lactose was removed from marketed Ventolin/Accuhaler™ products. Size 4 hard gelatin capsules were accurately hand-filled with approximately 0.0125 g of the blend.

2.3.8.3. Aerodynamic deposition assessment using next generation impactor

Aerosolisation studies were performed using the next generation impactor (NGI) with a model HCP5 vacuum pump (both from Copley Scientific Ltd., Nottingham, UK). In order to collect the drug-carrier mixture, each plate of the NGI was coated with 1% (w/v) silicone oil in n-Hexane, as described in Section 2.3.8.1. The NGI was then assembled as per the requirements in the British Pharmacopeia (Figure 2.3).

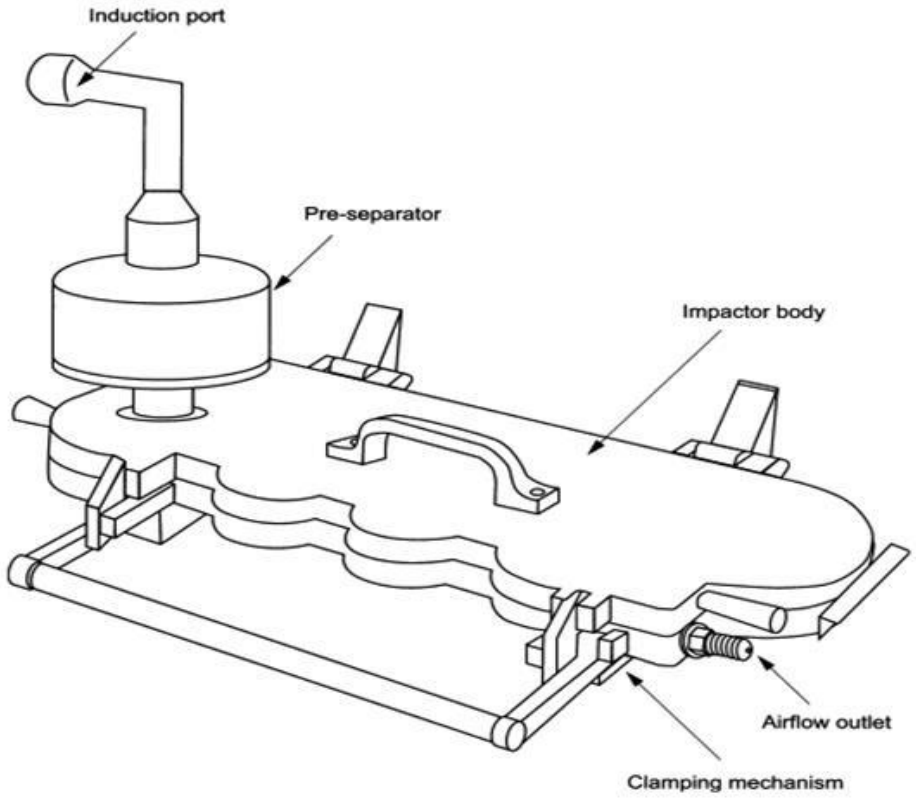

Figure 2.3. Scheme of next generation impactor according to the British Pharmacopoeia.

The Ventolin™ formulation was aerosolized using a Cyclohaler® device with and without the cyclone spacer. 15 ml of mobile phase was added to the central cup of the pre-separator and the flow rate was adjusted with the aid of a flow meter (Copley Scientific Ltd., Nottingham, UK) in order to reach 30, 45, 60, 75 or 100 $Lmin^{-1}$. When only the Cyclohaler® was employed for aerosolization, 6 Size 4 hard gelatin capsules (accurately hand-filled with 0.0125 g of the blend) were actuated. The aerosolization studies were performed at 30, 45, 60 and 75 and 100 L min^{-1} (= 4 kpa) with each actuation lasting 8, 5.3, 4, 3.2, 2.5 sec, respectively. A critical flow controller TPK (Copley Scientific Ltd., Nottingham, UK) was used to time the duration of the actuations. When the cyclone was employed as spacer device 8 filled capsules were actuated (12 capsules for 30 L min^{-1}). The aerosolisation studies were performed at 30, 45 and 60 $Lmin^{-1}$ as above (Figure 2.4) and the flow rate measured across the Cheng 1. The Cyclohaler ® was then attached to Cheng 1 and the capsules actuated.

Figure 2.4 Example of dry powder inhaler (Cyclohaler®) connected with the cyclone spacer (Cheng 1)

2.3.8.4. Recovery of deposited salbutamol sulphate from the impactor

In order to collect the drug, the Cyclohaler® and the capsules were washed with 20 ml of mobile phase and transferred into a volumetric flask. The bottom of the cyclone, the mouthpiece and the throat were each washed with 50 ml of mobile phase; whilst the upper section of the cyclone was washed with 10 ml. For collecting the drug from the pre-separator 100 ml of mobile phase was used for washing and dissolution of deposited drug. The volumetric flasks were sonicated using a sonicator (Kerry, Germany) for 2 min. When only the Cyclohaler® was employed, 10 ml of mobile phase was added to the first 5 stages, whilst 5 ml of solvent was used for the last 3 stages. All the stages were set on a laboratory rocker (Stirling Mixer, Sandrest Ltd, UK) and rocked for 2 min in order for the solvent to wash the entire surface. When the Cyclohaler® was employed with the cyclone, 5 ml of mobile phase was added to each stage. The concentration of the drug from each stage was determined by HPLC assay at 272 nm according to Section 2.3.3. After performing the experiments, each stage and the NGI were thoroughly cleaned with Millipore water and the coating was removed with acetone before rinsing with methanol.

2.3.9. Aerosolization studies using laser diffraction technique

Aerosolization was assessed by laser diffraction particle size analysis using the Sympatec Inhaler module (Inhaler Helos/KF, Sympatec Limited, Bury, UK) at 30, 45, and 60 $Lmin^{-1}$ for the Cyclohaler® device in the absence and presence of the Cheng 1. A carrier free DPI (Pulmicort/Turbuhaler®) was also tested at 2 and 4 kPa in the absence and presence of the cyclone-spacer. The lens used to detect the aerosol cloud was a R3 lens (0.5-175 μm). The measurement was set to trigger when the optical concentration was between 0.1 and 0.2 % for 5 sec duration (time base 1 ms).

2.3.10. Monodisperse aerosol study using Cheng 1

In order to estimate the cut off diameter of the Cheng 1, a VOAG (Vibrating Orifice Aerosol Generator, model 3450) was used. A solution of uranine (15%) and oleic acid (85%) was dissolved in isopropanol (IPA). In order to calculate the required solute concentration to generate a suitably sized aerosol (uranine and oleic acid) equation (2.6) was used:

$$(C + I) = \left(\frac{D_p}{D_d}\right)^3 \tag{2.6}$$

Where “C” is solute concentration, “I” is the impurity of the solvent, “D_p” is the final size of monodisperse aerosol to be generated (μm) and “D_d” is the diameter of the primary droplets (μm). When monodisperse aerosol was created with particle size (D_p) of 2 and 3 μm, the D_d was 40 μm, the solution feed through the orifice was set to speed rate 0.139 ml min^{-1} (flow rate of the solution to create the aerosol) and the vibration frequency for the orifice (20 μm) was set between 40-80 kHz (typically 69.13 kHz). In order to calculate the frequency needed the equation (2.7) was used:

$$f = \frac{6Q\ (C+I)}{\pi D_p^3} \tag{2.7}$$

To perform the experiment, the cyclone-spacer was placed facing the VOAG outlet. The outlet of the Cheng 1 was connected to an impinger (conical flask) to collect any

aerosol particles exiting the spacer. Airflow through the iminger and Cheng 1 in series was achieved with a vacuum pump. The flow rates used were 30, 45 and 60 $Lmin^{-1}$ to represent the aerosolisation studies. The flow rates were measured with a flow meter across the Cheng 1 prior the study. 20 ml of solution was used to clean the instrument and stabilise the jet. The dilution air to carry the air and particles into Cheng 1 was set to 30 L min^{-1} as it was the optimum air flow to avoid particle loss inside the VOAG tube. The duration of each measurement was 10 min. To collect the fluorescein aerosol, 50 ml of NaOH 0.1 M was used as washing solution [161] for the cyclone-spacer and the same volume to clean the conical flask impinger. To calculate the Cheng 1 efficiency Equation (2.8) was used:

$$\%\, Efficiency = \frac{mass\ of\ uranine\ in\ the\ spacer\ (\mu g)}{total\ mass\ of\ uranine\ collected\ (\text{spacer+impinger})(\mu g)} x100 \qquad (2.8)$$

2.3.11. Data analysis of impaction experiment

The % recovery was calculated, for full mass balance, as the total recovered drug (µg) on each stage and the device as a % of the total known mass of the drug actuated (i.e. the dose content). The recovered dose (RD) was calculated as the sum of the dose (µg) in each stage of the NGI and device or device and spacer. The emitted dose (ED) was calculated as the sum of the total dose recovered from NGI (or NGI and spacer) following actuation of the device. The spacer-emitted dose (sED) was calculated as the sum of the total dose recovered from the NGI only, when the spacer was used. The % retention of the cyclone was calculated as the mass of drug deposited in the spacer as a percentage of the ED. The % induction port/pre-separator (IP/PS) deposition was calculated as the mass of drug recovered on the IP/PS stage as a percentage of the ED or the sED. The % fine particle fraction below 5 µm (FPF 5µm) was calculated following interpolation of the cumulative particle size distribution of the dose deposited on the NGI stages as a percentage of the ED (i.e. ex device) or the sED (i.e. ex cyclone). The mass median aerodynamic diameter values (MMAD) were determined by interpolation of the cumulative particle size distribution of the dose deposited on the impactor stages.

2.3.12. Statistical analysis

Statistical analysis was performed in Minitab (version 15) using one-way ANOVA and post-hoc Tukey's test (multiple comparisons) or Student's two-tailed t-test for pair-wise comparisons, both at 95 % confidence intervals.

2.4. Results

2.4.1. Data analysis of high performance liquid chromatography assays

2.4.1.1. Assay linearity, precision and reproducibility

Linear regression analysis performed on raw data collected for three calibration series calibration is reported in Figure 2.5 for the SS.

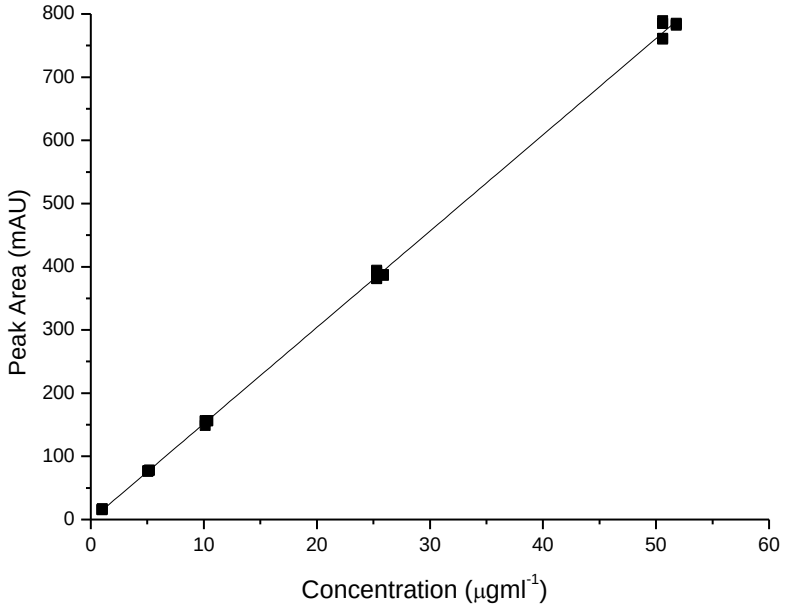

Figure 2.5. Linear regression analysis of peak area of salbutamol sulphate as a function of concentration (pooled raw data points of n=9 at each concentration level).

Regression results are reported in Table 2.2 .

Table 2.2. Regression results for peak area response plotted as a function of concentration for salbutamol sulphate (SS).

Day	Intercept	Standard deviation of the intercept	Slope	Standard deviation of the slope	Correlation coefficient (R^2)
1	-0.701	0.593	15.050	0.023	0.999
2	-0.493	0.856	15.105	0.032	0.999
3	-1.036	0.478	15.564	0.019	0.999
Pooled	-0.706	1.319	15.237	0.051	0.999

Intra-day variability of SS indicated good repeatability for SS between calibration range 1-50 µg/ml (Table 2.3).

Table 2.3. Intra-day variability of concentration range for salbutamol sulphate (n=3).

	% RSD				
	Concentrations (µg ml^{-1})				
	50	25	10	5	1
Day 1	0.10	0.08	0.04	0.15	0.74
Day 2	0.22	0.84	0.20	1.12	4.38
Day 3	0.30	0.59	0.26	0.45	2.79

Inter-day variability (Table 2.4) showed that at the lowest concentration for SS the reproducibility of the method was low.

Table 2.4. Table of data from inter-day variability (riproducibility of the relative standard deviation, RSD) for salbutamol sulphate (SS) (n=9).

Concentration (µg ml^{-1})	RSD (%)
50	1.49
25	2.17
10	1.34
5	0.67
1	3.29

2.4.1.2. Limits of detection (LOD) and limits of quantification (LOQ)

The sensitivity of the method used for SS was indicated by an LOD that was 0.26 µg ml^{-1} and LOQ that was 0.87 µg ml^{-1}. As the values are relatively low, the

method is suitably sensitive at low concentrations and lower than the lowest calibration standard.

2.4.1.3. Accuracy determination

The recoveries of SS alone and when lactose was added were 99.14 ± 2.33 % and 99.89 ± 2.44% respectively showing a high accuracy as the range was between 95 and 105 %. A two-tailed unpaired t-test revealed no significant difference when lactose was added (p value > 0.05) indicating that the carrier does not interfere with the detection of the drug.

2.4.2. Spectrofluorimetric assay for fluorescein disodium salt

Linear regression analysis performed on raw data collected for three calibration series is reported in Figure 2.6 for fluorescein disodium salt.

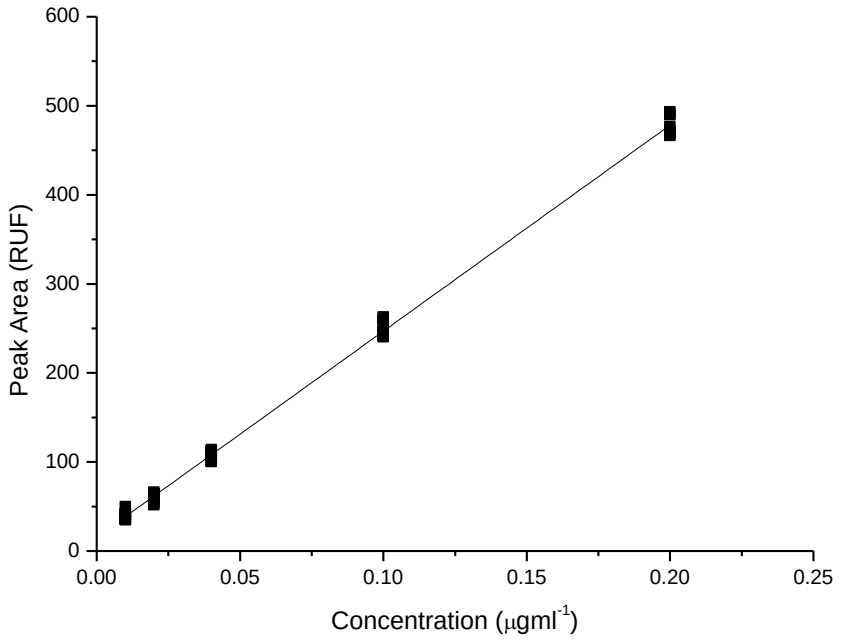

Figure 2.6. Linear regression analysis of peak area of fluorescein disodium salt as a function of concentration (pooled raw data points of n=12 at each concentration level).

Regression results are reported in Table 2.5.

Table 2.5. Intra-day variability of concentration range for fluorescein disodium salt (n=3).

Day	Intercept	Standard deviation of the intercept	Slope	Standard deviation of the slope	Correlation coefficient (R^2)
1	15.362	1.219	2391.679	11.945	0.999
2	14.650	1.273	2287.190	12.469	0.999
3	16.446	1.718	2263.492	16.830	0.999
Pooled	15.486	1.325	2314.120	12.985	0.998

Intra-day variability indicated good repeatability for the fluorescein disodium salt between calibration range 0.2-0.01 μg ml^{-1} (equivalent of 0.5-0.25 μM, Table 2.6) and inter-day variability (Table 2.7) are shown below. Intra-day variability showed poor repeatability at the lowest concentration, whereas poor reproducibility was seen at 0.02 and 0.01 μg ml^{-1}.

Table 2.6. Intra-day variability of concentration range for fluorescein disodium salt (n=3).

	% RSD				
Day	0.2 (μg ml^{-1})	0.1 (μg ml^{-1})	0.04(μg ml^{-1})	0.02 (μg ml^{-1})	0.01 (μg ml^{-1})
1	0.341	0.704	0.612	1.837	2.945
2	0.718	0.359	0.559	1.207	1.986
3	0.566	0.548	3.499	3.957	9.018

Table 2.7. Table of data from inter-day variability (riproducibility of the relative standard deviation, RSD) for fluorescein disodium salt (n=3).

Concentration (μg ml^{-1})	RSD (%)
0.2	2.179
0.1	3.331
0.04	4.967
0.02	8.480
0.01	11.616

The sensitivity of the method used was indicated by an LOD and LOQ that were 0.0017 and 0.0057 μg ml^{-1}, respectively.

2.4.3. Dose content assay

2.4.3.1. Dose content for mixture of salbutamol sulphate and lactose recovered from Ventolin/Accuhaler™ 200 µg/dose

The dose content of the mixture of SS and lactose formulation collected from the Ventolin/Accuhaler™ was 15.12 ± 0.49 $\mu g mg^{-1}$ (mean ± SD, n=6). The label claim was 200 µg/dose of SS. The mean of the six standards prepared from the mixture of SS and lactose determined using HPLC (Section 2.3.3) was 191.68 ± 7.50 µg/dose that corresponds to 95.84 ± 3.74 % (mean ± SD, n=6). The RSD was 3.91 %.

2.4.4. Resistance of Cheng 1

The cyclone-spacer posed high resistance to air flow (0.08 $kPa^{1/2}L^{-1}min$) as shown from the slope of the line in Figure 2.7.

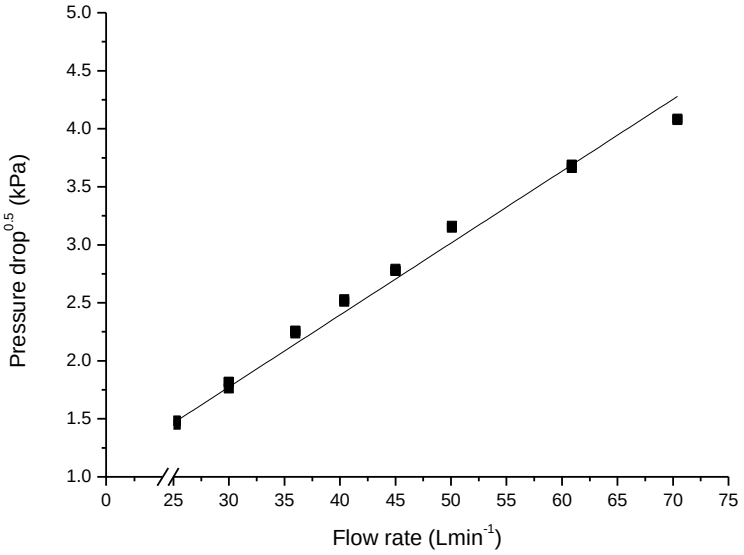

Figure 2.7. Linear relationship between pressure drop and flow rate across the Cheng 1 and Cyclohaler® in series (pooled raw data of n=3, at each data point. R^2 = 0.9891).

2.4.5. Impaction studies

2.4.5.1. Aerodynamic deposition assessment using next generation impactor for Cyclohaler®

The emission of SS from the Ventolin/Accuhaler™ formulation using a Cyclohaler® was assessed between 30-100 $Lmin^{-1}$ with the highest flow rate

corresponding to 4 kPa. The % drug recovery was adequate at all the flow rates ranging from 79.44 ± 2.90 % to 81.45 ± 3.14 %, according to the British Pharmacopoeia [147]. The drug retention in the Cyclohaler® did not change when the flow rate was increased (25.98 ± 8.07 % and 28.69 ± 10.69 % of recovered dose at 30 and 75 $Lmin^{-1}$ respectively, p value > 0.05, One way ANOVA). However, at 4 KPa, fewer drug particles were captured in the device (14.95 ± 3.00 %, p value < 0.05, One way ANOVA, Figure 2.8).

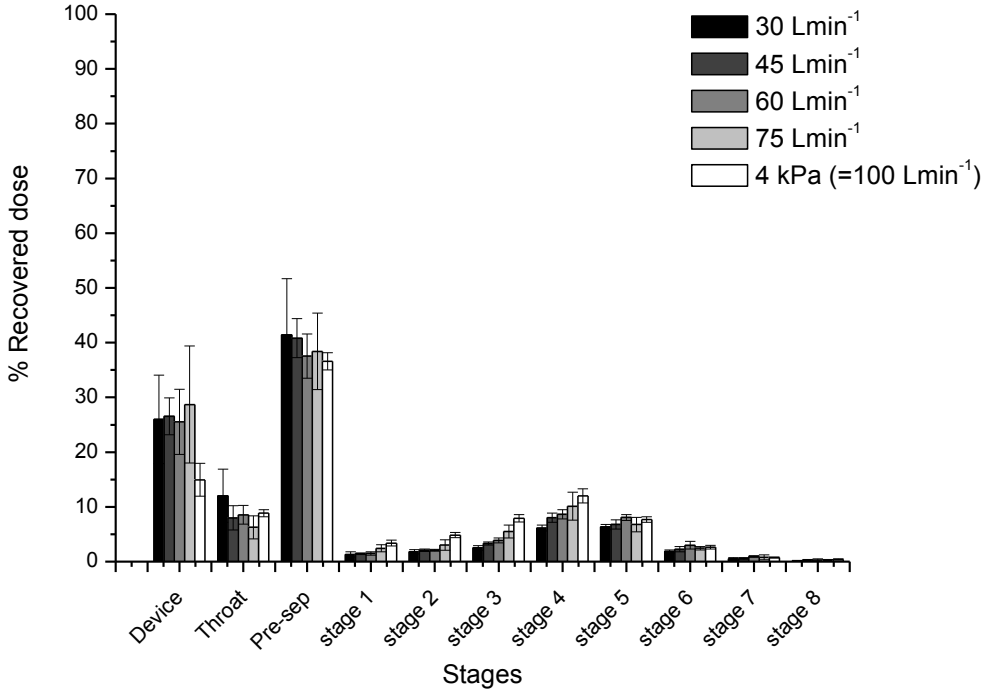

Figure 2.8. Recovered dose of salbutamol sulphate emitted from the Cyclohaler® at 30 $Lmin^{-1}$ (black bar), 45 $Lmin^{-1}$ (dark grey bar), 60 $Lmin^{-1}$ (grey bar), 75 $Lmin^{-1}$ (light grey bar) and 100 $Lmin^{-1}$ (white bar) (mean ± SD, n=4).

When the Cyclohaler® was assessed alone, increasing the flow rates led to a decrease in the throat deposition (ANOVA, p< 0.05, Table 2.8). The same trend was seen in the mass median aerodynamic diameter (MMAD), that was almost halved at 4 kPa compared to 30 Lmin-1. This led to a two-fold increase of the fine particle fraction (FPF) below 5 µm (i.e. the respirable fraction the patient would inhale) at the highest flow rate (p value< 0.05, Table 2.8). The FPF5µm from the Cyclohaler® increased from 20.83 ± 3.00% to 40.82 ± 2.53% when the flow rates were increased (ANOVA, p value < 0.05). The same trend was seen also for the fine particle dose (FPD) per actuation. An almost 100% increase in the FPD was seen at 100 L min-1 (e.g. 54.47 ± 5.02 µg/act) compared to 27.21 ± 4.33 µg/act at 30 L min-1 (Table 2.8).

Table 2.8. Aerosolisation metrics for salbutamol sulphate from a carrier based blend using the Cyclohaler® between 30 and 100 L min^{-1} (mean ± SD, n ≥ 4) (IP/PS – induction port/pre-separator deposition, MMAD - mass median aerodynamic diameter, $FPF_{5\mu m}$ (ED) - fine particle fraction < 5 µm of the emitted dose, FPD - fine particle dose).

Device	Flow rate ($Lmin^{-1}$)	IP/PS deposition (% ED)	MMAD (µm)	% $FPF_{5\mu m}$ (ED)	FPD (µg/act)
Cyclohaler®	30	70.22 ± 3.23	3.07 ± 0.26	20.83 ± 3.00	27.21 ± 4.33
	45	66.34 ± 3.38	2.49 ± 0.22	27.86 ± 3.50	32.67 ± 2.37
	60	61.74 ± 3.02	1.98 ± 0.09	33.84 ± 2.90	39.55 ± 3.58
	75	75.51 ± 16.70	2.07 ± 0.22	35.76 ± 1.51	38.76 ± 7.87
	100 (=4kPa)	52.75 ± 1.98	1.90 ± 0.06	40.82 ± 2.53	54.47 ± 5.02

2.4.5.2. Aerodynamic deposition assessment using the next generation impactor for Cheng 1

Impaction studies were performed using the Cheng 1 in series with the Cyclohaler® at the same conditions as when the Cyclohaler® was employed alone. However, when the Cheng 1 was added 75 $Lmin^{-1}$ and 4 kPa (corresponding to 100 $Lmin^{-1}$) were not achievable due to the high resistance of the spacer. Altering the flow rate did not significantly alter the % deposited within the Cyclohaler® device (18.02 ± 4.50 % to 21.51 ± 3.70 % at 30 and 60 $Lmin^{-1}$, respectively p value > 0.05, one way ANOVA) when the Cheng 1 was employed. The deposition within the Cheng 1 was high, although it did decrease with increasing flow rate (from 81.68 ± 6.88 % to 55.90 ± 10.64 %, at 30 and 60 Lmin-1, p value < 0.05, Figure 2.9).

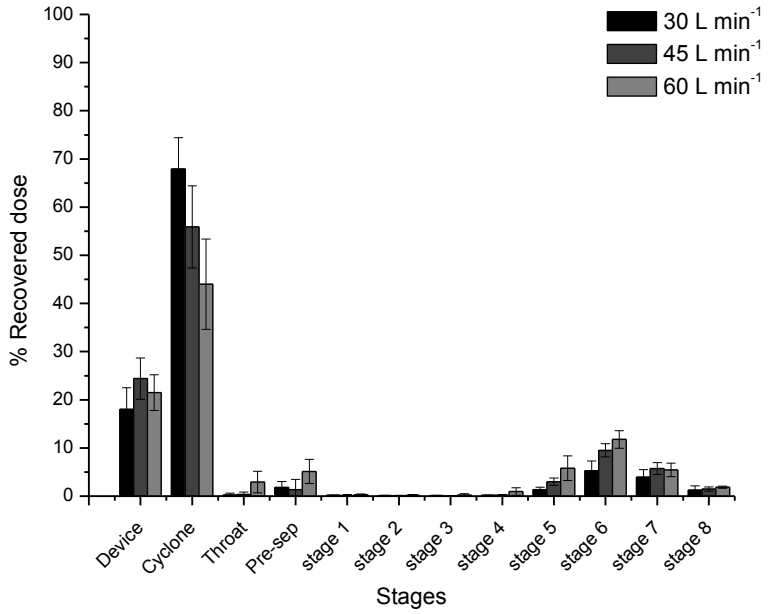

Figure 2.9. Recovered dose of salbutamol sulphate emitted from the Cyclohaler® in combination with the Cheng 1 at 30 $Lmin^{-1}$ (black bar), 45 $Lmin^{-1}$ (dark grey bar) and 60 $Lmin^{-1}$ (mean ± SD, n=4).

When the Cheng 1 was employed a dramatically decreased induction port/pre-separator (IP/PS) deposition was seen ($p<0.05$, Table 2.9) compared to when the Cyclohaler® was assessed alone. The extent of IP/PS deposition was unaffected by the change in the flow rate ($p > 0.05$) due (in part) to the variability between replicate analyses. When the Cheng 1 was added in series with the Cyclohaler®, the results indicate that the presence of the cyclone did not change the FPD of the emitted dose at 45 and 60 $Lmin^{-1}$ (Table 2.9).

Table 2.9. Aerosolisation metrics for salbutamol sulphate from a carrier based blend using the Cyclohaler® in presence of the Cheng 1 at 30, 45 and 60 L min^{-1} (mean ± SD, n ≥ 4) (IP/PS – induction port/pre-separator deposition, MMAD - mass median aerodynamic diameter, $FPF_{5\mu m}$ (ED) - fine particle fraction < 5 µm of the emitted dose, FPD - fine particle dose).

Device	Flow rate (L min^{-1})	MMAD(µm)	IP/PS deposition (% ED)		% $FPF_{5\mu m}$(ED)		FPD (µg/act)
			Expressed as % of dose emitted from DPI (%ED)	Expressed as % of dose emitted from Cheng I (%sED)	Expressed as % of dose emitted from DPI (%ED)	Expressed as % of dose emitted from Cheng I (%sED)	Expressed as dose emitted from DPI
Cyclohaler® + Cheng 1	30	0.90 ± 0.06	2.45 ± 1.18	14.82 ± 7.80	14.48 ± 5.84	82.75 ± 7.34	18.41 ± 6.63
	45	0.76 ± 0.04	2.32 ± 2.77	6.95 ± 7.91	26.44 ± 4.34	92.24 ± 7.74	29.51 ± 3.45
	60	0.76 ± 0.14	9.56 ± 6.50	22.27 ± 9.96	33.42 ± 5.86	77.0 ± 10.07	39.44 ± 7.67

The $FPF_{5\mu m}$ of SS was expressed as the percentage of the emitted dose (ED) of the drug when escaping either the Cyclohaler® (%ED) or the cyclone spacer (%sED). No statistical difference was observed in the $FPF_{5\mu m}$ (% ED, Table 2.9) between 45 and 60 $Lmin^{-1}$ (26.44 ± 4.34% and 33.42 ± 5.86 %, respectively) and when the Cyclohaler® was used alone at the same flow rate (Table 2.8). At low flow rate, however, both FPD and $FPF_{5\mu m}$ (%ED) of SS emitted decreased compared to the Cyclohaler® when used alone: FPD of 27.21 ± 4.33 μg/dose for SS when emitted for Cyclohaler® and FPD of 18.41 ± 6.63 μg/dose when Cheng 1 was in place ($p<0.05$). When the $FPF_{5\mu m}$ (%sED) was considered, an improved specificity of the particle delivery was seen compared to the emitted dose from the Cyclohaler® (Table 2.9, $p < 0.05$). The $FPF_{5\mu m}$ (%sED) did not change significantly upon increasing the flow rate ($p>0.05$). However, a high variability was seen in the $FPF_{5\mu m}$ at the highest flow rate (77.0 ± 10.07%). However, the metric FPD should be considered for comapring the dose as it would be respirable for the patient. When the Cheng 1 was employed the FPD increased with the flow rates with a similar trend of the FPD calculated to when the Cyclohaler® was employed alone. Almost double the amount of FPD was seen at 60 L min^{-1} compared to 30 L min^{-1} (39.44 ± 7.67 μg/act vs.18.41 ± 6.63 μg/act, respectively, Table 2.9). The median aerodynamic diameter (MMAD) values (Table 2.9) were ~3 times smaller with the Cheng 1 in place than for the Cyclohaler® alone (ANOVA, post-hoc Tukey's test, $p < 0.05$). The MMADs were, however, unchanged upon altering the flow rate with the cyclone in place (ANOVA, $p > 0.05$).

2.4.6. Aerosolization studies using laser diffraction analysis

2.4.6.1. Aerosolization studies for Cyclohaler®

The aerosol size distribution was tested using laser diffraction analysis. When the Cyclohaler® was tested alone, consistency was seen between flow rates (Figure 2.10). However, 100 L min^{-1} could not be tested due to the low power of the pump. The carrier-based formulation showed the presence of large agglomerates escaping with fine particles from the DPI (e.g. the volume median diameter (Dv50) was between 40.04 ± 4.03 μm and 50.12 ± 6.97 μm at 30 and 75 L min^{-1}, respectively).

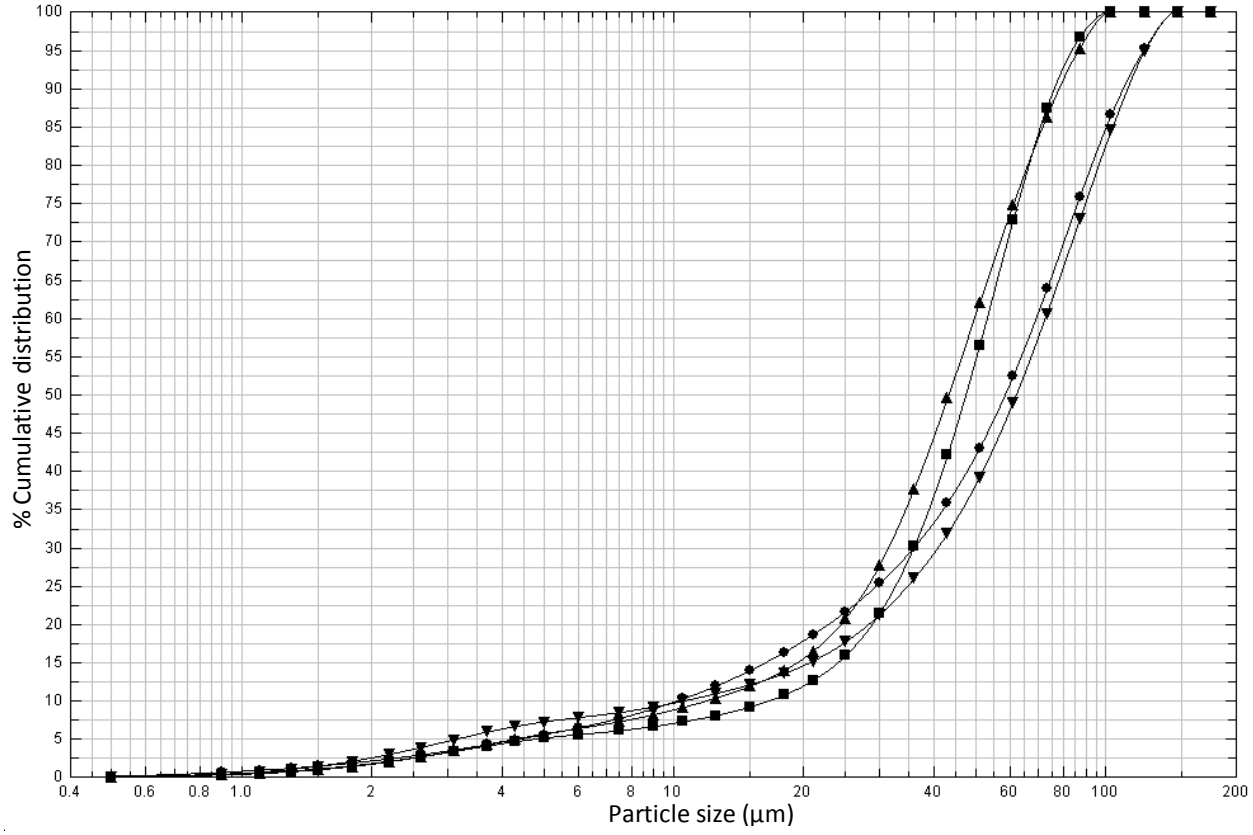

Figure 2.10. Representative particle size distributions of salbutamol sulphate from the Cyclohaler® at 30 $Lmin^{-1}$ (●), 45 $Lmin^{-1}$ (▲).60 $Lmin^{-1}$ (■) and 75 $Lmin^{-1}$ (▼).

2.4.6.2. Aerosolization studies using laser diffraction technique for Cheng 1

In order to understand the lower $FPF_{5\mu m}$ and FPD and the variability in IP/PS deposition with the cyclone at 60 $Lmin^{-1}$, laser diffraction analysis (LDA) on the emitted aerosol cloud was performed for the Cheng 1. LDA also displayed the potential of the cyclone to retain both large agglomerates of micronized drug and the carrier particles. The volume median diameter (Dv50) of the aerosol cloud released from the cyclone at 30 $Lmin^{-1}$ was 1.03 ± 0.01 µm which was of the same order of magnitude as the MMAD and substantially lower than when the cyclone was absent (40.04 ± 4.03 µm). The same trend was seen at 45 and 60 $Lmin^{-1}$ when the Dv50 was 1.18 ± 0.03 µm and 0.96 µm respectively. Only one value is reported for the highest flow rate because of the variability from actuation to actuation. In fact, variability was observed in the particle size distributions of the aerosol emitted from the cyclone (an example of two size distribution measurements at 60 $Lmin^{-1}$ are presented in Figure 2.11).

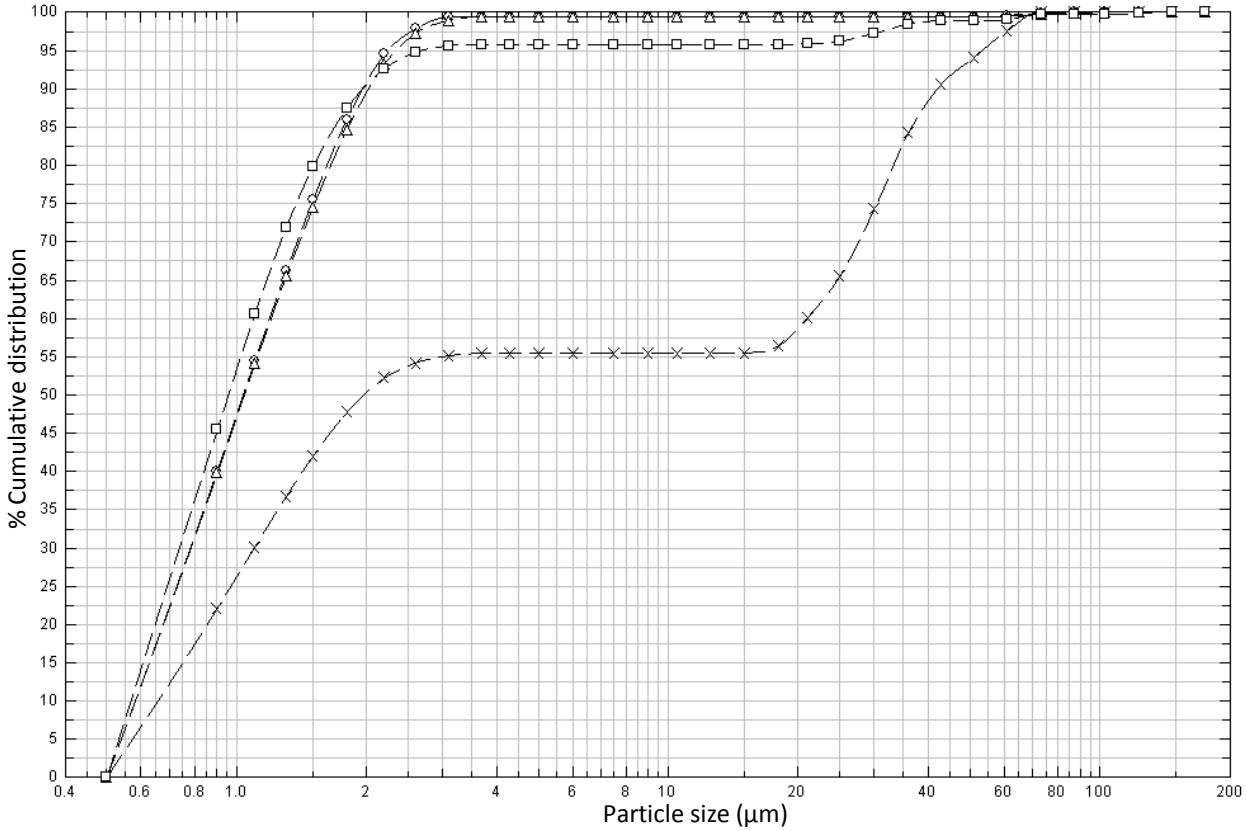

Figure 2.11. Representative particle size distributions of salbutamol sulphate from Cheng 1 at 30 $Lmin^{-1}$ (○), 45 $Lmin^{-1}$ (Δ) and 60 $Lmin^{-1}$ (□). At 60 $Lmin^{-1}$ some agglomerates have been detected emitted from the Cheng 1 (x) causing a bi-modal distribution.

The bi-modal PSD indicated that some fine material is emitted at 60 $Lmin^{-1}$ as well as at the other flow rates. However, at the highest flow rate, a plateau size is reached suggesting for particle size of 3 µm (e.g. no particles are delivered between 3 and 20 µm). Additionally, at 30 µm, some agglomerates and/or carrier particles escaped the cyclone which would have resulted in IP/PS deposition (observed in Figure 2.9). However, the latter observations of agglomerate emission displayed variability from actuation to actuation.

2.4.6.3. Aerosolization studies using laser diffraction technique for Pulmicort/Turbuhaler® with Cheng 1

The Pulmicort/Turbuhaler® device, which does not contain lactose monohydrate as a carrier in the formulation, was tested with and without Cheng 1. In Figure 2.12 the cumulative distribution of budesonide (Bud) particles emitted from

the Turbuhaler® shows that the formulation is composed of micronized particles without the presence of the carrier (e.g. Dv50 = 5.84 ± 0.31 at 2 kPa). Therefore, when the DPI was tested in presence of the spacer, it was difficult to obtain particle size distributions consistent with the Cyclohaler®, especially at 4 kPa where only one measurement was obtained (Dv50 = 0.97 μm) suggesting that the Cheng 1 worked only with carrier based formulations. Insufficient optical concentration of particles was achieved, which indicated poor emission of drug from the Turbuhaler into the Cyclone, or excessive drug retention by the Cyclone.

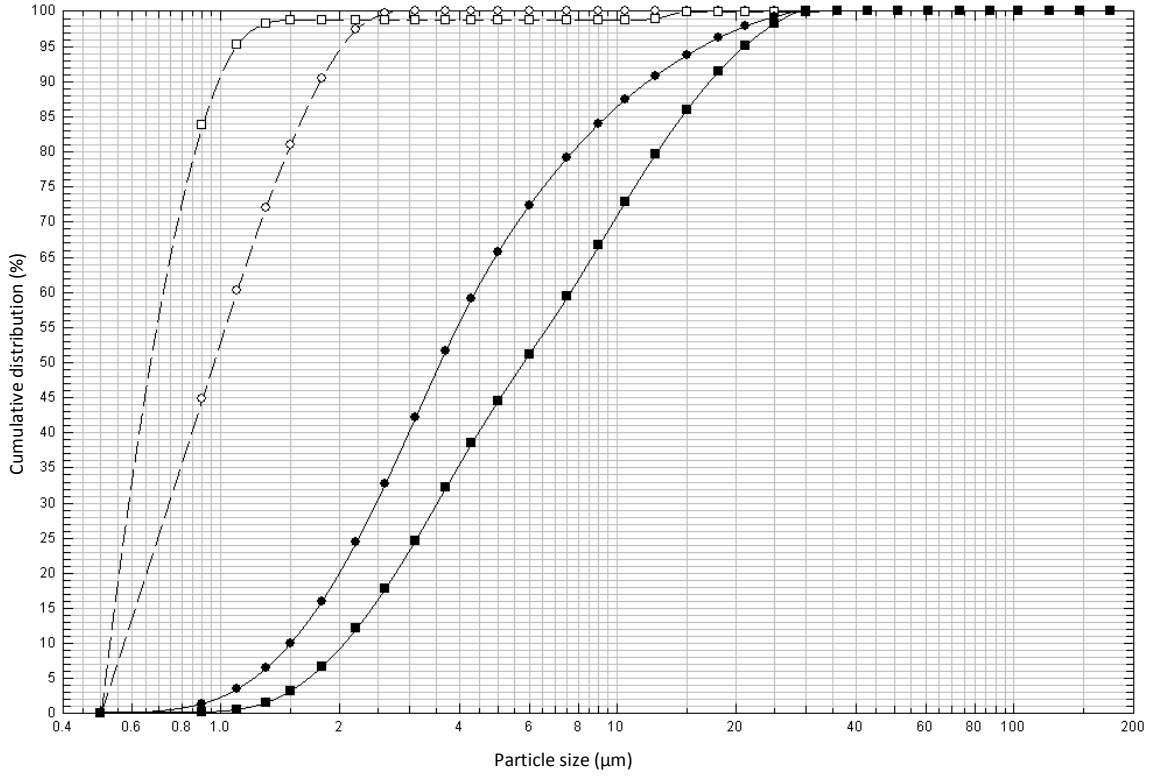

Figure 2.12. Representative particle size distributions of Bud from the Pulmicort/Turbuhaler® at 2 (■) and 4 kPa (●) and from the Cheng 1 at 2 (□) and at 4 kPa (○) (mean ± SD, n≥2).

2.4.7. Monodisperse aerosol study using the Cheng 1

The Cheng 1 showed 100% efficiency in collecting the monodisperse aerosol particles of fluorescein (particle sizes of 2 and 3 μm) between 30-60 L min^{-1}. The cyclone retained between 14.45 ± 4.32 μg and 17.12 ± 7.12 μg at 30 and 60 L min^{-1} respectively with orifice diameter of 20 μm and particle size of 3 μm. However, when the particle size was 2 μm (with orifice diameter of 20 μm), the cyclone retained 0.59 ± 0.41 μg and 1.68 ± 0.62 μg at 30 and 60 L min^{-1}, respectively. The concentration of fluorescein aerosol was too low in the conical flask to be detected by

spectrofluorimetric assay. This was probably due to the very low cut off diameter of the spacer and the unavailability of a lower diameter orifice for monodisperse aerosol testing of the Cyclone.

2.5. Discussion

Whilst DPIs have been accepted to treat asthma and COPD, the lung deposition and throat impaction is still very variable and dependent on the patient inhalation strength [152, 154]. Many studies have been conducted to improve the device design for a better pulmonary delivery [79, 93]. However, the variability of the patient's inhalation flow still affects the amount of emitted fine particles and their size. Therefore, the aim of the current work was to manufacture and characterise a cyclone spacer with reverse flow cyclone technology for use with DPIs.

The main outcome was to assess the ability of a cyclone spacer (Cheng 1) to decrease throat deposition using a wide range of flow rates (30-60 L min^{-1}). The Cyclohaler® was used as a trial DPI to emit the SS formulation recovered from the Venolin/Accuhaler™. A HPLC assay was validated for detection of SS, which is a hydrophilic weak base and β_2 agonist and therefore, used as a bronchodilator for treatment of asthma and COPD. SS has two pK_a values from the amino group and from the phenol group (9.3 and 10.3, respectively). Therefore, the ionization of SS varies with the pH. The mobile phase used was an 80:20 (v/v) mixture of 0.6% (w/v) aqueous ammonium acetate: methanol and the pH was adjusted to 4.5 with HCl 1M to ionize the drug completely. The stationary phase was a C18 column with particle size of 3 µm to increase the surface area and therefore to improve interaction with the stationary phase. The HPLC method in this study was validated with regards to the linearity, LOD, LOQ, accuracy and precision. The calibration curves generated for quantification of SS showed a good linearity (R^2=0.999) and high sensitivity at low concentrations. The reproducibility of the SS assay was acceptable. The accuracy studies performed on drug alone and with lactose confirmed that the carrier did not interfere with the detection of the drug (% accuracy between 99.14 ± 2.33 and 99.89 ± 2.44 %, respectively). Therefore, the blend mixture of SS and lactose collected from a marketed product Accuhaler™ could be used for cascade impactor analysis

for studying the variance in deposition and FPF of emitted particles with Cheng 1 in place. SS was studied as a pilot drug for this current project for a better comparison with a previous study that used a reverse cyclone technology DPI to deliver the same drug (i.e. the Conix™[162]).

The Cyclohaler® was chosen for this project as it is a single-unit dose inhaler that consists in a capsule to be pierced prior the dose delivery and replaced after each actuation. Upon inhalation, collisions between drug, the grid and the capsule occur and, due to increasing air velocity, turbulence increases [163, 164]. Together with the type of formulation, the design of the DPI affects the deagglomeration of the blend. The main features of the Cyclohaler® are air inlet size, the presence of the capsule and the grid [95, 164-166]. The latter has been the subject of many studies to improve the Cyclohaler® design (or Aerolizer®, which has a very similar shape to the Cyclohaler®) as it does affect the deagglomeration of the particles from the carrier.

When breathing through the Cyclohaler®, cyclonic turbulent flow predominates, leading to collision between particle-particle and particle-device wall. This would enhance deagglomeration of the emitted dose and, therefore, the FPF [95, 163]. However, the presence of the grid straightens the flow and helps the particle-mouthpiece or particle-particle interactions. Some studies indicated that the dispersion of the aerosol cloud inside the inhaler is also due to the movement of the capsule leading to a greater number of particle-wall collisions than otherwise would not be detected if the capsule was absent [153]. Increasing the flow, the turbulence and the dispersion of agglomerates increase, leading, however, to increased retention inside the device [167]. This would lead to a dependency on the delivered dose with such inhaler. The design of the DPI improves the deagglomeration of the emitted particles upon increasing the flow rate [166]. However, changing the design of the DPI will change the resistance to the airflow and the device resistance is the key element of evaluating how comfortable and easy it is for a patient to breathe through his/her inhaler [81, 125]. The resistance of the Cyclohaler is 0.02 $kPa^{0.5}L^{-1}min$ [168]. In vitro studies have investigated how the emitted dose and particle size change with increases of the flow rate to confirm the findings of in vivo studies.

In the current study, the Cyclohaler® was tested alone using the impaction technique at different flow rates (30 - 100 $Lmin^{-1}$). The flow rates tested were chosen based on flow rates achievable by patients through the device to aerosolize the drug particles [153]. It is reported that the aerosolization of the particles depends either on the design of the DPI or mainly on the inhalation strength of the patients [85, 153]. Also, the variability in patients' inhalation profiles [77, 85, 169] lead to high variability in fine particle liberation from DPI formulations and devices [12, 125].A good % drug recovery from Cyclohaler® was seen between 30 - 100 $Lmin^{-1}$. The % emission did not change when the flow rate increased for the Cyclohaler®, when used alone (74.02 ± 8.08% at 30 $Lmin^{-1}$, 73.45 ± 3.36 at 45 $Lmin^{-1}$, 74.44 ± 5.95 at 60 $Lmin^{-1}$). This is in accordance with a study from Srichana *et al*. [153] where the drug deposition of SS (400 µg) was studied from different devices at 30, 60 and 90 $Lmin^{-1}$ in the twin-stage impinge (TSI). Also Taki et al. [170] showed a good delivered dose (>82.5% from the Aerolizer® for FP and SX at 60 $Lmin^{-1}$ with the NGI). The deposition of a combined formulation of the two drugs was studied. Although using a different active pharmaceutical ingredient (API)-lactose blend, the % of deposition of the drug on the throat and pre-separator (IP/PS deposition) agrees with the current study, i.e. ~60%.

Srichana et al [153] showed an increased FPF with the flow rate for a wide range of DPIs. The Cyclohaler® showed an increased FPF of approximately 10 % from 30 to 90 L min^{-1}. A previous study [163] showed that increasing the airflow in the Aerolizer®, the turbulence inside the DPI increased significantly as well as the number and intensity of particle-device collisions. This did increase the overall potential of deagglomeration of the mannitol powder used. Increases were seen especially between 30 and 75 L min^{-1}, although after this flow rate, increasing the flow rate was not significant. This is in accordance (except at 100 $Lmin^{-1}$) with the results of the current project where the FPF of the emitted SS from the Cyclohaler® were not significantly different between 60 and 75 L min^{-1} (p value>0.05,

Table 2.8). It was previously suggested [163] that the flow rate where any change in the dispersion system is not significant is 65 L min^{-1}. Our study is in accordance as no difference was seen in both the FPF or in the recovered dose in device and throat between 60 and 75 L min^{-1}. However, a much reduced amount of particles retention in the device was seen at 100 L min^{-1} (Figure 2.8), whereas, Coates et al [163] showed no difference above 60 L min^{-1}, although they used micronized mannitol. They also showed a great reduction in recovered dose in the device between 30 and 60 L min^{-1} (50% to 5.1%, respectively) which is not shown in the current project. This is presumably due to the different powder used in the two studies. Increasing the air flow leads also to a reduced MMAD [149]. In the current study at the highest flow rates the MMAD of SS was halved when the Cyclohaler® was employed alone (Table 2.8).

Previous studies showed that the cyclone technology helped to retain large agglomerates and enhance the liberation of fine particles from DPIs. The Conix™ DPI, developed by Cambridge Consultants Ltd. [156] and licensed by 3M Drug Delivery Systems (3M Ltd.), was demonstrated to deliver an higher % of fine particles of SS and a better fine particle distribution than the Accuhaler™ [162]. At 4 kPa using the ACI the % of delivered dose of the SS from the Conix™ was 25 % in stage 4 and 5. The Accuhaler™ showed only 10 and 5 % of delivered dose on stage 4 and 5, respectively. Also, the MMAD of SS emitted from the Conix™ was halved (0.97 µm) compared to the MMAD from the Accuhaler™ (1.99µm). Additionally, the % FPF of the emitted dose was double that from the Accuhaler™ (~ 90 and ~ 40 %, respectively) [91]. Another DPI with a cyclone separator system, the AirMax™ showed a significant improvement of FPF of budesonide or salbutamol compared to the Turbuhaler® and more consistent dose delivered regardless the flow rates used [93]. Although cyclone technology inhalers showed efficiency in delivering a higher respirable fraction compared to more common DPIs, they do only provide the delivery of a specific formulation-device product [91-93, 146]. The idea of spacer for DPIs (as seen already for MDIs [171]) has been suggested and investigated. A spacer decreases aerosol velocity and particle size in order to prevent the oropharyngeal deposition of the biggest particles and to ensure smaller particles

reach the patient's airways [172]. The fine particle mass should be unchanged when a spacer is employed, and extra-thoracic deposition should be reduced [172]. The combination of spacer and DPI was previously suggested to reduce potential oropharyngeal deposition [173, 174]. However the authors failed to perform a full particle side distribution study. Thus, it is crucial to understand the impact of cyclone spacers on drug release and potential lung delivery.

Based on the cyclone separation technology applied to DPI development, CFD studies have been conducted towards miniaturization of reverse airflow cyclone-spacer prototypes (e.g. Cheng 1) [159] to classify particles based on size and enhance powder de-agglomeration at different flow rates. CFD revealed near-wall velocity and integral scale strain rates with enhanced aerodynamic separation and impaction forces. Therefore, the Cheng 1 (intended as a spacer for DPIs) was manufactured and assessed with the Cyclohaler®. The cyclone-spacer functions using reverse airflow cyclone technology theory. A vortex occurs when the airflow is drawn through the outlet and the centrifugal forces within the conical section (Figure 2.1) help the removal of fine particles from the coarse carrier that is retained within the conical section. The SS formulation was delivered using the Cyclohaler® instead of placing the powder in the conical section of the spacer because there was the need to create an aerosol cloud prior to entering the conical section of the cyclone spacer [95, 175]. CFD studies [159], also, suggested that impaction on the cyclone wall due to centrifugal forces occurs when vacuum is applied to the outlet of the cyclone and therefore, the velocity of the emitted particles from the Cyclohaler® would increase the particle-particle and particle-walls collisions inside the Cheng 1. Finally, due to the design of the Cheng 1, placing the powder inside the spacer was not trivial, and counter-productive to the concept of a generic spacer.

Initial experiments in the current study focussed on assessing the resistance of the cyclone spacer. The aim was to achieve 75 $Lmin^{-1}$ and 100 $Lmin^{-1}$ (= 4 kPa) through the spacer as already achieved for the Cyclohaler® alone. However, the resistance of the Cheng 1 was excessive (0.0805 $kPa^{1/2}$ /L min^{-1}) and therefore, the latter flow rates could not be reached. However, the study was carried out at three significant flow rates (30, 45 and 60 $Lmin^{-1}$) to investigate the flow rate dependence

of the emitted dose of a lactose/SS mixture using Cyclohaler® in series with the Cheng 1 spacer. Although the % recovery of the SS was within pharmacopoeial limits when the Cheng 1 was used, a high retention of the dose was seen within the spacer (e.g. 81.68 ± 6.88 % at 30 $Lmin^{-1}$). This is a common feature widely seen when spacers are employed with MDIs [143, 176]. Positively, spacer retention typically reduces the oropharyngeal deposition observed when the spacer is not employed. In the current study a much-reduced IP/PS deposition of SS was detected when the Cheng 1 was employed regardless of the flow rate (Table 2.9). Approximately a 3-fold decrease in the induction port/pre-separator deposition was seen with the Cheng 1 in place at 60 L min^{-1}, compared to the Cyclohaler® alone. This occurred principally because the cone section of the cyclone collected the non-inhalable fraction; i.e. d_{ae}> 10 µm [43]. The same trend was seen in a previous study [173] where terbutaline sulphate was emitted from the Turbuhaler® at 70 L min^{-1} with an add-on spacer chamber. The authors showed high retention in the spacer as well (approximately 25 % of the recovered dose of the drug). A filter collected 55.5 ± 3.3% of the emitted particles as being respirable and the remaining 20 % deposited in the throat [173]. Drug delivery efficiency was improved to 47% compared to 38.0 ± 2.4% delivery when the spacer was not used. Ehtezazi *et al* [174] confirmed that retention in the spacer reduced oropharyngeal deposition. When SS was emitted from the Clickhaler® with a long add-on spacer, 40.18 ± 6.94 % deposited in the oropharyngeal model compared to 70.86 ± 14.87 % without the spacer. The same trend has long been confirmed for MDIs with spacer chambers, showing that approximately 75 % of salbutamol emitted from the Ventolin™ with add-on spacer was collected inside the spacer [176]. In the current study, significant difference ($p < 0.05$) was observed in the IP/PS deposition when the flow rate was increased for the Cyclohaler® (70.22 ± 3.23 % - 75.51 ± 16.70% between 30 and 75 $Lmin^{-1}$, respectively). However, employing the cyclone significantly decreased the drug deposition in the throat and pre-separator due to both high retention in the cyclone and the liberation of only the finest particles that were likely to deposit in stages with a cut-off < 5 µm (i.e. the respirable fraction) [40, 44, 45].

High retention in the spacer indicates that in the presence of the cyclone increased less throat deposition may occur (Table 2.9). However, the respirable

dose expressed as FPD was unchanged when the spacer was used, except at low flow rate (i.e. 30 $Lmin^{-1}$, $p<0.05$). This suggests that at low flow rate, lower deaggregation forces occur inside the spacer and a lower respirable dose is emitted compared to when the DPI is used alone. This might lead to the high retention seen in the spacer [173] and potentially to an additional inhalation to be required for each actuation to achieve a consistent FPD between DPI alone and the DPI with the cyclone (i.e. uninhaled drug remains in the cyclone and may be inhaled more than once). The same trend of consistent FPF (%ED) was seen when Cyclohaler and spacer were compared (except for 30 $Lmin^{-1}$: 20.83 ± 3.00 % (30 $Lmin^{-1}$), 27.86 ± 3.50 % (45 $Lmin^{-1}$) or 33.84 ± 2.90 % (60 $Lmin^{-1}$) of the ED from the Cyclohaler® was potentially respirable vs. 14.48 ± 5.84 % (30 $Lmin^{-1}$), 26.44 ± 4.34 % (45 $Lmin^{-1}$) or 33.42 ± 5.86 % (60 $Lmin^{-1}$) when the Cheng 1 was in place. In this study a great increase in the % $FPF_{5\mu m}$ (%sED) has been shown with the Cheng 1 in place. The corresponding $FPF_{5\mu m}$ from the spacer (%sED) were between 82.75 ± 7.34 % and 77.00 ± 10.07 % at 30 and 60 $Lmin^{-1}$, respectively. However, it has to be kept in mind that $FPF_{5\mu m}$ (%sED) was calculated without considering the high retention of the particles in the conical section of the spacer. This great amount of powder that is not considered in the calculation would effectively increases the numerical value of the $FPF_{5\mu m}$ (%sED). It was promising to observe that the $FPF_{5\mu m}$ of the emitted particle from the Cheng 1 (%sED, and %ED Table 2.9) and the FPD was unaffected by the alteration of the flow rate at 45 and 60 $Lmin^{-1}$ with the cyclone in place because similar findings have not been revealed in previous studies using DPI spacers [173, 174, 177]. The only authors to suggested similar finding were Zeng *et al* [93] where they showed that the delivered dose of salbutamol emitted from the Airmax™ was within 85-115 % of the label claim at flow rates between 30-90 L min^{-1}. However, both FPD and $FPF_{5\mu m}$ of the emitted particle at the lowest flow rate from the Cyclohaler® with the Cheng 1 in place were affected by increasing the flow rate (Table 2.9). At 30 L min^{-1} both parameters were half those at 60 L min^{-1}. At lower flow rate the velocity of particle is diminished and therefore, more retention in the spacer was seen. This arises from the lower turbulence collision forces in the inner walls of the spacer than when the flow rate is 60 $Lmin^{-1}$. The force was not enough to lift the particles towards the outlet or to separate the micronized drug from the carrier, which is heavier and, therefore, deposits at the bottom of the conical section. Large particles (e.g. lactose carrier) have higher collision forces than micronized

particles. Hence the conical section of the Cheng 1 enhances deagglomeration of the former. Moreover, smaller particles, although emitted from the inhaler, would not impact on the cyclone wall with the same energy as the big agglomerates as their inertia is lower.

In addition the MMAD values (Table 2.9) with Cheng 1 in place were ~3 times smaller than for the Cyclohaler® itself (Table 2.8, ANOVA, post-hoc Tukey's test, $p < 0.05$) and this can potentially improve the specificity of lung deposition. Moreover, as the Cheng 1 is a classifier chamber that classifies the particle based on the size, the MMAD was unaltered upon increasing the flow rate (p value > 0.05). In fact, SS was emitted from the circular outlet of Cheng 1 that helped the consistency in the particle size. Thus the cyclone served to reduce potential oropharyngeal deposition (i.e. IP/ PS deposition) whilst limiting particle output to the respirable range, owing to the aerodynamic fractionation of the cyclone. This represents a major advantage compared to the use of the DPIs alone, where changes in MMAD are commonly observed due to differences in inspiratory parameters between patients [12, 81].

The cut off diameter of the spacer depends not only on the geometry and design of the outlet, but also on the air velocity pulled through it. Vortex instability occurring in the Cheng 1 might explain the variability in both IP/PS deposition and FPF at the highest flow rates (Table 2.9). Vortex instability was previously detected by CFD [159] and confirmed by LDA in the current work (Figure 2.11). The Cheng 1 showed a much reduced Dv50 (volume median diameter of 50 % of the particles population) when used compared to the Cyclohaler® by itself (1.03 ± 0.01 and 40.04 ± 4.03 µm, respectively at 30 $Lmin^{-1}$). However, at 60 L min^{-1}, a bi-model particle size distribution was observed confirming the escape of agglomerates or carrier lactose from the spacer, showing only 50 % of the volume distribution being below 3 µm. The prototype cyclone has shown the potential to be used as a classifier and spacer for DPI. However, when the Pulmicort/Turbuhaler™ was assessed, the LDA displayed micronized particles emitted from the device and the Cheng 1 decreased the Dv50 only at low pressure (2 kPa), failing to have reproducible data at the highest (4 kPa) (Figure 2.12). This confirms the theory that the cyclone spacer

worked only with carrier based DPI. A carrier-free formulation would be composed of only micronized material. The cyclone spacer appeared to classify the particles based on the size with retention of coarse carrier. If the formulation studied with the Cheng 1 was carrier-free, micronized particles would aerolize with a cohesive behavior, and due to their low momentum, they would not collide into the spacer's walls as seen for large particles. The cyclone technology operates with the presence of a coarse carrier for liberation of micronized drug. However, the LDA should not be used to evaluate the PSD alone [178]. The difference between laser diffraction and impaction techniques is that LDA provides information of the geometric particle size, whereas impaction gives information on the aerodynamic particle size and, therefore, a prediction of how particles will deposit in the lungs based on their aerodynamic size.

2.6. Conclusion

This study has shown the potential of a prototype cyclone spacer to be used with the Cyclohaler® to decrease predicted oropharyngeal deposition and to increase the respirable particle fraction of SS/carrier formulation. There was a high retention of non-respirable drug within the Cheng 1, a feature common to spacers. The MMAD of the emitted aerosol was shown to be determined by the low cut-off diameter (<5 µm) of the cyclone itself that also increased the respirable fraction (e.g. $FPF_{5\mu m}$). The Cheng 1, however, showed a high resistance leading to the inability to achieve flow rates above 60 L min^{-1}. Nevertheless, the mitigation of the flow rate dependence of the emitted dose and MMAD was a promising finding. However, the resistance of the spacer was too high and remanufacture will be necessary. Suggestions have been proposed to change the orifice diameter and shape from a cylindrical to a more oval shape to decrease the resistance. Moreover, increasing the cut off diameter from 2 to 5 µm would improve the liberation of fine particles and probably a more consistent delivery of the dose. Further study is required to focus on such a more suitable cyclone spacer prototype (Cheng 2) with a higher cut off and lower resistance than Cheng 1.

Chapter 3: Optimization of a reverse airflow cyclone-spacer for pulmonary delivery

3.1 Optimization of a reverse airflow cyclone-spacer for pulmonary delivery

3.1.1. The high variability of oropharyngeal and lung deposition from dry powder inhalers

Lung deposition from DPIs can be calculated from two variables: variability of the delivered dose and variability in the throat deposition. Higher throat deposition leads to lower lung deposition [179]. Many studies have focused on both oropharyngeal and lung deposition of the delivered dose emitted from DPIs either in vitro or in vivo. Many have suggested that on increasing the flow rates the particle size decreases leading to an increase peripheral lung deposition as smaller particles would be able to reach the small airways. Many others have also suggested there is a high variability between patients and devices used as represented in Table 3.1.

Table 3.1. Table of variability in oropharyngeal and lung deposition from dry powder inhalers at different flow rates. The sign "-"indicates not data were available for the specific parameter.

Authors	Inhalers	Flow rates ($Lmin^{-1}$)	Oropharyngeal Deposition (%)	Lung deposition (%)
Thorsson et al[180]	Diskus	-	-	13%
	Turbuhaler	-	-	36%
Newman et al[181]	Turbuhaler	60	21.4 %	54.8 - 80.0%
	ASTA Medica	45-90	19.9-32.1%	12.1-37.4%
Borgstrom et al[78]	Turbuhaler	35	66.6%	14%
Newman et al[79]	Genuair® DPI	80	61.9 %	34.0%
Newman et al[155]	MAGhaler	30-60	78.7%-72.5%	26.4%
	Novolizer	-	-	35.7%
	Pulvinal	-	-	14.8%
	Spinhaler	-	-	18.5%
Gibbons et al[182]	Handihaler	-	68%	18%
	Respira DPI	-	-	46%

3.1.2. In vitro simulation with mouth-throat models

Although in vivo study of throat and lung deposition of radiolabelled APIs could give a true estimate of the delivery performance of an inhaler, it requires ethical approval and it is time consuming. Therefore, many studies have focused on reproducing mouth-throat models to mimic oropharyngeal deposition of aerosols [183-186]. However it must be kept in mind that a human throat cast may show a

higher collection of the emitted particles compared to the standard throat used in impaction studies [187].

Zhou *et al* [185] and Zhang *et al* [186] showed that in vitro deposition with an idealized throat manufactured using computed tomography (CT) scanning of a human throat had a good correlation with in vivo deposition data. Using an idealized throat, the mouth-throat deposition of aerosol emitted from the Turbuhaler® was 67.8 ± 2.2 %, which showed a good correlation with in vivo values of 65.8 ± 10.1% [185]. Other studies have tested the mouth-throat cast at different flow rates (e.g. 15-90 $Lmin^{-1}$) with different nozzle exit diameters to represent marketed DPI [188, 189], suggesting that deposition in the mouth-throat cast of a monodisperse aerosol (e.g. 5 µm) emitted at low flow rates (e.g. 32 $Lmin^{-1}$) varied from 1.45% to 94.1 % when decreasing the diameter of the orifice inlet [188]. However, the deposition of the smallest particle (2 µm diameter) was unaffected by changes in mouthpiece diameter at all inspiratory flow rates [189]. This may be because 2 µm particles have lower inertia. Slower air velocity could result in a reduction in particle inertial values, decreasing the possibility of impaction of particles in the posterior oropharynx where the air stream changes its direction suddenly. Therefore, throat deposition would be high depending on the device design and on the flow rate used.

3.1.3. Improvement of in vitro drug delivery: the concept of a spacer for dry powder inhalers

Many studies have reported the in vitro variability on the particle size, fine particle fraction and fine particle dose with increasing the flow rates [149, 153-155]. Also, high throat deposition occurs in patients. Spacers for DPIs have been proposed in the last 20 years to decrease throat deposition of the emitted particles, as used for MDIs already [173, 174]. An example is shown in Figure 3.1.

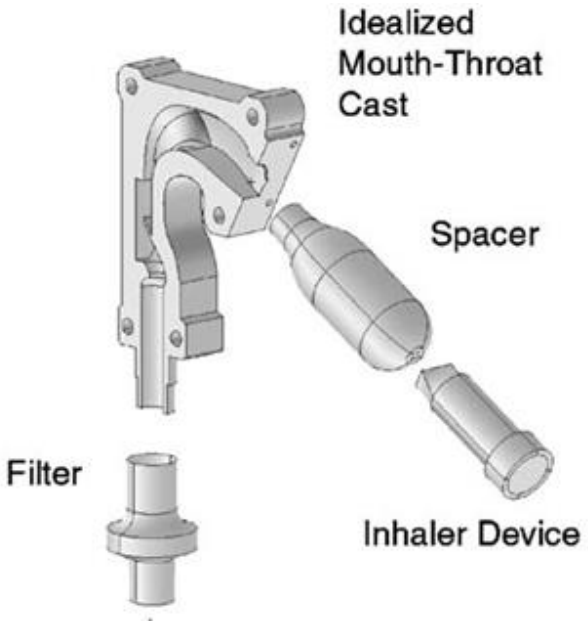

Figure 3.1. Diagram of a spacer used with inhaler devices for in vitro aerosolisation studies [174].

Although the reduction of the throat deposition was a promising finding, Matida et al. and Ehtezazi *et al*. [173, 174] did not perform a full particle size distribution with the spacers, which inhibits the potential to predict the aerosol deposition, which can be achieved with cascade impaction. They also showed that the spacers remained susceptible to the inter-patient flow rate-derived variability in fine particle characteristics (e.g. particle size and fine particle dose) from the DPI itself. However, Everard *et al* [177], showed an unchanged respirable fraction with an aerodynamic size below 6.8 μm emitted from the Turbuhaler with a spacer-chamber at 60 $Lmin^{-1}$, suggesting the spacer would not affect the lung deposition. Therefore, there is still potential for a spacer for dry powder inhalers although some consideration needs to be made regarding their design constraints.

3.1.4. Considerations regarding spacers with DPIs

The concept of the spacer is successful for MDIs because, broadly, the type of the formulation (except for the APIs) and design of the MDI device is identical between inhalers. Therefore, the aim of the spacer was mainly to reduce the throat deposition of the emitted aerosol [80, 190]. When a spacer is suggested for DPIs, two main things need to be taken into consideration: the design of the DPIs and the type of formulation. The design of the DPI affects the powder deagglomeration (together with the patient's inhalation strength) and the size of the internal diameter

of the device mouthpiece might affect the turbulence to air flow through each device [84]. This is important as turbulent flow would increase the deagglomeration of the emitted dose [95]. Additionally, Al-Sowair et al. [81] showed that the higher is the internal resistance of a DPI, the lower is the flow rate generated for a given pressure drop. This means that a patient would breathe fast across a low resistance device such as the Aerolizer, but for longer when a higher resistance device is used. Therefore, introducing a spacer to an already high resistance inhaler can increase the resistance of the DPI and the adherence of the patients to the therapy as they struggle to breathe through a high resistance device. As DPIs have a wide range of resistances to the air, manufacturing a generic spacer might be difficult to account for all the design of the inhalers.

3.1.5. Overview on commercial DPIs

It has been previously mentioned, many DPIs are available in the market [66]. The DPIs that will be studied in this chapter are Accuhaler™, Easyhaler™ and Cyclohaler® due to their different design and different formulations. Accuhaler™ is a multidose inhaler, Easyhaler™ is a reservoir inhaler and Cyclohaler® is a single dose inhaler. The different design would lead to different plume geometry between inhalers. If a spacer is used, this might affect the outcome of the emitted particles. For example, when using an Aerolizer (similar design to a Cyclohaler®), upon inhalation the velocity of the particles increases and more collision occurs between the drug and the grid which creates more energetic turbulence [95]. Thereby enhancing the FPF [95]. Turbulence is the major controlling factor on particle deagglomeration, and studies showed that inside the Aerolizer, turbulent flow (cyclonic flow) is predominant but approaches a maximum at 65 L min^{-1} [95]. By comparison, the Accuhaler device presents a cross-shape grid compared to the Cyclohaler®. This would affect the FPF, reducing the powder-grid impactions, and therefore the deagglomeration potential with increasing grid voidage [95]. This leads to an increased impaction in the mouthpiece and induction port stage for the Accuhaler™ [95, 166]. Another device that shows turbulent flow is the Easyhaler™. As a result, the FPF and the lung deposition ratio of drug particles are enhanced [86]. Both Easyhaler™ and Accuhaler™ show consistency in the delivered dose observed between the different flow rates [89, 152] However, dissimilarity was

observed with the Turbuhaler, which is subject to inconsistency in the delivered dose depending on the inhalation flow [191].

3.1.6. Cyclone technology applied for different formulations

Harrison *et al* [146] and Needham *et al* [91] studied SX/FP formulation and SS formulation emitted from the Conix™, respectively, as well as from the Accuhaler. Nine asthmatics were involved in the study comparing Accuhaler and the Conix [146]. They were prescribed with 100 µg/dose of FP and 50 µg/dose and SX, emitted from the Accuhaler and Conix. The study showed that FP was absorbed faster when emitted from the Conix in the first 2.5 h. In vitro studies showed that the Conix delivered a larger fraction of small particles than the Accuhaler for FP, with a lower MMAD [146]. This would explain a faster absorption in vivo because greater amount of small particles would reach the peripheral airways and pass through to the blood vessels. The same trend was seen for SX with a prolonged absorption from the Accuhaler (Diskus).

The formulations of SS and SX/FP emitted from the Conix showed a different IP/PS deposition although the cyclone technology was applied to both inhalers. Interestingly the combination of two drugs showed a higher IP/PS deposition (e.g. SX deposition was 76 % of the delivered dose) [146] than when only a single API was emitted from the Conix (e.g. SS deposition was 13% of the delivered dose) [91]. This may have been due to cohesive behaviour of SX when blended with coarse carrier that leads to less efficient deagglomeration processes than SS during emission from the device [98, 113].

Although in Chapter 2 neither cyclone-spacer retention nor IP/PS deposition was affected by the flow rate, the only API tested was SS/lactose. The Conix study, therefore, suggests that drug formulation/product type needs to be taken in consideration when applying new technology to DPIs, as they might not lead to an unaltered delivery of the dose. Therefore the aim of this chapter was to test the potential of a cyclone-spacer as a generic platform for a range of marketed DPI, with different device design and formulations.

3.2 Aim

A high resistance prototype spacer decreased the throat deposition of emitted aerosol particles and had potential to mitigate the flow rate dependency of the delivered dose and particle size of a carrier-based formulation. Moreover, it was able to capture the large particle size carriers (e.g. coarse lactose) emitted from the Cyclohaler®. The aim of the current chapter was to assess the potential of a low resistance cyclone-spacer to improve in vitro delivery of a range of commercial carrier based DPIs.

The objectives of the current work were:

- To manufacture a lower resistance cyclone-spacer than the Cheng 1 (i.e. Cheng 2)
- To test the resistance of the Cheng 2 in series with Cyclohaler®, Easyhaler and Accuhaler
- To assess Cheng 2 with carrier-based marketed inhalers to represent products regarded as a cohesive blend, an adhesive blend and a combination bronchodilator and corticosteroid formulation

3.3 Materials and methods

3.3.1 Materials

Micronized fluticasone propionate (FP) was purchased from Sicor de Mexico (Toluca, Mexico) and micronized budesonide (Bud, batch number U0015/1V040) was supplied from LGM Pharma (Boca Raton, USA). Salmeterol xinafoate (SX) was purchased from Vamsi Labs Ltd (Solapur, India). The DPIs tested were an Easyhaler/Budesonide™ 400µg/dose and Easyhaler /SS™ 200 µg/dose (purchased from Orion Pharma, Newbury, UK), a Seretide/Accuhaler™ 50 µg/500 µg/dose and Ventolin/Accuhaler™ 200 µg/dose (purchased from Allen & Hanburys, Uxbridge, Middlesex, UK). A Cyclohaler® device (obtained from AAH Hospital Supplies, Coventry, UK). Size 4 hard gelatine capsules were obtained from Meadow Laboratories Ltd. (Romford, UK). The cyclone spacer was manufactured in-house (University of Cambridge, UK) from a Perspex blocks (Engineering & Design Plastics Ltd, Cambridge, UK); the exit duct was cut and polished from stock brass tubing (Engineering Department Storeroom, University of Cambridge, UK) The flow meter

(model number DFM2), next generation impactor (NGI) and a model HCP5 vacuum pump were all purchased from Copley Scientific Ltd (Nottingham, UK).

3.3.2 Cyclone manufacture

A miniature reverse-flow cyclone (Cheng 2) was optimised from previous studies using empirical models [157] to have a theoretical particle cut-off diameter below 5 µm for flow rates between 30 and 120 $Lmin^{-1}$. The Cheng 2 was machined from Perspex with an oblong inlet orifice of 10.1 x 6 mm to facilitate relatively high inlet velocities with acceptable pressure drops. For dimensional accuracy, easy sample collection and interchangability, the Cheng 2 was manufactured in three separate sections as per Cheng 1 (Figure 3.2).

	Cheng 2
D	21
D_e	5.9
a^1	10.1
b^1	6
H	56.4
H	23.5
S	23.5
B	7.1

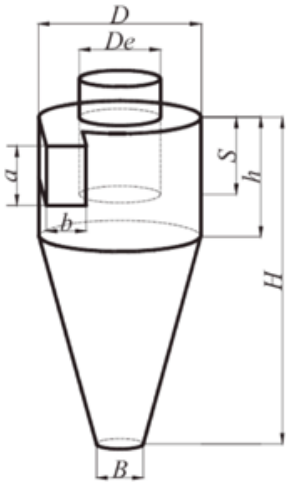

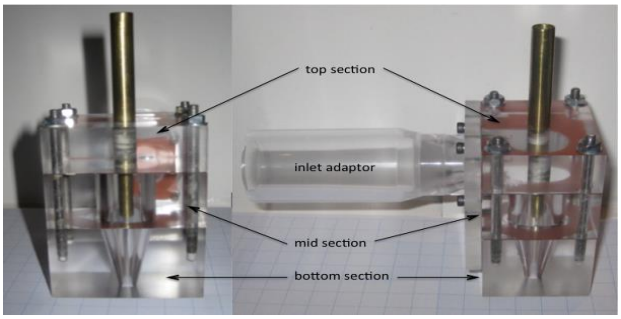

Figure 3.2. Dimensions of simulated cyclone geometries (units in mm)

3.3.3 High performance liquid chromatographic assay validation of active pharmaceutical ingredients

Three micronized active pharmaceutical ingredients (APIs) were tested using high performance liquid chromatographic (HPLC) assay: salmeterol xinafoate (SX), budesonide (Bud), fluticasone propionate (FP). A stock solution of each API was prepared by weighing accurately approximately 0.0025 g of the drug with an analytical balance (Mettler Toledo, UK), transferring it into a 50 ml volumetric flask and bringing the solution to volume with the appropriate mobile phase (Table 3.3). The stock solution was used in order to prepare a calibration series by pipetting the volumes shown in Table 3.3 and the set of calibration standards were run using HPLC (Agilent 1050 Series, Agilent Technologies UK Ltd., Edinburgh, UK) with a Luna 3 µm C18 column (150 mm x 4.6 mm x 3 µm) at 1 ml min^{-1} (the high performance liquid chromatographic conditions are reported in Table 3.3).

Table 3.2. Volume of stock solution (ml) required to prepare a calibration series in the concentration range of 0.05-50 µg ml^{-1}.

Theoretical concentration (µgml^{-1})	Volume of stock solution (ml)	Final volume (ml)
25	10	20
10	5	25
5	1	10
2	1	25
1	1	50
0.5	1 (from 1 µgml^{-1})	10

Table 3.3. High performance liquid chromatographic (HPLC) conditions for salmeterol xinafoate (SX), fluticasone propionate (FP), and budesonide (Bud).

Active pharmaceutical ingredients	Mobile phase	Column temperature (°C)	Injection volume (µl)	Detector Wavelength (nm)	Calibration range
SX	75:25 (v/v) mixture of methanol: 0.6% (w/v) aqueous ammonium acetate.	40	50	228	0.5-50 $\mu g ml^{-1}$
FP	75:25 (v/v) mixture of methanol: 0.6% (w/v) aqueous ammonium acetate	40	50	240	0.5-50 $\mu g ml^{-1}$
Bud	75:25 (v/v) mixture of methanol: 0.6% (w/v) aqueous ammonium acetate.	40	50	240	0.5-50 $\mu g ml^{-1}$

3.3.4 Data analysis of high performance liquid chromatography assays

3.3.4.1 Linearity assay precision and reproducibility

The linear regression analysis was performed according to Chapter 2, Section 2.3.4.1.

3.3.4.2 Limits of detection (LOD) and limits of quantification (LOQ)

The LOD and LOQ were calculated according to Chapter 2, Section 2.3.4.2

3.3.4.3 Accuracy determination

Two sets of five standard solutions were prepared; the first set were prepared with 0.002 g of the API dissolved into 20 ml of mobile phase and making a 1:10 dilution in order to obtain 10 µg/ml solution. The second set was prepared with 0.002 g of the API (FP, BUD or SX) and 0.048 g of lactose monohydrate dissolved into 50 ml of mobile phase and 1:4 dilutions were performed to obtain the same concentration to above. The peak area response of the standards when analyzed by HPLC according to the assay in Section 3.3.3 (Table 3.3) was determined. The amount of the API recovered was calculated using the calibration curve and the percentage recovery of the drug was calculated using the equation (3.1).

$$\% \text{ recovery} = \frac{calculated\ concentration\ (\mu g ml^{-1})}{theoretical\ concentration\ (\mu g ml^{-1})} \quad (3.1)$$

3.3.5 Dose content assay of emitted dose

The dose uniformity sampling apparatus (DUSA, Copley Scientific Ltd., Nottingham, UK) with a glass microfiber filter (Whatman, GE Healthcare Ltd., Buckinghamshire, UK) was used for the dose content determination (n=5). The pressure drop was set (2 and 4 kPa to represent values achievable by patients across the DPIs in series with the spacer Cheng 2). Then, the respective flow rate at the cyclone entrance was measured with a flow meter (Copley Scientific Ltd., Nottingham, UK). In Table 3.4 the flow rates at the spacer inlet corresponding to 2 and 4 kPa are reported for all the

DPIs tested. The drugs were collected from the DUSA and the filter with the appropriate mobile phase (Section 3.3.3). The concentrations were determined by HPLC assay (Section 3.3.3).

Table 3.4. Pressure drops and measured flow rates at the spacer inlet for dry powder inhalers tested at 2 and 4 kPa with the Cheng 2 (SS= salbutamol sulphate, SX= salmeterol xinafoate, FP = fluticasone propionate, Bud = budesonide). Pressure drop the flow rates generates through the DPI alone

Dry powder inhalers	Drug	Pressure drop (kPa)	Flow rates (L min^{-1})
Seretide/Accuhaler™	SX, FP	2	34
		4	50
Cyclohaler®	SS	2	37
		4	51
Easyhaler™	BUD	2	31
		4	43

3.3.6 Resistance of Cheng 2

The resistance of Cheng 2 was measured across the spacer and Cyclohaler®, Accuhaler™ and Easyhaler™, in series using a dose uniformity sampling apparatus (DUSA, Copley Scientific Ltd., Nottingham, UK). The DUSA was connected to a critical flow controller TPK (Copley Scientific Ltd., Nottingham, UK) to adjust the flow rate. Once the flow rate was set through the DUSA, the Cheng 2 with the inhaler was attached to the DUSA to record the pressure drop of the respective series device-spacer combinations. The range of flow rates tested was between 15-60 L min^{-1}. The pressure drops obtained were then plotted against the corresponding flow rates and the resistance calculated by interpolation.

3.3.7 Impaction studies using next generation impactor

Each DPI was tested at 2 and 4 kPa with and without Cheng 2 according to Sections 3.3.5. Prior to performing the measurements with the NGI, the desired flow rate was adjusted with a flow meter. Prior to measurement, 15 ml of mobile phase was added in the central cup of the pre-separator. When the Cyclohaler® was assessed alone, six Size 4 hard gelatine capsules were used. When the Cheng 2 was employed as spacer device, 12 capsules were actuated at 2 kPa and eight capsules at 4 kPa. When the Accuhaler™ and Easyhaler™ were used alone, six

actuations were counted at both pressure drops. When the cyclone was employed, 12 actuations were counted at 2 kPa and eight at 4 kPa for both the devices. In order to recover the drugs, the DPIs were washed with 20 ml of mobile phase. The bottom of the cyclone, the mouthpiece and the USP throat were each washed with 50 ml of mobile phase; whilst the upper section of the cyclone was washed with 10 ml. For collecting the drugs from the pre-separator 100 ml of mobile phase was used. The volumetric flasks were sonicated (Kerry, Germany) for 2 min. When only the DPIs were employed, 10 ml of mobile phase was added to the first 5 stages, whilst 5 ml of solvent was used for the last 3 stages. All the stages were set on a laboratory rocker (Stirling Mixer, Sandrest Ltd, UK) and rocked for 2 min in order to allow the solvent to clean the entire surface. When the cyclone was used, 5 ml of mobile phase was added to all the stages. The concentrations of the drugs from each stage were determined by HPLC assay as described in Section 3.3.3. After performing the experiments, each stage and the NGI were thoroughly cleaned with Millipore water and the silicone coating was removed with acetone before rinsing with methanol.

3.3.8 Aerosolization studies using laser diffraction technique

Aerosolization was assessed by laser diffraction particle size analysis using the Sympatec Inhaler module (Inhaler Helos/KF, Sympatec Limited, Bury, UK) at 2 and 4 kPa for all the DPIs with and without Cheng 2. The lens used to detect the aerosol cloud was an R3 lens (0.5-175 µm). The measurement was set to trigger when the optical concentration was between 1.0 and 1.1 % for 5 sec duration (time base 1 ms) to avoid reading of dust particles. The formulation was then recovered from each DPI and particle size tested with the Sympatec Rodos module to determine the DV50 for carrier particle size and the % of population with size < 5 µm. The trigger conditions were identical to when the inhaler module was used.

3.3.9 Statistical analysis

Statistical analysis was performed in Minitab (version 15) using one-way ANOVA and post-hoc Tukey's test (multiple comparisons) or Student's two-tailed t-test for pair-wise comparisons, both at 95 % confidence intervals. Data analysis was performed according to Chapter 2, Section 2.3.11.

3.4 Results

3.4.1 Resistance of the Cheng 2

The DPIs and the cyclone-spacer Cheng 2 on their own posed a wide range of resistances (slope of the curves in Figure 3.3). The Cheng 2 alone had 0.037 $kPa^{1/2}$ /L min^{-1} resistance, the Accuhaler had 0.032 $kPa^{1/2}$ /L min^{-1}, the Easyhaler, 0.054 $kPa^{1/2}$ /L min^{-1}, and the Cyclohaler 0.024 $kPa^{1/2}$ /L min^{-1}.

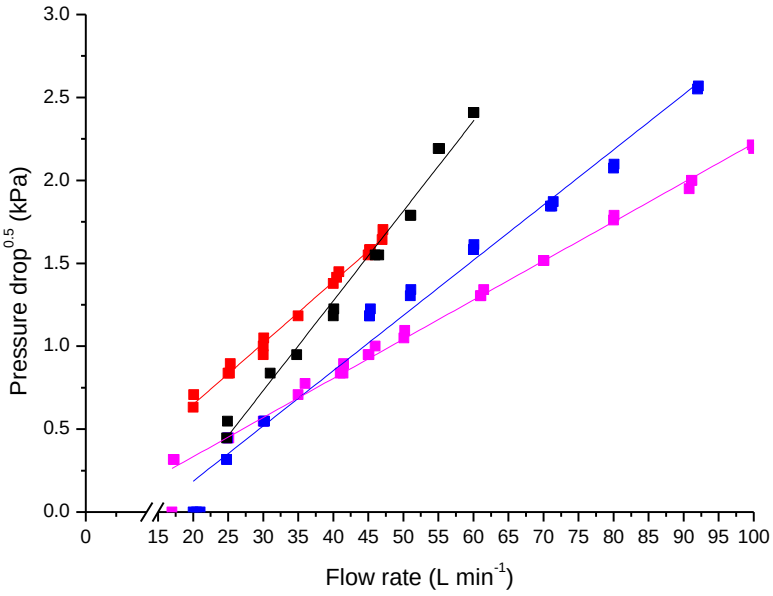

Figure 3.3. Linear relationship between pressure drop and flow rate across the inhalers alone (Easyhaler- black, Accuhaler – blue and Cyclohaler-pink) and Cheng 2 alone (red line).

However, when the resistance of Cheng 2 was tested together with the inhalers, it offered a more usable resistance (0.04 $kPa^{1/2}$ /L min^{-1}) than Cheng 1 resistance (0.08 $kPa^{1/2}$ /L min^{-1}) as showed from the slope of the curve in Figure 3.4, and was additionally consistant between devices.

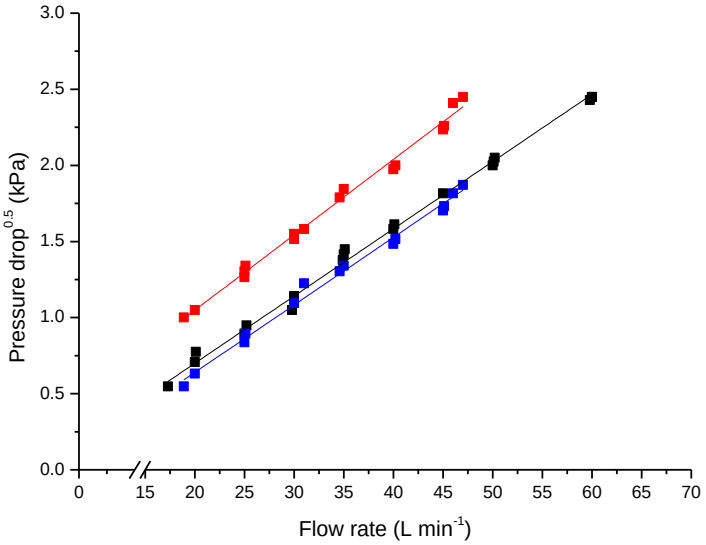

Figure 3.4. Linear relationship between pressure drop and flow rate across the Cheng 2 and Cyclohaler® as a whole device (black line), Cheng 2 and Accuhaler (blue line) and Cheng 2 and Easyhaler (red line).

3.4.2 Data analysis of high performance liquid chromatography assays

3.4.2.1 Assay Linearity precision and reproducibility

Linear regression analysis performed for peak area response as a function of drug concentration for three calibration series is reported in Figure 3.5 for all APIs used.

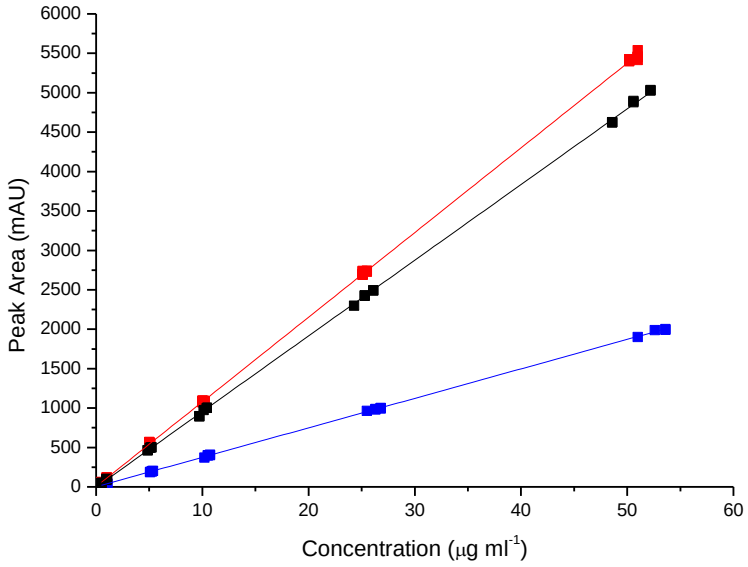

Figure 3.5. Linear regression analysis for budesonide (black), fluticasone propionate (red), and salmeterol xinafoate (blue) as a function of concentration (pooled raw data points of n=9, for each concentration level).

In Table 3.5 pooled linearity data of regression results are reported.

Table 3.5. Regression results for peak area response plotted as a function of concentration for fluticasone propionate (FP), budesonide (Bud), and salmeterol xinafoate (SX).

Day	Drug	Intercept	Standard deviation of the intercept	Slope	Standard deviation of the slope	Correlation coefficient (R^2)
1		5.982	2.537	108.514	0.206	0.999
2	FP	-1.124	1.929	107.743	0.083	0.999
3		0.346	4.210	107.122	0.177	0.999
Pooled		4.013	2.280	107.440	0.109	0.999
1		-7.832	3.857	95.175	0.170	0.999
2	Bud	-0.016	2.451	96.394	0.104	0.999
3		-5.403	2.891	96.310	0.119	0.999
Pooled		-4.816	3.209	96.000	0.137	0.999
1		-2.890	2.648	37.414	0.102	0.999
2	SX	0.829	1.566	37.696	0.064	0.999
3		3.151	1.034	37.138	0.041	0.999
Pooled		1.350	1.361	37.388	0.056	0.999

Intra-day variability indicated good repeatability for all the APIs within the calibration range 0.5-50 μg/ml (Table 3.6).

Table 3.6. Intra-day variability for peak area response plotted as a function of concentration for fluticasone propionate (FP), budesonide (Bud), and salmeterol xinafoate (SX).

		%RSD					
		Concentrations (μg ml^{-1})					
		50	25	10	5	1	0.5
SX	Day 1	0.01	0.03	0.11	0.14	1.49	0.63
	Day 2	0.05	0.38	0.64	0.19	0.57	2.25
	Day 3	0.26	0.24	1.10	0.10	0.41	5.37
FP	Day 1	N/A	0.32	0.69	0.95	3.04	4.26
	Day 2	0.21	0.16	0.59	0.33	1.08	3.09
	Day 3	0.81	0.18	0.30	0.48	1.85	4.08
BUD	Day 1	0.03	0.01	0.19	0.11	0.28	0.68
	Day 2	0.22	0.14	0.01	0.05	0.06	0.20
	Day 3	0.07	0.09	0.02	0.08	0.06	0.24

Inter-day variability (Table 3.7) showed that at the lowest concentration for all the drugs the reproducibility of the methods were low.

Table 3.7. Table of data from inter-day variability (reproducibility of the relative standard deviation, RSD) for fluticasone propionate (FP), budesonide (Bud), and salmeterol xinafoate (SX) assays (n=3).

	%RSD					
	Concentration (μg ml^{-1})					
	50	25	10	5	1	0.5
SX	0.75	0.68	2.24	1.21	3.28	9.29
FP	0.65	0.74	0.87	1.95	2.69	6.14
BUD	0.68	0.63	2.13	1.10	2.46	3.02

3.4.2.2 Limits of detection (LOD) and limits of quantification (LOQ)

The sensitivity of the method used for the FP was indicated by an LOD that was 0.06 μg ml^{-1} and LOQ that was 0.21 μg ml^{-1}. As the values are relatively low, the method was suitably sensitive at low concentrations. The same was indicated for Bud (LOD = 0.10 μg ml^{-1} and LOQ = 0.33 μg ml^{-1}), and for SX (LOD =0.11 μg ml^{-1} and LOQ =0.36 μg ml^{-1}).

3.4.2.3 Accuracy determination

The recoveries of FP alone and when lactose was added were 99.64 ± 2.57 % and 98.65 ± 1.86 % respectively showing a high accuracy as the range was between 95 and 105 %. A two-tailed unpaired t-test revealed no significant difference when lactose was added (p value < 0.05) as the carrier does not interfere with the detection of the drug. The same performance resulted for Bud, and SX. The % recoveries of the drugs were between 100.48 ± 2.19 % for Bud, and 100.30 ± 5.26 for SX.

3.4.3 Dose content assay of the emitted dose

The dose contents of the DPIs are reported in Table 3.8. The label claims were: Easyhaler/Budesonide™ 400μg/dose, Easyhaler/SS™ 200μg/dose, Seretide/Accuhaler™ 50 μg/500 μg/dose, Ventolin/Accuhaler™ 200 μg/dose.

Table 3.8. Emitted dose content of dry powder inhalers tested at flow rates corresponding to 2 and 4 kPa when the inhalers where tested with the Cheng 2 in series (SS = salbutamol sulphate, SX = salmeterol xinafoate, FP = fluticasone propionate, Bud = budesonide) (mean ± SD, n=5).

Dry powder inhalers	Drug	Flow rate ($Lmin^{-1}$)	Dose content (µg/dose)
Ventolin/Accuhaler™	SS	34	192.59 ± 8.53
		50	186.57 ±6.24
Seretide/Accuhaler™	SX	34	70.37 ± 18.99
		50	60.08 ± 9.71
	FP	34	491.75 ± 127.29
		50	350.64 ± 24.59
Easyhaler™	Bud	32	238.15 ± 15.16
		44	276.98 ±24.89
Easyhaler™	SS	32	191.92 ± 6.98
		44	199.59 ± 6.82

The dose emitted of SS for Ventolin/Accuhaler is in accordance with values reported in Chapter 2. Regarding Seretide/Accuhaler, the label claim is 50 µg of salmeterol base which is equivalent to 72.5 µg salmeterol xinafoate. FP however showed a much lower emitted dose compared to the label claim at the highest flow rate. The Accuhaler showed variable dose content values at different flow rates. Therefore, the flow did affect the emitted dose from the device when the spacer was used.

3.4.4 Impaction studies using next generation impactor

The DPIs were tested at the flow rates corresponding to at 2 and 4 kPa in the presence and absence of the spacer (Table 3.4). The Easyhaler/SS™ did not emit enough drug to be recovered from the impactor body of the NGI when the Cheng 2 was in place at both pressure drops. On the other hand, the Ventolin/Accuhaler™ emitted enough drug into the NGI body only at 4 kPa with the Cheng 2 for recovery above 75% as per the Pharmacopoeial limits [147]. At the lowest pressure drop SS did not leave the inhaler suggesting the Cheng 2 created lower collision forces between particle-spacer walls than Cheng 1. For all the other inhalers (i.e. Seretide/Accuhaler™, Cyclohaler® and Easyhaler/Bud™) the percentage recovery for all the APIs with and without the Cheng 2 was within pharmacopoeial limits (Table 3.9). The Cheng 2 showed high retention of non-respirable drug as observed for Cheng 1 (Chapter 2, Section 2.4.5.2) although no change was detected when the flow rate increased ($p > 0.05$,Table 3.9).

Table 3.9. Dose recovery (%), emission (% of RD) from the device (or Device - Cheng 2), retention within the Cheng 2 (%RD) and % induction port/pre-separator (%ED, IP/PS) deposition for salbutamol sulphate (SS), budesonide (Bud), salmeterol xinafoate (SX) and fluticasone propionate (FP) emitted from the Cyclohaler®, Easyhaler™ and Accuhaler™, with and without Cheng 2, respectively at 2 and 4 kPa (mean ±SD>4).

Device	Pressure drop(kPa)	Drug	% RD	% Emission Ex device (% RD)	% Retention in the cyclone (% ED)	IP/PS deposition (% ED)	IP/PS deposition (% sED)
Cyclohaler®	2	SS	85.68 ± 1.20	81.45 ± 3.14	N/A	67.28 ± 2.09	N/A
Cheng 2-Cyclohaler®			82.29 ± 3.98	11.61 ± 3.03	87.61 ± 2.96	N/A	15.87 ± 6.76
Easyhaler™		BUD	97.07 ± 3.78	97.62 ± 0.56	N/A	62.01 ± 2.52	N/A
Cheng 2-Easyhaler™			105.48 ± 3.69	24.51 ± 1.68	75.23 ± 1.70	N/A	15.65 ± 1.39
Accuhaler™		SX	88.94 ± 9.10	98.65 ± 0.27	N/A	78.27 ± 0.54	N/A
Cheng 2-Accuhaler™			89.56 ± 10.58	19.33 ± 0.46	80.48 ± 0.56	N/A	38.70 ± 4.56
Accuhaler™		FP	90.99 ± 7.92	98.84 ± 0.49	N/A	78.21 ± 1.87	N/A
Cheng 2-Accuhaler™			82.39 ± 4.43	18.13 ± 1.09	82.01 ± 1.18	N/A	35.03 ± 1.45
Cyclohaler®	4	SS	82.14 ± 2.19	78.59 ± 1.69	N/A	64.44 ± 2.49	N/A
Cheng 2-Cyclohaler®			79.66 ± 4.43	11.36 ± 0.93	85.69 ± 1.11	N/A	18.44 ± 2.79
Easyhaler™		BUD	104.61 ± 5.70	97.91 ± 0.56	N/A	63.18 ± 3.72	N/A
Cheng 2-Easyhaler™			104.50 ± 4.66	24.28 ± 2.41	75.12 ± 2.94	N/A	15.19 ± 1.74
Accuhaler™		SX	97.73 ± 2.96	99.05 ± 0.15	N/A	76.93 ± 2.39	N/A
Cheng 2-Accuhaler™			101.25 ± 13.56	16.16 ± 2.99	83.05 ± 3.67	N/A	36.01 ± 9.77
Accuhaler™		FP	115.61 ± 7.16	99.27 ± 0.19	N/A	75.53 ± 3.50	N/A
Cheng 2-Accuhaler™			102.68 ± 12.07	13.85 ± 2.01	85.70 ± 2.28	N/A	29.63 ± 5.85

The high retention in the spacer decreased the deposition of the particles in the induction port/pre-separator stages (Table 3.9) when the Cheng 2 was employed for all the DPIs tested. Interestingly the reduction of throat deposition with the cyclone-spacer in place was constant upon increasing the flow rate with the exception of FP/Accuhaler ($p<0.05$, Table 3.9). In the case of Cyclohaler/SS® and Easyhaler/Budesonide™, increasing the flow rate did not alter the IP/PS deposition ($p > 0.05$) both with and without the cyclone in place (e.g. for Easyhaler/Budesonide™ IP/PS deposition with Cheng 2 was 15.65 ± 1.39 % and 15.19 ± 1.74 % at 2 and 4 kPa, respectively). The decrease in the IP/PS deposition was due to the high retention of the emitted dose within the spacer. However, lower retention within the Cheng 2 cyclone was seen for Bud compared to SS (Table 3.9, $p< 0.05$). When the SX and FP were tested from the Seretide/Accuhaler™, even with the cyclone, the IP/PS deposition was double that of the other formulations at both flow rates ($p<0.05$, Table 3.9). The aerodynamic particle size distributions shown in Figure 3.6 for SS (A), BUD (B) and Figure 3.7 for SX and FP confirmed the reduction of IP/PS deposition (see arrows on Figure 3.6, A). The distribution shows the cyclone improved the % of particles with size < 5 µm (dashed line). Figure 3.6 and Figure 3.7 show an unconventional representation of the cumulative undersize distribution. The calculation was based following the method of Thiel et al [192] and Mitchell et al. [44]. Typically the aerosol PSD is normalized for the impactor sizeable fraction only. However, such a conventional representation does not demonstrate the extent of the IP/PS deposition, which is visible in Figure 3.6 and Figure 3.7 in the distributions calculated as % ED (solid line plot).

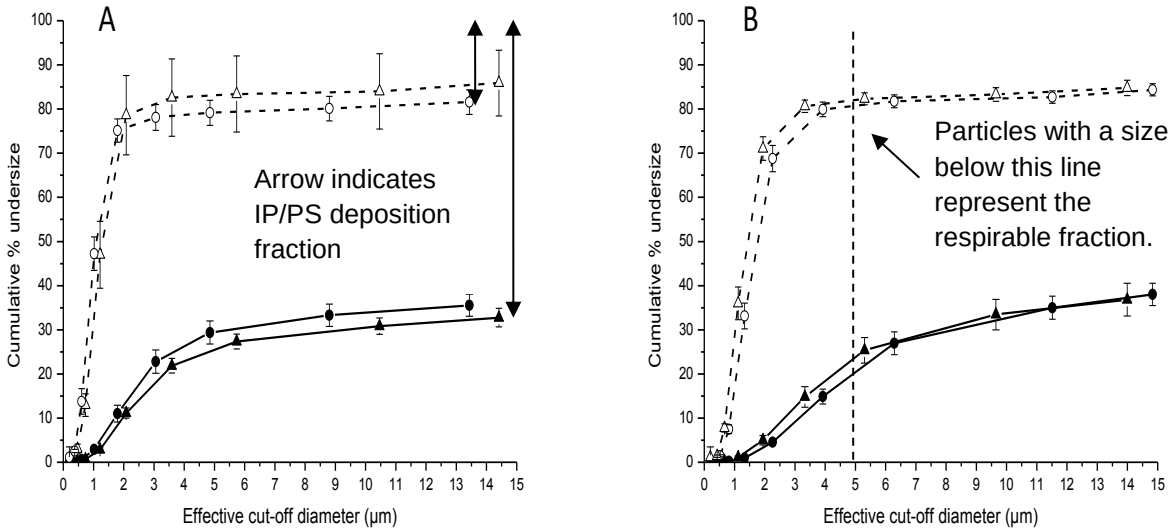

Figure 3.6. Cumulative aerodynamic undersize (%) of SS of emitted dose from Cyclohaler® at 2 kPa (▲) and 4 kPa(●) and from Cyclone (A) and of BUD emitted from Easyhaler™ and from Cyclone (B) at 2 kPa (Δ) and 4 kPa(○) (mean ± SD; n = 4).

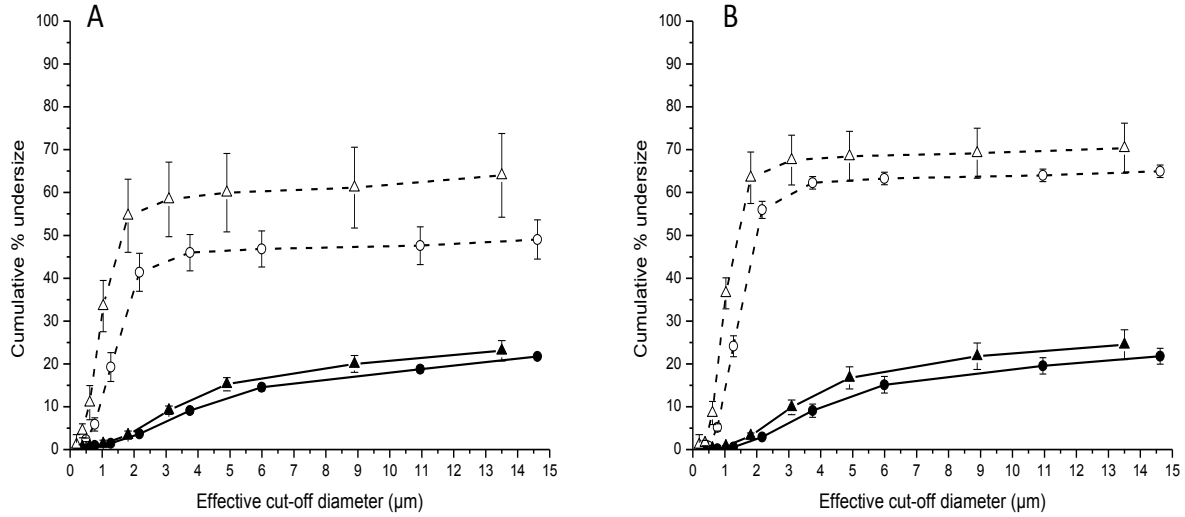

Figure 3.7. Cumulative aerodynamic undersize (%) of SX of emitted dose from Accuhaler™ at 2 kPa (▲) and 4 kPa(●) and from Cyclone (A) and of FP emitted from Accuhaler™ and from Cyclone (B) at 2 kPa (Δ) and 4 kPa(○) (mean ± SD; n = 4).

The FPD is the dose respirable by the patients below a particular size range (e.g. 5 µm). Similar trends to that reported for Cheng 1 of decreased MMAD and unchanged FPD values (Section 2.4.6.3) were observed for Cheng 2 compared to the devices alone.

Table 3.10. Mass median aerodynamic diameter (MMAD), fine particle fraction < 5 µm ($FPF_{5\mu m}$), and fine particle dose < 5 µm ($FPD_{5\mu m}$); of salbutamol sulphate (SS), budesonide (Bud), salmeterol xinafoate (SX) and fluticasone propionate (FP) emitted from the DPIs and from the DPIs through the Cheng 2 cyclone, (mean ± SX, n ≥ 4).

Device	Pressure drop(kPa)	Drug	$FPF_{5\mu m}$ (%ED)	$FPF_{5\mu m}$ (%sED)	$FPD_{5\mu m}$ (µm/dose)	MMAD (µm)
Cyclohaler®	2	SS	24.92 ± 1.61	N/A	31.64 ± 2.70	3.00 ± 0.12
Cheng 2-Cyclohaler®			12.90 ± 4.43	83.62 ± 6.88	15.13 ± 4.78	1.24 ± 0.10
Easyhaler™		BUD	20.41 ± 2.56	N/A	45.87 ± 3.72	4.72 ± 0.34
Cheng 2-Easyhaler™			19.44 ± 0.96	78.58 ± 1.69	48.37 ± 3.66	1.78 ± 0.05
Accuhaler™		SX	12.12 ± 0.47	N/A	7.49 ± 0.89	4.35 ± 0.36
Cheng 2-Accuhaler™			11.04 ± 0.83	56.81 ± 4.21	6.90 ± 0.69	1.54 ± 0.10
Accuhaler™		FP	12.25 ± 1.58	N/A	54.19 ± 8.42	4.48 ± 0.21
Cheng 2-Accuhaler™			11.26 ± 0.68	61.79 ± 1.51	45.43 ± 4.42	1.63 ± 0.14
Cyclohaler®	4	SS	25.29 ± 6.95	N/A	36.14 ± 5.04	2.65 ± 0.13
Cheng 2-Cyclohaler®			11.39 ± 0.64	79.66 ± 2.79	13.77 ± 1.67	1.05 ± 0.05
Easyhaler™		BUD	23.47 ± 2.65	N/A	66.73 ± 9.78	3.91 ± 0.24
Cheng 2-Easyhaler™			20.05 ± 2.02	81.63 ± 1.48	57.32 ± 5.78	1.45 ± 0.02
Accuhaler™		SX	14.38 ± 1.33	N/A	8.36 ± 0.81	3.67 ± 0.34
Cheng 2-Accuhaler™			9.71 ± 1.03	60.26 ± 9.18	5.84 ± 1.12	1.17 ± 0.08
Accuhaler™		FP	15.96 ± 2.44	N/A	64.21 ± 11.07	3.70 ± 0.07
Cheng 2-Accuhaler™			9.54 ± 1.46	68.70 ± 5.83	34.57 ± 8.67	1.20 ± 0.06

All the inhalers exhibited flow-rate dependence of the % $FPF_{5\mu m}$ (%ED) when employed alone (Table 3.10). Easyhaler/Budesonide was the only product where the change in flow rate altered the $FPF_{5\mu m}$ (sED) ($p<0.05$) when the cyclone was employed. The $FPF_{5\mu m}$ (%sED, fine particle fraction "ex-spacer") differed significantly between the products at both flow rates (SX Accuhaler™ < FP Accuhaler™ < Bud Easyhaler™ = SS Cyclohaler®, $p<0.05$). This was similar to the behaviour of the devices when tested without the cyclone (i.e. comparing $FPF_{5\mu m}$ %ED). When the cyclone was employed the fine particle dose (<5 µm, FPD) was unaffected by a change in flow rate ($p>0.05$), with the exception of the Easyhaler/Budesonide™ ($p <0.05$). However, with the exception of SX, the FPDs of all inhaled drugs were significantly lower ($p <0.05$) when Cheng 2 was employed (Table 3.10). By way of example, the FPD of SS combined with Cheng 2 (15.13 ± 4.78 µg and 13.77±1.67 µg at 2 and 4 kPa, respectively) was lower than from the Cyclohaler® alone (31.64 ± 2.70 µg and 36.14 ± 5.04 µg at 2 and 4 kPa, respectively). This was in accordance with data from Cheng 1, Section 2.4.5 that showed that the FPDs at 30 $Lmin^{-1}$ decreased compared to the Cyclohaler alone (e.g. 27.21 ± 4.33 µg/dose ex DPI and 18.41± 6.63 µ/dose ex Cheng 1). However, at 60 $Lmin^{-1}$ an equivalent FPD of SS was seen with Cheng 1 in place (39.55 ± 3.58 µg/dose ex DPI and 39.44 ± 7.67 µg/dose ex Cheng 1).

When the DPIs were tested alone, the MMADs decreased when the flow rate was increased (Table 3.10, $p <0.05$).The aerosols which would be inhaled by the patient (sED) possessed lower MMADs when emitted from the cyclone than from the devices alone (Table 3.10, $p <0.05$). For example, the MMAD of SS was halved when the cyclone was employed (Cyclohaler®: 3.00 ± 0.12 µm and Cheng 2: 1.24 ± 0.10 µm at 2 kPa). This showed the screening ability of Cheng 2; however unlike Cheng 1, the MMADs were lower for all formulations at the 4 kPa than 2 kPa flow rate with the cyclone in place (Table 3.10, $p <0.05$). The latter differences were not as large in magnitude as when the DPIs were tested without the spacer.

The size of the inlet of the cyclone was 6 mm x 10 mm with a cut-off size determined to be < 2 μm. Therefore, the spacer should classify the particles emitted from the devices. The fine particle ratio < 1.5 μm ($FPR_{1.5}$) was defined as equation (3.2):

$$FPR_{1.5} = \frac{Fine\ particle\ fraction\ _{1.5\mu m}\ (Cheng\ 2)}{Fine\ particle\ fraction\ _{1.5\mu m}\ (DPI)} \quad (3.2)$$

It was calculated as a measure of classification of particles below the cut-off diameter per Equation 3.2. Whilst accepting the undesirability of modifying the MMAD by spacer use, with the Cyclohaler/SS®, the $FPR_{1.5}$ was 1.73 ± 0.38 times higher at 2 kPa and 1.30 ± 0.18 at 4 kPa with the cyclone in place than without. For Accuhaler™/Cheng 2 the $FPR_{1.5}$ of SX was twice that without the cyclone (2.29 ± 0.31 and 1.98 ± 0.30 at 2 and 4 kPa, respectively) and of FP was 4.65 ± 0.12 and 2.63 ± 0.21 times at 2 and 4 kPa, respectively. The greatest $FPR_{1.5}$ was seen when the cyclone was tested for Bud emitted from the Easyhaler™ (6.70 ± 0.25 and 4.24 ± 0.29 times greater than Bud/Easyhaler™ at 2 and 4 kPa, respectively). This means that particles underwent deagglomeration within the cyclone spacer, since the proportion of fines < 1.5 μm had increased. However, the FPD was still lower when the Cheng 2 was employed due to the bigger agglomerates (1.5 - 5 μm) that are likely to be retained inside the cyclone as the cut off of the spacer was relatively low.

3.4.5 Aerosolization studies using laser diffraction technique

Laser diffraction analysis was performed on the aerosol emitted from the DPIs in presence and absence of the Cheng 2 at 2 and 4 kPa. The Dv50 (volume diameter of 50 % of the particle population) was dramatically decreased when the cyclone was employed for all the DPIs (Table 3.11).

Table 3.11. Values of volume median diameter (DV50) of the active pharmaceutical ingredient (API) emitted from the dry powder inhalers with and without the Cheng 2 (mean ± SD, n=3)

API	Device	DV50 (µm)	
Pressure drop		2 kPa	4 kPa
SS	Cyclohaler®	58.66 ± 3.42	61.56 ± 3.18
	Cheng 2-Cyclohaler®	1.29 ± 0.07	1.13 ± 0.02
Bud	Easyhaler™	32.68 ± 2.09	31.14 ± 2.12
	Cheng 2-Easyhaler™	1.88 ± 0.02	1.68 ± 0.05
SX/FP	Accuhaler™	48.13 ± 2.03	46.01 ± 2.99
	Cheng 2-Accuhaler™	1.73 ± 0.13	1.15 ± 0.12

However, when the Accuhaler™ was tested, some agglomerates escaped the Cheng 2 as shown in Figure 3.8 (the arrows in the figure indicate a shift in PSD to larger sizes caused by the agglomerates). A similar behaviour was already seen with the higher resistance Cheng 1 with SS at 60 $Lmin^{-1}$ (Chapter 2, Section 2.4.6.2).

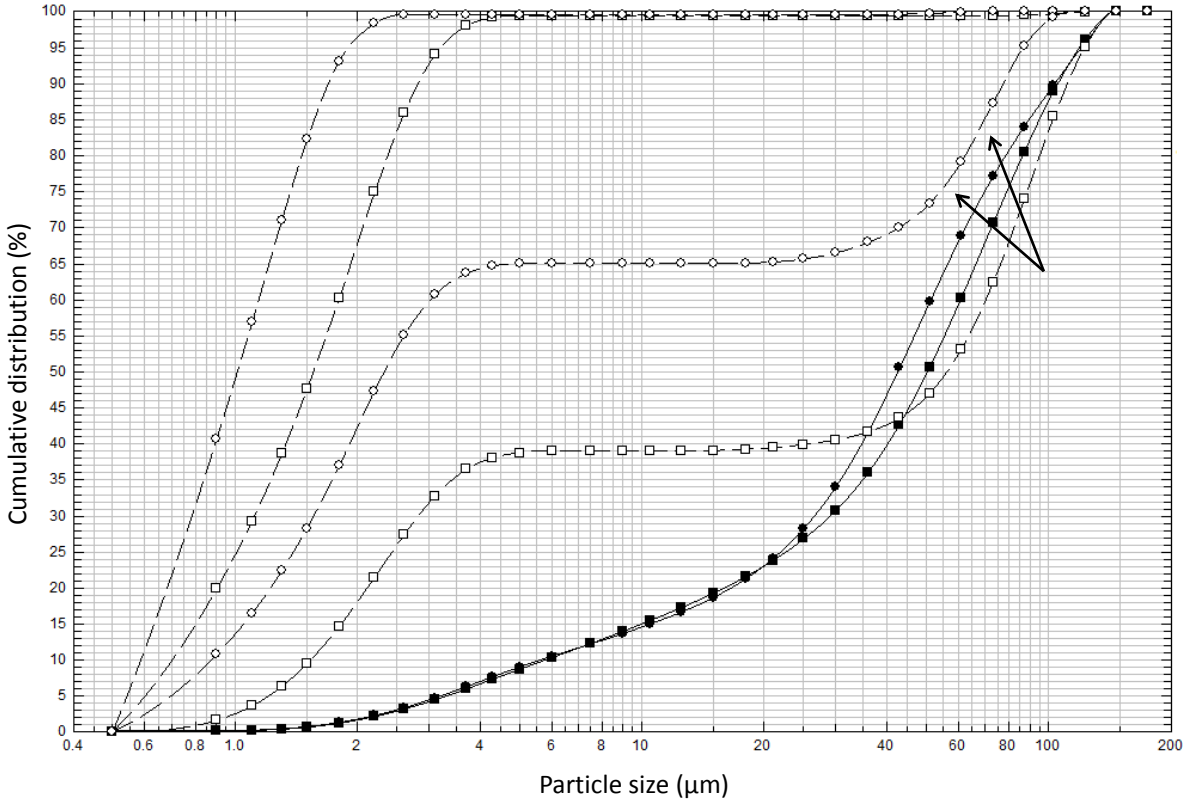

Figure 3.8. Representative particle size distributions of salmeterol xinafoate and fluticasone propionate from Seretide/Accuhaler™ at 2kPa (■) and 4 kPa (●) and from Cheng 2 at 2 kPa (□) and 4 kPa (○). The arrows indicate the agglomerates emitted from the cyclone for salmeterol xinafoate and fluticasone propionate at 2kPa (□) and 4 kPa (○).

The formulations were recovered from each DPI and the Sympatec Rodos module where used to determine DV50 of the carrier particle at 4 Bar dispersing pressure. The formulation collected from the Ventolin (SS/carrier lactose) and Seretide (SX/FP/carrier lactose) showed almost identical particle size for DV50 (63.46 ± 0.86 µm and 61.95 ± 0.46 µm, respectively, $p>0.05$). On the other hand, when formulation of SS + carrier lactose was recovered from the Easyhaler, the Dv50 was 52.06 ± 0.24 µm. Budesonide recovered from the Easyhaler showed the lowest Dv50 of all products (45.09 ± 0.36 µm, $p<0.05$). If the % of particle with size < 5 µm was taken in consideration, budesonide showed the greatest proportion compared to the other formulations (21.73 ± 0.85 %) whilst SS/Easyhaler showed the lowest (10.97 ± 0.42 %).

3.5 Discussion

In Chapter 2 the prototype cyclone-spacer Cheng 1 was manufactured and assessed with the Cyclohaler® using the SS/lactose formulation recovered from Ventolin/Accuhaler™. The Cheng 1 cyclone was tested between 30 and 60 L min^{-1} to evaluate its capacity to retain large agglomerates and particles. The reverse airflow cyclone technology is not new in the inhalation field to improve fine particle delivery [91-93]. However, previous applications of cyclones have been integrated into device platform to gain advantages of size selectivity and for improved deagglomeration. This was mirrored for a generic spacer approach in Chapter 2 when the Cyclohaler® delivered a constant FPD through the Cheng 1 (Chapter 2, Section 2.4.5.2, Table 2.9) at high flow rates. The spacer also reduced the MMAD, that also remained unchanged regardless of the flow rate tested. However, the spacer seemed to be incompatible with carrier-free formulations. When assessed with Turbuhaler® using LDA, the spacer did not show a similar trend to the SS/lactose formulation emitted from the Cyclohaler® (Section 2.4.6.3, Figure 2.12). The finding suggested that the spacer might only work with carrier-based formulations. Moreover, the prototype showed a high resistance to the air when tested there making difficult to reach flow rates above 60 L min^{-1}.

The aims of the current study were to manufacture a second prototype spacer (Cheng 2) with the same reverse airflow cyclone technology, but with lower flow rate resistance and different orifice design to allow a higher cut off diameter (target 5 µm) than Cheng 1. This was done to confirm whether a new manufactured spacer could still mitigate the dependence of the respirable dose and of the aerodynamic diameter on the inhalation flow rate. The Cheng 2 was then tested with a wide range of commercial carrier-based DPIs with different types of formulations. The Cyclohaler/SS® was tested again to confirm the capability of the Cheng 2 function to still retain agglomerates and it was used as a control device due to its assessment with Cheng 1. Easyhaler/SS™ 200 µg/dose and Ventolin/Accuhaler 200 µg/dose were also tested. However, the latter products did not release sufficient dose when tested with Cheng 2 for analysis suggesting, perhaps, the Cheng 2 might be ineffective with these products. This might be because Cheng 2 showed lower impaction forces and lower integral strain rate measurements by the inlet and at the vortex cone base than Cheng 1 which would promote fine particle detachment from carrier particles under impaction and turbulent shear forces [193].

Seretide/Accuhaler™ (SX and FP) and Easyhaler/Bud™ were also tested, together with Cyclohaler/SS® at 2 and 4 kPa to represent low and high pressure drops achievable by patients and to represent different formulations. SS was considered as an adhesively balanced blend when added to lactose [194], Bud as a cohesively balanced blend [195], and SX/FP was considered as a combination of anti-inflammatory and bronchodilator [196]. HPLC assays were validated with regards to the linearity, LOD, LOQ, accuracy and precision for Bud, SX and FP. The three drugs are highly lipophilic, therefore a 75:25 (v/v) mixture of methanol: 0.6% (w/v) aqueous ammonium acetate was used. Budesonide and fluticasone propionate are corticosteroids and they are used in asthma to treat inflammation in the lungs. Salmeterol xinafoate, on the other hand, is a bronchodilator for treatment of asthma and COPD. The stationary phase used for the APIs was a C18 column with particle size of 3 µm. The calibration curves generated for quantification of the APIs showed a good linearity (R^2 = 0.999) and high sensitivity at low concentrations with a coefficient of variance at 0.5 µg/ml above 5%, regarding the inter-day variability (e.g. SX = 9.29%, FP = 6.14%). Therefore, for SX and FP the method was not as robust as for BUD and SS and the reproducibility had to be tested for each run.

Spacers for DPIs have been suggested over the last 10 years [173, 174]. Such spacers showed a reduced deposition of emitted particles in the induction port stage when used with the Turbuhaler®. However, the authors suggested that the optimum length of the spacer should be used for low resistance devices [173]. Commercial DPIs have a small outlet that increases the turbulence upon inhalation. Therefore it has been suggested that spacer should have a greater outlet than the orifice of the DPI to decrease aerosol deposition in the mouth [188]. Moreover, the outlet of the spacer should have low resistance to reduce turbulence and, therefore, to reduce diffusion of respirable aerosol that otherwise will move toward the walls of the spacer. In the previous chapter, Cheng 1 showed a high resistance to the airflow due to the 4.1 x 4.1 mm circular shape of the orifice with cut-off diameter between 0.46 – 0.90 µm between 30-120 L min^{-1} (Chapter 2, Section 2.3.2). The modified Cheng 2 cyclone was manufactured with a 10.1 x 6 mm oval shape to decrease the resistance and achieve a cut-off diameter between 1.19 – 1.55 µm. In accordance with previous studies on the orifice of the inhalers [188], the Cheng 1 showed a greater tangential wall velocity than Cheng 2 at equivalent flow rates, indicating high impaction forces for Cheng 1 [159] and, therefore, impaction and deagglomeration forces would be higher for emitted masses passing through the Cheng 1. In addition, Cheng 1 produced higher integral strain rate measurements by the inlet and at the vortex cone base which would promote fine particle detachment from carrier particles under impaction and turbulent shear forces, which could explain the enhanced FPF and FPD for Cheng 1 at the highest flow rate, compared to Cheng 2 [193].

In Chapter 2, Cheng 1 showed high resistance to airflow (0.08 $kPa^{1/2}$ min L^{-1}) due to the circular inlet orifice (4.1 mm diameter). Therefore, the Cheng 2 was manufactured and it showed a lower resistance then Cheng 1 (0.04 $kPa^{1/2}$ min L^{-1}) that was also within the range of DPIs (Turbuhaler®, 0.03 $kPa^{1/2}$ min L^{-1} and Handihaler®, 0.05 $kPa^{1/2}$ min L^{-1}) acceptable to patients with obstructive lung disease [125, 168]. This was an improvement over Cheng 1 as patients with lung disease should be able to achieve a reasonable flow rate through the prototype.

Although studies have been shown that spacers can reduce the velocity of the emitted aerosol and, therefore, mouth and throat deposition, electrostatic charges

are common problems in the aerosol delivery especially for plastic spacers. The interactions between particles and spacer walls lead to acquisition of charges due to the stress in the electrical double layer. The increment of charge would alter the output of the aerosol, therefore, leading to a variable lung deposition, especially in the alveoli [197]. Moreover, this can lead to high retention of the aerosol inside the spacer [198, 199]. Wildhaber *el at* [198] showed that the charge in the Volumatic® spacer plays a major role in the delivery of salbutamol from pMDI at 60 $Lmin^{-1}$. They compared patients' old spacers with new ones and discovered that the delivery of particles with size < 6.8 µm into the multistage liquid impinge (MSLI) from a new spacer was lower than when the spacer was previously used (30 ± 3 % of the delivered dose vs. 37 ± 4 %, respectively), due to high electrostatic charges in the inner surface. The authors tested the spacer also after treatment with detergent to decrease static charge in the spacer, concluding that ionic detergent coating significantly improved the delivery of salbutamol < 6.8 µm. Kwok et al [200] also showed that detergent coated spacer for MDI decreased the deposition of the aerosol inside the chamber. In addition, DPIs shows electrostatic charges too. The material used to manufacture DPIs (mainly plastic) and the type of formulation lead to accumulation of electrostatic charges within the device, which affect the output of the delivered dose [201]. Therefore, when adding a plastic spacer to a DPI, the electrostatic charge effect would be enhanced, although in the current study, this was not controlled. It is important to note that this may account for the retention of drug in the spacers.

The previous chapter confirmed the ability of the Cheng 1 to retain the coarse carrier with an SS formulation; however, it was not tested with different formulations due to the high resistance of the spacer. Therefore, the Cheng 2 was tested with Seretide/Accuhaler™ that contains a combination of salmeterol xinafoate (SX) and fluticasone propionate (FP), Easyhaler/Budesonide™ and Cyclohaler® with SS/lactose blend recovered from the Ventolin/Accuhaler™ to assess the functionality of the prototype with a wide range of marketed inhalers. The % recovered doses for all the DPIs were within the pharmacopoeial limits with and without the spacer. When the Cheng 2 was employed the % emission into the impactor of the particles from the inhalers dramatically decreased as seen already for the Cheng 1. The % emission

calculated for the emitted dose of Bud from Easyhaler™ was 97.62 ± 0.56% at 2 kPa but dropped to 24.51 ± 1.68% with the cyclone in place. When the aerosolization of SX from Accuhaler™ was assessed, the % emission at 2 kPa was 98.65 ± 0.27% but 19.33 ± 0.46% with the Cheng 2. The same trend was seen for FP and SS from the Accuhaler™ and Cyclohaler® respectively. The reduced emission was due to the high retention within the spacer (almost 80% of the emitted drug was retained within the cyclone for all the formulations) due to the low cut off (< 2 µm) and possibly to the electrostatic charges of the emitted particles and the spacer walls, although a full study was not performed. The highest retention was seen for the Accuhaler™ formulation compared with Cyclohaler® and Easyhaler/Bud™. The high retention of the drug within the spacer was also shown for SS when using the Conix™ [91]. The author showed that almost 80 % of SS was recovered from the conical section.

By capturing the drug particles inside the spacer, throat deposition is reduced, which in clinical use serves to reduce oropharyngeal deposition [174]. Because of the high retention in the cyclone, the IP/PS deposition was reduced four-fold when the spacer was employed. However, the formulations showed different behaviours even with the cyclone in place. Interestingly, when the formulation containing SX and FP was tested, the IP/PS deposition was twice that of the Bud or SS emitted from Easyhaler™ and Cyclohaler®, respectively (e.g. 18.44 ± 2.79 % for SS, 15.19 ± 1.74 % for Bud, 36.01 ± 9.77 % for SX and 29.63 ± 5.85 % for FP at 4 kPa). Harrison *et al* [146] and Needham *et al* [91] studied an SX/FP formulation and an SS formulation emitted from the Conix™, respectively. The difference in the SS and SX IP/PS deposition that has been shown in the current project is in accordance with the Conix™ study. This was probably due to the combination of SX and FP. Their cohesive behaviour when blended with coarse carrier might lead to less efficient deagglomeration process than SS when emitted from a device, due to the strongly cohesive interaction forces [202] that would present large sized agglomerates, when drug particles redistribute in the interstitial spaces of the carrier in agglomerated form [203]. However, we need to keep in mind that the aerosolization studies were performed with an ACI for Conix/SS™ [91] and NGI for Conix/SX/FP™ [146], therefore the particle distribution in the impactor would be different. SS deposition in the throat was 13% (of the delivered dose) [91], whilst SX deposition was 76 % [146]. Although the label claim for the Conix™ and the DPIs studied in the current

project were different, the same trend of higher % throat deposition for SX than SS could be seen. As reported in Chapter 2, Section 2.4.5.2, neither cyclone retention nor IP/PS deposition was affected by the flow rate for SS formulation, nor for any of the drug-device formulations tested in the current study. Although the extent of IP/PS deposition and cyclone retention did depend on the drug formulation/product type (Table 3.9), the potential for flow-rate independence of oropharyngeal drug deposition for a specific formulation was a promising finding towards overcoming inter-patient variability in DPI deposition profiles.

The traditional view of spacer use with MDIs is that extra-thoracic deposition is reduced but that the fine particle deposition is unchanged when a spacer is employed [172]. The target with a DPI is therefore similar. While the cyclone was designed to emit a similar fine particle dose to the Cheng 1 for SS to improve in vitro drug delivery (Chapter 2) that was only accieved at 45 and 60 $Lmin^{-1}$, the current study showed that there was enhanced deagglomeration of Bud from the Easyhaler™ compared to SS from Cyclohaler® and SX and FP from Accuhaler™ (e.g. $FPR_{1.5}$ of 4.24 ± 0.29 times greater for Bud vs. 1.30 ± 0.18 for SS at 4 kPa with the cyclone in place than without). This means that particles underwent deagglomeration within the cyclone spacer, since the proportion of fines < 1.5 μm had increased. Nevertheless, the cyclone delivered a lower fine particle dose of the "inhalable" aerosol compared to when DPIs were tested alone only for SS and FP. This was attributed to the high fraction of the dose (>80 %) depositing in the cyclone. However, the cyclone managed to remove the non-sizeable fraction; i.e. d_{ae} > 10 μm [43] which has potential for high oropharyngeal deposition (e.g. IP/PS deposition >40% without cyclone in place). When the fine particle fraction was calculated as the % spacer-emitted dose, higher FPF (%sED) were seen for the formualtions compared to when the cyclone was not used. The results were in accordance with the Conix™ DPI [91], where almost 85 % FPF was detected for SS, whilst only 35 % was shown for the Accuhaler™. Although the FPF (%ED) of SS was approximately halved by the use of the cyclone ($p < 0.05$), with the exception of SX and FP at the highest flow rate (4 kPa, slightly lower, $p < 0.05$), there were no significant differences in the FPF (%ED) for Bud, SX or FP when the cyclone was added to the DPI product (Table 3.10). The latter findings were also reflected in the fine particle dose (FPD)

values (Table 3.10). As well as the comparability (excluding SS) to the DPI results, it was important to note that using the cyclone minimized (or removed) the magnitude of change in FPD and FPF (%ED), caused by increasing the flow rates. Differences in the FPF (% ED) when the cyclone was used indicate pharmaceutical non-equivalence.

It is also appropriate to compare the FPF as a %sED (i.e. the dose exiting the spacer) and examine its similarity when the cyclone is used (%sED) because this indicates the fraction which would be inhaled by the patient. The cyclone was designed to emit a similar $FPF_{5\mu m}$ (%sED) from all products. There were clear differences in the FPF (% sED) values observed in this study. The highest FPF was seen for SS and Bud (almost 80 % of the dose exiting from the spacer). A decrease in the FPF (%sED) was observed for the Accuhaler™ emission. The lower FPF was attributed to the higher IP/PS deposition of SX and FP even with the spacer in place (FPF was ~60 % of the emitted dose). Moreover, a much lower FPF (%sED) for SX was seen compared to SS emitted from the Conix™ (13 % vs. 85%, respectively). This was a consequence of the different % IP/PS deposition previously described for the two drugs. It was notable that the FPF (%sED) for SS from Cheng 2 was markedly lower than from Cheng 1, attributable to the higher retention of SS in Cheng 2 compared to Cheng 1 (Chapter 2, Section 2.4.5.2). The lower FPFs for Cheng 2 than Cheng 1 may be attributed to the different orifice geometry due to the narrower cyclone inlet of the latter [193].

It must be borne in mind that the factors governing deposition within induction ports appear to be drug specific [204]. However, it appeared from the current study that the functioning of the reverse-flow cyclone as a spacer may depend on the deagglomeration state of the drug particles entering the cyclone. For example, laser diffraction studies (Figure 3.8) of the Seretide/Accuhaler™ formulation revealed the emission of some agglomerates that escaped the cyclone similar to the Ventolin/Accuhaler. CFD studies highlighted the potential for vortex instability within the conical region of the spacer which would enable the escape of agglomerates [158, 159].

The design of the DPI helps the deagglomeration of the formulation, but the characterization of aerosol and plume geometry is also an important tool to study aerosol dispersion and it has been used widely to evaluate the performances of the valve and the actuator for MDIs [205]. Although FDA (Food and Drug Administration) introduced a CMC (Chemistry, Manufacturing and Controls) Guidance in 1998 for MDIs and DPIs, the study of spray pattern and plume geometry was only applied for MDI aerosols [150]. The guidance did not specify the need of this particular study for DPIs and there is also poor research on this particular field. However, Oxford Lasers [206] presented a study on the plume geometry and pattern of SV003 Lactose emitted from the Easyhaler, using FDA guidance. They showed that the plume degree was 15.89 ± 1.42 degrees with a mean plume length of 16.11 ± 0.92 cm. The plume width at 6 cm from the inhaler was 2.15 ± 0.28 cm. They also compared the spray pattern at 3 and 6 cm from the Easyhaler, showing that the pattern is more consistent at 6 cm [206]. Therefore, the plume geometry is important to consider when the aerosol enters the spacer as wide plume geometry would impact on the spacer walls, potentially leading to an enhanced deagglomeration.

The Easyhaler™ is designed to maximize the particle separation by changing the dimensions of the airflow path [207] with a cylindrical outlet with length of 3.28 cm. The mouthpiece of the Easyhaler is designed to re-disperse the micronized particles from the carrier. The dosing of the Easyhaler is based on the gravitational flowability of the powder which is dosed accordingly to the volume of the metering cavity. Easyhaler contained fine particles of lactose as an additive to improve flowability of the powder. The lactose used is large enough to avoid deposition in the lower part of the lungs to reduce irritation of the airways [208]. The Cyclohaler® shows a cylindrical outlet length of 4.80 cm, whilst the Accuhaler™ has a mouth shape outlet only approximately 0.80 cm. The entire design of the DPIs is very different between each other. The Cyclohaler® is a single dose inhaler consisting of a capsule that spins and the formulation is deagglomerated with the help of a grid [209]. The Accuhaler™ is a multi-unit dose inhaler contains a blister with multiple doses and due to the short outlet the formulation might not have sufficient opportunity to deagglomerate before reaching the patient's lung. Moreover, the mouth shape orifice with a cross shape grid might increase the dispersion of the particles in the air instead of leading the emitted dose through a cylindrical pathway

like in the Cyclohaler® and Easyhaler™, increasing therefore the impaction in the mouth and throat. More than 10 % difference was seen in the throat deposition between SS or Bud and SX or FP when emitted from Cyclohaler®, Easyhaler™ and Accuhaler™, respectively at 2 and 4 kPa. The literature [89] highlights that dose emission from an Easyhaler™ is constant regardless the flow. This is in agreement with the data showed in this study where the FPF of Bud from the Easyhaler™ alone was 20.41 ± 2.56 at 2 kPa and 23.47 ± 2.65 at 4 kPa. Therefore, spacers for DPIs might only be suitable for certain inhalers, such as the ones that do not show consistency of the emitted dose when changing the flow rates. For example, differences between the SS fine particle emission of Cheng 1 and Cheng 2 spacers was seen as well as the reduction of FPD for FP but not SX when the flow rate through the Seretide/Accuhaler™ was increased. There is potential that the cyclone does not solely behave as a classifier, but that deagglomeration also takes place within the cyclone vortices. Drug which adheres strongly to the carrier is more difficult to aerosolize than drug which forms agglomerates on the carrier surface [109]. Bud, which typically forms agglomerates with lactose, would be more easily removed at equivalent flow rates from the carrier surface than SS (which typically adheres to the surface), thereby leading to higher Bud FPF values. Collisions between particles and the cyclone wall or other particles in the cyclonic flow aids powder dispersal [146], particularly collisions with particles of large mass such as carrier lactose. Upon increasing the flow rate, sufficient force is provided to break up drug agglomerates further, but also aid removal of surface-adhered drug from the carrier.

The lower FPF when Accuhaler™ was tested was in accordance with Taki *et al* [170] who tested the aerosolization of SX and FP through the Accuhaler™ and through the Aerolizer® at 60 L min^{-1} with the NGI. The Accuhaler™ showed a much reduced FPF, higher MMAD values and higher IP/PS deposition compared to the Aerolizer®. In the current study, the FPF of SX and FP emitted from the Accuhaler™ were lower than the FPF of SS emitted from the Cyclohaler® (Table 3.10). In the current project, the decreased FPF from the Accuhaler™ could be explained by the higher IP/PS deposition compared to SS from Cyclohaler®. However, when the Ventolin/Accuhaler was tested to assess the SS distribution with Cheng 2, the

spacer did not perform as expected compared when it was used with the Cyclohaler to emit SS formulation recovered from the Ventolin/Accuhaler. Although the dose of the formulation was the same for both inhalers (label claim: 200 µg/dose of SS), the design of the DPI used (Accuhaler vs. Cyclohaler) played a major role on the emission of the dose into the spacer (Figure 3.8).

When FPD (fine particle dose) was assessed, Bud had an equivalent FPD with and without Cheng 2, unlike for the SS formulations (Table 3.10). The lower FPD for Bud when the cyclone was compared with Cyclohaler®/SS could be due to the higher affinity of SS to the lactose than Bud which would decrease the release of adhered SS particles from the carrier during passage through the spacer. Bud shows a cohesive behaviour with lactose compared to the more adhesive interaction of SS with the carrier [109, 194]. Begat *et al* [109], using SEM (scanning electron microscopy), showed that SS was equally distributed over the lactose surface, whereas, Bud was unevenly spread creating agglomerates on the carrier surface. However, the authors showed that for the same DPI the Bud delivery released a greater quantity of fine respirable particles than SS. This is probably due to the adhesive balance of SS with lactose, which decreases the degree of respirable particle dispersion leading to high emission yet poor fine particle fraction. On the other hand, Bud creates large agglomerates with greater aerodynamic drag forces than smaller agglomerates (e.g. SS). When the dose is emitted from the device into the spacer, the large agglomerates of Bud would collide better with the spacer's walls or outlet, enhancing the dispersion efficiency and creating greater percentage of fine respirable particles. The SX and FP showed a similar behaviour to the Bud. However, the extent of deagglomeration appeared lower.

The mass median aerodynamic diameter (MMAD) is one determinant (alongside inhalation parameters) of the potential deposition site of an inhaled aerosol. It would be expected that the MMADs for the aerosols emitted from the spacers would be limited by the effective cut-off diameters of the cyclone itself[158, 159] because the cyclone should act as a classifier, releasing only particles smaller than the cut-off size. Although different values were seen when DPIs were tested

alone (Table 3.10) as expected [170], when Cheng 2 was employed similar values of MMADs were seen for the formulations (Table 3.10), in keeping with other studies with reverse flow cyclone [91, 146]. Similar observations of reduction in the MMAD when Cheng 1 was used (Chapter 2, Section 2.4.5.2), were seen with Cheng 2 for all drugs studied. Indeed the MMADs were roughly equivalent to the calculated cut-off diameters of the cyclones (Cheng 1 ~0.9 µm, Cheng 2 ~2 µm). It appeared that both Cheng 1 and 2 functioned effectively as classifiers, a finding confirmed by laser diffraction analysis (Chapter 2), albeit with an indication of intra-cyclone deagglomeration occurring.

The MMAD was low because off the cut off size of Cheng 2. The $FPR_{1.5}$ calculates the extent of classification of particles below the cut-off diameter of the spacer and quantifies their deagglomeration. Bud showed the greatest deagglomeration as its $FPR_{1.5}$ with the Cheng 2 in place was 6.70 ± 0.25 and 4.24 ± 0.29 times greater than Bud/Easyhaler alone at 2 and 4 kPa, respectively. The same trend was seen for FP (4.65 ± 0.12 and 2.63 ± 0.21 times at 2 and 4 kPa, respectively). On the other hand, SS and SX showed the lowest $FPR_{1.5}$ at both pressure drops (e.g. 1.73 ± 0.38 times higher at 2 kPa for SS). An $FPR_{1.5} > 1.0$ indicates not solely classification but also deagglomeration occurring. The deagglomeration depended on the physico-chemistry of the particles, and the geometry of the conical section of the cyclone. This was confirmed by the variable IP/PS deposition seen from the NGI studies for SX/FP emitted from the Accuhaler™ with Cheng 2 in place (twice that of SS and Bud) and by the particle size distribution from the LDA. The variable deposition in the throat was confirmed by the laser diffraction studies, where some agglomerates escaped the cyclone, probably due to vortex instability within the spacer [210]. When aerosolized with the Cheng 2, agglomerates of FP and SX shifted the Dv50 to greater values (Figure 3.8). However, Cheng 2 exhibited lower impaction forces than Cheng 1, with decreased ability to improve the deagglomeration of low quantities of micronized material that are less likely to be detached from the coarse carrier. Therefore, the low % of micronized material recovered from the formulation of the Easyhaler/SS may have arisen due to difficulties in escaping the Cheng 2, revealing undetectable recovered dose in the cascade impactor. Moreover, the highest % of fine material from the

budesonide formulation might explain the highest FPF seen in the aerosolization study (Table 3.10) when using the spacer.

3.6 Conclusion

This chapter has explored the potential of the Cheng 2 spacer to be used with a wide range of DPIs to both decrease throat deposition and MMAD. Despite the high retention of the carrier within the spacer, attributed to the low cut-off diameter of the cyclone (< 2 µm), high FPF were seen for SS and budesonide emitted from Cyclohaler® and Easyhaler™, respectively. However, unchanged FPDs were only detected for Bud and SX when the cyclone was used. The IP/PS deposition was dramatically decreased with the cyclone in place. However, the formulation and the physico-chemistry of the APIs need to be considered for further studies, as they affected the deagglomeration within the spacer. When the Accuhaler™ was assessed, SX and FP showed a higher deposition in the throat and pre-separator stages than SS and Bud. This led to a much reduced FPF for SX and FP compared to SS and Bud. In the next Chapter, the Cheng 2 will be assessed with in-house manufactured “control” blends with different formulation behaviour (cohesive and adhesive) and with different grades of lactose to explore the physicochemical relationship further.

Chapter 4: Investigating deagglomeration mechanisms of inhaled formulations within a reverse airflow cyclone-spacer

4.1. Investigating deagglomeration mechanisms of inhaled formulations within a reverse airflow cyclone-spacer

4.1.1. Morphology of cohesive micronized particles

In the market, carrier free DPIs are available along with formulations containing different types of sugars such as mannitol, coarse lactose monohydrate, fine particles of lactose monohydrate, and combinations of coarse and fine lactose monohydrate. The absence of the coarse particle affects the formulations that contain only agglomerates [106, 211]. Budesonide (Bud), for example, is more cohesive the salbutamol sulphate (SS), showing bigger agglomerates under the SEM (scanning electron microscope) [212]. It has been suggested [212-214] that FP, like SX (salmeterol xinafoate) and Bud shows greater agglomeration forces then SS. However, the formation of agglomerates of micronized APIs leads to an increased entrainment of the drug particles, but poor blend flowability. Therefore, lactose or other sugars are usually present in the formulation acting as carrier particles to enhance flowability upon aerosoliation [103, 215].

4.1.2. Distribution of cohesive micronized particles on the carrier surface

Micronized material (e.g. FP (fluticasone propionate)) shows high cohesive behaviour forming big agglomerates, especially when carrier is added (DV50 40.15 ± 6.02 at 90 $Lmin^{-1}$) [202]. The authors [202] mixed coarse and fine lactose with the most cohesive batch of FP and the formulation generated a lower fine particle fraction then when the coarse carrier was not used. The authors [202] suggested that it was due to the presence of very large agglomerates of FP in the mixtures. In Chapter 3, the Cheng 2 spacer was tested with commercial carrier based formulations, showing that the deagglomeration behaviour of the particles within the spacer was affected by the type of formulation. It was suggested that this arose due to physico-chemical properties of micronized material when blended with coarse carrier. This would overcome the high energy between agglomerates, leading to the re-arrangement of the API on the surface of the carrier. The way of re-distribution of the API on the carrier particles differs from drug to drug (e.g. batch to batch variability of the same drug), and depends on how great is the cohesive force

between agglomerates [216]. Although all micronized particles are cohesive, when coarse carrier such as lactose is added to the formulation, the micronized material starts to redistribute on the lactose surface exhibiting very different behaviour [99, 109, 202]. For example, SS, which has been widely investigated [108, 109, 217], presents a rectangular or a plate-like shape when analysed under the SEM [217]. Other studies [108, 109] suggested that SS exhibits an adhesively balanced behaviour when added to coarse lactose and redistributes evenly on the lactose surface, with lower adhesive energy to the carrier with respect to other particles [109]. This is probably due to the relative balance of cohesive and adhesive interparticulate forces in binary (and ternary) formulations with carriers. SS showed also a lower cohesive energy compared to Bud, with SX also reported to exhibit a balance in favour of cohesion when added to lactose [104, 109, 194]. The interaction between lactose and drug molecules has to be strong enough to prevent segregation. However, upon aerosolization, the drug must be easily detached to allow lung deposition.

4.1.3. Effect of carrier and fine particles on aerosolization of the inhaled formulation

The design of the inhaler and the inhalation strength of the patients affect drug dispersion. In addition the forces of interaction within the powder formulation play a role in the aerosolization. Studies have demonstrated that the strong adhesion between API and coarse carrier, decreased the drug dispersion [99, 110]. Enhancement of the dispersion process (e.g. aerosol fraction of fine particles) and modification of inter-particulate forces within the powder formulation by the presence of ternary agent has been suggested [111, 112]. Adi *et al*. [99] showed that adding fine lactose improved the dispersion process of SX from the coarse carrier, because the interaction between the fine lactose and the SX produced mixed agglomerates. It may be the decreased drug/carrier adhesion energy or the easier break up of mixed agglomerates with low carrier adhesion that enhances dispersion efficiency.

It has been suggested that the addition of fine lactose would increase the respirable fraction [101], whilst the presence of coarse lactose improves the flowability of the formulation. However, Behara *et al* [113] showed that the presence

of coarse carrier is not necessary. The aerosolization was improved by increasing two-fold the concentration of fine lactose to SS (from 1:4 to 1:8). They suggested that increasing the concentration of fine lactose reduced the agglomerate strength between SS and fine lactose. SEM images indicate more diffuse agglomerates when SS-fine lactose (1:8) were analysed compared to SS-fine lactose (1:1) that showed a more agglomerated structural characteristics [113]. A comparison between SS and budesonide (adhesively and cohesively balanced particles, respectively), showed that FPF was greater when a cohesively balanced blend (Bud) was emitted from the Rotahaler (26.3 ± 6.2 %) than when SS was used (12.6 ± 1.2 %) [109]. However, the addition of fine particles does not always enhance the FPD (fine particle dose) as shown by Jones *et al* [203].

4.1.4. Empirical model for the study of deagglomeration mechanisms

The adhesion forces between drug and carrier consist mainly of inter-particulate forces such as van der Waals forces, electrostatic charges, and capillary interactions and influence aerosol dispersion from dry powder inhalers (DPIs) [40]. Studies have investigated the interaction between individual particles using atomic force microscopy (AFM) [218, 219]. However, the technique does not quantify the cohesion force of a powder bed as it only measures the interaction between one drug or excipient particle and the probe of the AFM. Laser diffraction techniques have been used for dry and liquid dispersion systems to study powder deagglomeration [220]. Airflow and pressure drop titration experiments have been performed [213, 220] to assess the change in particle size when a fine powder bed is subjected to an increasing pressure drop and empirical models have been proposed for micronized particles with or without the common carrier coarse lactose [213, 220, 221].

When only micronized APIs are present in the formulation alone or in presence of fine lactose, studies have suggested that the liberation of fine particles < 6 µm shows a sigmoidal trend with increasing airflow rate and a three-parameter sigmoidal equation has been used [220] as shown in equation (4.1):

$$y = \frac{a}{1+e^{-(x-x0)/b}} \tag{4.1}$$

With ‘a’ = maximum extent of deagglomeration, ‘x0’ = flow rate required to achieve 50% deagglomeration and ‘b’ = change in the deagglomeration with the flow rate.

However, the problem occurs when the coarse lactose is added to the formulation. Higher flow rates are required to deaggregate the mixture fully than if the lactose carrier was not present. Therefore, more energy is required to fully aerosolize micronized APIs away from the surface of the carrier. An equation similar to the Langmuir adsorption isotherm was proposed with the name of Powder Aerosol Deaggregation Equation (PADE, equation 4.2) [221]:

$$\frac{FPF}{FPF_{max}} = \frac{k_d \tau_s}{1+k_d \tau_s} \tag{4.2}$$

With FPF_{max}= FPF at maximum shear stress, τ_s=shear stress, k_d = deagglomeration constant. However, the latter equation implies that a cascade impactor should be used for the experiments affecting the deagglomeration of the particles. Moreover, Behara *et al*. [220] used the Rotohaler for the experiments, allowing the design of the DPI to affect the deagglomeration.

Adding a fine ternary agent to the formulation could be an important consideration for guiding formulation design, and may affect formulation suitability for the cyclone spacer. The spacer showed variable behaviour with different design of the DPIs and different formulations as shown by the PSD (particle size distribution) of SS and SX emitted from the Cyclohaler® and Seretide/Accuhaler® in Chapter 3. Perhaps, Cheng 2 only works with a particular device such as the Cyclohaler and the difference in the deagglomeration mechanism seen in Chapter 3 would not be present if the formulation was emitted from the same inhaler into the spacer, despite testing different APIs (active pharmaceutical ingredients). Studies [213, 220, 222] have been performed on the deagglomeration mechanism of micronized particles. Although these studies suggested a rapid methodology using laser diffraction, the models proposed to explain the deagglomeration process did not show any parameter with a physical meaning. This would be helpful to predict deagglomeration mechanisms of novel formulation and, particularly for the current study, to understand the impact of formulation design prior entering the cyclone-spacer.

4.2. Aims

Chapter 3 showed different behaviour for SS and SX formulations when emitted from the spacer. The Cheng 2 was still able to retain large agglomerates for carrier based commercial DPIs, however, the SS formulation showed a much reduced IP/PS deposition than the SX formulation when the spacer was used. The aim of the current chapter was to characterise and assess SS and SX in formulation with different grades of lactose in order to understand the deagglomeration behaviour of the API when emitted from the Cyclohaler® and its importance on performance of the spacer. This was done to assess whether the deagglomeration within the spacer was affected by the design of the device only or by the physico-chemical and blend properties of the formulation.

The objectives of the current work were:

- To prepare in-house manufactured blends of particles reported in the literature to be cohesively or adhesively balanced particles (SX and SS, respectively) with different grades of lactose carrier (fine lactose, coarse lactose and combination of both).
- To assess blend aerosolization with and without Cheng 2 using only the Cyclohaler®
- To characterize the blend morphology and particle distribution after aerosolization with scanning electron microscopy (SEM)
- To study the deagglomeration process of cohesively and adhesively balanced blends using an iterative empirical model

4.3. Materials and methods

4.3.1. Materials

Micronized salbutamol sulphate (SS, batch number B027798) was obtained from GlaxoSmithKline Research and Development (Ware, UK). Salmeterol xinafoate (SX)

was purchased from Vamsi Labs Ltd (Solapur, India). Lactose monohydrate, chromatography grade methanol, hydrochloric acid solution (HCl) 5M, sodium hydroxide and n-Hexane were purchased from FisherScientific (Loughborough, UK). Fine lactose (LH300) was a gift from Friesland Foods (The Netherlands). Hipersolv® grade ammonium acetate was purchased from Lab3 Ltd (Northampton, UK). A Luna 3 µm C18 column (150 mm x 4.6 mm x 3 µm) was obtained from Phenomenex (Macclesfield, UK). Silicone oil - Dow Corning Corporation 200® fluid was obtained from Sigma-Aldrich (Gillingham, UK). A Cyclohaler® device was obtained from AAH Hospital Supplies (Coventry, UK). Size 4 hard gelatine capsules were obtained from Meadow Laboratories Ltd. (Romford, UK). Cyclone spacer (Cheng 2) was manufactured in-house (University of Cambridge, UK) from a Perspex block (Engineering & Design Plastics Ltd, Cambridge, UK. The flow meter (model number DMF2), next generation impactor (NGI) and a model HCP5 vacuum pump were all purchased from Copley Scientific Ltd (Nottingham, UK). Adhesive carbon tabs and aluminium pin stubs were purchased from Agar Scientific Ltd (UK).

4.3.2. Preparation of API-blends

4.3.2.1. Lactose monohydrate sieving

Lactose monohydrate (Fisher Scientific, UK) was sieved to separate the 63-90 µm particle fractions. The lactose powder was placed on the 90 µm sieve which was above the 63 µm sieve and the mechanical sieve shaker (model - AS 200 digit, Retsch, Germany) was operated for 5 min at 100 amplitudes. The fraction of lactose between the sieves was collected to prepare the blends.

4.3.2.2. Particle size analysis

Salbutamol sulphate (SS), fine lactose (FL) salmeterol xinafoate (SX) and coarse lactose (CL) were tested for the homogeneity of the particle size using the laser diffraction technique. The Sympatec Rodos module (Inhaler Helos/KF, Sympatec Limited, Bury, UK) with Aspiros feeder was used. The speed of the feeder was set at 25 mm/sec. The pressure drops used were 2 and 4 bar in order to have a titration of the size and the duration of the measurements was 5 sec. The optimum concentration of the powder to be detected was in the range of 1.0 and 1.1 %.

4.3.2.3. Blend preparation

A total of 3 g of blends were prepared. The drug was sandwiched with coarse lactose (CL) in equal volumes. When the FL was used, it was first blended with the drug and the pre-mixture sandwiched with coarse lactose. Glass vials were used for the blending and vortexed (Vortex Genie 2, model G – 560E, Scientific Industries LTD, New York) for 2 min. The blending was carried out in a Turbula mixer (Turbula 2583, type +2C, Glen Mills, Clifton) for 40 min. In **Error! Reference source not found.** eights of the components and ratios are reported for all the blends.

Table 4.1. Blend preparation with ratios (API= active pharmaceutical ingredient, CL=coarse lactose, FL=fine lactose, SX=salmeterol xinafoate, SS= salbutamol sulphate)

Blend	Ratio (w/w)	Drug	Mass (g)
API:CL	1:67.5	SS or SX	0.044
		CL	2.970
API:FL:CL	1:4:63.5	SS or SX	0.044
		FL	0.176
		CL	2.794
API:FL	1:4	SS or SX	0.600
		FL	2.400

4.3.2.4. Dose content of the blends

Five samples of each blend were prepared by accurately weighing ~0.0125 g of each blend with dissolution into 20 ml of the respective mobile phase (Chapter 2, Section 2.3.3 and Chapter 3, Section 3.3.3). The concentration of the drugs was detected by HPLC assay (Chapter 2, Section 2.3.3 and Chapter 3, Section 3.3.3) and the dose content calculated using Equation (4.3) in order to identify the amount of drug per dose (µg/dose, where the capsule fill weight was ~0.0125 g):

$$\text{Dose content} = \frac{\text{mass of drug (µg)}}{\text{mass of blend (mg)}} \quad (4.3)$$

4.3.3. Impaction studies using Next Generation Impactor

Each blend was tested using the Cyclohaler® at 2 and 4 kPa with and without Cheng 2 according to Section 3.3.5. Prior to performing the measurements with the

NGI, the desired flow rate was adjusted with a flow meter. Prior the measurement, 15 ml of mobile phase was added in the central cup of the pre-separator. When the Cyclohaler® was assessed alone with blends with either CL or FL:CL, six Size 4 hard gelatin capsules were used. When the Cheng 2 was employed as spacer device, 12 capsules were actuated at 2 kPa and eight capsules at 4 kPa. When the drug:FL ratio was assessed with the Cyclohaler®, two capsules were actuated at both pressure drops and four when the Cheng 2 was employed. In order to collect the drugs, the DPIs were washed with 20 ml of mobile phase. The bottom of the cyclone was washed with 100 ml of mobile phase and the mouthpiece and the USP throat with 25 ml each; whilst the upper section of the cyclone was washed with 10 ml. For collecting the drugs from the pre-separator 100 ml of mobile phase was used. The volumetric flasks were sonicated (Kerry, Germany) for 2 min. When only the Cyclohaler® was employed, 10 ml of mobile phase were added at the first 5 stages, whilst 5 ml of solvent was used for the last 3 stages. All the stages were set on a laboratory rocker (Stirling Mixer, Sandrest Ltd, UK) and rocked for 2 min in order for the solvent to clean the entire surface. When the cyclone was used, 5 ml of mobile phase was added to all the stages. The concentrations of the drugs from each stage were determined by HPLC assay as described in Chapter 2, Section 2.3.3 and Chapter 3, Section 3.3.3. After performing the experiments, each stage and the NGI were thoroughly cleaned with Millipore water and the coating was removed with acetone before rinsing with methanol.

4.3.4. Particle size analysis

4.3.4.1. Laser diffraction analysis with Inhaler Module

Aerosolization was also assessed by laser diffraction particle size analysis using the Sympatec Inhaler module as described in Chapter 3 Section, 3.3.8.

4.3.4.2. Dry dispersion laser diffraction analysis with Rodos

The particle size distribution (PSD) of the blends was tested by laser diffraction using the Sympatec Rodos module (Sympatec Limited, UK) with Aspiros feeder. The lens used to detect the aerosol cloud was a R3 lens (0.5-175 µm). The speed of the feeder was set at 25 mm/sec and the duration of the measurement was 5 sec with optical concentration between 0.1-1.1 %. The pressure drop was set between 0.1 to

5 Bar in order to titrate the dispersion pressure. The PSD vas collected every 0.1 Bar when tested from 0.1-1 Bar and every 1 Bar when tested from 1-5 Bar.

4.3.4.3. Liquid dispersion laser diffraction analysis with Malvern Mastersizer

To measure the 'true' fully dispersed particle size, the blends were suspended in 0.5% Span 80 in cyclohexane (for SX blends, SX, FL, CL) and 1% Span 80 (for SS blends and SS). Malvern Mastersizer X (Malvern Instruments Ltd, UK) was used [213] with 100 mm focal length lenses (0.5-180 µm) and MS7 magnetically stirred cell. Prior to measurement, the solvents were saturated with the appropriate particles and sonicated for 30 min followed by overnight stirring. For the measurements, approximately 1 mg of powder was added to 2 ml filtered dispersant (0.2 µm cellulose acetate syringe filter, Sartorius Stedim Biotech., UK) and sonicated (Sonicleaner, DAWE, Ultrasonics Ltd, USA) for 1 min for SS, FL and CL and 5 min for SX. The stirring was set at 3 for all the powders with sweeps of 2500 for SX and 3500 for the other powders. A background reading was taken and the suspension was added to the sample cell until the obscuration was 10–30%. Following equilibration (60 s for SX and 30 s for the others), ten individual measurements were taken for n = 3 samples. From the instruments, Dv_{10}, Dv50, and Dv_{90} (corresponding to the cumulative percentage particle undersize values for 10%, 50% and 90% of the particles by volume), and the % volume < 5 µm were used for analysis.

4.3.5. Particle morphology

4.3.5.1. Preparation of the powder

Powder samples were transferred to adhesive carbon tabs, mounted onto aluminium pin stubs (Agar Scientific Ltd, England).

4.3.5.2. Collection of the powder from the impactor

Each blend was tested using the Cyclohaler® at 4 kPa with and without Cheng 2. Prior to performing the measurements with the NGI, the desired flow rate was adjusted with a flow meter. To collect the drug from the USP throat, a glass coverslip (diameter 12 mm, Scientific Laboratory Supplies, Nottingham, UK) was attached with a double side adhesive tape in the 90° angle. Glass coverslips of 22 mm diameter

were used for the pre-separator (placed in the middle of the collection cup), and stage 3 and 5 of the NGI (to represent the respirable fraction size range). The powder was then transferred to an adhesive carbon tab. When the Cyclohaler® was assessed alone with blends with either CL or FL:CL, six Size 4 hard gelatine capsules were used. The powder was collected from the capsules and transferred to an adhesive carbon tab. When the Cheng 2 was employed as spacer device, eight capsules were actuated. When the drug:FL ratio was assessed with the Cyclohaler®, two capsules were counted and 4 when the Cheng 2 was employed. The powder was collected from the bottom of the cyclone and transferred to an adhesive carbon tab.

4.3.5.3. Particle morphology using the scanning electron microscopy

To assess blend interactions, scanning electron microscopy (SEM, Jeol Carry Scope JCM 5700, Welwyn Garden City, UK) was performed. Samples were sputter coated with gold under argon for 4 min to achieve a thickness of approx. 30 mm using an Emitec SC 7620 coater (Quorum Technologies Limited, West Sussex, England). To view the particle morphology, the SEM operated at 15 kV in low vacuum mode and a working distance of 13 mm.

4.3.6. Statistical analysis

Statistical analysis was performed in Minitab (version 15) using one-way ANOVA and post-hoc Tukey's test (multiple comparisons) or Student's two-tailed t-test for pair-wise comparisons, both at 95 % confidence intervals. Non-linear regression analysis of the powder dispersion data was performed using OriginPro (ver. 8) and MatLab software (ver. R2013a). Data analysis from aerosolization studies has been done according to Chapter 2, Section 2.3.11.

4.4. Results

4.4.1. Preparation of API-blends

4.4.1.1. Particle size analysis

Due to the high variability of IP/PS deposition with the Seretide/Accuhaler™ formulation and the different deagglomeration behaviour compared to Cyclohaler/SS® when the Cheng 2 (Chapter 3) was employed, a deeper investigation was carried out. Two different APIs were taken into consideration: adhesively- and cohesively-balanced blend (SS and SX, respectively according to literature search) with lactose. The two drug were blended with different grades of lactose (FL, CL or combination of both) in order to understand the deagglomeration process that might occur within the cyclone. Both the APIs and the FL were micronized as detected by the laser diffraction Figure 4.1). However, the coarse lactose showed a small shoulder in the fine particle size range due to the presence of fine lactose already present in the coarse carrier formulation (Figure 4.2).

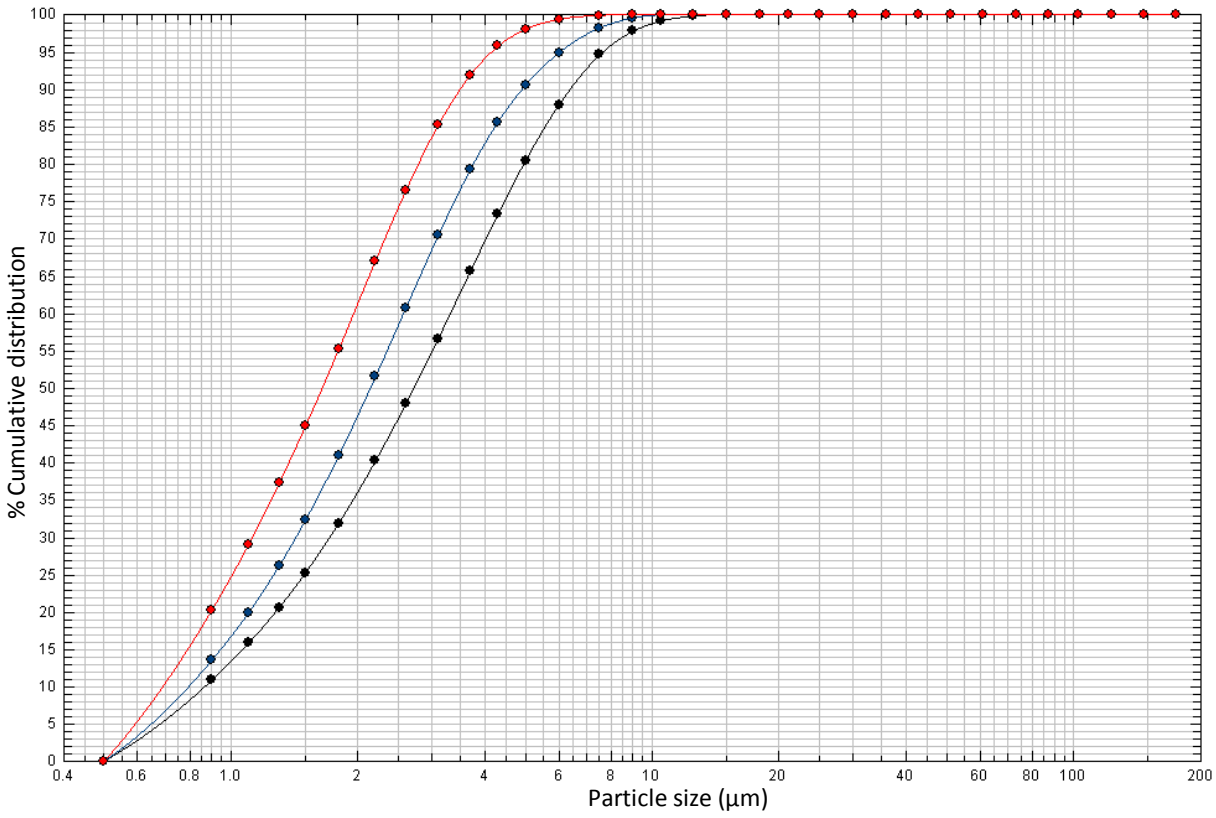

Figure 4.1. Representative particle size distributions for salbutamol sulphate (●), salmeterol xinafoate (●) and micronized lactose (●).

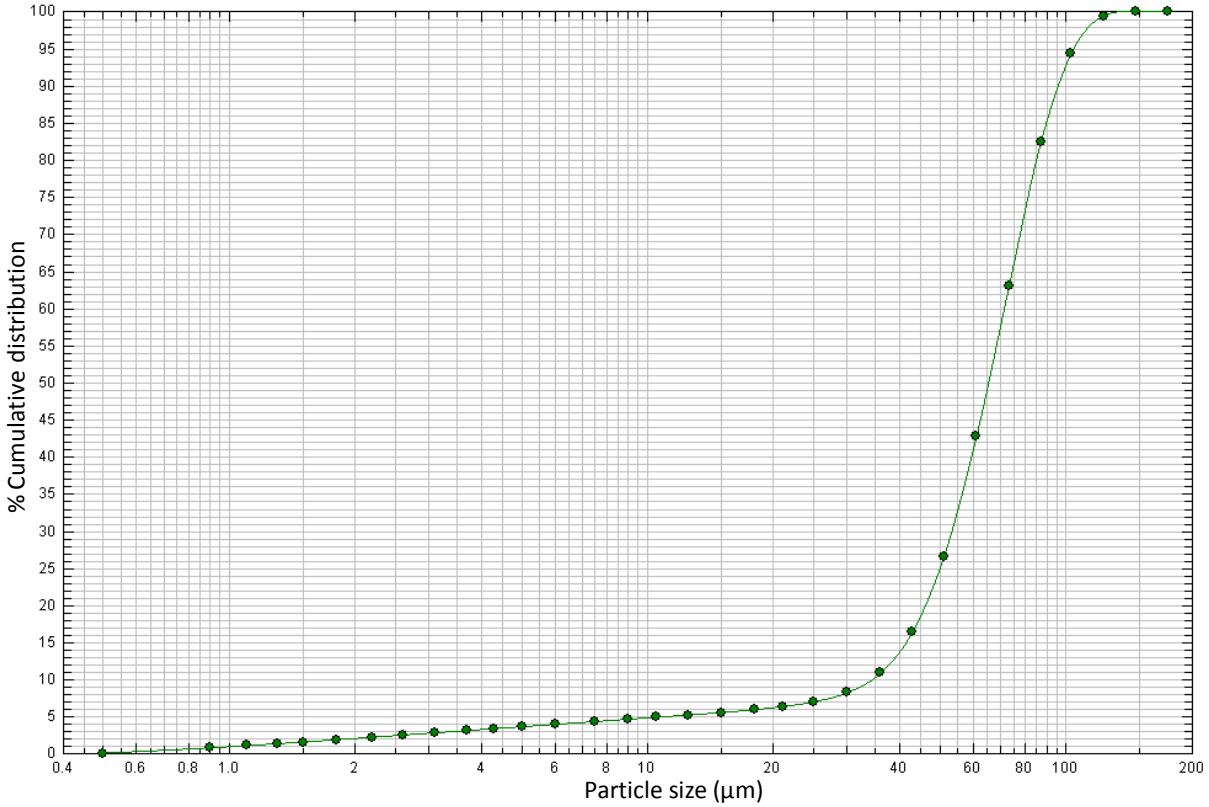

Figure 4.2. Representative particle size distribution for coarse lactose (●).

The DV50 at 4 kPa were: 1.65 ± 0.01 µm for SS, 2.14 ± 0.01 µm for SX, 2.72 ± 0.04 µm for LH300, 65.78 ± 0.44 µm for coarse lactose.

4.4.1.2. Dose content of the blends

In Table 4.2 the dose content for each blend is shown with the coefficient of variance expressed as percentage (%CV). The %CV for all particles, with the exception of SS:FL and SX:FL:CL was acceptable. For the latter blends, replicates were made (n≥5) in order to understand the variance.

Table 4.2. Dose content for all blends with coefficient of variance (CV) (mean ± SD, n ≥ 5). (SS= salbutamol sulphate, CL=coarse lactose, FL= fine lactose, SX=salmeterol xinafoate).

Blends	Ratio	Dose content (µg/mg)	% CV (n>5)
SS:CL	1:67.5	14.41 ± 0.16	1.31
SS:FL:CL	1:4:63.5	15.41 ± 0.28	1.35
SS:FL	1:4	212.32 ± 12.60	5.94
SX:CL	1:67.5	14.42 ± 0.05	0.32
SX:FL:CL	1:4:63.5	14.93 ± 0.79	5.32
SX:FL	1:4	197.43 ± 6.25	3.17

4.4.2. Impaction studies using next generation impactor

Aerosolization studies were performed on the blends with and without Cheng 2 and emitted from the Cyclohaler®. The pressure drops used were 2 and 4 kPa as per Chapter 3. The % recovery of all the blends was adequate and within the limits of 75 and 125 % as recommended by the British Pharmacopoeia (e.g. 91.52 ± 2.20% for SS:FL:CL at 2kPa using the Cyclohaler® and 78.92 ± 4.63% for SX:CL at 4 kPa with the cyclone added at the Cyclohaler®). As seen already in Chapter 3, the retention of the drug within the cyclone was high especially for the blend with fine lactose only (e.g. 95.76 ± 0.67 % and 96.83 ± 0.34 % for SS and SX). Cohesively-balanced formulations (SX) demonstrated higher emission from the Cheng 2 than adhesively-balanced blends (SS) especially for drug:FL:CL blends at 4 kPa: 2.54 ± 0.47% for SS:FL, 10.25 ± 3.85% for SS:CL and 22.86 ± 4.30 % for SS:FL:CL vs. 1.71 ± 0.36 % for SX:FL, 16.30 ± 3.25 % for SX:CL and 30.64 ± 10.44 for SX:FL:CL ($p<0.05$).

When the Accuhaler™ was previously assessed a high IP/PS deposition was still seen when the cyclone was employed (Chapter 3, Section 3.4.4). The comparison between SS and SX blends confirmed the finding (Table 4.3). IP/PS deposition for the cohesively-balanced SX formulation was almost double that of adhesively-balanced SS blends when only coarse lactose was used as carrier with Cheng 2 was in place (Table 4.3). However, when FL was added to the formulation, a similar IP/PS deposition was seen for both SS and SX blends.

Table 4.3. Induction port/pre-separator (IP/PS) deposition of all the blends emitted from the Cheng 2 at 2 and 4 kPa (mean ± SD, n > 3). (ED = emitted dose).

Blends	Ratio	Pressure drop (kPa)	IP/PS deposition (% ED)	Pressure drop (kPa)	IP/PS deposition (% ED)
SS:CL	1:67.5	2	32.52 ± 9.24	4	29.65 ± 4.82
SS:FL:CL	1:4:63.5		24.24 ± 16.45		15.53 ± 2.25
SS:FL	1:4		0.00 ± 0.00		0.00 ± 0.00
SX:CL	1:67.5		46.56 ± 13.51		58.71 ± 8.30
SX:FL:CL	1:4:63.5		24.53 ± 2.90		21.74 ± 1.66
SX:FL	1:4		0.00 ± 0.00		0.00 ± 0.00

The greater IP/PS deposition for SX blends led to a decreased fine particle fraction compared to SS blends. The aerodynamic PSD at 2 kPa (Figure 4.3, A) showed that the blends with coarse lactose containing SS released a higher respirable fraction of the particles < 5 µm compared to the blends containing SX regardless of the device used to deliver the dose (e.g. Cheng 2 vs. Cyclohaler). Moreover, as reported in Figure 4.3, B an increased % of the FPF was seen for both API when FL was added at the formulation (Figure 4.3, B). The same trend was observed at 4 kPa (Figure 4.4, A-B). The difference in the FPF for both materials when either the Cheng 2 or the Cyclohaler was used decreased when fine lactose was employed in the formulation.

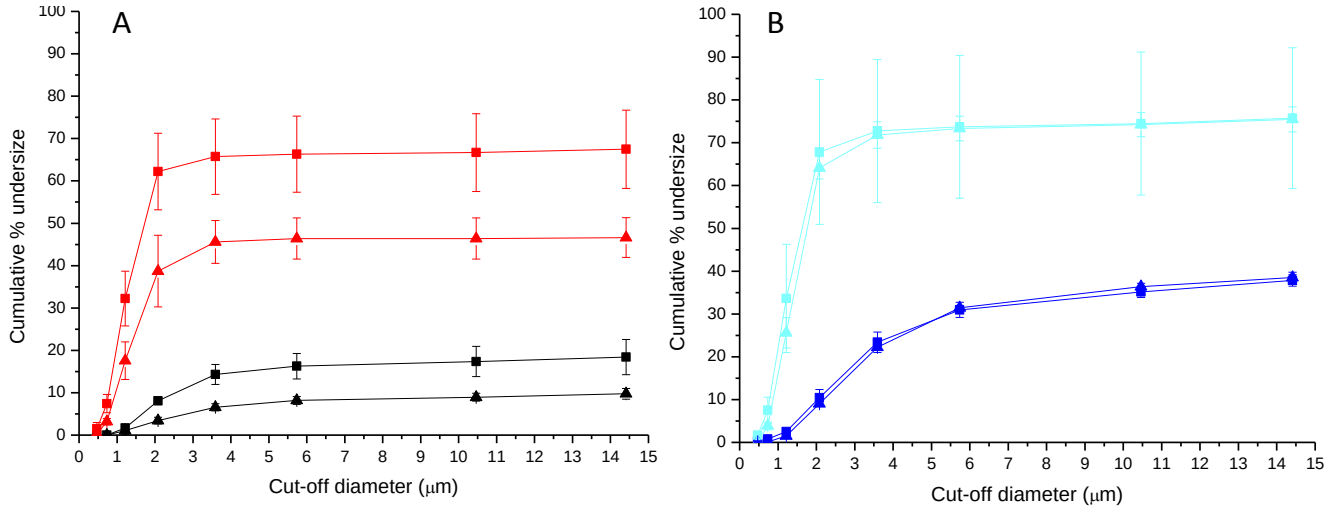

Figure 4.3. Particle size distribution expressed as cumulative % undersize (%) of the emitted dose of SS:CL (■-Cyclohaler, ■-Cheng 2), SX:CL (▲-Cyclohaler, ▲-Cheng 2), (A) and of SS:FL:CL (■-Cyclohaler, ■-Cheng 2), SX:FL:CL (▲-Cyclohaler,▲-Cheng 2), (B) at 2 kPa (mean ± SD; n > 3).

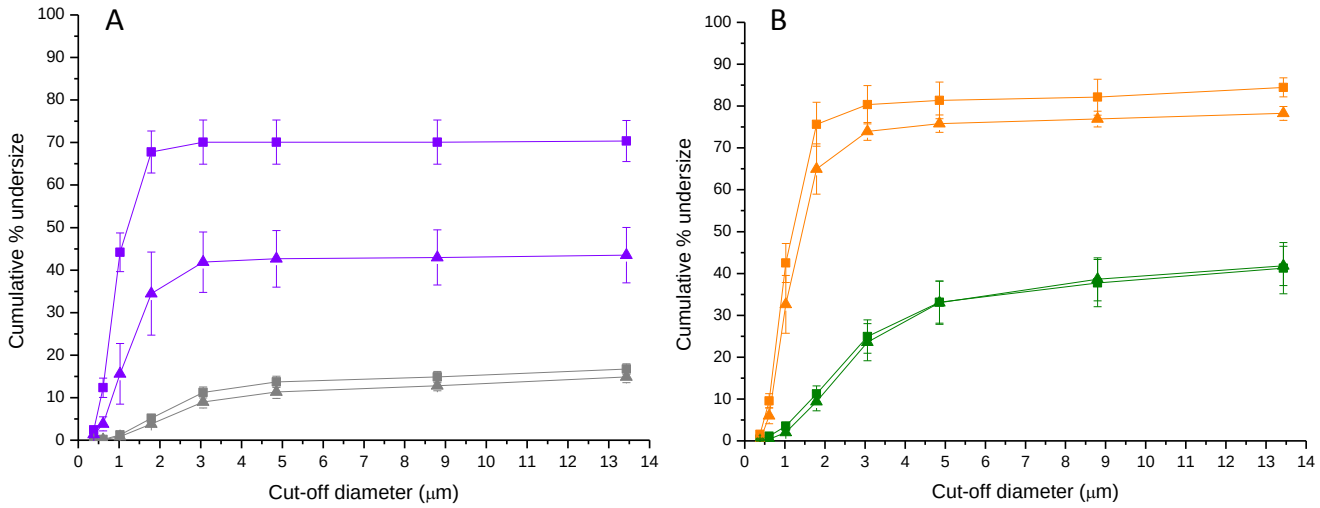

Figure 4.4. Particle size distribution expressed as cumulative % undersize (%) of the emitted dose of SS:CL (■-Cyclohaler, ■-Cheng 2), SX:CL (▲-Cyclohaler,▲-Cheng 2), (A) and of SS:FL:CL (■-Cyclohaler, ■-Cheng 2), SX:FL:CL (▲-Cyclohaler,▲-Cheng 2), SX (B) at 4kPa (mean ± SD; n > 3).

If the values of the fine particle fraction are analysed, SS blends showed a higher FPF than SX ($p<0.05$). However, the FPF is a metric of a proportion of the particles below a certain size (e.g. 5 μm) and does not provide a clear explanation on the PSD like the Figure 4.3 and Figure 4.4. When the highest flow rates are taken into account, a higher FPF was seen only for SX:FL, whilst the remaining blends for SS show an improvement compared to the other SX blends in the FPF. The ratios of fine particles with size < 1.5 μm are more important to consider as they might explain the propensity and extent of deagglomeration of the blend within the cyclone. The FPRs < 1.5 μm (FPR1.5) were calculated as a measure of quantifying emission of particles below the cut-off diameter of the cyclone (i.e. 2 μm) according to Equation (3.2) (Table 4.4).

Table 4.4. Fine particle fraction (FPF) below 5 µ, and fine particle ratios (FPR) below 1.5 µm of SX and SS blends emitted from the Cheng 2 with different grade of lactose

Blends	Ratio	Pressure Drop (kPa)	$FPF_{5\mu m}$ Ex-Cheng 2 (% sED)	$FPR_{1.5\mu m}$ (ED)
SS:CL	1:67.5	2	65.53 ± 8.99	1.45 ± 0.31
SS:FL:CL	1:4:63.5		72.68 ± 16.83	2.01 ± 0.52
SS:FL	1:4		85.39 ± 0.99	1.03 ± 0.27
SS:CL	1:67.5	4	70.14 ± 5.15	1.97 ± 0.22
SS:FL:CL	1:4:63.5		81.83 ± 4.11	2.18 ± 0.18
SS:FL	1:4		86.45 ± 3.02	0.43 ± 0.32
SX:CL	1:67.5	2	45.83 ± 5.03	2.34 ± 0.61
SX:FL:CL	1:4:63.5		71.76 ± 2.80	2.82 ± 0.24
SX:FL	1:4		94.54 ± 1.01	0.87 ± 0.27
SX:CL	1:67.5	4	43.06 ± 6.88	1.67 ± 0.49
SX:FL:CL	1:4:63.5		76.66 ± 1.35	3.44 ± 0.34
SX:FL	1:4		91.27 ± 12.28	0.37 ± 0.20

Despite the higher IP/PS deposition, a cohesively-balanced blend with fine lactose added to coarse carrier improved deagglomeration within the cyclone. Also, blends with the carrier showed a higher FPF and FPR for both SS and SX compared to blends with only fine lactose. Therefore, blends should have CL present in the formulation to enhance deagglomeration in the cyclone.

4.4.3. Particle size analysis

4.4.3.1. Laser diffraction analysis with inhaler module

The LDA was performed on the SS and SX blends with different grades of lactose. When the fine lactose was present in the blends, the % of particles emitted with a size < 5µm increased compared to the blends with only coarse lactose (Table 4.5).

Table 4.5. Table of values for % of particles with size < µm emitted from the blends when Cyclohaler® and Cheng 2 were used (mean ± SD, n=3).

Cyclohaler	Ratio	Pressure drop (kPa)	% < 5µm	DV50 (µm)
SS:CL	1:67.5	2	4.64 ± 1.20	63.31 ± 1.57
SS:FL:CL	1:4:63.5		12.6 ± 2.00	60.11 ± 0.37
SS:FL	1:4		52.90 ± 3.07	4.74 ± 0.28
SX:CL	1:67.5		4.31 ± 0.91	67.94 ± 4.17
SX:FL:CL	1:4:63.5		17.05 ± 0.42	53.29 ± 1.55
SX:FL	1:4		52.76 ± 3.62	4.76 ± 0.33
SS:CL	1:67.5	4	5.39 ± 0.56	64.86 ± 1.71
SS:FL:CL	1:4:63.5		22.51 ± 1.57	50.20 ± 1.12
SS:FL	1:4		68.76 ± 3.24	3.59 ± 1.14
SX:CL	1:67.5		5.79 ± 1.84	66.61 ± 2.40
SX:FL:CL	1:4:63.5		15.37 ± 0.65	55.36 ± 1.13
SX:FL	1:4		61.66 ± 2.26	3.95 ± 0.21
Cyclone	**Ratio**	**Pressure drop (kPa)**	**% < 5µm**	**DV50 (µm)**
SS:CL	1:67.5	2	98.65 ± 2.33	1.96 ± 0.04
SS:FL:CL	1:4:63.5		100.00 ± 0.0	1.81 ± 0.12
SS:FL	1:4		100.00 ± 0.0	1.64 ± 0.12
SX:CL	1:67.5		100.00 ± 0.0	1.83 ± 0.04
SX:FL:CL	1:4:63.5		100.00 ± 0.0	1.50 ± 0.12
SX:FL	1:4		100.00 ± 0.0	2.05 ± 0.01
SS:CL	1:67.5	4	100.00 ± 0.0	1.65 ± 0.36
SS:FL:CL	1:4:63.5		100.00 ± 0.0	1.19 ± 0.04
SS:FL	1:4		100.00 ± 0.0	1.26 ± 0.03
SX:CL	1:67.5		100.00 ± 0.0	1.26 ± 0.08
SX:FL:CL	1:4:63.5		100.00 ± 0.0	1.26 ± 0.04
SX:FL	1:4		100.00 ± 0.0	1.49 ± 0.04

When the cyclone was employed an improved deagglomeration occurred at the highest flow rate. The LDA confirmed that the blends that contained fine lactose released the finest aerosol compared to other blends ($p<0.05$) (Table 4.5). However, a change in size with the Cheng 2 in place was seen between the blends. The blends with CL showed a greater Dv50 at 2kPa ($p<0.05$, Table 4.5). The Dv50 for the blends with carrier when emitted from the Cyclohaler at 2 and 4 kPa were unchanged regardless the formulation (e.g. Dv50 for SS:FL:CL was 50.20 ±1.12 µm at 4 kPa, whilst the Dv50 for SX:FL:CL was 55.36 ± 1.13 µm at 4 kPa). On the other hand, when CL was absent from the formulation and only FL was used, the Dv50 of the blends emitted from the Cyclohaler was 3.59 ± 1.14 µm and 3.95 ± 0.21 µm at 4 kPa for SS:FL and SX:FL, respectively.

4.4.3.2. Dry dispersion laser diffraction analysis

SX and FL showed a bi-modal distribution at 0.5 bar, indicating a fraction of poorly dispersed agglomerates (Figure 4.5, A and B) due to the low force applied to deaggregate the mixture. However, SS showed the same behavior also at 1 bar (Figure 4.5, C), indicating a poorer deagglomeration response of the agglomerates compared to the previous FL particles.

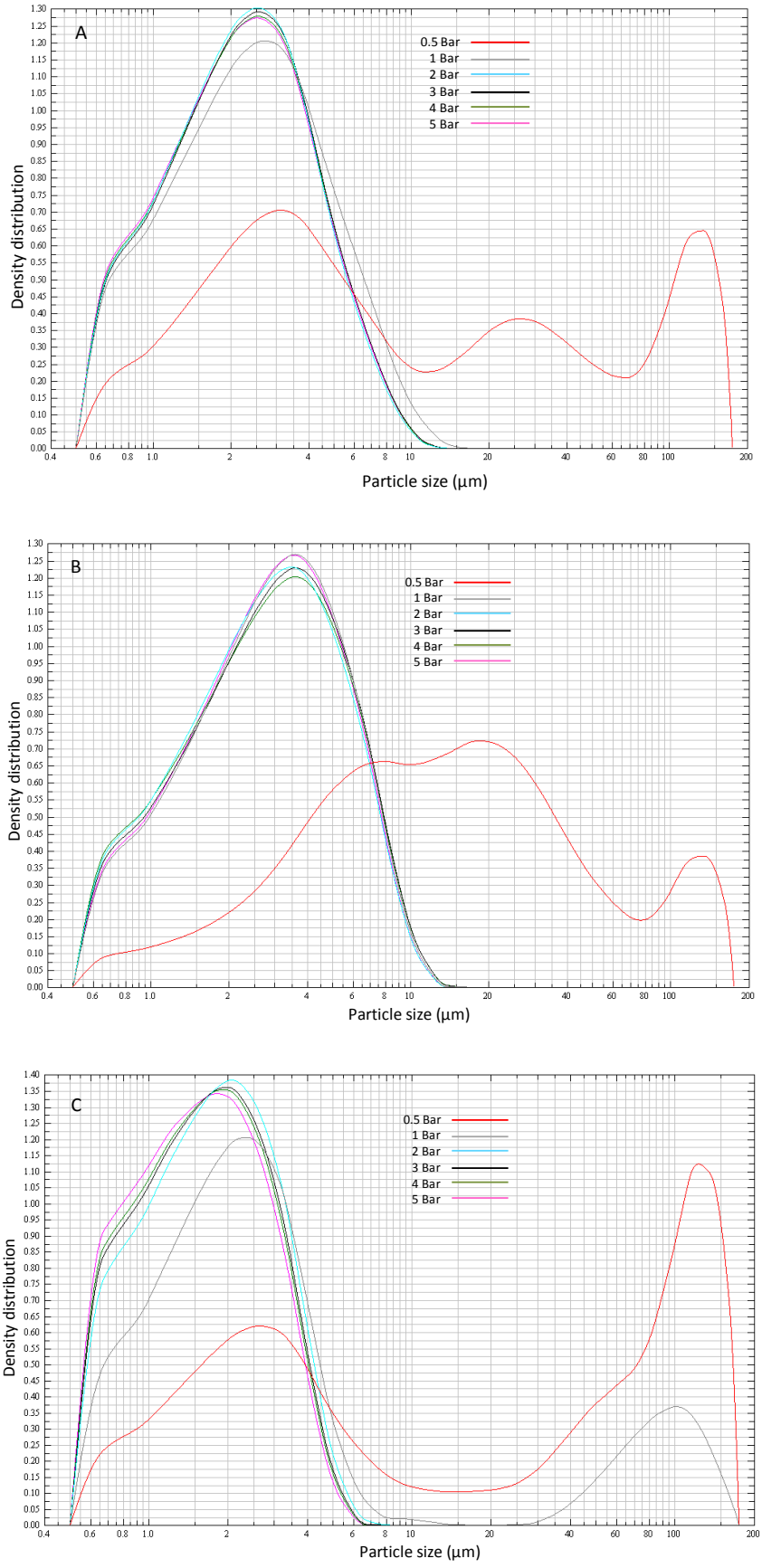

Figure 4.5. Density distribution of size of salmeterol xinafoate (A), fine lactose LH300 (B) and salbutamol sulphate (C) between 0.5 and 5 Bar.

When FL was added to SX or SS, the same trend of bi-modal distribution was observed at 0.5 Bar (Figure 4.6, A and B). However, SS:FL showed a much bigger shoulder in the 100 µm range than SX:FL (Figure 4.6, A) at low pressure, due to the more strongly cohesive forces of the agglomerates detected for SS alone compared to SX. However, the addition of FL enhanced deagglomeration of SS as at 1 Bar, as a monomodal distribution is detected (Figure 4.6, A) compared to when SS was tested alone at 1 Bar.

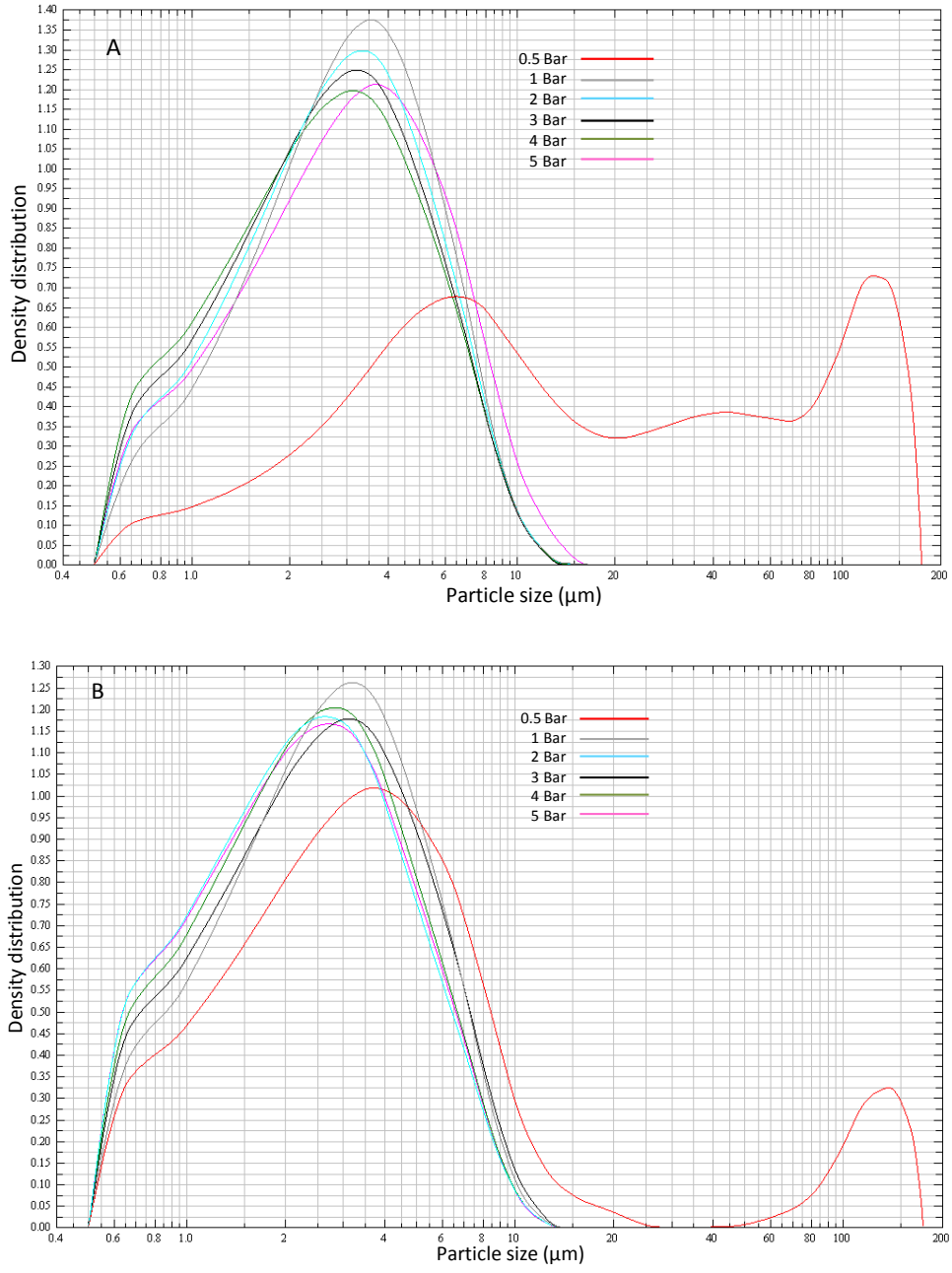

Figure 4.6. Density distribution of size of salbutamol sulphate: fine lactose blends (A) and salmeterol xinafoate: fine lactose blend (B) between 0.5 and 5 Bar.

A larger particle size mode (seen already for the blends of micronized particles) was observed for the blends with either CL or FL:CL (Figure 4.7, A). However, when FL was added to the formulation API:CL, a shift towards the respirable range was seen due to a greater amount of fine particles present in the mixture (Figure 4.7, B).

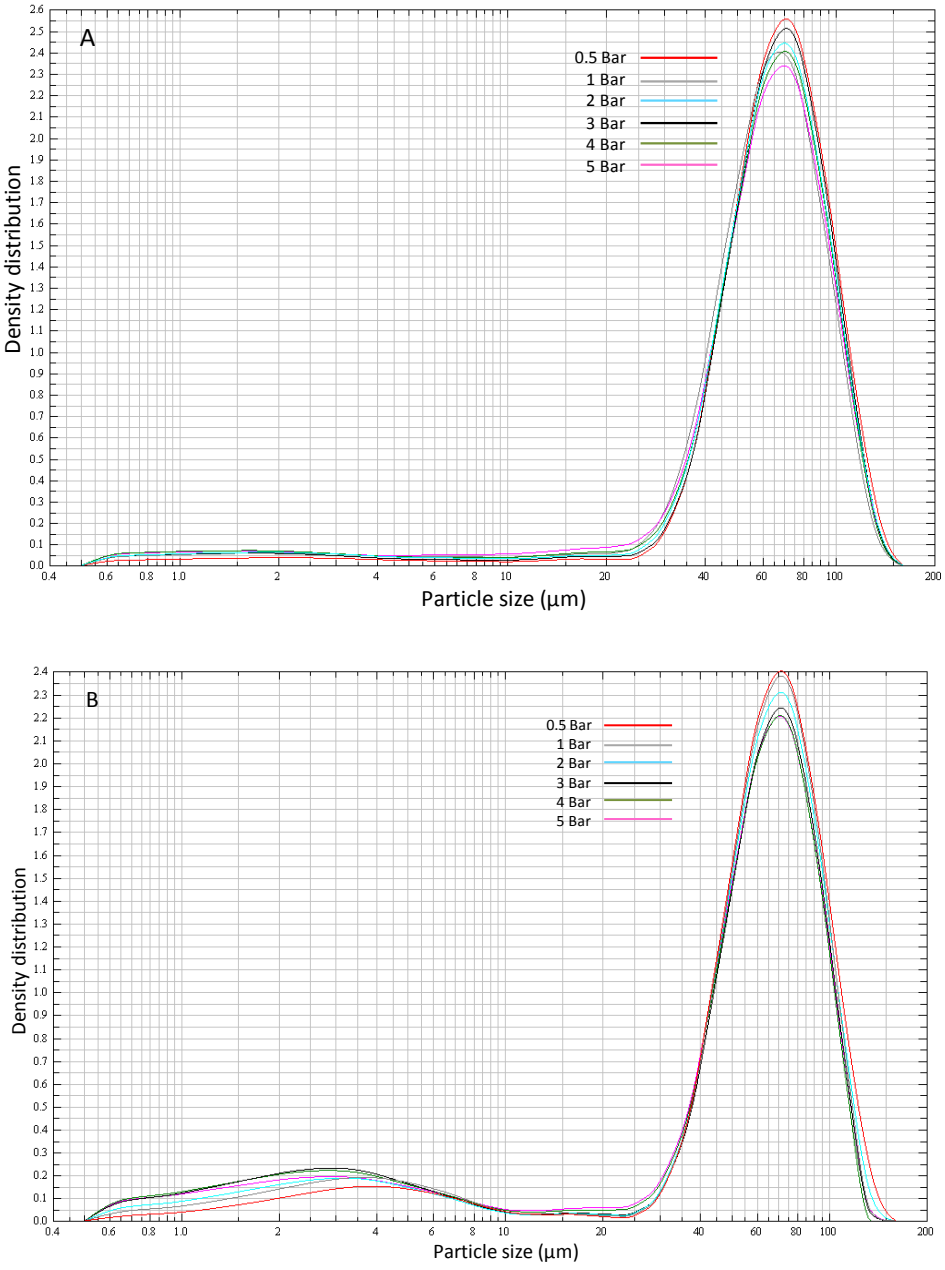

Figure 4.7. Density distribution of size of salbutamol sulphate: coarse lactose blend (A) and salmeterol xinafoate: fine lactose: coarse lactose blend (B) between 0.5 and 5 Bar.

The bimodal distribution of certain blends was attributed to the presence of coarse carrier in the formulation that, when pressure was applied led to a release of easily dispersible agglomerates (fine particles) and a poorly dispersible fraction of large cohesive agglomerates. At high pressures there was an increase in the release of fine particles, corresponding to the increased FPF as seen in the cascade impaction study (Table 4.4). Upon increasing the pressure, the Dv50 decreased (Figure 4.8, A). For formulations with fine particles only, a plateau particle size was reached suggesting that complete particle dispersion was achieved (Figure 4.8, B).

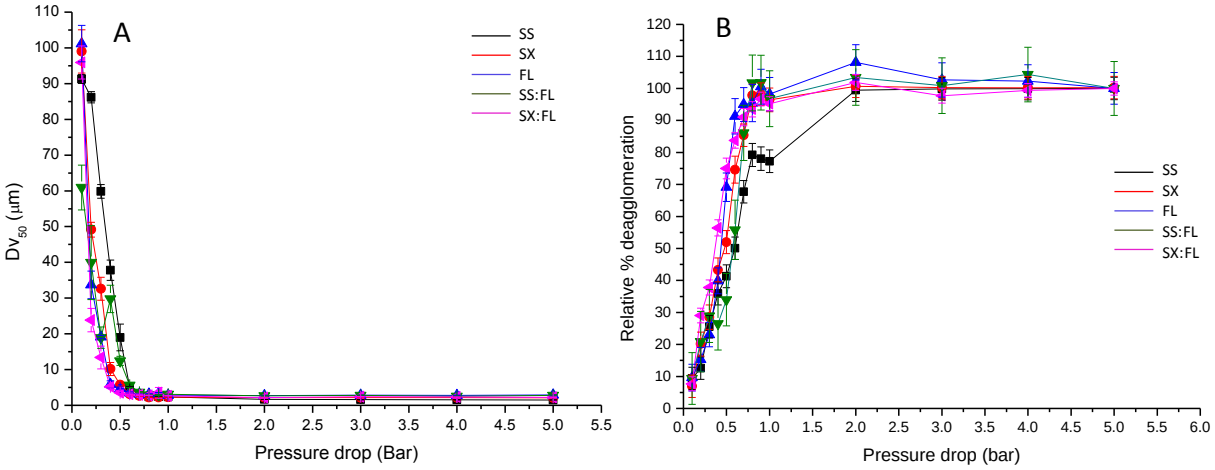

Figure 4.8. Median particle size (A) and deagglomeration behaviour (B) as a function of pressure drop for micronized salmeterol xinafoate (SX, red), salbutamol sulphate (SS, black), fine lactose (FL, blue), salbutamol sulphate: fine lactose (SS:FL, green) and salmeterol xinafoate: fine lactose (SX:FL, pink) (mean ± SD, n=3).

The descending part of the graph prior the plateau shows different deagglomeration behaviour between particles and formulations (e.g. SS vs. SX and FL in Figure 4.8, A). The difference, especially at low pressure drops, suggests variability in agglomerate size and strength as suggested from the density distributions of size in Figure 4.5. The degree of deagglomeration was calculated following Equation 4.4 [213] and plotted against the pressure drops (Figure **4.8**, B).

$$\mathrm{DA} = \frac{\mathrm{Dv}_{50}\,(\mu\mathrm{m},\ \text{fully dispersed})}{\mathrm{Dv}_{50}(\mu\mathrm{m},\ \text{primary pressure})} \tag{4.4}$$

Where DA is the degree of de-agglomeration.

The % relative deagglomeration for micronized particles could also be calculated, instead, using the model proposed by Behara *et al* [220] in Equation (4.5).

$$\mathrm{RD} = \frac{\%\ \text{volume}{<}5\mu m\ (\text{dry dispersion})}{\%\ \text{volume}{<}5\ \mu m\ (liquid\ dispersion)} * 100 \tag{4.5}$$

Where RD is the relative deagglomeration.

SX reached the maximum deagglomeration earlier than SS which, on the other hand, seemed to not reach a constant particle size at the highest pressure (Figure 4.8, B). FL instead reached the plateau at lower pressure than the other APIs. When FL was added to both APIs, an increase in the degree of deagglomeration was seen at 2 Bar, which then decreased at 3 Bar (Figure 4.8, B). This was probably due to the instability of the formulation at high pressure drops.

4.4.3.3. Liquid dispersion laser diffraction analysis

The liquid dispersion laser diffraction was used to determine the fully dispersed particle size of the API and blends. The results confirmed the dry dispersion values as the Dv50 of the blends with the carrier were shifted to higher values than when the drugs were blended with fine lactose only (Table 4.6). On the other hand, the micronized API possessed a PSD within the micron size range (Table 4.6).

Table 4.6. Particle size distribution for pure material and blends of salbutamol sulphate (SS) and salmeterol xinafoate (SX) with lactose using liquid dispersion laser diffraction (mean ± SD, n=3) (FL=fine lactose, CL=coarse lactose).

Materials	Ratio	Dv_{10} (µm)	Dv50 (µm)	Dv_{90} (µm)	Volume%<5 µm
SX	n/a	0.90 ± 0.01	3.01 ± 0.05	7.40 ± 0.33	76.15 ± 1.22
SS	n/a	1.38 ± 0.03	3.63 ± 0.05	10.02 ± 0.40	66.15 ± 0.56
LH300	n/a	1.51 ± 0.01	3.40 ± 0.07	6.76 ± 0.13	75.71 ± 1.25
SS:CL	1:67.5	4.96 ± 3.11	53.42 ± 8.75	92.76 ± 2.83	13.36 ± 6.87
SS:FL:CL	1:4:63.5	4.60 ±1.27	57.36 ± 4.07	95.24 ± 1.68	11.45 ± 2.74
SS:FL	1:4	1.38 ± 0.04	3.60 ± 0.16	9.03 ±1.07	68.76 ± 2.69
SX:CL	1:67.5	4.79 ± 3.65	56.05 ± 3.98	89.32 ± 11.57	12.50 ± 3.98
SX:FL:CL	1:4:63.5	2.11 ± 0.43	43.35 ± 12.68	84.82 ± 8.61	22.87 ± 7.76
SX:FL	1:4	1.23 ± 0.03	3.15 ± 0.06	6.73 ± 0.23	77.89 ± 0.82

When the blends containing coarse lactose were analysed equation (4.5) was used to calculate % relative deagglomeration and plotted against the pressure drop (Figure 4.9).

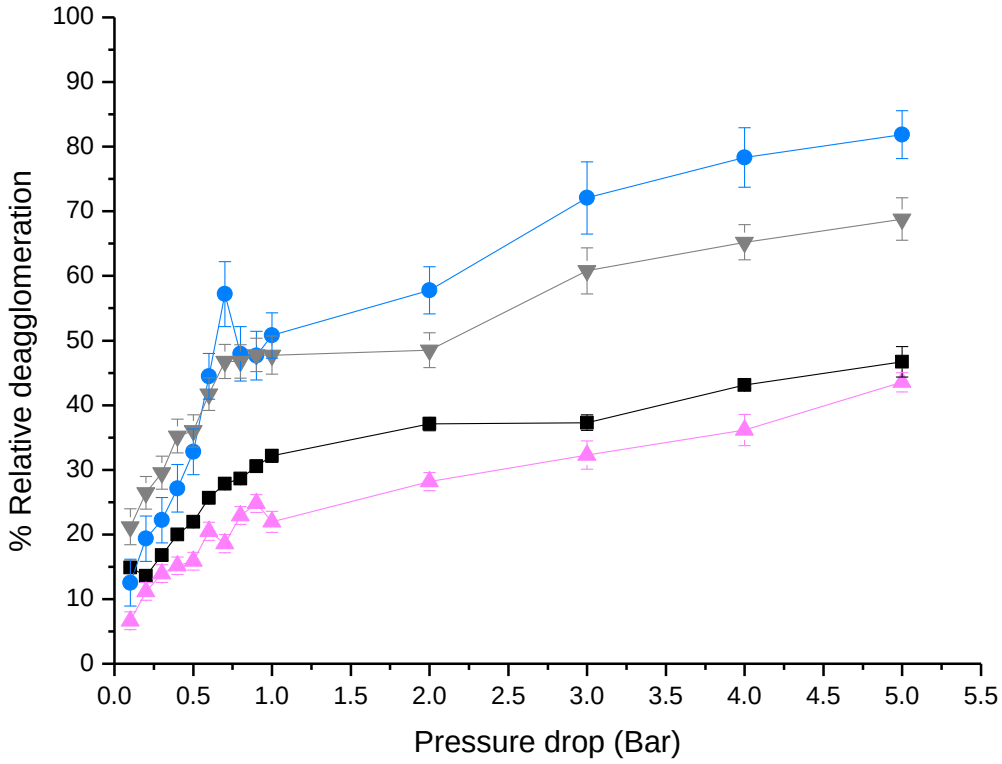

Figure 4.9. Bi-exponential distribution of the % relative deagglomeration for salbutamol sulphate and salmeterol xinafoate blended with coarse lactose (SS:CL black, SX:CL pink) and with fine lactose (SS:FL:CL blue, SX:FL:CL grey) (mean ± SD, n=3).

Unlike the micronized API and blends with FL only, the formulation containing both CL and FL or only CL did not show a plateau in the particle size. The graph shows a bi-exponential distribution with the first part showing an easily dispersed fraction and a second part showing a less easily dispersed fraction. The trend of the latter seemed to be the same for all the formulations. However, the first part of the curve shows difference in the deagglomeration behaviour of the blends. SS:CL seemed to have the steepest curve compared to the other API:CL blends. As expected, API:FL:CL blends, showed a steeper slope in the first fraction then API:CL blends (Figure 4.9).

4.4.4. Empirical model

The % relative deagglomeration for micronized particles and micronized formulations showed a mono-exponential trend when a pressure drop was applied to the agglomerates. The trend could be explained by the equation (4.6):

$$y=m(1-e^{-(x/x0)^n}) \quad (4.6)$$

The deagglomeration mechanism depends on the distribution of the APIs either alone or in combination with FL in formulation. The slope of the curve is the maximum gradient and represents how easily the deagglomeration process occurs before the drug reaches the plateau size. A plateau particle size was reached suggesting fully dispersed particles (Table 4.7; the positive asymptote or 'm' parameter).The deagglomeration behaviour can be described by the critical primary pressure at 95 % (CCP95, pressure where the degree of deagglomeration has reached 95 % of its final value) of the positive asymptote (m = maximal deagglomeration, Table 4.7). The deagglomeration response is described by ‘n’ (deagglomeration exponent) and ‘x0’, which reflect the agglomerate structure and deagglomeration mechanism. The maximum gradient of the fit (Table 4.7) defined the sensitivity of the deagglomeration response to increasing airflow. SX achieved full deagglomeration at lower pressures than SS (Table 4.7, Column CCP_{95}), whilst SS reached the maximum deagglomeration process at higher pressure compared also to FL (Table 4.7, $p<0.05$), indicating that higher pressure was needed to deaggregate SS fully. However, the addition of FL to SS improved the

deagglomeration mechanism of the latter, as shown by an increased maximum gradient (Table 4.7, $p<0.05$) and increased the exponent two-fold, indicating easier deagglomeration due to an altered agglomerate structure. On the other hand, FL reduced the deagglomeration exponent of SX (Table 4.7, $p<0.05$). Due to the high variability in the repeats, an artificial error was added when normalizing the data.

Table 4.7. Mono-exponential deagglomeration parameters for salbutamol sulphate (SS), salmeterol xinafoate (SX), fine lactose (FL) and SS-FL or SX-FL blends.

Materials	m (%)	x0 (bar)	n	Maximum Gradient (bar^{-1})	CPP_{95} (bar)	R^2
FL	101.99 ± 3.00	0.49 ± 0.02	2.65 ± 0.35	289.05 ± 32.08	0.74 ± 0.05	0.98274
SX	101.18 ± 2.19	0.53 ± 0.03	2.03 ± 0.27	194.27 ± 9.67	0.90 ± 0.05	0.98606
SS	99.89 ± 2.61	0.69 ± 0.04	1.53 ± 0.17	108.88 ± 5.06	1.25 ± 0.19	0.98587
SS:FL	103.40 ± 5.40	0.61 ± 0.04	2.71 ± 0.71	230.20 ± 34.34	0.84 ± 0.08	0.93928
SX:FL	99.40 ± 1.60	0.43 ± 0.01	1.68 ± 0.12	207.35 ± 6.1	0.82 ± 0.04	0.99360

m= positive asymptote

x0= pressure value in the x axis which takes a value of $n \geq 0$

n= deagglomeration exponent

Maximum gradient= slope of the curve

CPP_{95} = critical primary pressure where the degree of deagglomeration has reached the 95 % of its final value

R^2= value of the best fitted line

When CL was added to the formulation, the plateau was not reached when the blends containing CL were analysed. Instead, the formulations showed a bi-exponential trend (Figure 4.9), highlighting an easily dispersed fraction and a second poorly dispersible fraction of respirable particles. This response is described by Equation (4.7).

$$y = A(1-e^{-(x/x1)}) + H(x-x_W)(100-A)(1-e^{-(x/x2)}) \qquad (4.7)$$

'A' represents the amplitude of the easily dispersed fraction (i.e., extent of deagglomeration), whereas 100 - 'A' represents the deagglomeration extent of the poorly dispersed fraction; 'x_w' is the pressure when the poorly dispersible fraction starts to deagglomerate; 'H' is the Heaviside-function (1 if $x>x_w$, 0 if $x<x_w$); x_1 and x_2

are pressure points when the deagglomeration response is at maximum for the easily and poorly dispersed fractions, respectively. With the exception of SX:CL, all blends exhibited an 'x_w' value (Table 4.8). Greater deagglomeration responses for the easily dispersed fraction were seen for blends with FL:CL (e.g. 170.97 ± 12.74 bar^{-1} for SX:FL:CL) than with CL (e.g. 71.64 ± 7.42 bar^{-1} for SX:CL). The presence of ternary agent improved the liberation of the finest particles (higher 'A' parameter, Table 4.8). The greatest 'A'-value was observed for SS:FL:CL (Table 4.8).

Table 4.8. Parameters from a bi-exponential equation for salbutamol sulphate (SS) blends (FL=fine lactose, CL=coarse lactose) and salmeterol xinafoate (SX) blends.

Blends	A (%)	x_1 (bar)	x_2 (bar)	$x_w;y_w$ (bar;%)	R^2
SS:CL	37.6 ± 0.7	0.5 ± 0.0	11.2 ± 2.8	3.0 ± 0.3; 37.4 ± 0.8	0.81143
SS:FL:CL	61.4 ± 2.6	0.6 ± 0.1	3.7± 1.0	2.0 ± 0.3; 59.8 ± 6.4	0.91714
SX:CL	17.8 ± 2.8	0.3 ± 0.1	14.0 ± 1.0	0;0	0.88214
SX:FL:CL	48.7± 1.8	0.3 ± 0.0	5.6 ± 1.4	1.9 ± 0.4; 48.6 ± 1.6	0.91714

4.4.5. Particle morphology

4.4.5.1. Micronized particle and blend morphology

Microscopy was employed to examine blend structure. The micronized SS and SX showed a very similar elongated shape (Figure 4.10, left and right).

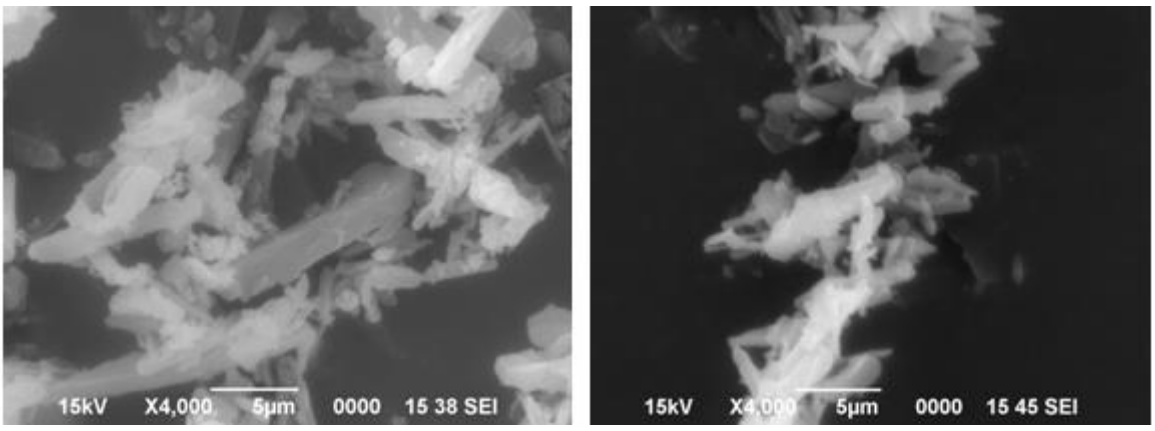

Figure 4.10. Scanning electron microscopy images for salbutamol sulphate (left image) and salmeterol xinafoate (right image).

Alone, the drugs created agglomerates. However, when the coarse lactose was added, the distribution of SS and SX on its surface did not show any difference (Figure 4.11).

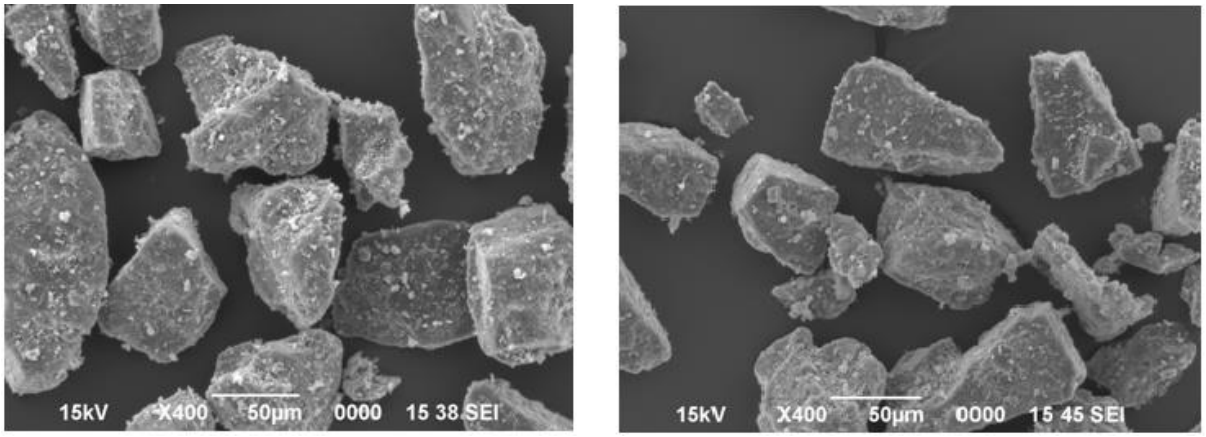

Figure 4.11. Scanning electron microscopy images for salbutamol sulphate:coarse lactose(left image) and salmeterol xinafoate:coarse lactose (right image).

However, when FL was added to SX:CL (Figure 4.12, left), clearly more agglomerates can be seen at the extremities of the surface of the carrier. Interestingly, when the fine lactose was added to SS:CL, “free” agglomerates of FL:SS were visible in the space between carrier particles (Figure 4.12, right). When energy is applied, these agglomerates would be dispersed more easily compared to those adhered to the surface of the carrier (e.g. in SX:FL:CL); leading to the higher % deagglomeration for the SS:FL:CL compared to SX:FL:CL (“A” parameter, Table 4.8). However, the adhesive strength predicted (Table 4.8) of the CL-SS interactions in the agglomerates would require high pressure to achieve full deagglomeration (“x_1” parameter in Table 4.8).

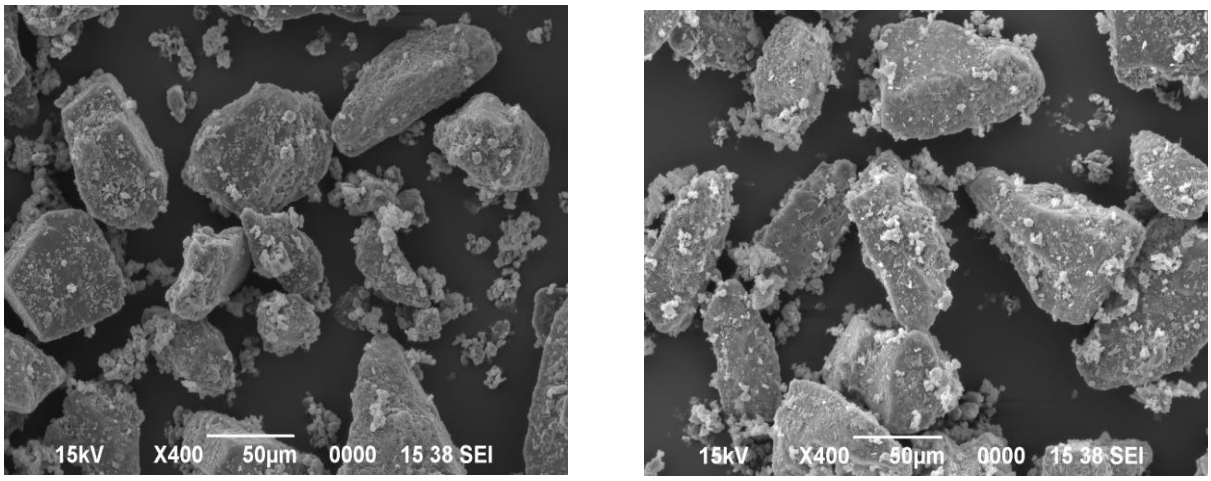

Figure 4.12. Scanning electron microscopy images for salbutamol sulphate blended with fine and coarse lactose (SS:FL:CL – left image) and salmeterol xinafoate blended with fine and coarse lactose (SX:FL:CL – right image)

4.4.5.2. Agglomeration state of the deposited fraction

SEM was carried out on particles emitted from both the Cyclohaler® and the Cyclohaler-Cheng 2 cyclone in series at 4 kPa into the impactor. The stages where the particles were collected were: capsule, 90° angle of USP throat, central cup of the pre-separator and stage 5, to represent the particle cut off size at 4 kPa. In Figure 4.13 the formulations emitted from the Cyclohaler® are reported.

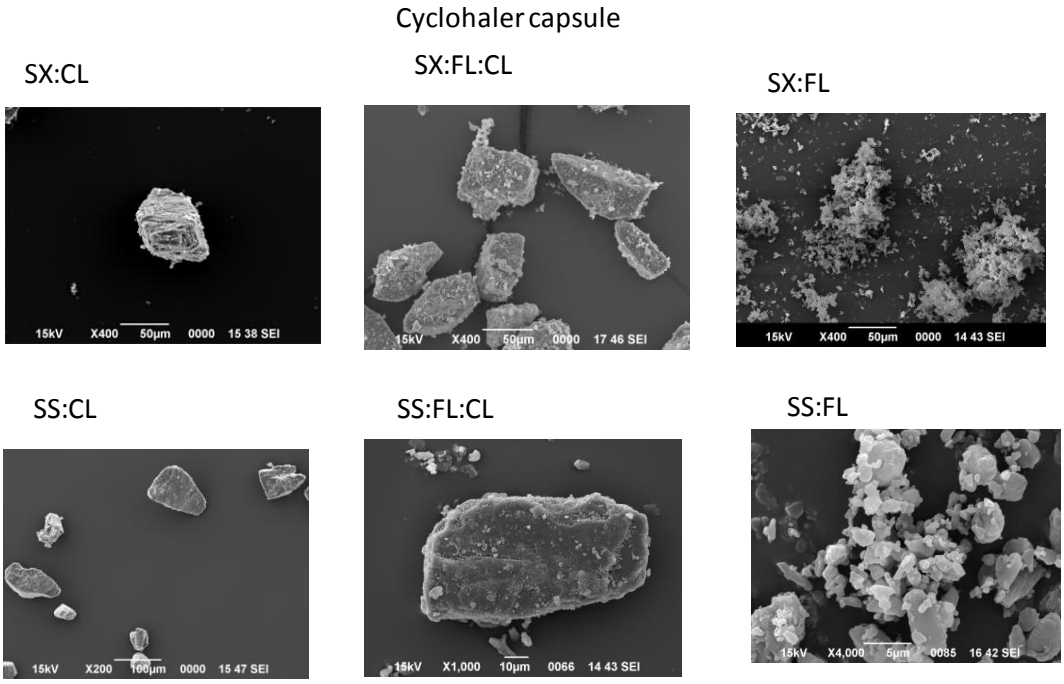

Figure 4.13. Scanning electron microscopy images for all the blends emitted using the Cyclohaler (capsule/stage).

Powder collected from the capsules showed the presence of fine particles when FL:CL blends were tested compared to API:CL blends. Some difference of the effect of the fine lactose when added to the formulation is seen on the SX:FL:CL blends when emitted from the Cyclohaler. Agglomerates can be seen on the extremities of the carrier. SX was assumed to be the cohesively-balanced particles when added to the lactose and FL helped the deagglomeration mechanism (Table 4.8). However, when FL was added to SS:CL blends, the particles typically regarded as adhesive did not behave similarly to SX. When the mixture of SS:FL:CL was collected form the capsule (Figure 4.13), some “free” agglomerates was seen in the surrounding space of the carrier than when the formulation SX:FL:CL was analysed (Figure 4.13). When SS:CL and SX:CL formulation were analysed, no difference was observed (Figure 4.13) or when the Cheng 2 was employed (Figure 4.14). When Cheng 2 was used (Figure 4.14), the deposition in the capsules was unchanged in respect of the Cyclohaler alone.

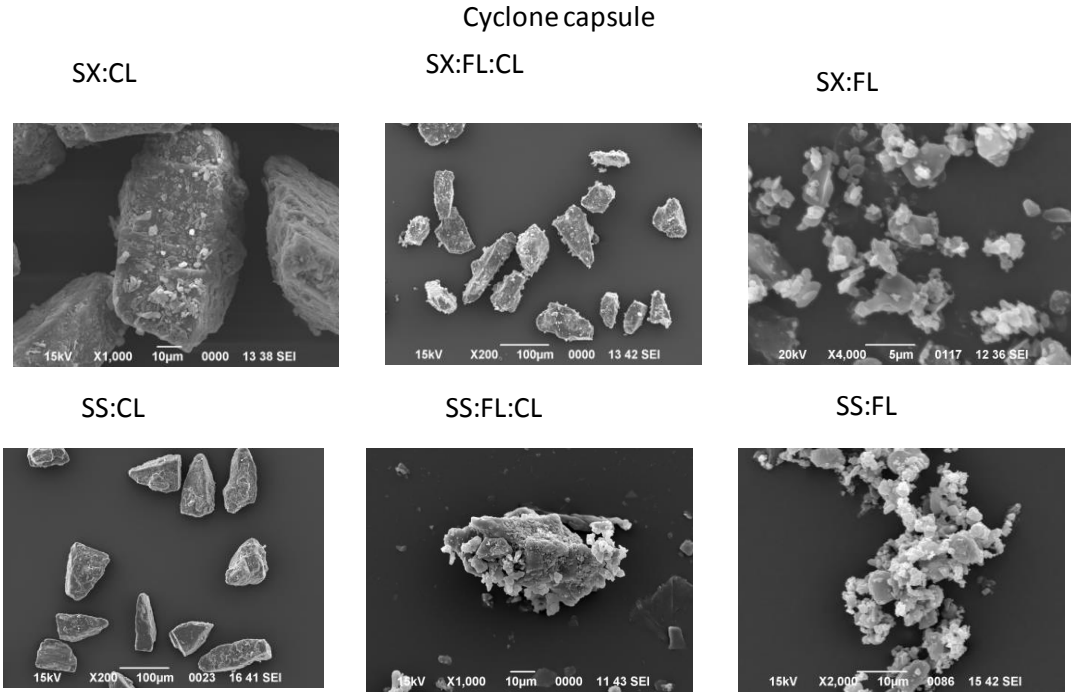

Figure 4.14. Scanning electron microscopy images for all the blends emitted using the Cyclohaler/Cheng 2 Cyclone in series (capsule/stage).

A great amount of the blends was detected in the inlet of the Cheng 2 (Figure 4.15). SX:FL:CL showed “free agglomerates” inside the conical section of spacer. In contrast to the SX:FL:CL collected from the Cheng 2, SS:FL:CL did not show “free” agglomerates (Figure 4.15).

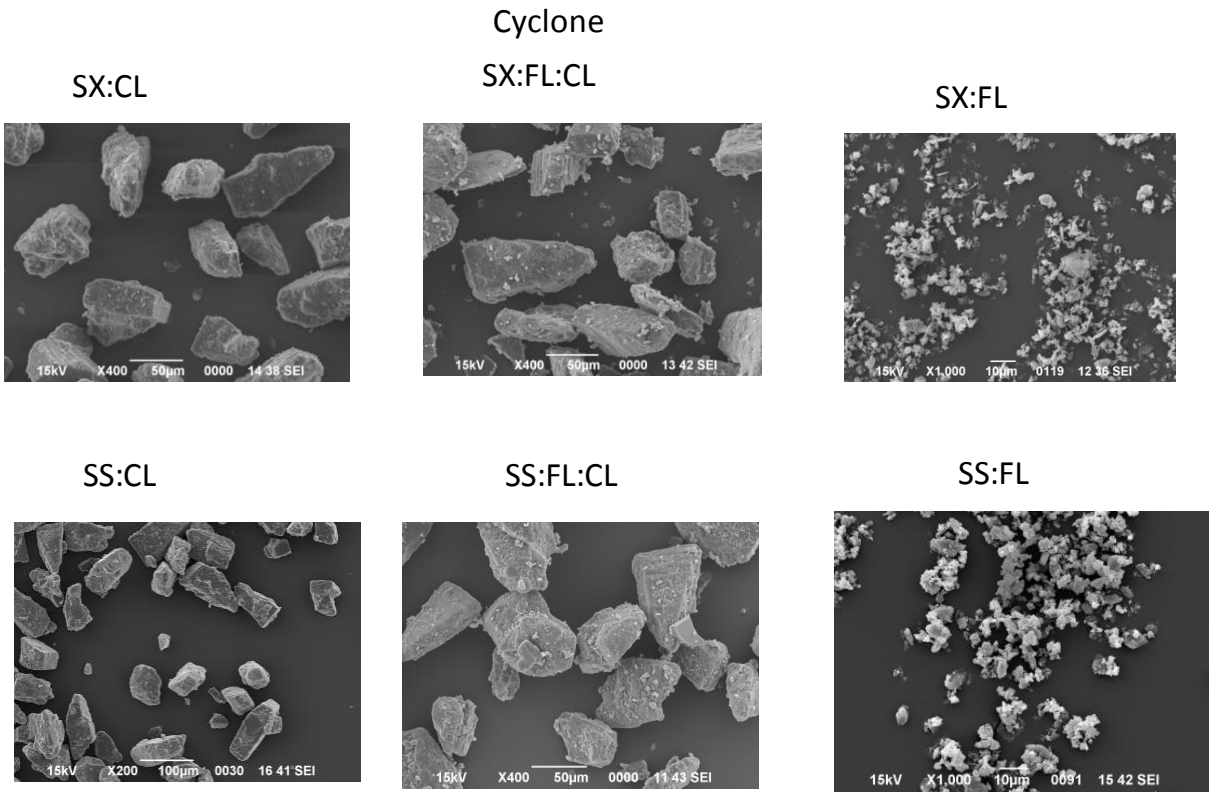

Figure 4.15. Scanning electron microscopy images for all the blends emitted using the Cheng 2 (inlet of cyclone-spacer).

As already described in Section 4.4.2, some agglomerates and carrier particles were detected in the IP/PS stage for all the blends when the Cyclohaler was used alone (Figure 4.16). For SS blends, drug was trapped in the asperities of the lactose. Therefore, the force was not sufficient enough to detach all SS from the high energy sites.

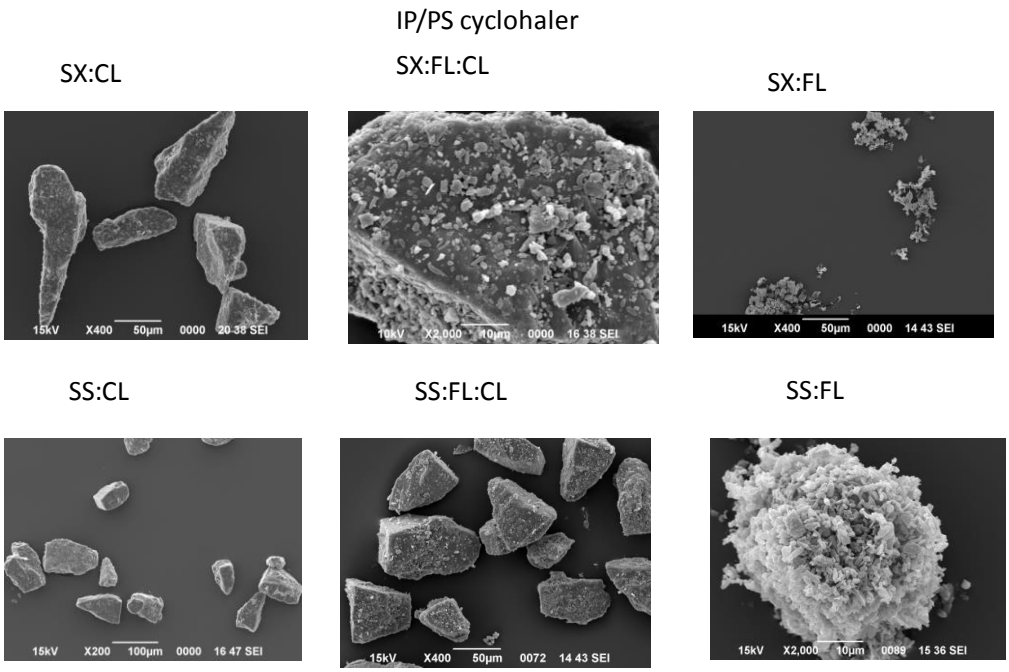

Figure 4.16. Scanning electron microscopy images for all the blends emitted using the Cyclohaler (IP/PS stage).

Agglomerates that would have been retained inside the Cyclone (Figure 4.15) were seen in the IP/PS stage when Cyclohaler was used alone (Figure 4.16). Fewer coarse carrier particles were detected in the IP/PS stage when Cheng 2 was used Figure 4.17).

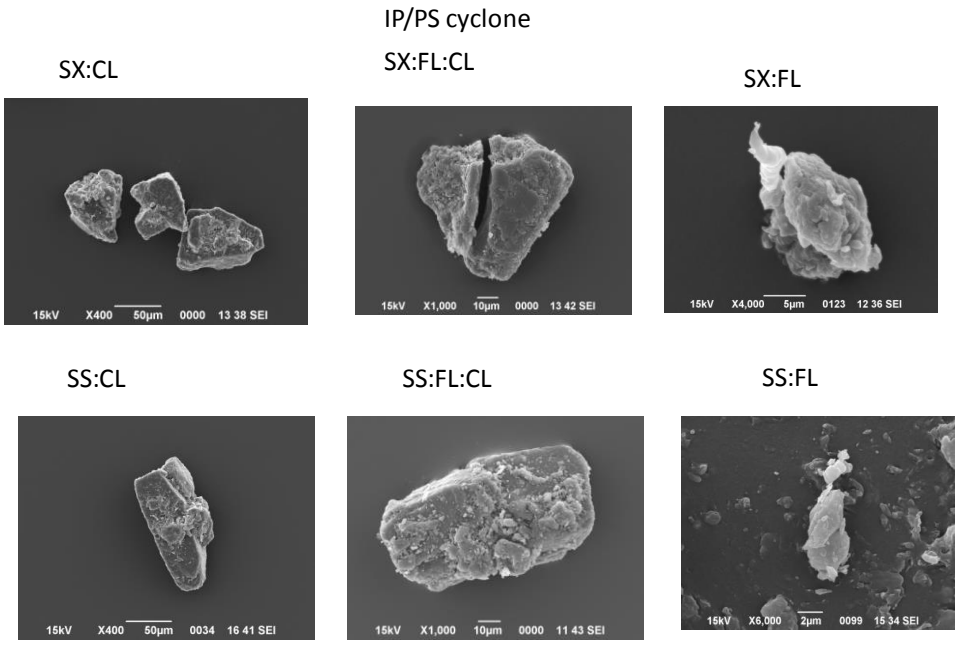

Figure 4.17. Scanning electron microscopy images for all the blends emitted using the Cyclohaler/Cheng 2 (IP/PS stage).

In general, when the blends were emitted from the Cyclohaler® only, more powder was collected from the throat and pre-separator stage than when the Cheng 2 was employed (e.g. Figure 4.16 and Figure 4.17). A higher magnification of the microscope in the pre-separator stage (Figure 4.16) showed agglomerates of SX with FL on the carrier surface. When Cheng 2 was used, some carrier particles were detected with clearly some SX still attached or in the surrounding space in the IP/PS stage (Figure 4.17). However, the vacuum of the sputter coating process fragmented one particle that was recovered from the throat stage (Figure 4.17).

As expected, in stage 5 only micronized particles were collected (Figure 4.18). However, the presence of fine lactose in the blends enhanced the detachment of drug from the carrier surface resulting in higher deposition of the micronized mixture in stage 5 compared to when blends with CL only were assessed for both Cyclohaler and Cheng 2. This was previously reported in the impaction data (Table 4.4).

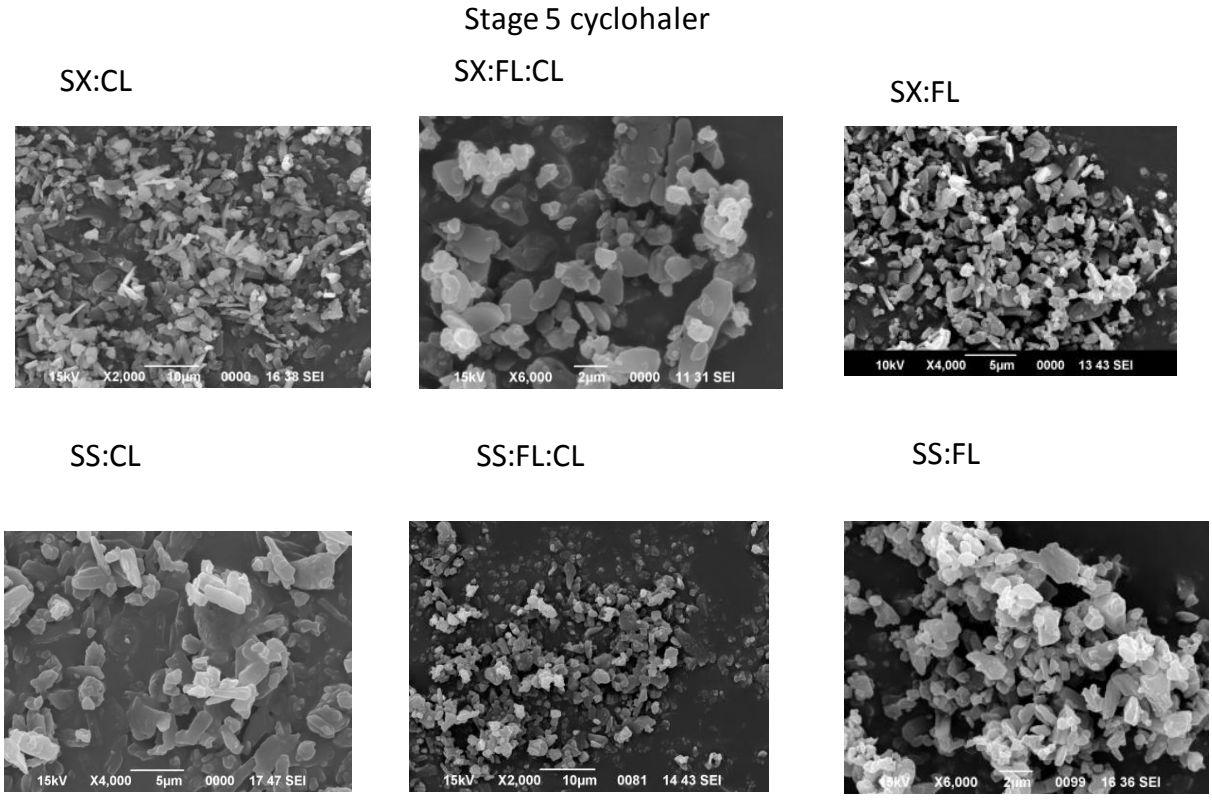

Figure 4.18. Scanning electron microscopy images for all the blends emitted using the Cyclohaler (stage 5).

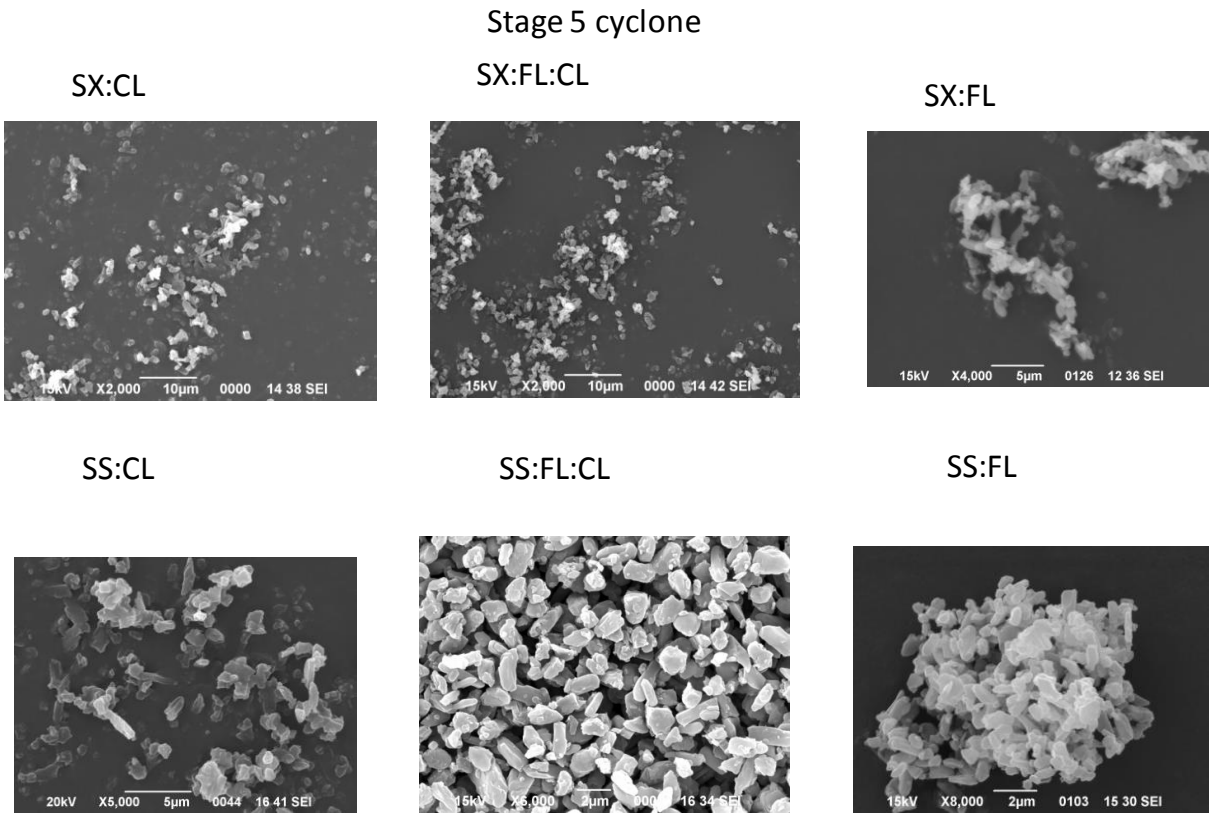

Figure 4.19. Scanning electron microscopy images for all the blends emitted using the Cyclohaler /Cheng 2 (stage 5).

4.5. Discussion

Due to interesting results from the Accuhaler™ formulation in Chapter 3, a study of aerosolization using the cyclone with blends containing different APIs with different grades of lactose was assessed. A variable IP/PS deposition was seen for SS and SX emitted from the Cyclohaler® and Accuhaler™, both in series with Cheng 2, respectively (Chapter 3). The throat deposition was almost doubled for SX leading to a much reduced FPF than SS. Although the data were obtained when the Cheng 2 was in place, which was supposed to retain only the large carrier particles, the APIs seemed to deagglomerate differently inside the conical section of the spacer. In order to understand the mechanism better, blends with either SX or SS were manufactured in-house with different grades of lactose and their aerosolization, was studied with the Cyclohaler® in the presence or absence of the Cheng 2 spacer at 2 and 4 kPa. For the purpose of the study and to understand the different deagglomeration mechanism of SX and SS, the former was considered cohesively-balanced when added to the lactose, due to its tendency to create agglomerates on

the carrier surface [104]. On the other hand, SS was considered due to its adhesively balanced behaviour when added to lactose as previously described [108]. This considerations were based on literature search. The concentration of the SS and SX was 1.48% w/w and they were blended with either FL (1:4), coarse lactose (1:67.5) or both (1:4:63.5). In the current chapter FPF and $FPR_{1.5}$ were considered as metrics to undertstand the extend of deagglomeration of the blends and not for any clinical purpose (e.g. understanding the potential respirable fraction when using the spacer). This was decided due to the variability of the Cheng 2 with commercial blends. Therefore, comparison between blends when tested with or without the spacer was made only to propose a theory of different behaviour relating to the chemical entities (e.g. API) and the presence of fine carrier.

The PSD (particle size distribution) of the APIs confirmed that the drugs were micronized (Figure 4.1 and Figure 4.2). Although the lactose was sieved in the fraction 63-90 µm, its Dv50 was 65.78 ± 0.44 µm. This is probably due to the presence of fine lactose on the surface of the carrier that affected the particle size. CL is well known to be used to improve aerosolization and flowability of micronized drug [108, 223]. However, a strong adhesion of the API to the carrier would decrease the drug dispersion[99, 110]. Therefore, ternary agents (or fine lactose) are usually added to the formulation to compete with the drug on the active sites of the carrier. Saturating the sites, the drug is detached easily from the carrier upon aerosolization [98, 100]. Many studies suggest an increase of fines would increase the FPF of the API because fines create agglomerates [99]. However, the different behaviour of the drug when mixed with the carriers must be kept in mind. Behara et al [113] showed that the presence of coarse carrier was not necessary as by increasing the concentration of fines, the agglomerate strength is reduced leading to a better aerosolization. Moreover, Islam et al [224] indicated that SX dispersion increased as the amount of FL increased. On the other hand, Jones et al [203] demonstrated that the addition of fines does not always enhance the FPD. They tested the aerosolization of Bud and formoterol fumarate dihydrate in combination with erythriol or trehalose fines. They found that the FPD did not increase compared to the binary formulation of the drug with the carrier lactose (e.g. 18.6 ± 3.3 % vs. 22.0 ± 1.2 % for budesonide binary formulation and budesonide/erythriol fines formulation, respectively).

In the current study, the emission from the Cyclohaler® alone did not differ between SS and SX formulations (88.20 ± 2.86% for SS:CL and 89.05 ± 2.12% for SX:CL at 4 kPa, $p>0.05$). However, it decreased when FL was added to the formulations (e.g. 89.05 ± 2.12% for SX:CL vs. 75.70 ± 2.00 for SX:FL:CL at 4 kPa). On the other hand, when the Cheng 2 was used, greater emission was seen for the SX blends than for the SS formulation (10.25 ± 3.85% for SS:CL and 22.86 ± 4.30 % for SS:FL:CL vs. 16.30 ± 3.25 % for SX:CL and 30.64 ± 10.44 for SX:FL:CL at 4 kPa, $p<0.05$). In the conical section of the Cheng 2, deagglomeration processes probably occur, leading to better emission of what could be stong agglomerates of SX from the spacer than SS. As previously suggested [224], adding FL in SX formulations (with CL) the SX deagglomeration occurred to a greater extend. This also led to a reduced IP/PS deposition for the blend with the ternary agent compared to when fine lactose was absent from the formulation (Table 4.3). Greater throat deposition was seen for SX blends than SS formulations. The same finding was reported when Cyclohaler/SS and Accuhaler/SX/FP were tested with Cheng 2 in Chapter 3.

In Chapter 3, the retention of the drug within the cyclone was high shown to be high for all drugs. Here the cyclone retention was especially high for the blends with fine lactose only (e.g. 95.76 ± 0.67 % and 96.83 ± 0.34 % for SS and SX). This is probably due to the presence of small particles that have low inertia and therefore, experience low deagglomeration forces. Also, when only micronized particles were in the formulation (e.g. SS:FL or SX:FL), no throat deposition was detected when the Cheng 2 was in place, as the drug particles remained inside the spacer which has been shown not to work efficiently with only micronized material. Therefore, when hitting the spacer walls, the particles do not re-disperse in the air. In fact, as seen in Chapter 2 with the Symbicort/Turbuhaler®, when coarse carrier was absent from the formulation, the majority of the particles were collected within the conical section of the spacer. This confirms that the cyclone spacer did not function effectively with agglomerated micronized material alone. Fine lactose and cohesive micronized particles create agglomerates [113]. The absence of the coarse lactose affects the flowability of the formulation [96] and therefore, when entering the spacer, the agglomerates are subjected to more adhesion to the cyclone's walls than the other type of formulations with a coarse carrier. In fact, the highest retention within the spacer was seen for SS:FL and SX:FL (64.14 ± 6.20% and 52.39 ± 4.73 % at 4 kPa,

respectively). This was confirmed by the SEM images (Figure 4.15) where particles were detected as agglomerates.

The lower deposition in the IP/PS for SS than SX formulations when CL or FL:CL was used than SX formulation lead to a variable PSD between the formulations when the spacer was used. Interestingly, when the Cheng 2 was not employed, the blends showed an almost identical PSD at both flow rates (Figure 4.3 and Figure 4.4). In fact, the same FPF (% ED) of the aerosol emitted from the inhaler alone was unchanged for both APIs (13.08 ± 1.29 % for SS:CL vs. 10.86 ± 1.31% for SX:CL, $p>0.05$ and 31.95 ± 4.76% for SS:FL:CL and 32.2 ± 5.08% for SX:FL:CL, $p>0.05$). FPF seems dependent on the composition of lactose used [225].

The presence of cohesively balanced particles, and therefore, high interaction forces between drug-drug, would lead to a reduced FPF of the drug upon aerosolization [104]. This was observed when Cheng 2 was employed. A reduced FPF (%sED) of SX:CL emitted from Cyclohaler into the spacer was observed than when SS:CL was assessed (Table 4.4). The SS, probably due to its stronger forces of interaction with the lactose [108] showed an higher FPF than SX (%sED) (65.83 ± 8.99 % vs.45.83 ± 5.035 % for SS:CL and SX:CL, respectively at 2 kPa and 70.14 ± 5.15% and 43.06 ± 6.88 %, for SS:CL and SX:CL, respectively at 4 kPa, $p<0.05$). It seems that the deagglomeration forces inside the conical section of the spacer have a greater impact on the formulation when the carrier is used. Interestingly, adding FL to the formulation led to an enhanced FPF (%sED) for formulations of both SS or SX with a much greater improvement for SS blends (e.g. 81.83 ± 4.11 % for SS:FL:CL vs 70.15 ±5.15 % for SS:CL at 4 kPa). Literature search suggests that SX exhibits a more cohesive behaviour than SS [99]. However, when added to the FL and CL, the fine particles competed with SX leading to a similar FPF of SS:FL:CL and SX:FL:CL (72.68 ± 16.83 % for SS:FL:CL and 71.76 ± 2.80% for SX:FL:CL at 2 kPa). Therefore, the CAB theory cannot be fully applied to the proposed project. However, it seems that the presence of the ternary agent improved the dispersion of the drug probably due to stonger FL deagglomeration forces that break up the weak mixed agglomerates [99].

Due to the cut off size of the cyclone being < 2 µm, $FPR_{1.5}$ were calculated dividing the FPF1.5 of the blends emitted from the spacer by the $FPF_{1.5}$ of the same

formulation emitted from the Cyclohaler®. This was done as $FPF_{1.5}$ could be used as a parameter to assess the extent of deagglomeration of the emitted dose within the spacer. It was calculated as a measure of classification of particles below the cut-off diameter. Although SS:CL had higher FPF than SX:CL, the latter exhibited a greater $FPR_{1.5}$ (Table 4.4). The same trend was seen when FL was added to the formulations, with expected greater ratios for the formulation with fine lactose than with CL (2.01 ± 0.52 for SS:FL:CL vs. 2.82 ± 0.24 for SX:FL:CL at 2 kPa and 2.18 ± 0.18 for SS:FL:CL vs. 3.44 ± 0.34 for SX:FL:CL at 4kPa). This was confirmed by the maximum gradient (slope in Figure 4.9) of SS:FL:CL and SX:FL:CL (in the easily dispersed fraction curve), indicating SX:FL:CL to have a greater gradient than SS:FL:CL. Therefore, a better deagglomeration seems to occur for SX particles as it should be expected also in the absence of the carrier (Figure 4.8, B) [99]. In Chapter 3, the same trend was seen for SS formulation and SX formulation emitted from the Cyclohaler and Accuhaler, respectively in the presence of the spacer (1.96 ± 0.30 for SX and 1.30 ± 0.98 for SS at 4 kPa). Although the respirable fraction was higher for the SS formulation, the potential of enhanced deagglomeration of SX would lead to a more potential lung deposition in the small airways for this particular API, where a longer bronchodilation than SS would be required for severe asthmatic patients [226, 227]. This is probably because SS alone is not present as agglomerates unlike when is in presence with the lactose. Moreover, SX presents agglomerates on the carrier surface (Figure 4.12), leading to a greater deagglomeration than SS blends (e.g. $FPR_{1.5}$ in Table 4.4). From the SEMs, it is clear that SS:FL agglomerates, when mixed with CL, tend to re-distribute in the surrounding spacer of the carrier unlike SX:FL agglomerates when mixed with CL.

Using laser diffraction techniques, the effect of the addition of either fine lactose or coarse lactose to the API was shown [224]. Studying the particle size distribution of SX with fine lactose, Islam *et al* [224] indicated that SX dispersion increased as the amount of FL increased. On the other hand, adding coarse carrier to the mixture shifted the distribution to a larger size range [224]. However, adding lactose with size between 45-63 µm, led to almost double the FPF (fine particle fraction), compared to when the coarse lactose with size > 63 µm. Particle size distribution using laser diffraction showed a greater fraction of particles with size < 5 µm when SS blends were emitted from the Cyclohaler® (Table 4.5). As already discussed in Chapter 3,

the cyclone spacer, Cheng 2, especially its conical section, behaves differently between formulations. Studying the deagglomeration process of the dispersed powder at different flow rates prior to entering the spacer is important to understand the outcome when a DPI is used to effect powder emission. Although this issue has featured widely in the literature, a few studies have investigated the deagglomeration trend of either the powder bed [213] or the aerosol emitted from a Rotohaler [220]. These studies proposed a quick methodology to assess deagglomeration of the formulation upon increasing flow rate or pressure drop. Laser diffraction analysis such as Sympatec and Malvern instrument [213, 220] were used. However, the studies seem to focus on the fine particles, rather than on the formulation with coarse carrier.

High flow rates are required to deaggregate blends if lactose carrier is present, due to the adhesion of the micronized particle to its surface. Only several studies have investigated the powder dispersion when coarse lactose was employed [221, 228]. The authors used Standardized Entrainment Tubes (SETs) to generate the aerosols using then cascade impactor (twin-stage liquid impinger and Andersen cascade impactor) to characterize the formulation at 60 $Lmin^{-1}$ [221]. The FPF was then correlated to the SET shear stress and an equation proposed similar to the Langmuir adsorption isotherm, called the powder aerosol deaggregation equation (PADE) [221]. However, the study implies that a cascade impactor should be used to study the deagglomeration of the particles. The same issue of modifying the deagglomeration process with an inhaler was reported by Behara et al, [220] when the Rotohaler was used. The aim of the current chapter was to understand the deagglomeration behaviour of the formulation itself prior to entering the cyclone spacer. Therefore the models proposed by these studies were not used. Other studies investigated the interaction between individual particles using atomic force microscopy (AFM) [218, 219]. However, the technique does not quantify the adhesion force of the powder bed as it only measure the interaction between one particle or excipient and the probe of the AFM.

Other techniques have been proposed to study the interaction between particles. For instance, inverse phase gas chromatography [229] showed potential to

understand the interaction between carrier and API, where the formulation is placed inside a packed columns and a gas (e.g. helium) is passed through it. The API with higher affinity to the carrier, would elute later than the one with less affinity. This is due to the higher surface energy between API particles and carrier. Studying the retention of a range of probes with different polarity and chemistry, the cohesion strength can be calculated [229]. Another technique to study the different behaviour of blends under applied forces are powder rheometry (where flow properties are studied by studying the movement of an impeller through blends under a specified force, such as torque) [230] and centrifugation of micronized material [231]. In this chapter only cascade impactor, laser diffraction and SEM techniques were used to propose a deagglomeration theory.

When the APIs were dispersed using the Sympatec/RODOS for pressure drop titration, both SX and FL showed a bi-modal PSD at 0.5 Bar (Figure 4.5 A, B). The same trend was seen also for SS that exhibited a similar behaviour at 1 Bar too (Figure 4.5, C), suggesting a greater energy is required for the deagglomeration mechanism to occur for SS compared to SX and FL. However SS, SX and FL showed a bell-shaped distribution at higher pressure drops as confirmed in previous studies [96, 232]. When FL was added to the APIs, a more consistent distribution when increasing the pressure was seen for both drugs, although SS-FL deagglomeration at low pressure (0.5 Bar) did not occur completely (shoulder in the large particle size range in Figure 4.6, A). The same trend was seen by Jaffari et al [213] with SX, and by Behara et at for SS:FL [220]. However, the bi-modal distribution was not present for SS:FL at 1 Bar unlike for SS alone, probably due to the addition of the FL leading to disruption of SS agglomerates and enhanced deagglomeration [113].

When the formulations containing either CL or FL:CL were analysed, the lactose carrier showed a distribution in the 60-90 µm range (Figure 4.7 A). However, in blends also containing FL, a shoulder was seen in the micronized region due to the greater amount of fine particles present in the mixture (Figure 4.7, B). The formulations showed a bi-modal distribution due to the presence of easily-dispersible agglomerates (small shoulder in the respirable range) and a poorly-dispersible fraction of drug still attached to the carrier (big shoulder) [98, 213] that could be

explained by the bi-exponential trend when an increased pressure drop is applied (Figure 4.9). At high pressures there was an increase in the release of fine particles, corresponding to the increased FPF as seen in the cascade impaction study (Table 4.4). The presence of ternary agent would help the detachment of the micronized API from the surface of the carrier, resulting in greater FPF than when the formulation was composed of CL only [101] (Table 4.4). Jones et al [203] confirmed it when also other ternary agents were added to a binary formulations showing and increased mode in the respirable fraction for Bud ternary formulation with erythriol fines.

In accordance with Jaffari et al [213], formulations with fine particles only reached a plateau when the pressure drop was increased. The trend could be described by a mono-exponential function (equation 4.6) which is a modification from the Johnson-Mehl-Avrami-Kolmogorov (JMAK) equation [233]. The plateau size represents the maximum deagglomeration ("m" parameter in Table 4.7 define the positive asymptote of the curve) which varied with the type of particle (Table 4.7). The slope of the curve in Table 4.7, B represents the deagglomeration sensitivity (e.g. the maximum gradient). SS showed the lowest maximum gradient (indicating a deagglomeration process less sensitive to airflow) when pressure is applied compared to the other micronized materials (Table 4.7). The difference, especially at low pressure drops, suggests variability in agglomerate size (i.e. x0 in Equation 4.6) and strength between agglomerates [194, 214]. In order to compare the drugs and blends, the critical pressure point (CPP), the pressure point corresponding to reaching 95% of the maximum deagglomeration was calculated. SS started to reach the plateau at 1.25 ± 0.19 Bar, at a much greater pressure than SX or FL (Table 4.7). However, when FL was added to SS, the CCP95 was reached at lower pressure than when SS was analysed alone (0.84 ± 0.08 Bar, $p < 0.05$) and the greater maximum gradient was seen for FL than SS (Table 4.7).The maximum gradient is a vector of the derivative of the function. This indicates the rate of ascent of the curve, therefore, the rate of the degree of deagglomeration. If a small tangent is drawn in a selected point (in this case x0;y0), then the maximum gradient refers to the slope of the tangent.

The enhanced degree of deagglomeration seen for SS when FL was added could be explained by the fact that adding FL, agglomerates with potential low cohesive strength are created between fine carrier particles and drug that otherwise would not be overcome [113, 220]. Therefore, the force of adhesion between agglomerates of API is reduced. SX:FL had a poor deagglomeration compared to FL or SX, suggesting that maybe the addition of FL to very cohesive agglomerates does not improve the deagglomeration mechanism [203]. In accordance with this theory, Adi et al [104] showed that increasing the shear pressure to formulations of SX containing FL with different size range (3.0 and 7.9 µm) is required especially for formulation containing FL 3.0 µm. This might lead to segregation in the formulation, especially at high pressure drops, a phenomenon already reported with other formulations in Chapters 2 and 3. The parameters ‘x0’ and ‘n’ are dependent on each other. The parameter ‘x0’ has a similar meaning like the one proposed by Behara et al [220]. The authors used a Rotahaler with Spraytec to study the deagglomeration behaviour of either SS or FL. They suggested that the parameter was the dispersion energy required to overcome internal interaction of the agglomerates. In the current project we suggested that ‘x0’ could be seen as an inflection point and it is the pressure at which the deagglomeration attempts to reach the maximum point. In accordance with Behara et al [220], the blends with fine particles and FL alone showed similar ‘x0’ values (Table 4.7, $p>0.05$) with the exception of SS. The parameter ‘n’ is the trend of the first part curve between 0.1 and x0 Bar. SS:FL exhibited the highest deagglomeration exponent whilst, SX:FL showed the smallest. This indicates a different deagglomeration mechanism when the fine lactose overcomes SS-SS and SX-SX interactive forces. Moreover, the blend structure plays a role. Adding the fine lactose would modify the adhesive strength between particles and enhance the detachment of the API (Table 4.7, maximum gradient was greater for SS:FL than SX:FL).

When the blends containing coarse lactose or fine lactose and coarse lactose were analysed, they did not show a plateau size. The graph shows a bi-exponential distribution (Figure 4.9) that could be described by Equation (4.7) with the first part showing an easily dispersed fraction and a second part showing a less easily dispersed fraction. The trend of the latter seemed to be the same for all the formulations. However, the first part shows difference in the deagglomeration

behaviour of the blends. SS:CL seemed to have the steepest curve than the other API:CL blends, expressed by the maximum gradient. As expected, API:FL:CL blends, showed a more rapid slope in the first fraction than API:CL blends (Figure 4.9). They showed also a greater % of deagglomeration expressed by the parameter "A" in equation (4.7) reported in Table 4.8. This might explain the greater FPF seen for blends with FL when either the Cyclohaler or the Cheng 2 was used in the aerosolization studies (Table 4.4). Equation (4.7) shows the Heaviside function which is usually used in engineering to represent a parameter that changes abruptly at specified values of time t. For example, it is usually applied when a voltage is switched on or off in an electrical circuit at a specified value of time t. In many circuits, waveforms are applied at specified intervals other than t = 0 [234, 235]. In the current model the step function (or Heaviside function) was applied to the bi-exponential trend. If noticed in Figure 4.9, between 1.0 and 2.0 Bar, between the end of the deagglomeration of the easily dispersed fraction and the beginning of the deagglomeration of the poorly dispersed fraction, there is a small plateau [235]. *'H'* was applied to the deagglomeration mechanism of the blends with coarse carrier, where the "H" parameter of the function was 1 if $x>x_w$, with x_w being the pressure when the poorly dispersed fraction starts to deagglomerate (the delayed unit), or 0 if x<xw. All the formulations with the exception of SX:CL showed the plateau between the easily and the poorly dispersed fraction, with SS:CL showing the highest pressure value. This suggested that this particular formulation required the highest pressure to deagglomerate. The addition of FL led to a greater deagglomeration as the pressure (x_w) decreased by 1 unit. Furthermore, the corresponding % deagglomeration to xw was the highest between all the formulations (Table 4.8).

SEM was used to study the morphology of the APIs and blends. Unlike some studies have suggested [109, 213], SS did not exhibit a plate-like shape, whereas both APIs created elongated agglomerates without clear differentiation in their shape (Figure 4.10). Moreover, When added to coarse lactose, no difference in the APIs' distribution was seen on the surface of the carrier (Figure 4.11). This particle behaviour is different to what is proposed in the literature. Begat et al suggested that SS distributes evenly on the surface of the carrier [109], whilst SX that created agglomerates due to the fact that SX–lactose blends are dominated by SX cohesive interactions [99]. However, this is not showed in the current work. Nevertheless,

clearly different re-distribution of the APIs with the lactose was seen when FL was added to the mixture (Figure 4.12). The agglomerates of FL-SX were clearly not distributing homogenously on the lactose surface, presenting larger agglomerates on the extremities of the carrier compared to when FL was absent in the formulation. This was probably due to the weak adhesion of FL to the carrier surface, and therefore, its tendency to agglomerate with SX [98]. This suggests that SX-FL have stronger adhesion than FL:FL. The same tendency to create agglomerates was seen for FL-SS. The maximum gradient value for SS:FL (Table 4.7) was greater than SX:FL, suggesting that the deagglomeration of the former was enhanced in presence of the fine lactose that can be seen also when the coarse carrier is present (e.g. % relative deagglomeration in Table 4.8). The SX:FL agglomerates did not redistribute on the lactose surface, but in the spaces between carrier particles showing a greater amount of “free” agglomerates for SS:FL than SX:FL. This might explain the greater % deagglomeration seen for SS:FL:CL than SX:FL:CL (Table 4.8) as less energy is required to release the agglomerates form the carrier surface. However, the adhesion between SS and lactose carrier does require higher flow rates to be overcome (x_w= 3.0 ± 0.3 for SS:CL in Table 4.8).

In order to understand impaction data and correlate to the empirical model proposed, SEM was also used on the powder deposited on specific stages of the NGI (device, Cheng 2, throat, pre-separator, stage 5). No great difference was seen between SS:CL and SX:CL when deposited in each stage between Cyclohaler® tested alone and when Cheng 2 was employed. However, slightly difference of the effect of the fine lactose when added to the formulation was seen for SX:FL:CL (Figure 4.15 and Table 4.8). It appeared that individual SX particles remain in the capsules compared to SS (Figure 4.13). The Cheng 2 is known to retain big agglomerates. This is shown by the SEM images (Figure 4.15) and cascade impactor studies (retention within Cheng 2 for 65.54 ± 10.08 for SS:CL and 67.82 ± 10.24 for SX:CL at 4 kPa). This helps to decrease the IP-PS deposition of the formulation. However, as already seen in Chapter 3 with Cyclohaler/SS and Accuhaler SX/FP, SS:CL and SX:CL emitted from the Cheng 2 showed a different deposition in the throat and pre-separator stages (Table 4.3). This was confirmed by SEM, as shown in Figure 4.17. Small agglomerates of SX were detected in the USP throat with size less than 10 µm. Aersolization studies showed the IP/PS deposition

was doubled when SX:CL was emitted from the Cheng 2 than SS:CL (29.65 ± 4.82 for SS:CL vs. 58.71 ± 8.30 for SX:CL at 4 kPa). The rotation of the capsules increases the deagglomeration process [164]. Large agglomerates tend to be deagglomerated better during aerosolization than small agglomerates as the contact surface is smaller.

The addition of fines together with the presence of coarse carrier might increase the deagglomeration due to the fact the particle-particle collisions increase in these types of formulation rather than when only CL is present [203]. This was confirmed by both aerosolization studies and $FPR_{1.5}$ (Table 4.4) of SX:FL:CL and SS:FL:CL emitted from Cheng 2. Collection of carrier particles was seen in the spacer (Figure 4.15), that prevented their deposition in the throat (Figure 4.17). Compared to SX:FL:CL, when Cheng 2 was employed, SEM showed the lack of agglomerates in the spacer for SS:FL:CL (Figure 4.15). This indicates the fine particles are removed from the carrier leading to slightly higher respirable fraction for this formulation rather than SX:FL:CL (81.83 ± 4.11 and 76.66 ± 1.35 at 4 kPa, respectively). This is in accordance with Adi et al [98] who showed less fine particle detachment from the carrier for low % of SX with FL. The particles adhered to the wall of the gelatine capsule and the inhaler used in the study, causing a low FPF of SX. Although, the difference in the SEM for stage 5 between devices and blends is not very clear, higher % deagglomeration for SS:FL:CL formulation was seen than SX:FL:CL (61.4 ± 2.6 vs. 48.7 ± 1.8, respectively, Table 4.8). Nevertheless, the $FPR_{1.5}$ was greater for SX blends than SS blends (Table 4.4). However, when the fines (SX and FL) concentration was increased, a better detachment from the lactose and a greater amount of agglomerates was seen in stage 1 of the twin-stage impinger, because of saturation of the active sites on the carrier[98]. This led to a better interaction between SX and FL causing agglomeration and surface detachment. The authors proposed this is due to the fact that adhesion force between SX-CL was lower than SX-SX and SX-FL [98]. This potentially shows the strong cohesive behaviour of SX particles that is likely to create agglomerates. However, SEM was not a successful technique to help understand the deagglomeration extent of formulation, although it is was a useful tool for assessing particle morphology.

4.6. Conclusion

This chapter has shown that the cyclone spacer Cheng 2 does behave in a different manner for different formulations, despite using the same inhaler to emit the blend. Higher deposition in the IP/PS stages was seen for SX:CL and SX:FL:CL when Cheng 2 was employed, leading to a lower FPF (%sED) than SS:CL and SS:FL:CL, but higher deagglomeration ($FPR_{1.5}$). This was suggested by SEM studies only for SS:FL:CL which showed a greater number of free agglomerates in the formulation than SX:FL:CL, leading to higher dispersion of the micronized material. Moreover, an empirical model has been suggested as a fast approach to understand deagglomeration behaviour of the formulation that enters the spacer which could guide future mixture preparation and design of new cyclone geometry. The empirical parameterization described agglomerate structure and deagglomeration mechanisms. The micronized particles showed different deagglomeration processes to each other suggesting variability in agglomerate size and strength between agglomerates. On the other hand, the presence of the coarse carrier and fine lactose did modify the deagglomeration process suggesting that two different type of fraction of dispersed particles can be identified when increasing the pressure drop.

Chapter 5: Development of a strategy to determine the influence of inter-patient variability on the product performance of dry powder inhalers

5.1. Development of a strategy to determine the influence of inter-patient variability on the product performance of dry powder inhalers

5.1.1. The importance of device choice in patient disease management

Although asthma and COPD (chronic obstructive pulmonary diseases) affect almost 6% of UK population, there is not exact definition for the former, whilst patients with COPD are affected also by heart problems and the cost of management is increasing due to the poor disease control [68]. The causes of poor management are many such as underestimated symptoms, lack of adherence of the patients or incorrect use of the available inhalers [74, 132, 135]. To overcome the adherence issue, a constant improvement of the device design has been recently made by pharmaceutical innovators and engineering design companies, such as GSK (Ellipta), Pfizer (Exubera), Novartis (Breezehaler) or Team Consulting (StarHaler). The main problem is that patients have difficulties in using the appropriate technique through their device [69, 74]. The majority of the patients is not aware of the different techniques in using MDIs (metered dose inhalers) or DPI (dry powder inhalers), resulting in the dose delivered to the lungs being compromised [69]. For an MDI a slow and deep manoeuvre is needed when inhaling the formulation, whilst for DPIs, a fast and deep inhalation is required in order to create turbulent energy for aerosolization of the dose [74].

5.1.2. Inspiratory airflow power and guidance for inhaler selection

The ability of an individual to inhale with sufficient strength through an inhaler, especially dry powder inhalers (DPI), depends on both the lung function and device design [84]. The device design creates a resistance to the air that is almost a fingerprint for each inhaler and a wide range of resistances can be achieved [85]. Typically, high flow rates are achieved through DPIs such as Diskus and Aerolizer which have low resistance compared to high resistance DPIs such as Easyhaler, Turbuhaler and Handihaler [81, 85]. In vivo studies [84, 125, 236] suggested that prolonged peak inspiratory flow (PIF) is achievable with high resistance device, although some patient might find it uncomfortable. Many studies report both high inter and intra-patient flow rate variability that leads to a variable respirable dose and its particle size [12]. It has been shown that the delivered dose and the de-

aggregation force depend on the full inhalation manoeuvre of the patients and not only on the peak inspiratory flow [126]. Using simulated patients' inhalation profiles, Kamin *et al*. [12] tested the variability of the mass output and mass median aerodynamic diameter (MMAD) from two DPIs (Turbuhaler and Accuhaler). The Turbuhaler showed the highest variance in particle output with range of fine particle fraction (FPF) between 3.4% to 22.1% of label claim (at 30 and 75 $Lmin^{-1}$, respectively), whereas the Diskus was less dependent on variations (10.6% to 18.5% of label claim) [12].

Some studies [237, 238] have focused their aims on assessing the peak inspiratory flow (PIF) of a group of COPD (chronic obstructive pulmonary disease) patients through particular devices. Dewar *et al*. [238] suggested that some patients can inhale correctly through the device provided (e.g. Turbuhaler for COPD patients) and Janssens et al. [237] suggested that, especially in elderly patients, the flow rate achievable could be compromised probably due to the high resistance of the inhaler prescribed. Other groups [239, 240] have focused their work on creating or collecting inhalation profiles for in vitro testing of inhalers. Therefore, the inhalation manoeuvre is important to consider when choosing the appropriate device. Some studies in the US and in the EU have been completed [13, 241] on collection of inhalation profiles through specific devices. The authors used a pneumotrac spirometer attached to marketed devices and measured the inhalation profile using the inhalation manager (i.e. a computer-controlled flow-volume simulator). Although their methods gave interesting information regarding the inhalation profiles, it required multiple inhalers with placebo or medicine. Sometimes a propellant might be involved that can increase the risk of having aerosol impacting on the patient's throat.

5.1.3. Incorporating patient performance when assessing product performance

The British and US Pharmacopoeia [147] stated that the aerosol deposition from an inhaler needs to be tested at a constant flow. This is mainly for quality control purposes. However, it does not represent the actual use of inhalers, as patients do not inhale with a constant flow. It has been reported [12, 13] that the inhalation manoeuvres of a patient consist of an initial flow acceleration, when the

dose is usually delivered [126], a maximum peak inspiratory flow that is the maximum flow that the patient achieves, and a deceleration of the flow, that indicates the manoeuvre is terminated. As the assessment of the dose deposition is important to be tested at constant flow, the full inhalation profile needs to be taken in consideration, too (e.g. Figure 5.1).

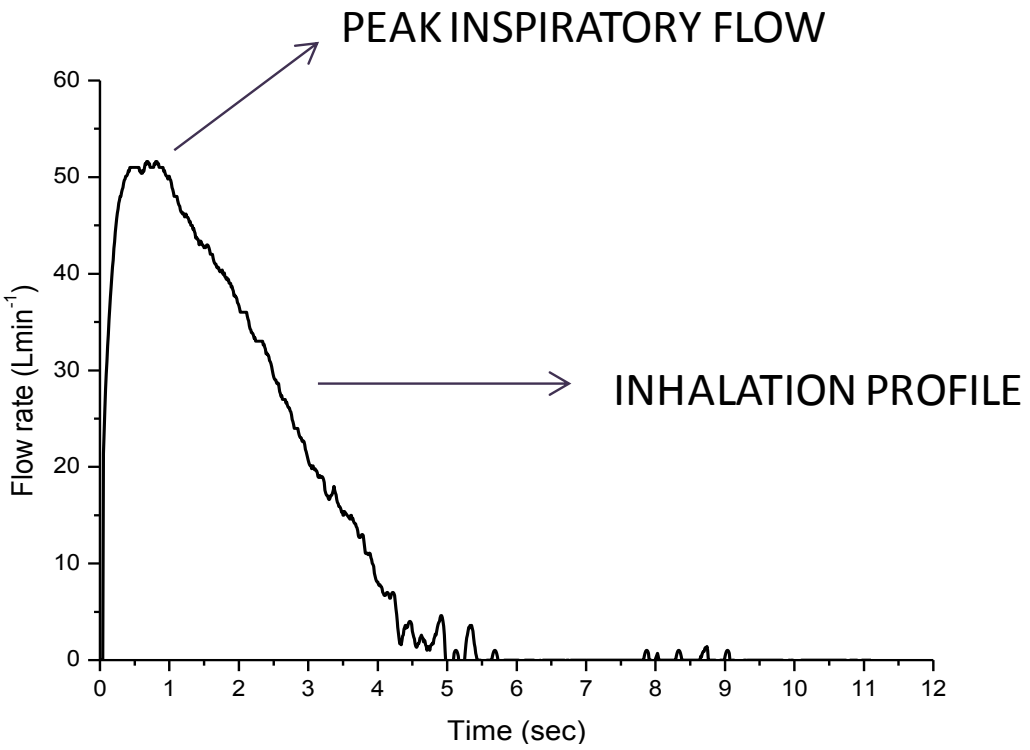

Figure 5.1. Inhalation profile and peak inspiratory flow of a healthy volunteer through Cheng 2 spacer-device.

Studies showed that patients are able to maintain the PIF for longer when the resistance of the device is high [13, 125, 236] rather than when the resistance is low. Also, the dose is released rapidly for devices such as Diskus and Turbuhaler, although the dose emitted from capsule-containing devices such as the Cyclohaler is released over a longer period of time [242]. It has been shown that the powder emptying rate from inhalers appears to increase when the acceleration slope increases [243].

Parameters, such as flow acceleration, inhalation volume, time to reach peak inspiratory flow, post peak deceleration [13] need to be considered when testing aerosol deposition. The electronic lung device (ELD) has been used [126, 127, 244]

in order to determine the aerosol deposition using both inhalation profiles and steady flow. The dose dispersion from the inhaler is driven by the patients' profiles that can be loaded into the ELD, whilst the steady flow allows the particle size determination into the impactor [244]. However, inhalation profiles are required. In Figure 5.1 an example of inhalation profile is shown.

Some authors [245] attempted to predict the slope of the inhalation pressure profiles using the PIFs through inhalers. Correlation was seen between PIF and slopes for Diskus and Turbuhaler (13.5 ± 5.0 and 13.8 ± 4.7 kPa s^{-1}, respectively) [245]. The authors suggested that PIF could be used to predict the inhalation slope if the inhaler resistance is known. However, they pointed out that for a given PIF, a wide range of slopes can be achieved. Previous studies recorded inhalation profiles through inhalers such as Turbuhaler and Diskus [246] to assess the ex-vivo performance of the inhalers. Variability was seen within inhalers. Diskus showed a more accurate and reproducible dose emission across the range of tested flow rates than Turbuhaler [152] and the latter trend was seen regardless of the inhalation profile used [246]. The Turbuhaler delivered only 68.1% of the labelled dose when inhalation profiles of COPD patients were used and a correlation between total emitted dose or fine particle mass with PIF showed that the Diskus performed independently of the PIF unlike the Turbuhaler [246]. Other authors have studied the change in the particle size when using a constant flow or an inhalation profile. Finlay *et al* [247] suggested that the aerosol particle size is unchanged when peak inspiratory flow is chosen instead of the breath simulated profiles as long as the flow rates are set as near as possible of the PIF achieved in the profile.

5.1.4. Throat models for in vitro studies (AIT)

The use of human mouth-throat cast models (e.g. Alberta Idealized Throat, AIT) have started to appear in published papers [183-186] as a substitute for the USP throat for aerosolization studies with cascade impactors. The AIT was first proposed ten years ago by the Aerosol Research Laboratory at the University of Alberta, Canada[248]. The cast has been validated on computed tomography (CT) scans of human throats. Using the AIT would help the prediction of real mouth and throat

deposition and enable a real comparison between in vivo and in vitro data [185, 186]. Zhang et al [185] showed a good correlation between in vivo deposition of particles emitted from the Turbuhaler® (65.8 ± 10.1%) and in vitro deposition using an idealized throat (67.8 ± 2.2 %,). A further, more recent study [249] reported that a good correlation between in vitro and in vivo lung and throat deposition was seen for marketed inhalers such as Handihaler, Diskhaler, Easyhaler, Turbuhaler and Aerolizer. Lung deposition was reported to be 17.3 ± 1.2%, 22.6 ± 1.1%, 29.0 ± 1.1%, 28.0 ± 3.0%, 21.7 ±1.2%, respectively. The throat deposition followed a similar trend [249]. Other studies tested the mouth-throat cast at different flow rates [188, 189] suggesting that small particle deposition decreased under a slow flow rate due to a low particle inertia values. Delvadia *et al* [250] tested inhalers with simulated inhalation profiles using an equation based on the PIFs (peak inspiratory flows) to extrapolate the full profile. However, the state of the disease of the patient needs to be considered, including how this affects their inhalation strength. Consequently accurate inhalation profiles need to be collected from the patients through each device used.

5.2. Aims

The aim of this chapter was to investigate the potential influence of flow-rate control with DPIs on potential disease management in asthmatic patients and those affected by COPD. This involved the collection of preliminary data on the future applicability of a diagnostic tool to guide DPI choice based on inhalation profiles achieved by asthmatic and COPD patients. It also involved establishing a methodology to assess the impact of patient-focussed aerosolization testing to improve inhaled product development. In Chapter 4, the potential of a cyclone spacer to mitigate flow rate dependence of particle size and respirable fraction was examined, revealing different behaviour depending on formulation and API (active pharmaceutical ingredient) choice. However, the biorelevance of employing constant airflow for aerosolization of DPIs needs to be considered. This chapter further aimed to pilot a more patient-relevant testing regime during device and product development in an *ex vivo* pilot study.

The objectives of the current work were:

- To establish and pilot an inspiratory manoeuvre testing system and protocol using clinically-employed spirometry through the Cheng 2 spacer with healthy volunteers
- To design a statistically appropriate study protocol and obtain ethical and R&D approval for a full clinical spirometry study in the NHS
- To identify appropriate asthmatic (moderate, severe) and COPD patients and establish metrics that stratify inter-patient and inter-device variability in dry powder inhaler use.
- To assess the difference in aerosol deposition when employing the Cheng 2 spacer with the standard metric of square wave peak inhalation flow compared to a full inhalation profile.

5.3. Materials and methods

5.3.1. Materials

Micronized salbutamol sulphate (SS, batch number B027798) was purchased from GlaxoSmithKline Research and Development (Ware, UK). Salmeterol xinafoate (SX) was purchased from Vamsi Labs Ltd (Solapur, India). Lactose monohydrate, chromatography grade methanol, hydrochloric acid solution (HCl) 5M, sodium hydroxide and n-Hexane were purchased from FisherScientific (Loughborough, UK). Fine lactose (LH300) was purchased from Friesland Foods (Netherlands). Hipersolv® grade ammonium acetate was purchased from Lab3 Ltd (Northampton, UK). A Luna 3 µm C18 column (150 mm x 4.6 mm x 3 µm) was obtained from Phenomenex (Macclesfield, UK). Silicone oil - Dow Corning Corporation 200® fluid was obtained from Sigma-Aldrich (Gillingham, UK). A Cyclohaler® device was obtained from AAH Hospital Supplies (Coventry, UK). Size 4 hard gelatine capsules were obtained from Meadow Laboratories Ltd. (Romford, UK). The cyclone spacer (Cheng 2) was manufactured in-house (University of Cambridge, UK) from a Perspex block (Engineering & Design Plastics Ltd, Cambridge, UK); the exit duct was cut and polished from stock brass tubing (Engineering Department Storeroom, University of Cambridge, UK). The flow meter (model number DMF2), next

generation impactor (NGI), Breath Simulator (BRS 3000), Albert Idealized throat and a model HCP5 vacuum pump were all purchased from Copley Scientific Ltd (Nottingham, UK).

The spirometer (Vitalograph Pneumotrac) with software IV, filters and mouthpieces were kindly donated by Vitalograph (Buckingham, UK). A Pneumotrac (MasterScreen™ Pneumo Spirometer) was purchased from CareFusion (Basingstoke, UK) and a mouthpiece containing a rotating disk that contained holes that mimic the resistance of MDI, Turbuhaler and Accuhaler was removed from the In-Check Dial (Clement Clarke International Ltd., Harlow, UK). Clement Clark International kindly provided two devices that mimic the resistances of Handihaler and Aerolizer. Filters purchased from CareFusion (Basingstoke, UK) were used between patients to avoid microbial contamination.

Statistical analysis including one-way ANOVA and post-hoc Tukey's test (multiple comparisons) or Student's two-tailed t-tests (paired and unpaired as appropriate) for pair-wise comparisons was performed in Minitab or OriginLab.

5.3.2. Performance of in vivo measurements with healthy volunteers

5.3.2.1. Ethical review and study protocol

An internal ethical approval (number PHAEC/12-77) was obtained from the ethics committee (Professor Brown, Dr O'Neill, Dr Trainor, Mr Caserta, Mrs Fuller) in order to assess inhalation profiles of 10 healthy subjects through a cyclone-spacer prototype using the Vitalograph Pneumotrac spirometer. The participants were requested to fill in a questionnaire about their demographic data (weight, height, gender, age, smoking habit, previous attack of asthma) in order to ensure the health of the volunteers. Once the volunteers were identified, they were requested to perform a full lung function test (Section 5.3.2.2) and to breathe through a cyclone spacer (Engineering & Design Plastics, Cambridge, UK) attached to a spirometer in order to record an inhalation profile (Section 5.3.2.3). The volunteers were fully trained before performing the test. Exclusion criteria for participants were:

- Had a chest infection or were recovering from it.
- Patients with pneumonia unless fully recovered from the condition
- Patients who smoked unless free from smoking for 24 hours
- Patients with pneumothorax
- Patients with myocardial infarction within 8 weeks preceding the test
- Patient with abdominal, chest, throat or eye operations within 6 weeks preceding the test
- Patients with any form of aneurism
- Patient with uncontrolled angina
- Patients with uncontrolled blood pressure
- Patients with asthma or chronic obstructive pulmonary disease
- Participants, who when screened presented with a lung function test indicating obstruction or restriction (i.e. FEV_1/FVC ratio less than 70%; FVC less than 80% and FEV_1 less than 80%). However, spirometry was carried out if at least 5 weeks have passed from the last antibiotic treatment for chest infection.

5.3.2.2. Full lung function testing

Prior to the start of the test, weight, height, gender and ethnic background were recorded in the software (Spirotrac) to confirm the health of the volunteer. Then, the subject exhaled into a disposable filter (to avoid contamination between volunteers) in order to measure slow vital capacity (SVC), forced expiratory volume in 1 second (FEV_1), forced vital capacity (FVC), and peak expiratory flow (PEF). A minimum of three tests were measured. In order to define healthy volunteers, the ratio between FEV_1 and FVC had to be > 0.7 and PEF> 75 % of the predicted value. The FVC had to be > 80% and FEV_1> 80% of the predicted value [11]. The values were assessed in accordance to ATS/ERS (American Thoracic Society/European Respiratory Society) criteria.

5.3.2.3. Collection of inhalation profiles and Peak Inspiratory Flow through Cheng 2

Following lung function screening, the volunteers inhaled through the cyclone spacer attached to the spirometer to assess the inhaled volume (IV) and the peak

inspiratory flow (PIF) through the device and in order to record the inhalation profiles. A disposable mouthpiece (sterile plastic tubing) was attached to the cyclone to avoid contamination between volunteers (Figure 5.2). A minimum of three tests were measured for each volunteer and exported as an MS Excel spreadsheet. PIF was measured using the ATS equation from the inhalation profiles.

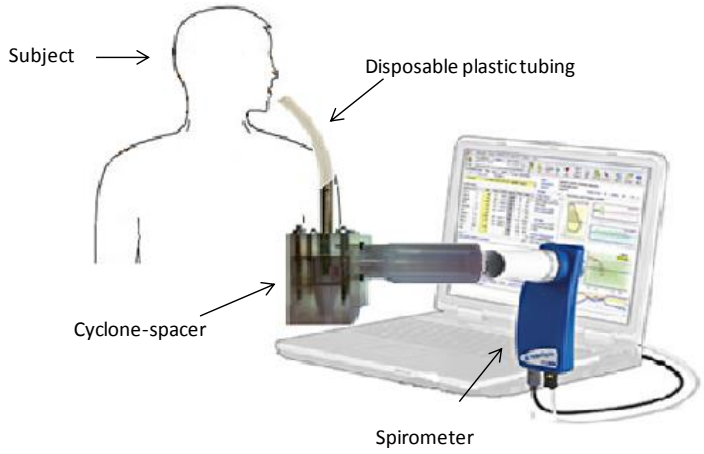

Figure 5.2 Diagram of how the in-vivo study was performed

5.3.3. Clinical study

5.3.3.1. NHS protocol

An ethical and R&D approval (REC number: 13/LO/0970 and Study ID: 122645) was obtained through the Royal Brompton Hospital (Asthma Clinic, London) in order to recruit 80 patients (20 COPD and 20 mild, 20 moderate and 20 severe asthmatics, all adults) that were identified through medical records. For the purpose of this chapter, the data from only 20 severe asthmatics and 20 COPD patients were analysed due to failure to recruit sufficient numbers of patient to reach statistical power. The protocol was designed to identify patients through a clinician at the hospital who performed a full lung function test on the volunteers as a routine check. The volunteers were requested to inhale through an airflow-restricting device that mimics the resistance to airflow of marketed in order for their inhalation profile to be collected (Table 5.1).

Table 5.1 Devices and their resistance to the air tested with patients.

Device	Resistance ($kpa^{0.5}L^{-1}min$)
MDI	No resistance
Aerolizer	0.020
Handihaler	0.048

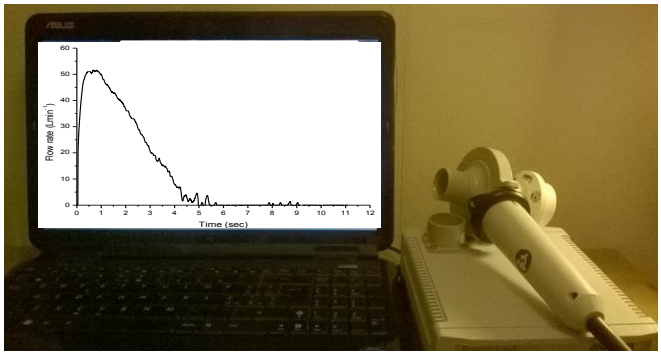

Participants were permitted to practice an inhalation manoeuvre under training prior to the recorded inhalation. The study was designed in a way that the patients would inhale air when performing the study as showed in above. No placebo powder or active pharmaceutical ingredient was used. Exclusion criteria for the patient recruitment to the clinical phase of study were identical to Section 5.3.2.1, above. Lung function testing was also performed as described in Section 5.3.2.2.

5.3.3.2. Sample size selection

The study was designed as a cross-over cohort observational study. Two statistical packages were employed for analysis. G*Power Ver. 3 (University of Duesseldorf) was used to assess the response of statistical power to effect size and sample number. Minitab Ver. 16.2 was employed to calculate statistical power. The data generated were assumed to represent a normal distribution of values. Literature review of clinical studies was performed to enable sample size analysis. The mean ($\bar{x}$) and standard deviation (*s*) values were taken into account. The measured (estimated) difference was calculated using Equation 5.1:

$$\Delta = \bar{x}_1 - \bar{x}_2 \qquad (5.1)$$

Assuming a normal distribution, the individual sample means ($\bar{x}_1, \bar{x}_2$) were estimates of the true population means (μ_1, μ_2). Hence the estimate of the differences between the means was also a normal distribution with a mean (μ_d) and a standard error (SE_d) and variance $(SE_d)^2$. The standard error of the difference can be calculated in Equation 5.2:

$$SE_d = \sqrt{\frac{(s_1)^2}{n_2} + \frac{(s_2)^2}{n_2}} \tag{5.2}$$

For Δ to reach significance, the test statistic of d/SE_d should be greater than the critical value $|u_\alpha|$. Here u_α is a value selected such that the standard normal distribution (mean 0, variance 1) > $|u_\alpha|$ with probability α. For example $u_{0.05} = 1.96$. In accordance with Bland *et al* [251] and Whitley *et al* [251, 252] statistical estimates of effect size were calculated from the differences (Δ) through the calculation of standardized differences (Cohen's effect size, [253]), d, according to equation 5.3 .

$$d = \frac{\bar{x}_1 - \bar{x}_2}{s} \tag{5.3}$$

In the first approach, the pooled standard deviation was calculated according to:

$$s_{pool} = \sqrt{\frac{(n_1 - 1)s_1^2 + (n_2 - 1)s_2^2}{n_1 + n_2}} \tag{5.4}$$

Where n_1, n_2 are the numbers of patients and $s_1$and s_2 are the standard deviations reported for study group 1 and 2, respectively, from the literature values. In the second approach the largest standard deviation (s_{max}) from the reported studies (e.g. when comparing PIFR for asthmatics through Turbuhaler vs. PIFR for asthmatics through Accuhaler) was employed in Equation 5.3, to provide the most conservative estimate of effect size (d_{max}).

The sample size was determined for at a significance level of 0.05 for a statistical power of 0.8 and 0.9 using Equation 5.5:

$$n = \frac{2f(\alpha, p)}{d^2} \tag{5.5}$$

The function *f(α,p)* is defined as:

$$f(\alpha, p) = \left(u_{\alpha} + u_{2(1-P)}\right)^2 \quad (5.6)$$

Where the values for the *f(α,p)* function were obtained from literature [251, 252].

5.3.3.3. Collection of inhalation profiles as a function of device resistance

After assessing the severity of the disease, the patients were required to inhale through an airflow-restricting device consisting of a rotating disk with holes that mimic the resistance to the air of marketed inhalers, within a sealed mouthpiece. By rotating the disk, each aperture diameter was selected in turn, thereby providing a range of resistances. The inhalation volume and full profile were recorded using spirometry for each patient over an inhalation period (measured in seconds), until the patient felt comfortable to inhale. A disposable mouthpiece was attached to the airflow-restricting device that was changed between patients to avoid cross-contamination. After the study the patients were rewarded economically.

5.3.4. Impaction studies with Cheng 2 using Next Generation Impactor at peak inspiratory flow

The formulations of SS:FL:CL and SX:FL:CL, prepared for the study in Chapter 4, were tested using the Cyclohaler® at the PIF values corresponding to the population undersize 10th, 25th, 50th, 75th and 90th percentiles with the Cheng 2 in place according to Section 4.3.5. Prior to performing the measurements with the NGI, the desired flow rate was adjusted with a flow meter. 15 ml of mobile phase was added to the central cup of the pre-separator. Eight capsules were actuated at each flow rate. In order to collect the drugs, the Cyclohaler, with the capsules, were washed with 20 ml of mobile phase. The bottom of the cyclone was washed with 100 ml, whilst the mouthpiece and the AIT (Alberta Idealized Throat) were washed with 25 ml of mobile phase.The upper section of the cyclone was washed with 10 ml. For collecting the drugs from the pre-separator 50 ml of mobile phase was used. The volumetric flasks were sonicated (Kerry, Germany) for 2 min. Mobile phase (5 ml) was added to each stage to recover deposited drug. All the stages were set on a laboratory rocker (Stirling Mixer, Sandrest Ltd, UK) and rocked for 2 min in order for the solvent to wash the entire surface. The concentrations of the drugs from each

stage were determined by HPLC assays as described in Chapter 2, Section 2.3.3 and Chapter 3, Section 3.3.3. After performing the experiments, each stage and the NGI were thoroughly cleaned with Millipore water and the coating was removed with acetone before rinsing with methanol.

5.3.5. Impaction studies with Cheng 2 using Next Generation Impactor with inhalation profiles

The inhalation profiles collected from the healthy volunteers through the spacer were uploaded in the Breath Simulator 3000 (Copley, Nottingham, UK). Prior to the test, the PIF from each profile was set with a vacuum pump at the outlet of the breath simulator attached to the NGI. With an air compressor, the flow was then set to zero to avoid air leak between actuations (Figure 5.3).

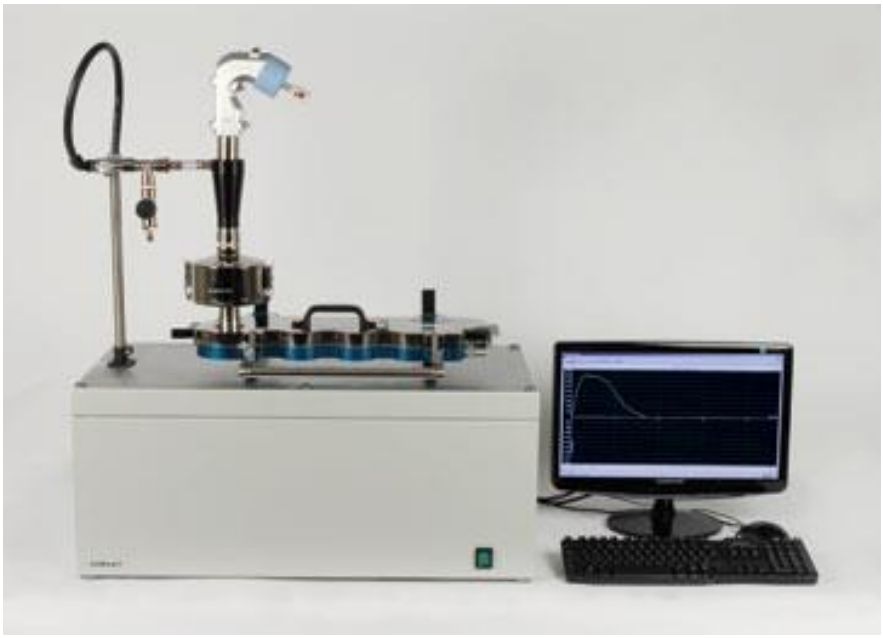

Figure 5.3. Breath simulator 3000 attached to a next generation impactor.

The inhalation profiles which possess the PIF corresponding to the 10^{th}, 25^{th}, 50^{th}, 75^{th} and 90^{th} percentile of PIFs of the population were employed. The Cheng 2 was used attached to the Cyclohaler. The same method was used as described in Section 5.3.4.

5.4. Results

5.4.1. Performance of in vivo measurements with healthy volunteers

5.4.1.1. Full lung function testing

All the volunteers utilized for the project were healthy (using the FEV_1/FVC being > 0.7) as demonstrated by the SVC, FEV_1 and PEF values in Table 6.2 (n=10).

Table 5.2. Table of parameters used to define healthy volunteers (FEV_1= forced expiratory volume in 1 sec; PEF = peak expiratory flow, SVC =slow vital capacity).

Parameters	Values (mean ± SD)
Female	5
Male	5
Smokers	0
FEV_1 % predicted	104.14 ± 8.51
PEF % predicted	103.87 ± 9.15
SVC	4.43 ± 0.87

5.4.1.2. Collection of inhalation profiles

The 10 volunteers were requested to inhale through the cyclone at maximal effort but not to cause discomfort [125]. Each volunteer repeated the inspiratory manoeuvre 3 times and the average result was 72.07 ± 12.03 $Lmin^{-1}$ with an inhaled volume of 2.96 ± 0.64 litres (n = 30). Cumulative frequency analysis (Table 5.3 and Figure 5.4) showed that one quartile of the volunteers was able to breathe through the spacer with a PIF greater than 79.93 $Lmin^{-1}$whilst the lower quartile used a PIF of 65.55 $Lmin^{-1}$or less. However, half of the volunteers managed to breathe with a PIF greater than 72.65 $Lmin^{-1}$. A wide range of flow rates were achievable with the Cheng 2 in the healthy population. In Figure 5.5 representative inhalation profiles through the Cheng 2 are shown.

Table 5.3. Values of peak inspiratory flow through the cyclone for 10%, one quartile, three quartile, half and 90% of the volunteers.

10%	25%	Median	75%	90%
52.83$Lmin^{-1}$	65.55 $Lmin^{-1}$	72.65 $Lmin^{-1}$	79.93 $Lmin^{-1}$	89.1$Lmin^{-1}$

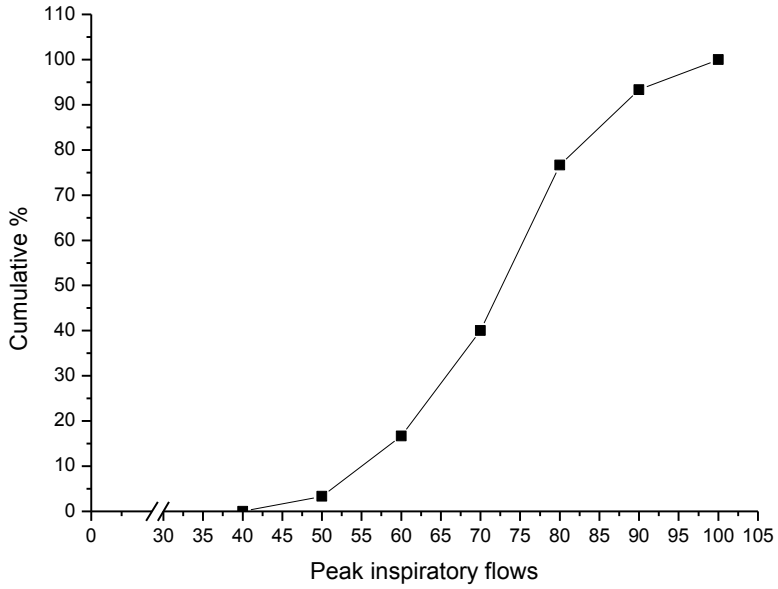

Figure 5.4. Cumulative frequency distribution of peak inspiratory flow rates achieved through the cyclone (n=30).

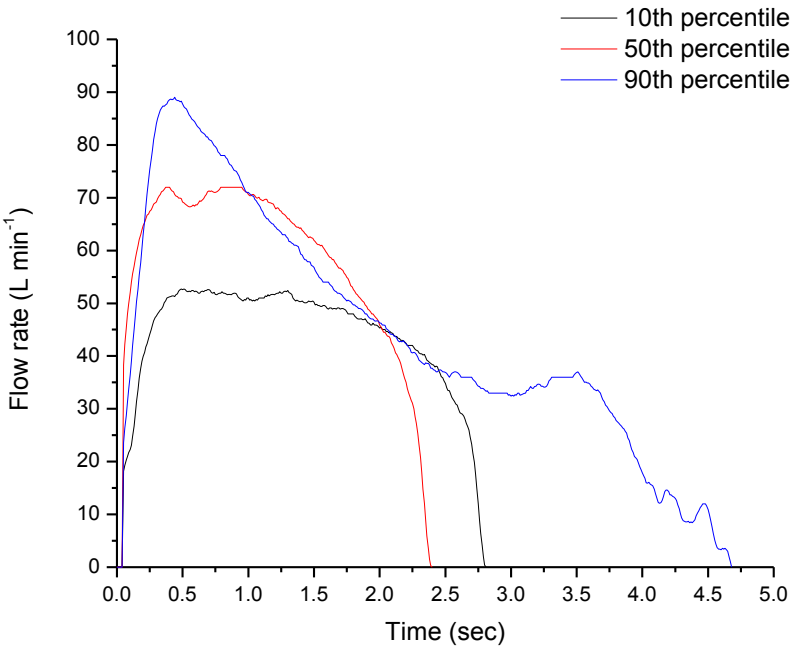

Figure 5.5. Representative inhalation profiles of a healthy volunteers through the Cheng 2 spacer-device.

5.4.2. Statistical design to measure inspiratory performance through dry powder inhalers using a clinically-applicable spirometry tool.

In order to establish an appropriate sample size a survey was conducted of previous similar studies from the literature where inhalation by patients through various devices was studied. The majority of the data were reported as mean ($\bar{x}$), standard deviation (*s*) and sample size (*n*) (Table 5.4). As the study was a cross-over cohort observational study the differentiating power was increased by allowing paired comparisons both within homogeneous groups and between heterogeneous groups. The study does not rely on independent group comparisons. A single metric from the inhalation profile (peak inspiratory flow rate, PIFR) has been used to assess the appropriateness of an emitted aerosol for inhalation therapy. Therefore the PIFR and the fine particle mass/fraction (i.e. that portion of the dose which is suitable for inhalation) were examined to assess the statistical power and an appropriate sample size for comparisons of relevance. The data from review of the cited studies are presented in Table 5.4.

The study's aim was to recruit equal numbers of patients for study in each group. Furthermore, it was clear from comparison of previous studies (Table 5.4), that variance in the sample estimates was not identical between study groups or conditions. Therefore, to provide the most conservative estimate of SE_d for sample size determinations, the largest value of the s of any two groups being compared was chosen (e.g. PIFR for asthmatics through Turbuhaler compared to PIFR for asthmatics through Accuhaler). The differences (Δ) from published reports as estimates of the anticipated differences in the current study along with their SE_{diff}, Cohen's effect size (*d*) and the most conservative effect size (d_{max}) are presented in Table 5.5 and the sample size and study power were determined for a significance level of $s = 0.05$.

Table 5.4. Sample mean values ($\bar{x}$), standard deviation (*s*) and sample number (*n*) from previous literature reports into inhalation performance through inhaler devices. COPD: chronic obstructive pulmonary disease, PIFR: peak inspiratory flow rate, FPM: fine particle mass following aerosolization and FPF: fine particle fraction following aerosolization.

	$\bar{x}$	*s*	*n*
Combined asthma & COPD, PIFR through devices [13]			
Turbuhaler	65.1 ($Lmin^{-1}$)	21.1	262
Accuhaler	103.3 ($Lmin^{-1}$)	42.0	341
Uncategorized COPD, PIFR through devices [81]			
Turbuhaler	47.8 ($Lmin^{-1}$)	14.7	163
Accuhaler	57.5 ($Lmin^{-1}$)	17.9	163
Handihaler	28.6 ($Lmin^{-1}$)	10	163
Uncategorized asthma, PIFR through devices [254]			
Turbuhaler	76.8 ($Lmin^{-1}$)	26.2	20
Accuhaler	94.7 ($Lmin^{-1}$)	32.9	20
PIFR for Turbuhaler, comparing diagnosis [13, 254]			
Asthma	76.8 ($Lmin^{-1}$)	26.2	20
COPD	47.8 ($Lmin^{-1}$)	14.7	163
PIFR for Accuhaler, comparing diagnosis [13, 254]			
Asthma	94.7 ($Lmin^{-1}$)	32.9	20
COPD	57.5 ($Lmin^{-1}$)	17.9	163
PIFR for grouped asthmatics & COPD [245]			
Turbuhaler	76.1 ($Lmin^{-1}$)	13.8	58
Accuhaler	108.3 ($Lmin^{-1}$)	20.4	58
PIFR for Turbuhaler: 4-year olds compared to 8-year olds as a surrogate measure for lung function/capacity [255]			
4 years	53.0 ($Lmin^{-1}$)	23.0	18
8 years	76.0 ($Lmin^{-1}$)	10.0	20
PIFR for Accuhaler: 4-year olds compared to 8-year olds as a surrogate measure for lung function/capacity [255]			
4 years	70.0 ($Lmin^{-1}$)	23.0	18
8 years	105.0 ($Lmin^{-1}$)	14.0	20
FPM when inhalation profiles tested ex vivo for Accuhaler: 4-year olds compared to 8-year olds as a surrogate measure for lung function/capacity [255]			
4 years	15.0 (µm)	2.0	18
8 years	18.0 (µm)	2.0	20
FPM when inhalation profiles tested ex vivo for Turbuhaler: 4-year old compared to 8-year olds as a surrogate measure for lung function/capacity [255]			
4 years	21.0 (µm)	10.0	18
8 years	32.0 (µm)	9.0	20
Uncategorized asthma, FPM when inhalation profiles tested *ex vivo* [254]			
Turbuhaler	20.4 (µm)	4.8	20
Accuhaler	23.1 (µm)	12.9	20

Table 5.5 . Measured difference (*d*) and standard error of the difference (SE_{diff}) and effect sizes (*d* and d_{max}) for literary comparisons in peak inspiratory flow values (PIFR). COPD is chronic obstructive pulmonary disease.

	Δ	SE_{diff}	***D***	d_{max}
To compare PIFR between Turbuhaler & Accuhaler in asthmatics & COPD patients [13]	38.2 ($Lmin^{-1}$)	2.6	1.11	0.91
To compare PIFR between two devices in uncategorized COPD patients [81]				
Turbuhaler vs Accuhaler	9.7 ($Lmin^{-1}$)	1.8	0.59	0.54
Turbuhaler vs Handihaler	19.2 ($Lmin^{-1}$)	1.4	1.53	1.31
Accuhaler vs Handihaler	28.9 ($Lmin^{-1}$)	1.6	1.99	1.62
To compare PIFR between Turbuhaler & Accuhaler in uncategorized asthmatics patients [254]	17.9 ($Lmin^{-1}$)	9.4	0.62	0.54
To compare PIFR between Turbuhaler & Accuhaler for patients with uncategorised lung disease [256]	32.2 ($Lmin^{-1}$)	3.2	1.87	1.58
To compare PIFR between asthmatics and COPD patients for a specific device [81, 254]				
Turbuhaler	29.0 ($Lmin^{-1}$)	6.0	1.79	1.11
Accuhaler	37.2 ($Lmin^{-1}$)	7.5	1.87	1.13
To compare PIFR between lung function for a specific device [242]				
Turbuhaler	23.0 ($Lmin^{-1}$)	5.9	1.36	1.00
Accuhaler	35.0 ($Lmin^{-1}$)	6.3	1.91	1.52

From Table 5.5, it is clear that the required sample size for group comparative studies ranges is subject to a wide degree of variability in estimated effect size from a low of 0.54 [81] to a high of 1.62 [81]. This was expected to lead to a disparity between the estimated sample size required for some comparisons when the various studies are examined. The response of sample power to effect size was determined for total sample sizes ranging between 80 and 160 patients (Figure 5.6). In the current study, it was proposed that 20 patients would be recruited for each category of lung disease (i.e. a total of 80 patients). It is clear that for the lowest effect size (d_{max} = 0.54) a large sample size of >55 patients per treatment arm would be required to achieve statistical power of 80 % with an independent comparison of mean PIFR for two devices. However, the cross-over design ensures 80 patients in each measurement arm (equivalent to a total of 160 patient comparisons). Pooling standard deviation when comparing two different devices in the same patient population may not be a suitable approach due to the potential for vastly different variability in the data (cf. SE_{diff} in Table 5.5). To account for this and provide the most discerning test for difference, the mean PIFRs for two devices in the heterogeneous

patient group are compared as independent means. From Figure 5.6, when the assumption was applied to the 80 patient-comparison, the study design provides for in excess of 80 % power at the 5 % confidence interval even with the low *d* = 0.54.

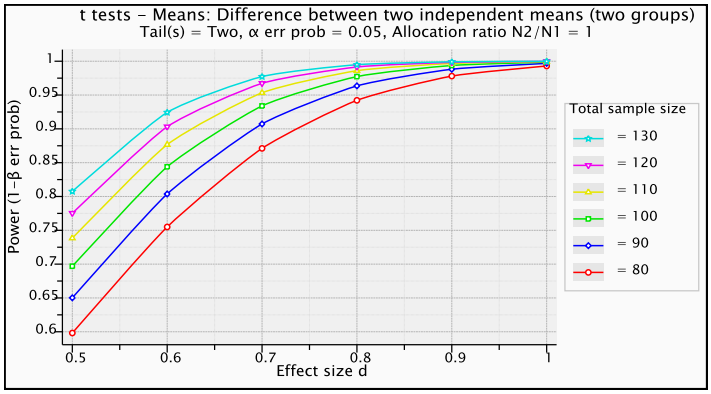

Figure 5.6. Simulation of effect size (Cohen's d value) on the statistical power at a confidence level of α = 0.05 for a two-tailed independent t-test comparing mean PIFR between two different devices total sample of 80 (red), 90 (blue), 100 (green) 100 (yellow), 120 (purple) and 130 (cyan) patients.

The design of the current study employs a paired analysis, thereby offering 80 uncategorised patients per device (i.e. 20 mild, 20 moderate, 20 severe, 20 COPD). From Figure 5.7, it is clear that the 80 patients achieved by pooling patients from all four groups together would achieve a power in excess of 90 %. Within a homogeneous treatment group, it would be expected that the effect of changing device would be lowest for mild asthmatics, but highest for severe asthmatic patients. The simulation performed assuming the lowest effect size of any of the reported studies (d_{max}=0.54) was chosen to represent the mild asthmatic group and also to account for the fact that the COPD group to be recruited is likely to be heterogeneous in their disease state. In considering the effect of changing the device on PIFR (Figure 5.7, red) it is clear that a sample size of 26 patients would be sufficient to determine differences at 75 % power within the classified groups. However, cross comparison of all three studies indicates that in actual fact a d_{max}> 0.54 is to be expected in a homogeneous patient group and therefore recruiting 20 subjects in each disease severity category would provide for sufficient statistical power using the proposed design.

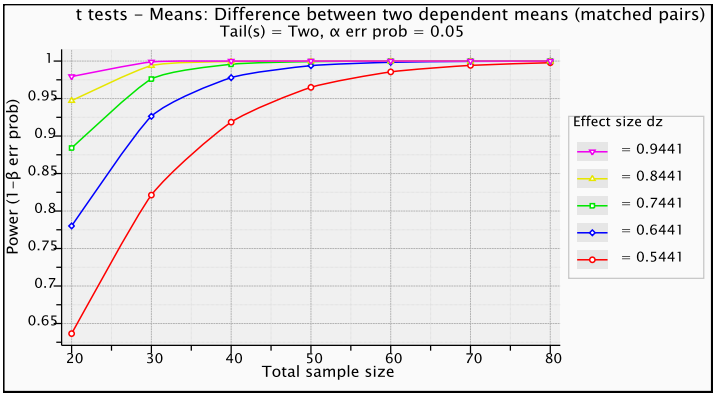

Figure 5.7. Simulation of effect sample number on the statistical power at a confidence level of α = 0.05 for a two-tailed paired t-test comparing mean PIFR between two different devices for an effect size of sample of 0.54 (red), 0.64 (blue), 0.74 (green), 0.84 (yellow) and 0.94 (purple).

The change in PIFR when using the same device in a sample of asthmatics compared to a sample of COPD patients is presented in Table 5.5. It can be seen that even comparing two heterogeneous patient populations (i.e. uncategorised asthma and uncategorised COPD), the disease state is predicted to have a large effect on the PIFR. Employing the lowest d_{max} value (1.11) would result in a power > 99 % (Figure 5.7) for comparing a group of 20 asthmatics with 20 COPD patients in the current study. The strength of the latter observations suggests that a sample size of 20 patients in each disease group would provide for a sufficiently powered study to assess differences between disease state and PIFR for a particular device. The stratification of patients into homogeneous groups defined by disease severity was assessed using a surrogate marker for lung function/capacity (i.e. age) is considered for children (Table 5.5), since the latter population shows highly variable inhalation abilities [255]. In this instance the lowest effect size observed was 1.00 (comparing the same device between two age groups) and a sample size of 20 patients in each group would provide a power of 86.9 % when comparing independent means. Thus classification of patients into categories of disease severity (i.e. mild, moderate, severe asthmatics and COPD patients) provides a sufficient statistical power for the most conservative estimates of effect size (d & d_{max}), both for paired group (device-

device) and unpaired group (disease condition-disease condition) comparisons when studying inhalation profiles in asthmatic patients.

5.4.2.1. Inhalation performance and parameterisation of patients with lung disease

The full lung function testing (FEV_1, forced expiratory volume in 1 s, FVC, forced vital capacity and the ratio of the two values) are reported in Table 5.6.

Table 5.6. Forced expiratory volume in 1 sec (FEV_1), forced vital capacity (FVC) and ratio between FEV_1 and FVC for COPD and severe asthmatics patients involved in the study (mean ± SD, n=20).

Parameters	COPD	Severe asthma
FEV_1 (% pred)	54.79 ± 26.61	63.21± 27.09
FVC (% pred)	87.79 ± 27.87	80.89 ± 24.27
FEV_1/FVC (%)	62.13 ± 18.19	77.52 ± 23.51

In Figure 5.8 (A, B) a representative inhalation profile for each 'device' resistance is presented for the two groups of patients.

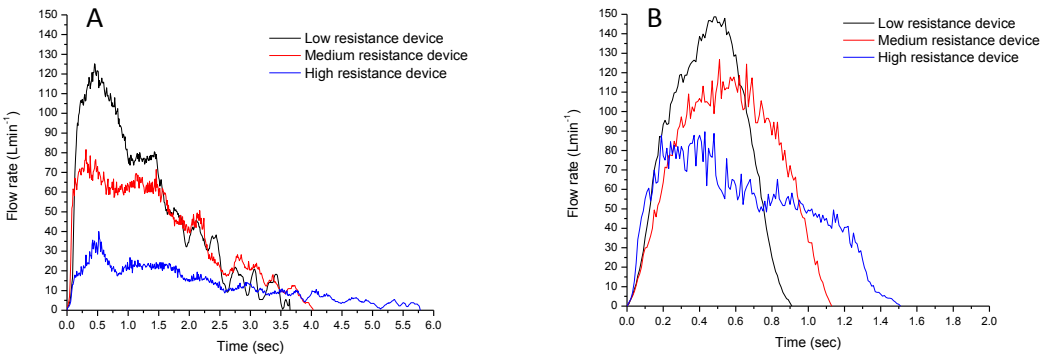

Figure 5.8. Representative inhalation profiles against time through resistance simulating a low resistance device (red), the medium resistance device (blue) and the high resistance device (green) devices a COPD patient (A) and a severe asthmatic patient (B).

The majority of the patients demonstrated inappropriate technique when inhaling through the low resistance device as shown in Figure 5.8 (black line). On the other hand, when testing the device with resistance of 0.04 $kpa^{0.5}L^{-1}min$ a more prolonged flow was observed (Figure 5.8, blue line). In Table 5.7, metrics recorded from the inhalation profiles of the patients and used for statistical analysis are reported.

Table 5.7. Values of peak inspiratory flow (PIF), inhaled volume (IV), time of inhalation, time to reach the PIF, PIF at 50,70, 90%, acceleration measured for two groups of patients through three inhalers (mean ± SD, n=20)

Metrics	Resistances ($kpa^{0.5}L^{-1}min$)	COPD	Severe asthma
PIF (l/min)	No resistance	147.57 ± 43.71	141.72 ± 53.21
	0.02	133.33 ± 43.30	133.44 ± 41.19
	0.04	82.51 ± 28.64	77.89 ± 28.05
IV (L)	No resistance	2.39 ± 0.95	2.09 ± 0.72
	0.02	2.51 ± 0.96	2.06 ± 0.73
	0.04	2.09 ± 0.86	1.59 ± 0.68
Time of inhalation (sec)	No resistance	3.06 ± 1.36	1.89 ± 1.01
	0.02	3.02 ± 1.90	1.85 ± 0.97
	0.04	4.12 ± 1.88	2.78 ± 1.81
Time to PIF (sec)	No resistance	0.72 ± 0.73	0.71 ± 0.44
	0.02	0.83 ± 1.89	0.64 ± 0.54
	0.04	0.82 ± 0.95	0.78 ± 1.09
Time above 50% (sec)	No resistance	1.22 ± 0.50	1.03 ± 0.44
	0.02	1.14 ± 0.43	1.02 ± 0.30
	0.04	1.58 ± 0.62	1.41 ± 0.54
$Acceleration_{50}$ (l/sec^2)	No resistance	7.26 ± 5.15	7.45 ± 5.91
	0.02	8.35 ± 5.22	8.59 ± 5.44
	0.04	4.04 ± 2.33	4.65 ± 2.64
$Acceleration_{70}$ (l/sec^2)	No resistance	7.37 ± 4.92	7.35 ± 5.47
	0.02	6.97 ± 3.51	8.29 ± 5.07
	0.04	2.92 ± 1.55	4.21 ± 2.27
$Acceleration_{90}$ (l/sec^2)	No resistance	6.08 ± 3.46	5.98 ± 3.97
	0.02	8.09 ± 4.39	6.83 ± 4.90
	0.04	3.74 ± 2.04	3.40 ± 1.80
Acceleration (l/sec^2)	No resistance	4.87 ± 2.90	4.52 ± 2.68
	0.02	5.42 ± 3.15	5.32 ± 3.82
	0.04	2.47 ± 1.32	2.83 ± 1.67

The PIFs achieved for the low resistance device were high compared to the DPIs used due to the patients' poor inhalation technique. However, for within disease group comparisons, patients inhaling through the medium resistance device (e.g. Aerolizer), achieved a greater PIF and IV than following inhalation through the high resistance device (e.g. Handihaler, paired t-test, $p<0.05$, Table 5.7). No significant difference was seen when any specific inhaler was compared between asthmatics and COPD patients (unpaired t-test, $p>0.05$, Figure 5.9). A similar trend to the PIF was observed for the high IV achieved by the patients for a medium resistance device compared to high resistance device. Unlike the PIF, a significant difference was seen for IV between disease groups for the medium and the high resistance device (unpaired t-test, $p<0.05$, Table 5.7).

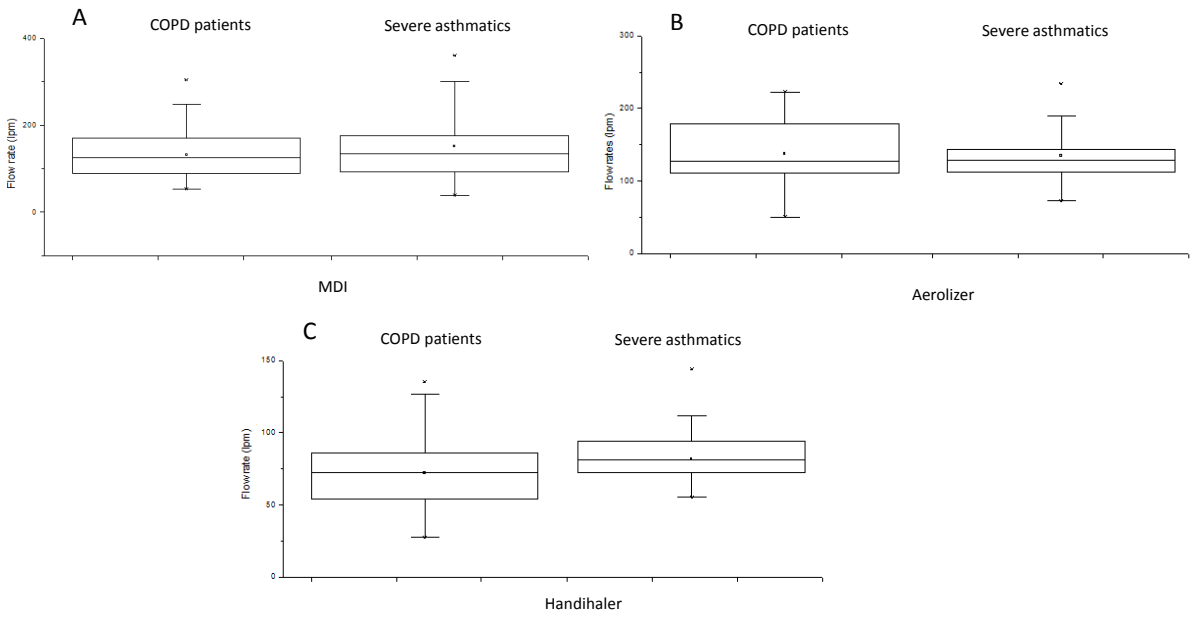

Figure 5.9.Statistical analysis of PIF (peak inspiratory flow) on MDI (A), Aerolizer (B) and Handihaler (C) between groups of patients (mean ± SD, n=20).

Interestingly patients affected by COPD had a longer inhalation time for all the inhalers than asthmatic patients ($p<0.05$, Table 5.7) and, in addition, a longer inhalation manoeuvre for the highest resistance device ($p<0.05$, Table 5.7). No statistical difference was observed for the % of PIFs (Table 5.7, $p>0.05$) between diseases, although the % of PIFs were greater for the no resistance device compared to the medium resistance device and then high resistance inhaler within the same patient group. The same trend was observed when the acceleration was analysed, although no statistical significance was observed for inter-disease group comparisons for any specific device and inter-device comparisons for a particular patient group for time to reach the PIF ($p>0.05$, Table 5.7). Moreover, higher acceleration was observed during the inhalation profiles for both groups of patients when the resistance of the device decreased (Table 5.7).

5.4.3. Aerosolization studies with Cheng 2 at peak inspiratory flow

Aerosolization studies of SX:FL:CL and SS:FL:CL were performed using the NGI with the AIT at the PIF of the 10^{th} – 90^{th} percentile of the population. The PIF identified were 52.83 $Lmin^{-1}$ for 10 %, 65.55 $Lmin^{-1}$ for 25 %, 72.65 $Lmin^{-1}$ for 50 %, 79.93$Lmin^{-1}$ for 75 % and 89.1 $Lmin^{-1}$ for the 90^{th} percentile. The Cyclohaler was used in series with the Cheng 2. The recovery was within the pharmacopoeial limits

for both drugs at each flow rate (e.g. 75.16 ± 0.34% – 76.34 ± 2.04 for SS:FL:CL and 77.57 ± 2.44 % - 76.25 ± 1.29 % for SX:FL:CL% between 10^{th} – 90^{th} percentile of the PIFs). Similar to previous observations (Chapter 4) the emission from the Cheng 2 was higher for SX:FL:CL (range: 16.02 ± 7.13 % to 16.51 ± 1.42 %) between the flow rates tested. For SS:FL:CL the % emission ranged from between 12.59 ± 0.95% to 12.14 ± 0.94%. Although the emission form the Cheng 2 was higher for SX:FL:CL, the FPF (%sED) was lower for this blend than SS:FL:CL, due to a higher AIT deposition for the SX formulation (21.66 ± 3.02% at the 10^{th} percentile) than SS where AIT deposition was not detectable at any flow rate tested. On the other hand, %FPF (ED) was almost unaltered between blends, whilst the FPD (especially for 10^{th} and 90^{th} percentile PIFs) showed differences between blends (Table 5.8).

Table 5.8. Fine particle fraction (FPF) and fine particle dose (FPD) for salbutamol sulphate (SS): fine lactose (FL): coarse lactose (CL) and salmeterol xinafoate (SX): FL: CL emitted from the Cheng 2 in series with the Cyclohaler® at the peak inspiratory flow at 10^{th}, 25^{th}, 50^{th}, 75^{th}, 90^{th} percentile of the population (mean ±SD, n = 4).

Blends	% of population	Peak inspiratory flow ($Lmin^{-1}$)	% FPF (ED)	% FPF (%sED)	FPD (µg/ml)
SS:FL:CL	10	52.83	13.38 ± 2.63	86.71 ± 16.02	14.18 ± 0.44
	25	65.55	14.14 ± 5.58	99.93 ±0.08	13.29 ± 6.59
	50	72.65	14.71 ± 2.38	99.97 ± 0.03	15.62 ± 2.28
	75	79.93	18.57 ± 4.64	99.85 ± 0.15	16.33 ± 3.77
	90	89.10	16.96 ± 1.99	99.90 ± 0.03	16.28 ± 1.34
SX:FL:CL	10	52.83	17.05 ± 2.12	74.09 ± 5.12	15.96 ± 8.14
	25	65.55	16.25 ± 3.11	69.23 ± 3.75	18.70 ± 4.02
	50	72.65	19.23 ± 3.93	72.39 ± 3.92	21.50 ± 4.52
	75	79.93	17.78 ± 3.52	71.91 ± 1.97	20.34 ± 3.88
	90	89.10	14.72 ± 0.72	73.00 ± 3.05	15.52 ± 1.36

The FPF (%ED) was calculated as a fraction of the particles emitted from the Cyclohaler entering the spacer. The almost unchanged FPF (%ED) was already seen for the Cheng 2 spacer in Chapter 4, Section 4.4.4. On the other hand, if FPF (%sED) is analysed, a difference is seen in the formulations (Table 6.8, SX < SS for low flow rate profiles), due to the deagglomeration process that occurs in the cyclone-spacer, already proposed in Chapter 4.

5.4.4. Aerosolization studies with Cheng 2 using inhalation profiles

The inhalation profiles of healthy volunteers were collected through the Cheng 2 and tested in the NGI for SX:FL:CL and SS:FL:CL. The comparison of the aerosol deposition with the impactor was made when inhalation profiles were tested vs. PIF. The recovered dose was within the pharmacopoeial limits for both formulations (e.g. 77.96 ± 2.44% for SS:FL:CL for the 10th percentile and 84.40 ± 5.93% for SX:FL:CL at 90th percentile).

Table 5.9.% Emission (%sED) from the Cyclohaler in series with Cheng 2 and % AIT/PS Alberta idealized throat/pre-separator) deposition for salbutamol sulphate (SS): fine lactose (FL): coarse lactose (CL) and salmeterol xinafoate (SX):L fine lactose (FL): coarse lactose (CL)at the peak inspiratory flow (PIF) and inhalation profiles (IP) corresponding to the 10th, 25th, 50th, 75th, 90th percentile of the population (mean ±SD, n = 4).

Blends	%	% Emission (%sED) from IP	% Emission (%sED) from PIF	AIT/PS deposition (%)from IP	AIT/PS deposition (%)from PIF
SS:FL:CL	10	2.55 ± 1.00	12.59 ± 0.95	0.00 ± 0.00	0.00 ± 0.00
	25	5.46 ± 1.62	10.52 ± 4.09	0.00 ± 0.00	0.00 ± 0.00
	50	6.67 ± 3.75	10.66 ±1.52	0.00 ± 0.00	0.00 ± 0.00
	75	4.20 ± 1.29	13.62 ± 3.21	0.00 ± 0.00	0.00 ± 0.00
	90	2.13 ± 0.23	12.14 ± 0.94	0.00 ± 0.00	0.00 ± 0.00
SX:FL:CL	10	6.25 ± 2.01	16.02 ± 7.13	37.86 ± 6.93	21.66 ± 3.02
	25	3.46 ± 0.46	17.89 ± 2.98	25.41 ± 2.69	27.89 ± 3.32
	50	6.16 ± 0.56	20.89 ± 4.04	45.06 ± 1.27	30.14 ± 1.73
	75	8.00 ± 1.39	19.58 ± 3.46	40.45 ± 5.86	26.48 ± 2.04
	90	6.59 ± 1.06	16.51 ± 1.46	44.53 ± 0.99	25.45 ± 3.08

The emission of the SX blend was higher than SS formulation (Table 5.9) when inhalation profiles were used. However, for both formulations, the % emission was dramatically reduced compared to when PIF were used. This probably occurred as, during the inhalation profiles, steady flow is not present. Instead, there are acceleration and deceleration phases. Therefore, there is probably lower force involved to aerosolise the particles. On the other hand, the IP/PS deposition for SX:FL:CL was higher when the inhalation profiles were used ($p<0.05$). Therefore, when the Cheng 2 was assessed with reproduced 'real' inhalation manoeuvres, the flow rate dependency of the throat deposition was not mitigated for low flow rates (10th and 25th percentiles, $p<0.05$). However, for flow rates above 70 Lmin^{-1}, the

deposition on the throat did not vary between flow profiles. The % cumulative undersize collected form the PSD decreased when inhalation profiles were tested rather than when peak inspiratory flows were used for both formulations (Figures 5.10 and 5.11). This is correlated with the difference in the % emission seen already (Table 5.9).

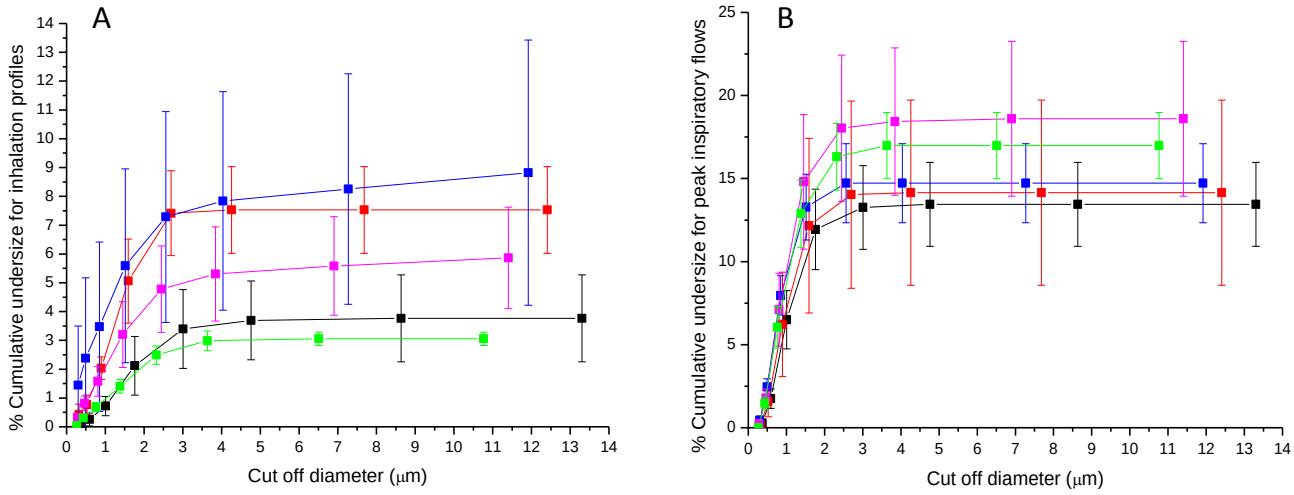

Figure 5.10. Cumulative aerodynamic undersize (%) of SS:FL:CL of emitted dose from Cheng 2 using inhalation profiles (A, Black: 10th, Red: 25th, Blue: 50th, Pink: 75th, Green 90th percentile) and using peak inspiratory flow (B, Black: 10th, Red: 25th, Blue: 50th, Pink: 75th, Green 90thpercentile) (mean ± SD, n = 4)

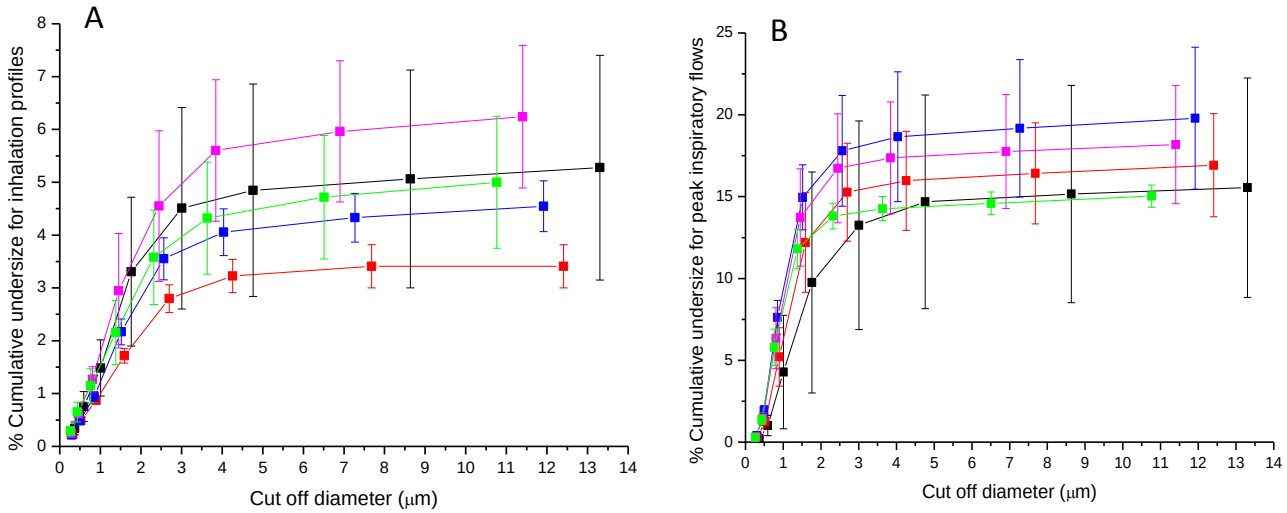

Figure 5.11. Cumulative aerodynamic undersize (%) of SX:FL:CL of emitted dose from Cheng 2 at inhalation profiles A, Black: 10th, Red: 25th, Blue: 50th, Pink: 75th, Green 90th percentile) and using peak inspiratory flow (B, Black: 10th, Red: 25th, Blue: 50th, Pink: 75th, Green 90thpercentile) (mean ± SD, n = 4)

The FPF (%sED) were higher when PIF were tested compared to when inhalation profiles were used for both formulations (Table 5.10). The SX formulation showed a slightly higher FPF compared to SS:FL:CL when square wave flow profiles were used, although for the inhalation profiles of the 25th and 50th percentile PIF, SS showed a greater FPF than SX (Table 5.10). A similar trend was seen for the FPD, the dose respirable by the patients (Table 5.10). Clearly, the physico-chemical properties of the APIs affect the deagglomeration mechanism inside the Cheng 2. Furthermore, using a constant flow (e.g. PIF) would lead to a constant energy provision for the aerosolization of the particles, whilst, when employing a flow rate loop (e.g. an inhalation profile) the flow is no longer constant, as acceleration and deceleration are present. This would lead to decreased values for FPF and FPD when inhalation profiles are used. The Cheng 2 showed variable FPF and FPD especially at highest flow rates (75 and 90%, Table 5.10). As previously reported (Chapter 3 and 4), at high flow rates some uncontrolled vortex instability occurs inside the cyclone.

Table 5.10. Fine particle fraction < 5 µm ($FPF_{5\mu m}$), Fine particle dose < 5 µm ($FPD_{5\mu m}$), and Mass median aerodynamic diameter (MMAD) of salbutamol sulphate (SS) and salmeterol xinafoate (SX) formulation with fine lactose (FL) and coarse lactose (CL) emitted from the Cyclohaler in sequence with the Cheng 2 at the peak inspiratory flow (PIF) and inhalation profiles (IP) of the % of the population (mean ± SD, n = 4).

Blends	Inhalation profiles of population (%)	% FPF (ED)	FPD (µg/ml)	MMADs (µm)
SS:FL:CL	10	3.67 ± 1.46	3.42 ± 1.28	1.54 ± 0.23
	25	7.20 ± 1.85	6.70 ± 1.62	1.25 ± 0.08
	50	8.01 ± 3.89	8.04 ± 4.63	1.11 ± 0.29
	75	5.54 ± 1.75	5.44 ± 1.67	1.25 ± 0.07
	90	2.93 ± 0.23	2.33 ± 0.39	1.28 ± 0.13
SX:FL:CL	10	4.83 ± 2.00	5.70 ± 2.38	1.46 ± 0.11
	25	3.20 ± 0.37	3.88 ± 0.61	1.33 ± 0.10
	50	4.15 ± 0.45	5.63 ± 0.49	1.48 ± 0.02
	75	5.73 ± 1.35	7.06 ± 2.12	1.46 ± 0.13
	90	4.52 ± 1.12	4.78 ± 0.26	1.38 ± 0.02
Blends	PIF ($Lmin^{-1}$)	% FPF (ED)	FPD (µg/ml)	MMADs (µm)
SS:FL:CL	52.83	13.38 ± 2.63	14.18 ± 0.44	1.02 ± 0.09
	65.55	14.14 ± 5.58	13.29 ± 6.59	0.98 ± 0.12
	72.65	14.71 ± 2.38	15.62 ± 2.28	0.79 ± 0.06
	79.93	18.57 ± 4.64	16.33 ± 3.77	0.94 ± 0.07
	89.10	16.96 ± 1.99	16.28 ± 1.34	0.93 ± 0.04
SX:FL:CL	52.83	17.05 ± 2.12	15.96 ± 8.14	1.63 ± 0.38
	65.55	16.25 ± 3.11	18.70 ± 4.02	1.35 ± 0.08
	72.65	19.23 ± 3.93	21.50 ± 4.52	1.15 ± 0.17
	79.93	17.78 ± 3.52	20.34 ± 3.88	1.14 ± 0.03
	89.10	14.72 ± 0.72	15.52 ± 1.36	1.05 ± 0.08

When MMADs are considered (Table 5.10), Cheng 2 decreased the aerodynamic diameter of the emitted particles upon increasing the flow rates only for SX:FL:CL. When Inhalation profiles were used, the MMADs for the formulation did not change. On the other hand, unaltered MMADs was seen for SS at PIFs unlike when inhalation profiles were used.

5.5. Discussion

The design of the inhaler plays a major role on its resistance to airflow and this influences the correct inhalation technique through the device [132]. In vitro studies showed that, when testing a dry powder inhaler (DPI), increasing the flow rate would increase the FPF (fine particle fraction) of the aerosol deposited in the cascade impactor body [148, 153]. Although a constant flow is used for in vitro studies of aerosol deposition as requested from regulatory agencies, it cannot be solely employed to recreate the realistic scenario that occurs in the clinics. Researchers have started taking into account the inhalation manoeuvre from patients [126, 240, 256]. However, authors have used devices containing propellant or placebo to collect inhalation profiles through inhalers from patients affected by lung diseases [13, 257]. This would be difficult to implement routinely in clinical settings and provide meaningful information to prescribers about the suitability of devices for their patients. The aim of this chapter was to understand metrics collected from real inhalation profiles when inhalers with different resistances to airflow were used with patients. This was achieved in three principal studies: (1) a pilot study assessing the feasibility of modified spirometry to collect inhalation profiles from healthy volunteers, using an inhalation device (i.e. the cyclone spacer); (2) to apply the spirometry method to record inhalation profiles from real patients in the clinic suitable to assess patient-use issues; and (3) to employ recorded profiles understand the potential in vivo performance aspects during development of inhalation devices and formulations (i.e. a generic spacer for DPIs).

For quality control the BP and USP [147] state that airflow through an inhaler corresponding to 4 kPa is required to test a new device. Moreover, either 4 L (BP) or 2 L (USP) of air are required to calculate the time for each actuation of the inhaler when testing using a cascade impactor. However, a new monograph in the Pharmacopoeia mentioned the used of the breath simulation to test the emitted dose of nebulizers. Although the constant flow is an appropriate metric to measure the particle size distribution and the deagglomeration process of the emitted aerosol, it cannot be solely employed to recreate the realistic scenario that occurs in the clinic. This is due to the fact that patients do not use a constant flow to inhale the medication emitted from an inhaler. Therefore, a more accurate and realistic assessment of the aerosol deposition is required, not only in the research field, but also in the industry guidance for inhalation. When a patient inhales, an acceleration of inhalation first occurs, followed by attaining a maximum flow achievable and it terminates with a deceleration to conclude the manoeuvre [12, 13]. Typically, the dose is delivered before the maximum peak flow is reached [126]. Some authors showed that patients are able to maintain a prolonged inhalation time for devices with high resistance, and this was confirmed in Section 5.4.2.1 [13, 125, 236]. The use of realistic as well as predicted inhalation profiles has been recently reported [152, 245, 246].

Previously it was shown that the Cheng 2 spacer enhanced the deagglomeration of mixed drug agglomerates containing lactose (Chapter 4), although the nature of whether blends are potentially adhesively- or cohesively-balanced may play a major role in the deagglomeration process both in aerosol clouds entering the spacer, and for agglomerates present within the spacer (Chapter 4). Healthy volunteers were recruited to enter a pilot study where their inhalation profiles were collected through the Cheng 2. The spacer showed high resistance to airflow in the range of Turbuhaler and Handihaler (Chapter 4). However, it was suitable for the pilot study as the participants were not affected by impaired lungs. De Boer et al [258] showed that the volunteers in their study preferred a medium to high resistance device when DPIs with different resistance were tested due to the prolonged inhalation profile. Also, the dose is released rapidly for devices such as Diskus and Turbuhaler (the latter presents high resistance), although the dose

emitted from capsule-containing devices such as the Aerolizer (resistance: 0.02 $kpa^{0.5}L^{-1}min$) is released over a longer period of time [242]. The range of PIFs achievable when inhaling through the spacer was large; between 52.8 $Lmin^{-1}$ to 89.1 $Lmin^{-1}$ were achievable by the population recruited, whilst a narrower distribution was seen for patients for the high resistance device (Table 5.7). The feasibility of employing modified spirometry to record inhalation profiles through devices in a rapid manner was demonstrated in the pilot study, which enabled the development of a protocol for translation to the clinical environment.

The clinically-based study was designed to collect inhalation profiles using a rotating disk with five holes that mimic the resistance of marketed inhalers from 80 patients, in the chapter only 40 patients (20 COPD and 20 severe asthmatics) were analysed and three inhalers (Aerolizer, MDI and Handihaler) were taken into account for statistical analysis. The study was designed to provide a sufficient number of participants in each of four study groups to investigate the presence of any significant differences in inspiratory flow characteristics through inhalation devices depending on the disease state of the individual. Several studies were identified which addressed the inhalation of patients/volunteers through devices [13, 81, 254, 256, 259]. The majority of the latter studies did not characterize the full inhalation profile. In addition, the results for patients stratified according to the disease severity were only reported in a single study [260]. However, the latter study did not report the data in a manner suitable for statistical design of the experiment (i.e. no tabulated data). Peak inspiratory flow rate (PIFR) through a device has been correlated previously to the severity of lung disease, as well as to the appropriateness of an emitted aerosol for inhalation therapy. Therefore the PIFR was examined in the sample size measurement to estimate an appropriate sample size for the patient populations in question. The data in Table 5.4 confirm that variance was dissimilar between studies and, between study treatments (for a given study group). In only one study was it possible to calculate a pooled variance for both study groups for the PIFR in uncategorized asthmatics [254]. The purpose of the current study was to recruit equal numbers of patients in each of four groups. The data reported in Table 6.4 demonstrated the PIFR, FPF and FPM and a similar finding was reported with respect to the Forced Expiratory Volume in 1 second (FEV_1) which is the directly opposite metric (exhalation) to the PIFR measurements

reported by Bland *et al* [251]. The measured (estimated) difference (Δ) between reported metric means was calculated and the standardized differences (referred to as the effect size throughout) were calculated using the method of Cohen [253].Two approaches were used to calculate the effect size. In the first, approach the pooled standard deviation of two independent means was employed (referred to as *d*, below). In the second approach the largest standard deviation of the two compared studies was employed to provide the most conservative estimate of effect size (referred to as d_{max}, below). Sample sizes and statistical power at a significance level of 0.05 were calculated using values of the $f(\alpha,p)$ function obtained from literature [251, 252]. In all cases the sample size numbers were increased to the nearest whole patient number. The absolute magnitude of difference in PIFR between devices would be anticipated to be larger when comparing devices which differ more in their resistance. This is seen in Table 5.5, for example by comparing Turbuhaler vs. Accuhaler and Accuhaler vs. Handihaler comparisons.

In heterogeneous patient populations with high measurement variance [13] the effect size (d, d_{max}) was observed to be large. An equally large effect size was calculated from the reports of Broeders *et al*. [256]. When examining a more homogeneous group of patients (i.e. COPD only [81]) the effect sizes calculated were medium-to-large (e.g. d_{max} 0.54 – 1.62). However, the latter study did not stratify the COPD patients according to disease severity. Similarly, the PIFR was compared in uncategorized asthmatic patients [254] for two different devices. In this instance the d_{max} values corresponded to a moderate effect level. In attempting to estimate the required sample number for the proposed study, the approach was taken of using the lowest identified effect size (d_{max}= 0.54 [191]). The response of sample power to effect size was determined for total sample sizes ranging between 80 and 120 patients (Figure 5.6).The simulation performed assuming the lowest effect size of any of the reported studies (d_{max} = 0.54) was chosen to represent the mild asthmatic group and also to account for the fact that the COPD group to be recruited is likely to be heterogeneous in their disease state. It can be seen that even comparing two heterogeneous patient populations (i.e. uncategorized asthma and uncategorized COPD), the disease state is predicted to have a large effect on the PIFR. Employing the conservative value of effect size for the latter comparisons

(d_{max} = 1.11) would result in a power > 99 % (Figure 5.7) for comparing a group of 20 asthmatics with 20 COPD patients in the current study. The strength of the latter observations suggests that a sample size of 20 patients in each disease group was appropriate to provide a sufficiently powered study to assess differences between disease state and PIFR for a particular device.

Several studies have collected the inhalations of patients/volunteers through devices [81, 242, 256, 261, 262]. As already reported [81] the PIF achieved by the patients though a high resistance device (e.g. 0.048 $kpa^{0.5}L^{-1}min$) were low compared to low resistance inhaler (Table 5.7). It has been shown that slow flow rates were achieved by COPD patients and that it was proportional to the severity of their lung disease [81]. Although some authors suggested that a low to medium resistance device is a suitable option for those types of patients [81, 246], other authors recommended a high resistance device as a more prolonged flow is achievable [125, 236, 249]. The latter statement is in accordance with the data collected using the Handihaler (resistance 0.048 $kpa^{0.5}L^{-1}min$, Figure 5.5).

As previously reported [125], the patients showed a prolonged breath profile with the Handihaler and this can be beneficial as longer inhalation time could lead to better coarse particle deagglomeration. This is in accordance with the current study where the inhalation time was double for COPD patients than asthmatics when inhaling to the highest resistance device (0.048 $kpa^{0.5}L^{-1}min$, Table 5.7). Moreover, the expected flow rate was achieved for that particular inhaler (e.g. 40 $Lmin^{-1}$ for the Handihaler) suggesting that potentially air was still drawn in the lungs during inhalation. It has been suggested [164, 166] that when flow is applied to a modified device with the same resistance of the Handihaler the turbulence through the inhaler increases, enhancing the potential deagglomeration of the emitted dose. De Boer *et al* [258] showed that the volunteers in their study preferred the medium to high resistance device when DPIs with different resistance were tested due to the prolonged inhalation profile. Janssens *et al*. [237] showed that the majority of the patients with COPD were able to achieve flow rates > 45 $Lmin^{-1}$ when the In-Check Dial was used. The In-Check Dial is a device that mimics the resistance of marketed

inhalers such as Aerolizer, Diskus, Turbuhaler and MDI. When the Aerolizer was used, 87.5% of the population achieved inspiratory flow > 45 $Lmin^{-1}$ as well as at 30 $Lmin^{-1}$. In the current study the patients inhaled with a much higher flow rate for the medium resistance device representing the Aerolizer (Table 5.7). Moreover, when patients inhaled through the spirometer with the mouthpiece that mimics the resistance of the MDI inappropriate technique was recorded (Figure 5.8) [74]. The rapid manoeuvre was achieved owing to the poor perception of flow rate against the low resistance. The MDI is an ultralow-resistance device, which means that it is relatively easy to generate too great an inspiratory flow, which is a common error in the use of MDIs [74]. The PIFs achieved for the MDI were higher the previously reported data for patients with good technique [85], although patients with poor technique do inhale as rapidly as 240 $Lmin^{-1}$ [263]. The inhalation volume achieved by the asthmatic patients through both Aerolizer and Handihaler are in agreement with the data shown by Delvadia *et al*. [249], although the authors generated empirically the inhalation profiles from healthy volunteers. Moreover, as previously suggested [125, 236, 249], patients to inhale longer for a high resistance devices (Table 5.7), although inter-patient variability is still shown.

The aerosol deposition of strongly (SX:FL:CL) and weakly (SS:FL:CL) agglomerating blends in the cascade impactor was assessed using both inhalation profiles and peak inspiratory flows collected from the volunteers. The emission from the spacer was higher for the SX blends than SS formulations (16.02 ± 7.13 % for SX vs. 12.59 ± 0.95% for SS), which led to a greater throat deposition for the former and a greater FPF (%sED and %ED) for the latter, although unchanged with increasing flow rate (Table 5.8). When comparing PIF vs. inhalation profiles, the % emission had the same trend, although was lower for both formulations when using the inhalation profiles. The particle size distribution (PSD) differed between the inhalation profiles and PIF (e.g. compare the ranking of the distributions for the 90^{th} (green) and 75^{th} (pink) percentiles (Figure 5.10 and 5.11) for both SS:FL:CL and SX:FL:CL. It has been suggested [247] that the particle size of the aerosols is unchanged when constant flow or breath simulated profiles are employed, as long as the flow rates are set as near as possible the PIF achieved in the profile. When employing PIFs a lower FPF (%sED) was observed ($p<0.05$) for SX:FL:CL (e.g.

72.39 ± 3.92% for the 50th percentile PIF) than SS:FL:CL (e.g. 99.97± 0.08% for the 50th percentile PIF).

In Chapter 4, the aerosolization of SS was dominated by impaction events in the cyclone unlike SX blends. The contrasting behaviour for SS and SX when comparing PIF to inhalation profiles presumably occurs as, during the inhalation profiles, the steady flow is not present. Instead, due to the acceleration and deceleration it is hypothesized that lower force is applied to aerosolize the particles [12, 13]. This would also explain the variable % emission when comparing the two metrics. An interesting result, when using the inhalation profiles as metric to assess the aerosol distribution, was that the AIT/PS deposition for the formulations was not constant when increasing the flow, unlike when the PIF was used. The flow rate dependence of the throat deposition was not mitigated with the Cheng 2 in place especially at low inhalation profiles. Less AIT/PS deposition was observed when the Cheng 2 was used with PIFs, but not when the profiles were used, instead. Interestingly, this phenomena did not happen at flow rates above 70 Lmin^{-1}, probably due to more control of the volunteers at maintaining the flow through a high resistance device [125].

As previously showed in Chapter 4, SX blends showed a greater throat deposition than weakly agglomerated particles. Interestingly, the throat deposition was doubled when the IP was used due to the low acceleration during the inhalation profile than when PIF was used. The respirable fraction of SX formulations were slightly higher than SS blends (Table 5.10) when low inhalation energy was supplied (e.g. at inhalation profiles and at low PIF). This is probably due to both physico-chemical properties of the APIs (e.g. the deagglomeration process is affected due to different agglomeration strength of SS and SX particles with lactose, respectively) and to the use of a constant energy that enhanced deagglomeration of the weakly agglomerated SS blends (e.g. PIF). Together with the % emission, also the FPD values were decreased when the inhalation profiles were used compared to the PIF. The Cheng 2 showed relatively consistent MMADs but variable FPDs, especially at low flow rates and inhalation profiles (Table 5.10). This is probably due to the fact

that at low energy the capsule does not spin in the device, releasing a lower dose than when high flow rates are employed [175]. The current project showed that the PIF was probably not an adequate metric to assess inter-subject variability in fine particle delivery from the cyclone spacer.

5.6. Conclusions

This chapter has developed, piloted and implemented a rapid screening modified spirometric method for rapid identification of the ability of patients to inhale through inhalation devices with a wide range of resistances to inhalation. The study showed no significant difference for the majority of the metrics of inhalation performance (e.g. the peak inspiratory flow) between patient disease groups when examining specific inhalation device resistances, although within groups, patients achieved low flow rates and longer inhalation time for a device with high (0.048 $kpa^{0.5}L^{-1}min$) resistance to airflow (i.e. Handihaler) than a device with 0.020 $kpa^{0.5}L^{-1}min$ resistance to the air (Aerolizer). Significant difference was seen in the IV, instead, suggesting the using only the PIF as a sole metric is not appropriate. Variability in the flow achievable by the patients is still an issue. This is expected to lead to variable lung deposition, oropharyngeal impaction and a high particle size of the dose. It is apparent that strategies to mitigate against the variability are therefore required, analogous to the use of spacer devices for metered dose inhalers. Accordingly the pilot study conducted with inhalation profiles collected from healthy volunteers were employed in patient-centred device testing. The full assessment of spacer functionality showed that a simulation of real-life inhalation conditions is required to understand the device performance. The crucial dependence of drug delivery performance on physico-chemical properties of the formulation (e.g. cohesive vs. adhesive balance) was revealed by the mismatch between fine particle delivery when square wave peak inspiratory flows were tested compared to the profiles of real volunteer inhalations, as acceleration and inhaled volumes are parameters to consider. The observation that, by using the cyclone spacer, the variability in the aerodynamic diameter and fine particle delivery were consistently minimized alongside the reduction in throat deposition, represent highly positive finding of relevance to realistic application to patient therapy.

Chapter 6: General Discussion

Asthma and COPD (chronic obstructive pulmonary disease) are considered diseases of major burden worldwide. The WHO (World Health Organization) estimated that 64 million people have COPD, 3 million people died of COPD and 235 million people suffer from asthma. These diseases could be a cause of death worldwide in the near future [264]. Moreover, they are common in both high income and developing countries. In the latter, between 6.5 to 7.7 % of the population suffers from chronic bronchitis due to open-fire cooking with high child mortality [16]. In the UK, the NHS registered more than 1,200 deaths per year from asthma [11] and increased rates of hospitalization for both asthmatic and COPD patients [67]. Metered dose inhalers (MDIs) and dry powder inhalers (DPIs) have been used widely with consistent improvements in the user-friendliness and efficiency of delivered dose for these portable therapies over the last fifty years. However, poor response to inhaled medicine is still common probably due to underestimated symptoms, poor adherence of patients or due to incorrect inhalation technique. This thesis has sought to address several poorly investigated issues relating to poor management of lung disease using DPIs. The latter issues were: physical capacity to use inhalers correctly; specificity of lung deposition of inhaled formulations; and reduction of oropharyngeal deposition as a potential strategy to improve compliance.

Poor management of asthma leads to a progression of the disease and needs to be controlled as exacerbations lead to poor quality of life. It has been reported [11, 68] that patients are not familiar with the prescribed medications and/or are not well aware of their symptoms. This leads to a poor adherence/concordance of the patient to/with their inhalation therapy and, subsequently poor disease control. Moreover, due to their inexperience, a poor inhalation technique is displayed [11, 68, 69]. The medical staff is frequently unaware of the patient's poor technique and the incorrect inhaler may be prescribed. Especially when MDIs are used, patients do not inhale properly through the device (i.e. slow and deep inhalation) [74]. In the current study the highest peak inspiratory flows recorded for asthmatic patients through an MDI were 287 $Lmin^{-1}$ and 248 $Lmin^{-1}$ for COPD patients. The issue of high flow rates through the MDI as an incorrect inhalation technique was previously reported [263]. Patients, often do not differentiate the inhalation technique from an MDI and a DPI (i.e. "inhale as fast and as deep as you can" manoeuvre). The inhalation strength required for DPIs is to create turbulent energy for aerosolization of the dose [74].

Failing to achieve that, the dose delivered to the lungs can be compromised [69]. Moreover, due to the different types of asthma and lung diseases, high inter-patient variability in the achieved peak flow rate is reported [77, 85]; although considering only the peak flow rate ignores the potential source of variability. In fact, the variability seen between patients lies mainly in the first, acceleration part of the inhalation manoeuvre, and many studies reported that the medication is inhaled before the peak inspiratory flow in reached [12, 125, 126].

The achieved airflows and profiles variability lead to low deposition of the emitted dose of the medication in the specific lung regions for therapeutic effect. Also, due to the low inhalation strength of the patients during therapy, most of the emitted powder impacts on the throat. This leads to side effects with corticosteroid medications. Available already in the market, there are some training tools to help the patients understand the appropriate technique to use when inhaling through a device, such as the Flo-Tone or the Novolizer. These device emit signals that either inform the patients of the appropriate inhalation technique used or whether sufficient drug has been delivered to the lungs [145]. Pharmaceutical companies are also moving forward in the design technology, leading to inhalers that liberate fine particles suitable to deep lung deposition. Some example are the Airmax® [92, 93] that has a design similar to MDI and the Conix® [91, 146] that contains a miniature reverse airflow cyclone to capture coarse carrier that might impact in the patient throat during inhalation. Although similar technologies have addressed and attempted to overcome the main issues of DPI delivery of carrier particles, inter-patient variability in the particle size and delivered dose is still observed. Moreover, the technology is applied only to specific branded inhalers and not necessarily the required drug substance for a patient.

The primary aim of this PhD thesis was to investigate strategies to minimize the flow rate-derived variability of performance when using DPIs. This was achieved using prototype reverse airflow cyclones that were intended to function as a spacer (Cheng 1 and Cheng 2) for DPIs in order to collect large agglomerates during dose emission. This study focused on characterizing the spaces using both marketed and in-house formulations and varying flow rates and flow regimes. The secondary aim was to formulate a patient-centred testing approach using both healthy volunteers

and patients with obstructive lung disease to understand their inhalation profile variability when inhaling against different resistances to airflow.

Each inhaler available in the market has its own typical resistance to inhaled airflow. Typically, high flow rates are achieved through DPIs such as Diskus and Aerolizer which have low or medium resistance compared to high resistance DPIs such as Easyhaler, Turbuhaler and Handihaler [81, 85]. In collaboration with the Department of Engineering at Cambridge University, a prototype cyclone spacer called Cheng 1 was manufactured to be used with DPIs. The cyclone spacer was engineered to retain particles down to a micron-scale size range with the aim of creating an classifier with cut off diameter <2 μm. Cascade impactor testing was performed at 3 flow rates (30, 45 and 60 L min^{-1}) using a Cyclohaler® and aerosolizing the formulation collected from the Ventolin/Accuhaler™. In Chapter 2 a much lower throat deposition in the Next Generation Impactor (NGI) was observed when the Cyclohaler® was used in series with the Cheng 1 spacer. However the spacer did not improve the FPD (fine particle dose) for the 'inhalable' aerosol when the Cheng 1 was present except at low flow rates. This is possible as at low flow rates, lower deagglomeration forces occur and during aerosolization the axially downward-flowing vortex and the secondary axially upward-flowing vortex in the Cheng 1 might not work properly. This led to high retention of the emitted powder in the conical section of the spacer (~ 60% of the emitted powder) and subsequently reduced throat deposition [173]. Interesting, the conical section of the Cheng 1 did collect the big agglomerate as seen during laser diffraction analysis (Figure 2.11). Particles of large mass and inertia are retained in the cone, and only the finest particles (e.g. < 5 μm) can escape the cyclone for inhalation [91]. Data shown in Chapter 2 suggested that the spacer might reduce the FPD flow rate dependency; although without improvement.

An improved FPF of the aerosol that escapes the cyclone (% sED) can be seen with the spacer in place. It has been reported that with the Cyclohaler, a cyclonic turbulent flow is predominant, increasing the collisions between particle-particle and particle-device wall. This would enhance deagglomeration of the emitted dose and,

therefore, the FPF [95, 163]. Such deagglomeration was continued and enhanced inside the conical section of the Cheng 1 [159].

When considering the Cyclohaler alone, the FPFs of the emitted SS increased from 30 to 60 L min^{-1} (p value>0.05, Table 2.8) with consequently decreased in the IP/PS deposition [163]. Another feature of the cyclone was that the MMAD (mass median aerodynamic diameter) was halved for SS and mitigated at 45 and 60 $Lmin^{-1}$ suggesting the potential of an enhanced deagglomeration process with the spacer. However, because the emitted aerosol size was lower than one expects during inhalation therapy (e.g. 0.76 ± 0.04 μm at 60 L min^{-1} with Cheng 1), the spacer needed some engineering improvement. However, it has to be taken into consideration that the engineering of the spacer was only proposed to collect big agglomerates, without knowledge on potential creation of sub-micronized particles.

CFD revealed near-wall velocity and integral scale strain rates with enhanced aerodynamic separation and impaction forces [159]. Moreover, CFD studies [159] suggested that impaction on the cyclone wall due to centrifugal forces occurs when flow rate is applied at the outlet of the cyclone and therefore, the velocity of the emitted particles from the Cyclohaler® would increase the particle-particle and particle-wall collisions inside the Cheng 1. However, the resistance of the Cheng 1 was excessive (0.0805 $kPa^{1/2}$ /L min^{-1}) and not acceptable for use in patients with obstructive lung disease. Moreover, when using a carrier-free product (e.g. Turbuhaler/Symbicort), no difference in aerosol emission using the Cheng 1 was observed with laser diffraction techniques. On the other hand, large agglomerates were observed escaping the Cheng 1 at 60 $Lmin^{-1}$ as a bi-modal particle size distribution was detected by laser diffraction.

Therefore, a second prototype (Chapter 3) with a much reduced resistance (0.04 $kPa^{1/2}$ min L^{-1}) was manufactured modifying the outlet orifice diameter from a circular to an oval shape. The device resistance was within the range of existing DPIs (Tubuhaler®, 0.03 $kPa^{1/2}$ min L^{-1} and Handihaler®, 0.05 $kPa^{1/2}$ min L^{-1}) acceptable by patients even with severe COPD [125, 168]. This was an improvement as patients with lung disease should be able to achieve a reasonable flow rate

through the prototype. The new design was also engineered to allow a higher cut off diameter (e.g. < 5 μm) than Cheng 1 (which was in the region of 1.0 μm). However, due to manufacturing issues, this was not achieved, resulting in a cut off diameter which was also very low, although it was higher than Cheng 1 (1.19 – 1.55 μm for Cheng 2 and 0.46 – 0.90 μm for Cheng 1). In Chapter 3 the impaction testing using Cheng 2 was performed to ensure that the spacer could still mitigate the dependence of the respirable dose and of the MMADs on the inhalation flow rate using marketed inhalers. The SS was still recovered from the Ventolin/Accuhaler™ and emitted through the Cyclohaler® for comparison. The Cheng 2 was then tested with: Cyclohaler/SS®, Easyhaler/Budesonide (Bud™ 400 μg/dose) and Seretide/Accuhaler™ (Salmeterol xinafoate, SX) 50 μg/dose and fluticasone propionate, FP) 500μg/dose). SS was considered as it is reported that it forms adhesively-balanced blends when added to lactose [194], Bud is reported to form cohesively- balanced blends [195], and SX/FP was considered due their therapeutic use as a combination of anti-inflammatory and bronchodilator [196]. In the study, 2 and 4 kPa were used to aerosolise the formulation in order to represent low and high pressure drop achievable by patients and to represent different formulations.

The engineering issue in designing the Cheng 2 led its axial velocity to be lower than Cheng 1. This led to high near wall tangential velocities in the latter allowing greater impaction and deagglomeration forces for emitted masses passing through the spacer. This potentially may have allowed large agglomerates to exit the cone as seen during laser diffraction testing (Figure 3.8). The near wall tangential velocity was 3-fold lower for Cheng 2 than Cheng 1 leading to higher impact mass though the former. The greater integral strain rate of Cheng 1 led, in fact, to a greater fine particle detachment then when Cheng 2 was used. For instance, the FPF (%ED) for SS when Cheng 1 was used was 14.48 ± 5.84 μm at 30 L min^{-1}, whilst when Cheng 2 was used for the same API, the FPF (%ED) was 12.90 ± 4.43 μm at 37 L min^{-1}. The same trend was observed when the flow rate increased (e.g. 33.42 ± 5.86 μm at 60 L min^{-1} when Cheng 1 was employed and 11.39 ± 0.64 μm at 51 L min^{-1} when Cheng 2 was used). Cheng 2 showed lower impaction forces and lower integral strain rate by the inlet and at the vortex cone base than Cheng 1 [193]. Nevertheless, similar to Cheng 1, high retention of the formulations was detected in Cheng 2 possibly due to electrostatic charges occurring in plastic spacers, but also

due to the retention of large agglomerates and carrier-bound drug particles. In fact, the % emission calculated for the emitted dose of APIs emitted from the inhalers when Cheng 2 was employed was low (e.g. 24.51 ± 1.68 % and 19.33 ± 0.46 % for Bud and SX respectively at 2 kPa). The low emitted fractions were due to the high retention within the spacer (almost 80% of the emitted drug) as seen already for the Conix™(80 %) [91]. This would allow decreased in vivo throat deposition [174]. The trend of reduced throat deposition seen already for Cheng 1 was observed also for Cheng 2 in Chapter 3 for all the formulations tested. However, there was a formulation dependency in the performance behaviour with the cyclone in place. For instance, the IP/PS deposition for SX and FP was twice that of the Bud or SS (e.g. 18.44 ± 2.79 % for SS, 15.19 ± 1.74 % for Bud, 36.01 ± 9.77 % for SX and 29.63 ± 5.85 % for FP at 4 kPa). Harrison et al [146] and Needham et al [91] showed similar findings when testing SX/FP formulation and SS formulation emitted from the Conix™. SX and FP cohesive behaviour when blended with coarse carrier might lead to a less efficient deagglomeration process than SS when emitted from a device as their interaction to the carrier has higher energy than SS [202]. In accordance with data shown in Chapter 2, neither cyclone retention nor IP/PS deposition was affected by the flow rate for the SS formulation, nor for any of the drug-device formulations tested. Although the extent of IP/PS deposition and cyclone retention did depend on the drug formulation/product type (Table 3.9), the potential for flow-rate independence of oropharyngeal drug deposition for a specific formulation was a promising finding towards overcoming inter-patient variability in DPI deposition profiles.

While the cyclone was designed to emit a similar fine particle fraction to the inhaler for SS to improve in vitro drug delivery (Chapter 2), it was seen to fail in tis aim, since a lower fraction was emitted for SS, and the FPDs of the tested drugs decreased compared to the inhalers tested alone with the exception of Bud/Easyhaler™ (Table 3.10). Although, the FPDs were lower with the Cheng 2 in place than without, the consistency of FPD (and MMAD) between flow rates confirmed that the spacer might mitigate the flow rate dependence of the emitted aerosol for all formulations. Although the spacer did not perform with pharmaceutically equivalence to the inhalers regarding the FPD (i.e. FPDs changed when the spacer was used) and very fine particles (e.g. MMADs) were emitted due to the less-than-desirable excessively low cut off diameter, the difference in the

IP/PS deposition between SS and SX or BUD and FP (that lead to similar difference in the FPFs, Table 3.10) was worth being investigated. Therefore, in Chapter 4, in-house made blends were prepared using what the literature suggested being cohesive balanced blends (SX/Lactose) and adhesive balanced blends (SS/lactose).

Similar to when commercial products were tested, variable IP/PS deposition and respirable fractions were observed when Cheng 2 was assessed with in-house manufactured blends of strongly agglomerating- (SX) and weakly agglomerating- (SS) particles with different grades of lactose when Cyclohaler® was used. Although the data obtained when the Cheng 2 was in place suggest retention of large agglomerates, the APIs seemed to deagglomerate differently inside the conical section of the spacer. In Chapter 4, it was observed that the presence of FL would improve the emission of both strongly agglomerated- (SX) and weakly agglomerated- (SS) particles in presence of the spacer (10.25 ± 3.85% for SS:CL and 22.86 ± 4.30 % for SS:FL:CL vs. 16.30 ± 3.25 % for SX:CL and 30.64 ± 10.44 for SX:FL:CL at 4 kPa, $p<0.05$). This is probably due to the fact that SS is still attached to the lactose and has low impaction forces in the spacer. On the other hand, the creation of small SX agglomerates may lead to greater % of emitted dose. However, the SX agglomerates seemed not to break-up as the FPF (%sED) was lower than the SS FPF (%sED): e.g. 76.66 ± 1.35 % for SX:FL:CL vs. 81.83 ± 4.11 % for SS:FL:CL at 4 kPa). The same difference was observed in the IP/PS deposition with SX blends having higher impaction in this particular stage then SS (65.83 ± 8.99 % vs. 45.83 ± 5.04 % for SS:CL and SX:CL, respectively). It seems that the deagglomeration forces inside the conical section of the spacer have a greater impact on the formulation when a large particle size carrier is used.

Studying the deagglomeration process of the dispersed powder as a function of the flow rate prior to entering the spacer is important to understand the outcome when a DPI is used for the powder emission. Fine particle formulations showed an exponential trend in the deagglomeration process when a pressure drop was applied, reaching a plateau point of maximum deagglomeration. On the other hand, when coarse lactose was added to the micronized material, a bi-exponential trend was observed without a maximum deagglomeration. As expected, API:FL:CL blends,

showed a greater % of deagglomeration than API:CL formulation. This might explain the greater FPF seen for blends with FL when either the Cyclohaler or the Cheng 2 was used in the aerosolization studies (i.e. because of enhanced mixed agglomerate liberation from the formulation prior to entering the cyclone. This was confirmed by SEM (scanning electron microscopy) study. SX:FL:CL showed agglomerates on the lactose surface and a greater quantity of "free agglomerates" than SS:FL:CL, explaining the greater % deagglomeration seen for SS:FL:CL than SX:FL:CL (Table 4.8), as lower energy was required to release the agglomerates form the carrier surface.

The data shown in Chapters 2, 3 and 4 were obtained using constant (square-wave) airflow. However, in reality, patients breathe using an inhalation loop with acceleration and deceleration of the flow. Therefore, a patient-centred study approach was developed and performed using the Cheng 2 with healthy volunteers, and a mouthpiece air-restrictor that can vary the resistance to inhalation airflow with asthmatics and COPD patients. This was performed to collect inhalation profiles through multiple devices and obtain a measure of inter-patient variability. Using a breathing simulator, inhalation profiles of healthy volunteers were used for in vitro testing. A wide range of flow rates were achieved by the volunteers through the Cheng 2. Aerosolization studies of SX:FL:CL and SS:FL:CL were performed using the NGI with the idealized throat at the PIF (peak inspiratory flow) and inhalation profiles for those corresponding PIFs in the range 10 – 90% of the population PIF distribution. The Cyclohaler® was used in series with the Cheng 2.

The particle size distribution (PSD), differed between the inhalation profiles and PIF for both SS:FL:CL and SX:FL:CL. It had been suggested [256] that the particle size of an aerosol is identical for a constant flow and an inhalation profile provided the constant flow rate approximates the PIF achieved in the profile. Although emission of SX from the spacer was higher than the SS formulation when inhalation profiles were used, the % emission was dramatically reduced compared to when PIFs were used instead. The throat deposition for SX blends was similar for all the PIFs tested (e.g.27.89 ± 3.32% for the 25^{th} percentile PIF and 25.45 ± 3.08% for the

90^{th} percentile PIF). Interestingly, when employing PIFs a lower FPF (%sED) was observed ($p<0.05$) for SX:FL:CL (e.g. 72.39 ± 3.92% at 50^{th} percentile PIF) than SS:FL:CL (e.g. 99.97± 0.08% at 50^{th} percentile PIF). In Chapter 3 and 4, the data showed that aerosolization of weakly agglomerated SS blended with lactose was dominated by impaction events in the cyclone unlike aerosolization of small but strongly coherent agglomerates of SX. The contrasting behaviour for SS and SX when comparing PIF to inhalation profiles presumably occurs as, during the inhalation profiles, the steady flow required to release SS from the carrier is not present. Instead, due to the acceleration and deceleration, it is hypothesized that lower force is applied to aerosolize the particles. Therefore, it is evident that the PIF was not an adequate metric to assess inter-subject variability in fine particle delivery from a dry powder inhaler.

The study used spirometer technology to collect inhalation profiles from patients in an attempt to identify metrics to quantify inter-patient variability in inhalation for use in patient-centred testing designs. The study was performed in respiratory clinics through a mouthpiece air-restrictor that mimic the resistance of inhalers available in the market. Data suggested that when patients inhaled though a very low resistance device such as an MDI, patients tended to inhale rapidly, which is an incorrect technique for MDIs but may be appropriate for low resistance DPIs [74]. This led to flow rate above 200 $Lmin^{-1}$ being achieved, however the duration of inhalation was typically shorter than recommended. Interestingly, when a high resistance mouthpiece was used, patients, especially COPD volunteers, tended to inhaler longer than through low resistance device, suggesting that air was still entering into the distal lung regions (e.g. alveoli) [125, 236, 249]. Therefore, although some authors suggested that a low to medium resistance device is a suitable option for those types of patients [81, 246], probably a higher resistance device should be preferred due to the longer inhalation time allowing the formulation to deaggregate better and reach the lower regions of the lung during the lengthy inhalation[125, 236, 249].

The work of this thesis has shown, in vitro, that a prototype spacer based on reverse airflow cyclone technology offers some potential to mitigate the flow rate dependency of aerodynamic particle size. However, the respirable dose represented by the FPD did decrease with the spacer. This was unexpected, as was the enhanced delivery of sub-micron particles which may not be suitable for inhalation therapy – and certainly could not be considered pharmaceutically equivalent. Also, consideration regarding the physicochemical properties of the API in the formulation needs to be made prior using the spacer. The thesis has also shown that considering only the PIF is not a realistic metric when attempting to address the bio-relevance of in vitro aerosolisation performance studies, despite the acceptance of square-wave PIFs in quality control testing. Inhalation profiles should be taken into account with compendial testing in order to achieve a more realistic scenario and data for interpretation during inhaled product design. Therefore acceleration, inhalation volume and other parameters that account for the full inhalation profiles should be considered during in vitro study. Aerosolisation studies in the future must take into account the inhalation profiles achieved by those patients being treated. This thesis has also shown the necessity to develop appropriate and reliable tools for clinicians to facilitate prescribing of a product which maximizes specific lung deposition for their patients, and which addresses the preponderance for throat deposition, an all-too-frequent cause for poor patient compliance with inhaled therapies.

Reference

1. Rowe, B.H., et al., *Corticosteroid therapy for acute asthma.* Respiratory medicine, 2004. **98**(4): p. 275-284.
2. Wall, D.A., *Pulmonary Absorption of Peptides and Proteins.* Drug Delivery, 1995. **2**(1): p. 1-20.
3. Person, A. and M.L. Mintz, *Anatomy and physiology of the respiratory tract*, in *Disorders of the Respiratory Tract*2006, Springer. p. 11-15.
4. Weibel, E.R., *Morphometry of the human lung*1963, New York: Academic Press.
5. Cotes, J.E., D.J. Chinn, and M.R. Miller, *Lung Function: Physiology, Measurement and Application in Medicine*, M. Khan and R. Blundell, Editors. 2006, Jhon Wiley & Sons.
6. S. Whittemore and D.A. Cooley, *The Respiratory System (Human Body: How it Works)* 2009: Chelsea House Publishers.
7. Criée, C., et al., *Body plethysmography-Its principles and clinical use.* Respiratory medicine, 2011.
8. Wanger, J., et al., *Standardisation of the measurement of lung volumes.* European Respiratory Journal, 2005. **26**(3): p. 511.
9. Hayes, D. and S.S. Kraman, *The physiologic basis of spirometry.* Respiratory care, 2009. **54**(12): p. 1717-1726.
10. Miller, M.R., et al., *Standardisation of spirometry.* European Respiratory Journal, 2005. **26**(2): p. 319-338.
11. British, Thoracic, and Society, *British Guideline on the Management of Asthma: A national clinical guideline*, S.I.G. Network, Editor 2012.
12. Kamin, W.E.S., et al., *Mass output and particle size distribution of glucocorticosteroids emitted from different inhalation devices depending on various inspiratory parameters.* Journal of Aerosol Medicine-Deposition Clearance and Effects in the Lung, 2002. **15**(1): p. 65-73.
13. Kamin, W.E.S., et al., *The inhalation manager: a new computer-based device to assess inhalation technique and drug delivery to the patient.* Journal of aerosol medicine, 2003. **16**(1): p. 21-29.
14. Sterner, J.B., et al., *Inspiratory flow-volume curve evaluation for detecting upper airway disease.* Respiratory care, 2009. **54**(4): p. 461-466.
15. Hogg, J.C., et al., *The nature of small-airway obstruction in chronic obstructive pulmonary disease.* New England Journal of Medicine, 2004. **350**(26): p. 2645-2653.
16. McKay, A.J., et al., *Prevalence of COPD in India: a systematic review.* Prim Care Resp J, 2012. **21**.
17. Diette, G.B., et al., *Environmental issues in managing asthma.* Respiratory Care, 2008. **53**(5): p. 602-617.
18. Apfelbacher, C.J., et al., *Measuring asthma-specific quality of life: structured review.* Allergy, 2011. **66**(4): p. 439-457.
19. Cazzola, M., et al., *Outcomes for COPD pharmacological trials: From lung function to biomarkers.* European Respiratory Journal, 2008. **31**(2): p. 416-468.
20. Institute, N.H.L.a.B., *COPD: are you at risk?*, U.S.D.o.H.a.H. Service, Editor 2011.
21. Tantucci, C. and D. Modina, *Lung function decline in COPD.* International Journal of Chronic Obstructive Pulmonary Disease, 2012. **7**: p. 95.
22. Chang, C.L., et al., *Biochemical markers of cardiac dysfunction predict mortality in acute exacerbations of COPD.* Thorax, 2011. **66**(9): p. 764-768.
23. Donaldson, G.C., et al., *Increased risk of myocardial infarction and stroke following exacerbation of COPD.* CHEST Journal, 2010. **137**(5): p. 1091-1097.
24. Sin, D.D. and S.P. Man, *Why are patients with chronic obstructive pulmonary disease at increased risk of cardiovascular diseases? The potential role of systemic inflammation in chronic obstructive pulmonary disease.* Circulation, 2003. **107**(11): p. 1514-1519.

25. Drost, E., et al., *Oxidative stress and airway inflammation in severe exacerbations of COPD.* Thorax, 2005. **60**(4): p. 293-300.
26. Sumi, Y. and Q. Hamis, *Airway remodeling in asthma.* Allergology International, 2007. **56**(4): p. 341-348.
27. Ward, C., et al., *Reduced airway distensibility, fixed airflow limitation, and airway wall remodeling in asthma.* American journal of respiratory and critical care medicine, 2001. **164**(9): p. 1718-1721.
28. Bousquet, J., et al., *Asthma: a disease remodeling the airways* European Journal of Allergy and Clinical Immunology, 1992. **47**(1): p. 3-11.
29. Lieberman, P., *Pulmonary remodeling in asthma.* 1000F Medicine Reports, 2010. **2**(74).
30. Ebina, M., et al., *Cellular hypertrophy and hyperplasia of airway smooth muscles underlying bronchial asthma: A 3-D morphometric study.* American Review of Respiratory Disease, 1993. **148**(3): p. 720-726.
31. Homer, R.J. and J.A. Elias, *Airway Remodeling in Asthma: Therapeutic Implications of Mechanisms.* Physiology, 2005. **20**(1): p. 28-35.
32. Tiddens, H., et al., *Cartilaginous airway dimensions and airflow obstruction in human lungs.* American journal of respiratory and critical care medicine, 1995. **152**(1): p. 260-266.
33. Fath, M.A., et al., *Interaction of secretory leukocyte protease inhibitor with heparin inhibits proteases involved in asthma.* Journal of Biological Chemistry, 1998. **273**(22): p. 13563-13569.
34. Abbinante-Nissen, J.M., L.G. Simpson, and G.D. Leikauf, *Corticosteroids increase secretory leukocyte protease inhibitor transcript levels in airway epithelial cells.* American Journal of Physiology-Lung Cellular and Molecular Physiology, 1995. **268**(4): p. L601-L606.
35. Bates, J.H. and B. Suki, *Assessment of peripheral lung mechanics.* Respiratory physiology & neurobiology, 2008. **163**(1): p. 54-63.
36. Beekman, A.J., E.H. Bel, and P.J. Sterk, *Recurrent exacerbations in severe asthma are associated with enhanced airway closure during stable episodes.* American journal of respiratory and critical care medicine, 2000. **161**(6): p. 1902-1906.
37. Aikawa, T., et al., *Marked goblet cell hyperplasia with mucus accumulation in the airways of patients who died of severe acute asthma attack.* CHEST Journal, 1992. **101**(4): p. 916-921.
38. SAETTA, M., et al., *Goblet cell hyperplasia and epithelial inflammation in peripheral airways of smokers with both symptoms of chronic bronchitis and chronic airflow limitation.* American Journal of Respiratory and Critical Care Medicine, 2000. **161**(3): p. 1016-1021.
39. Carvalho, T.C., J.I. Peters, and R.O. Williams, *Influence of particle size on regional lung deposition - What evidence is there?* International Journal of Pharmaceutics, 2011. **406**(1-2): p. 1-10.
40. Zeng, X.P., G.P. Martin, and C. Marriott, *Particulate Interaction in Dry Powder Formulation for Inhalation*2001, London, UK: Taylor & Francis.
41. Darquenne, C., *Particle Deposition in the Lung*, in *Encyclopedia of Respiratory Medicine*, G.J. Laurent and S.D. Shapiro, Editors. 2006, Academic Press.
42. Bailey, A.G., *The inhalation and deposition of charged particles within the human lung.* Journal of Electrostatics, 1997. **42**(1-2): p. 25-32.
43. Heyder, J., *Deposition of inhaled particles in the human respiratory tract and consequences for regional targeting in respiratory drug delivery.* Proc Am Thorac Soc, 2004. **1**(4): p. 315-320.
44. Mitchell, P. and M.W. Nagel, *Particle Size Analysis of Aerosols from Medicinal Inhalers.* Kona, 2004. **22**: p. 32-65.
45. Cryan, S.A., N. Sivadas, and L. Garcia-Contreras, *In vivo animal models for drug delivery across the lung mucosal barrier.* Advanced Drug Delivery Reviews, 2007. **59**(11): p. 1133-1151.

46. Heyder, J., et al., *Deposition of particles in the human respiratory tract in the size range 0.005-15 Î¼m.* Journal of Aerosol Science, 1986. **17**(5): p. 811-825.
47. Barnes, P.J., *Mechanisms of Disease. Airway receptors.* Postgraduate Medical Journal, 1989. **65**: p. 532- 542.
48. Proskocil, B.J. and A.D. Fryer, *{beta}2-Agonist and Anticholinergic Drugs in the Treatment of Lung Disease.* Proc Am Thorac Soc, 2005. **2**(4): p. 305-310.
49. Rudolf, G., et al., *Regional Aerosol Deposition in Man—A Statistical and Algebraic Model.* Annals of Occupational Hygiene, 1994. **38**(inhaled particles VII): p. 1-14.
50. Breysse P and L.P.S. J., *Particulate matter*, T.J.H. University, Editor.
51. Edwards, D.A., et al., *Large porous particles for pulmonary drug delivery.* Science, 1997. **276**(5320): p. 1868-1871.
52. Vanbever, R., et al., *Formulation and physical characterization of large porous particles for inhalation.* Pharmaceutical Research, 1999. **16**(11): p. 1735-1742.
53. Allen, T., *Powder sampling and particle size determination*2003: Access Online via Elsevier.
54. Shekunov, B.Y., et al., *Particle size analysis in pharmaceutics: Principles, methods and applications.* Pharmaceutical Research, 2007. **24**(2): p. 203-227.
55. Dunbar, C. and J. Mitchell, *Analysis of cascade impactor mass distributions.* Journal of Aerosol Medicine, 2005. **18**(4): p. 439-451.
56. Lenzer, J., *Inhaled insulin is approved in Europe and United States.* Bmj, 2006. **332**(7537): p. 321.
57. Nelson, H.S., et al., *Enhanced synergy between fluticasone propionate and salmeterol inhaled from a single inhaler versus separate inhalers.* Journal of Allergy and Clinical Immunology, 2003. **112**(1): p. 29-36.
58. Barnes, P.J., *Inhaled Corticosteroids.* Pharmaceuticals, 2010(3): p. 514-540.
59. Juniper, E.F., et al., *Effect of long-term treatment with an inhaled corticosteroid (budesonide) on airway hyperresponsiveness and clinical asthma in nonsteroid-dependent asthmatics.* American Review of Respiratory Disease, 1990. **142**(4): p. 832-836.
60. Pauwels, R.A., et al., *Early intervention with budesonide in mild persistent asthma: a randomised, double-blind trial.* The Lancet, 2003. **361**(9363): p. 1071-1076.
61. Greening, A., et al., *Added salmeterol versus higher-dose corticosteroid in asthma patients with symptoms on existing inhaled corticosteroid.* The Lancet, 1994. **344**(8917): p. 219-224.
62. Gibson, P.G., H. Powell, and F.M. Ducharme, *Differential effects of maintenance long-acting β-agonist and inhaled corticosteroid on asthma control and asthma exacerbations.* Journal of allergy and clinical immunology, 2007. **119**(2): p. 344-350.
63. Cohen, A.B. and W.M. Gold, *DEFENSE-MECHANISMS OF LUNGS.* Annual Review of Physiology, 1975. **37**: p. 325-350.
64. Knowles, M.R. and R.C. Boucher, *Mucus clearance as a primary innate defense mechanism for mammalian airways.* Journal of Clinical Investigation, 2002. **109**(5): p. 571-577.
65. Lombry, C., et al., *Alveolar macrophages are a primary barrier to pulmonary absorption of macromolecules.* American Journal of Physiology - Lung Cellular and Molecular Physiology, 2004. **286**(5 30-5): p. L1002-L1008.
66. Lavorini, F., et al., *Retail sales of inhalation devices in European countries: so much for a global policy.* Respiratory medicine, 2011. **105**(7): p. 1099-1103.
67. NHS. *The NHS Information Centre, Hospital episode statistics.* 2010; Available from: http://www.hscic.gov.uk/hes.
68. GINA, *Global strategy for asthma management and prevention*, 2011.
69. Haughney, J., et al., *Achieving asthma control in practice: understanding the reasons for poor control.* Respiratory medicine, 2008. **102**(12): p. 1681-1693.
70. Hickey, A.J., *Back to the future: Inhaled drug products.* Journal of Pharmaceutical Sciences, 2013.

71. Sanders, M., *Inhalation therapy: an historical review.* Prim Care Respir J, 2007. **16**(2): p. 71-81.
72. Hallworth, G.W., *An improved design of powder inhaler.* Br J Clin Pharmacol, 1977. **4**(6): p. 689–690.
73. Dolovich, M.B. and R. Dhand, *Aerosol drug delivery: developments in device design and clinical use.* The Lancet, 2011. **377**(9770): p. 1032-1045.
74. Broeders, M.E.A.C., et al., *The ADMIT series - Issues in Inhalation Therapy. 2) Improving technique and clinical effectiveness.* Primary Care Respiratory Journal, 2009. **18**(2): p. 76-82.
75. Aulton, M.E., ed. *Pharmaceutics. The Science of Dosage Form Design*. 2002, Elsevier Limited.
76. Thorsson, L., S. Edsbacker, and T. Conradson, *Lung deposition of budesonide from Turbuhaler is twice that from a pressurized metered-dose inhaler P-MDI.* European Respiratory Journal, 1994. **7**(10): p. 1839-1844.
77. Borgstrom, L., et al., *Variability in lung deposition of inhaled drug, within and between asthmatic patients, with a pMDI and a dry powder inhaler, Turbuhaler (R).* International Journal of Pharmaceutics, 2000. **193**(2): p. 227-230.
78. Borgstrom, L., et al., *Lung deposition of budesonide inhaled via Turbuhaler: a comparison with terbutaline sulphate in normal subjects.* European Respiratory Journal, 1994. **7**(1): p. 69-73.
79. Newman, S., et al., *Lung deposition of aclidinium bromide from Genuair®, a multidose dry powder inhaler.* Respiration, 2009. **78**(3): p. 322-328.
80. Pauwels, R., S. Newman, and L. Borgstrom, *Airway deposition and airway effects of antiasthma drugs delivered from metered-dose inhalers.* European Respiratory Journal, 1997. **10**(9): p. 2127-2138.
81. Al-Showair, R.A.M., et al., *Can all patients with COPD use the correct inhalation flow with all inhalers and does training help?* Respiratory Medicine, 2007. **101**(11): p. 2395-2401.
82. Buhl, R., *Local oropharyngeal side effects of inhaled corticosteroids in patients with asthma.* Allergy, 2006. **61**(5): p. 518-526.
83. Telko, M.J. and A.J. Hickey, *Dry powder inhaler formulation.* Respiratory care, 2005. **50**(9): p. 1209-1227.
84. de Koning, J.P., et al., *Effect of an external resistance to airflow on the inspiratory flow curve.* International Journal of Pharmaceutics, 2002. **234**(1-2): p. 257-266.
85. Chrystyn, H., *Is inhalation rate important for a dry powder inhaler? using the In-Check Dial to identify these rates.* Respiratory medicine, 2003. **97**(2): p. 181-187.
86. Islam, N. and M.J. Cleary, *Developing an efficient and reliable dry powder inhaler for pulmonary drug delivery–A review for multidisciplinary researchers.* Medical engineering & physics, 2012.
87. Chrystyn, H., *The DiskusTM: a review of its position among dry powder inhaler devices.* International journal of clinical practice, 2007. **61**(6): p. 1022-1036.
88. Chrystyn, H., *Closer to an 'Ideal Inhaler'with the Easyhaler®.* Clinical drug investigation, 2006. **26**(4): p. 175-183.
89. Palander, A., et al., *In vitro comparison of three salbutamol-containing multidose dry powder inhalers: Buventol Easyhaler, Inspiryl Turbuhaler and Ventoline Diskus.* Clinical Drug Investigation, 2000. **20**(1): p. 25-33.
90. Rönmark, E., et al., *Correct use of three powder inhalers: comparison between Diskus, Turbuhaler, and Easyhaler.* Journal of Asthma, 2005. **42**(3): p. 173-178.
91. Needham M, Cocks P, and Fradley G. *Investigating the Efficiency of the 3M Conix™ Reverse Cyclone Technology for DPI Drug Delivery*. 3M Drug Delivery Systems, 3M Healthcare Ltd. [cited 2013 29th April]; Available from: http://solutions.3m.com/3MContentRetrievalAPI/BlobServlet?lmd=1320272822000&locale=en_WW&assetType=MMM_Image&assetId=1319208813657&blobAttribute=ImageFile.

92. Zeng, X.M., et al., *Delivery of formoterol from a novel multi-dose inhaler Airmax ™.* Respiratory medicine, 2002. **96**(6): p. 397-403.
93. Zeng, X.M., et al., *Delivery of salbutamol and of budesonide from a novel multi-dose inhaler Airmax™.* Respiratory medicine, 2002. **96**(6): p. 404-411.
94. Voss, A. and W.H. Finlay, *Deagglomeration of dry powder pharmaceutical aerosols.* International Journal of Pharmaceutics, 2002. **248**(1): p. 39-50.
95. Coates, M.S., et al., *Effect of design on the performance of a dry powder inhaler using computational fluid dynamics. Part 1: Grid structure and mouthpiece length.* Journal of Pharmaceutical Sciences, 2004. **93**(11): p. 2863-2876.
96. Young, P.M., et al., *The influence of dose on the performance of dry powder inhalation systems.* International Journal of Pharmaceutics, 2005. **296**(1): p. 26-33.
97. Tykhoniuk, R., et al., *Ultrafine cohesive powders: from interparticle contacts to continuum behaviour.* Chemical Engineering Science, 2007. **62**(11): p. 2843-2864.
98. Adi, H., et al., *Role of agglomeration in the dispersion of salmeterol xinafoate from mixtures for inhalation with differing drug to fine lactose ratios.* Journal of Pharmaceutical Sciences, 2008. **97**(8): p. 3140-3152.
99. Adi, H., I. Larson, and P.J. Stewart, *Adhesion and redistribution of salmeterol xinafoate particles in sugar-based mixtures for inhalation.* International Journal of Pharmaceutics, 2007. **337**(1-2): p. 229-238.
100. Zeng, X.M., et al., *The role of fine particle lactose on the dispersion and deaggregation of salbutamol sulphate in an air stream in vitro.* International Journal of Pharmaceutics, 1998. **176**(1): p. 99-110.
101. Jones, M.D. and R. Price, *The influence of fine excipient particles on the performance of carrier-based dry powder inhalation formulations.* Pharmaceutical Research, 2006. **23**(8): p. 1665-1674.
102. Steckel, H. and B.W. Müller, *In vitro evaluation of dry powder inhalers II: influence of carrier particle size and concentration on in vitro deposition.* International Journal of Pharmaceutics, 1997. **154**(1): p. 31-37.
103. Zeng, X.M., et al., *Lactose as a carrier in dry powder formulations: the influence of surface characteristics on drug delivery.* Journal of Pharmaceutical Sciences, 2001. **90**(9): p. 1424-1434.
104. Adi, H., et al., *Agglomerate strength and dispersion of salmeterol xinafoate from powder mixtures for inhalation.* Pharmaceutical Research, 2006. **23**(11): p. 2556-2565.
105. Srichana, T., G.P. Martin, and C. Marriott, *On the relationship between drug and carrier deposition from dry powder inhalers in vitro.* International Journal of Pharmaceutics, 1998. **167**(1-2): p. 13-23.
106. Wetterlin, K., *Turbuhaler: a new powder inhaler for administration of drugs to the airways.* Pharmaceutical Research, 1988. **5**(8): p. 506-508.
107. Young, P., et al., *Characterization of a surface modified dry powder inhalation carrier prepared by "particle smoothing".* Journal of Pharmacy and Pharmacology, 2002. **54**(10): p. 1339-1344.
108. Kaialy, W., M. Ticehurst, and A. Nokhodchi, *Dry powder inhalers: Mechanistic evaluation of lactose formulations containing salbutamol sulphate.* International Journal of Pharmaceutics, 2011.
109. Begat, P., et al., *The cohesive-adhesive balances in dry powder inhaler formulations II: Influence on fine particle delivery characteristics.* Pharmaceutical Research, 2004. **21**(10): p. 1826-1833.
110. Kawashima, Y., et al., *A new powder design method to improve inhalation efficiency of pranlukast hydrate dry powder aerosols by surface modification with hydroxypropylmethylcellulose phthalate nanospheres.* Pharmaceutical research, 1998. **15**(11): p. 1748-1752.

111. Louey, M.D., S. Razia, and P.J. Stewart, *Influence of physico-chemical carrier properties on the in vitro aerosol deposition from interactive mixtures.* International Journal of Pharmaceutics, 2003. **252**(1): p. 87-98.
112. Young, P.M., et al., *The influence of relative humidity on the cohesion properties of micronized drugs used in inhalation therapy.* Journal of Pharmaceutical Sciences, 2004. **93**(3): p. 753-761.
113. Behara, S.R.B., et al., *Structural influence of cohesive mixtures of salbutamol sulphate and lactose on aerosolisation and de-agglomeration behaviour under dynamic conditions.* European Journal of Pharmaceutical Sciences, 2011. **42**(3): p. 210-219.
114. Marple, V.A., et al., *Next generation pharmaceutical impactor (A new impactor for pharmaceutical inhaler testing). Part II: Archival calibration.* Journal of Aerosol Medicine-Deposition Clearance and Effects in the Lung, 2003. **16**(3): p. 301-324.
115. Marple, V.A., et al., *Next generation pharmaceutical impactor (A new impactor for pharmaceutical inhaler testing). Part I: Design.* Journal of Aerosol Medicine-Deposition Clearance and Effects in the Lung, 2003. **16**(3): p. 283-299.
116. De Boer, A.H., et al., *Characterization of inhalation aerosols: A critical evaluation of cascade impactor analysis and laser diffraction technique.* International Journal of Pharmaceutics, 2002. **249**(1-2): p. 219-231.
117. Usmani, O.S., et al., *Effects of bronchodilator particle size in asthmatic patients using monodisperse aerosols.* Journal of Applied Physiology, 2003. **95**(5): p. 2106-2112.
118. Zanen, P., L. Go, and J. Lammers, *Optimal particle size for beta 2 agonist and anticholinergic aerosols in patients with severe airflow obstruction.* Thorax, 1996. **51**(10): p. 977-980.
119. Berglund, R.N. and B.Y. Liu, *Generation of monodisperse aerosol standards.* Environmental Science & Technology, 1973. **7**(2): p. 147-153.
120. TSI, *Model 3450 Vibrating Orifice Aerosol Generator*, 2002.
121. De Boer, A.H., et al., *Design and application of a new modular adapter for laser diffraction characterization of inhalation aerosols.* International Journal of Pharmaceutics, 2002. **249**(1-2): p. 233-245.
122. Ziegler, J. and H. Wachtel, *Comparison of cascade impaction and laser diffraction for particle size distribution measurements.* Journal of Aerosol Medicine-Deposition Clearance and Effects in the Lung, 2005. **18**(3): p. 311-324.
123. Mitchell, J.P., et al., *Laser diffractometry as a technique for the rapid assessment of aerosol particle size from inhalers.* Journal of Aerosol Medicine: Deposition, Clearance, and Effects in the Lung, 2006. **19**(4): p. 409-433.
124. de Boer, G.B.J., et al., *Laser Diffraction Spectrometry: Fraunhofer Diffraction Versus Mie Scattering.* Particle & Particle Systems Characterization, 1987. **4**(1-4): p. 14-19.
125. Clark AR and H. AM., *The relationship between powder inhaler resistance and peak inspiratory conditions in healthy volunteers-implications for in vitro testing.* J Aerosol Med, 1993. **6**(2): p. 99-110.
126. Martin, G.P., C. Marriott, and X.M. Zeng, *Influence of realistic inspiratory flow profiles on fine particle fractions of dry powder aerosol formulations.* Pharmaceutical Research, 2007. **24**(2): p. 361-369.
127. BRINDLEY, A., B.S. SUMBY, and I.A.N.J. SMITH, *The characterisation of inhalation devices by an inhalation simulator: the Electronic Lung™.* Journal of aerosol medicine, 1994. **7**(2): p. 197-200.
128. Haupt, D., K. Krigsman, and J.L.G. Nilsson, *Medication persistence among patients with asthma/COPD drugs.* Pharmacy World and Science, 2008. **30**(5): p. 509-514.
129. Krigsman, K., et al., *Refill adherence by the elderly for asthma/chronic obstructive pulmonary disease drugs dispensed over a 10-year period.* Journal of Clinical Pharmacy and Therapeutics, 2007. **32**(6): p. 603-611.

130. Lindsay, J.T. and L.G. Heaney, *Nonadherence in difficult asthma–facts, myths, and a time to act.* Patient preference and adherence, 2013. **7**: p. 329.
131. Gamble, J., et al., *Difficult asthma: people's perspectives on taking corticosteroid therapy.* Journal of Clinical Nursing, 2007. **16**(3a): p. 59-67.
132. Dekhuijzen, P., A. Magnan, and M. Kneussl, *The ADMIT series-issues in inhalation therapy. 1) The goals of asthma treatment: can they be achieved.* Prim Care Resp J, 2007. **16**(6): p. 341-8.
133. NAEPP. *Expert Panel Report 3:Guidelines for the Diagnosis and Management of Asthma*. National Heart, Lung and Blood Institute 2007; Available from: http://www.nhlbi.nih.gov/guidelines/asthma/asthgdln.htm.
134. Giavina-Bianchi, P., et al., *Difficult-to-control asthma management through the use of a specific protocol.* Clinics, 2010. **65**(9): p. 905-918.
135. Horne, R., et al., *Can asthma control be improved by understanding the patient's perspective?* BMC Pulmonary Medicine, 2007. **7**(1): p. 8.
136. Levy, M.L., et al., *International Primary Care Respiratory Group (IPCRG) Guidelines: diagnosis of respiratory diseases in primary care.* Primary Care Respiratory Journal, 2006. **15**(1): p. 20-34.
137. Smith, A.D., et al., *Use of exhaled nitric oxide measurements to guide treatment in chronic asthma.* New England Journal of Medicine, 2005. **352**(21): p. 2163-2173.
138. Battaglia, S., et al., *Small airways function and molecular markers in exhaled air in mild asthma.* Thorax, 2005. **60**(8): p. 639-644.
139. Pliss, L., E. Ingenito, and R. Ingram Jr, *Responsiveness, inflammation, and effects of deep breaths on obstruction in mild asthma.* Journal of Applied Physiology, 1989. **66**(5): p. 2298-2304.
140. van Veen, I.H., et al., *Alveolar nitric oxide versus measures of peripheral airway dysfunction in severe asthma.* European Respiratory Journal, 2006. **27**(5): p. 951-956.
141. Stoloff, S.W. and H.A. Boushey, *Severity, control, and responsiveness in asthma.* Journal of Allergy and Clinical Immunology, 2006. **117**(3): p. 544-548.
142. Aaron, S.D., *Combination Inhaler Therapy for Chronic Obstructive Pulmonary Disease.* Annals of Internal Medicine, 2007. **146**(8): p. I-12.
143. Lavorini, F. and G.A. Fontana, *Targeting drugs to the airways: the role of spacer devices.* Expert Opinion on Drug Delivery, 2009. **6**(1): p. 91-102.
144. ClementClarke. *Improving patient's inhaler technique*. 2012; Available from: http://www.clement-clarke.com/NewsEvents/FloToneTrainer.aspx.
145. Meda, *Novolizer®.* 2013.
146. Harrison, L.I., et al., *Comparative pulmonary function and pharmacokinetics of fluticasone propionate and salmeterol xinafoate delivered by two dry powder inhalers to patients with asthma.* Journal of aerosol medicine and pulmonary drug delivery, 2011. **24**(5): p. 245-252.
147. Commission, B.P., *Appendix XII C. Consistency of Formulated Preparations* in *Brithis Pharmacopoeia*2011, The Stationery Office.
148. Feddah, M.R., et al., *In-vitro characterisation of metered dose inhaler versus dry powder inhaler glucocorticoid products: Influence of inspiratory flow rates.* Journal of Pharmacy and Pharmaceutical Sciences, 2000. **3**(3): p. 317-324.
149. Zanen, P., et al., *THE EFFECT OF THE INHALATION FLOW ON THE PERFORMANCE OF A DRY POWDER INHALATION SYSTEM.* International Journal of Pharmaceutics, 1992. **81**(2-3): p. 199-203.
150. FDA, *Guidance for Industry Metered Dose Inhaler (MDI) and Dry Powder Inhaler (DPI) Drug Products Chemistry, Manufacturing, and Controls Documentation*, h.w.f.g.d.D.G.u.p. U.S. Department of Health and Human Services, Editor 1998.
151. Magnussen, H., et al., *Peak inspiratory flow through the Genuair< sup>®</sup> inhaler in patients with moderate or severe COPD.* Respiratory medicine, 2009. **103**(12): p. 1832-1837.

152. Hill, L.S. and A.L. Slater, *A comparison of the performance of two modern multidose dry powder asthma inhalers.* Respiratory medicine, 1998. **92**(1): p. 105-110.
153. Srichana, T., G.P. Martin, and C. Marriott, *Dry powder inhalers: The influence of device resistance and powder formulation on drug and lactose deposition in vitro.* European Journal of Pharmaceutical Sciences, 1998. **7**(1): p. 73-80.
154. Munzel, U., et al., *Variability of fine particle dose and lung deposition of budesonide delivered through two multidose dry powder inhalers.* Current Medical Research and Opinion®, 2005. **21**(6): p. 827-833.
155. Newman, S., et al., *Lung deposition of salbutamol in healthy human subjects from the MAGhaler dry powder inhaler.* Respiratory medicine, 2002. **96**(12): p. 1026-1032.
156. Smith Simon James, et al., *Cyclone inhaler*, C. Consultants, Editor 2007: UK.
157. Hoffmann, A.C. and L.E. Stein, *Gas cyclones and swirl tubes: principles, design and operation*2002: Springer Verlag.
158. Cheng S.J. and Symons D.D. *Optimisation of Dry Powder inhalers throught Robust CFD Simulation of Air Classifiers*. in *Drug Delivery to the Lungs 21*. 2010. Edinburgh.
159. Cheng, S.J., *Numerical and Experimental Study of Cyclone Separators for Aerosol Drug Delivery, PhD Thesis*, in *Department of Engineering*2012, University of Cambridge: Cambridge. p. 1-262.
160. Bright, F.V., G.H. Vickers, and G.M. Hieftje, *Use of time resolution to eliminate bilirubin interference in the determination of fluorescein.* Analytical chemistry, 1986. **58**(6): p. 1225-1227.
161. Tolocka, M.P., P.T. Tseng, and R.W. Wiener, *Optimization of the wash-off method for measuring aerosol concentrations.* Aerosol Science & Technology, 2001. **34**(5): p. 416-421.
162. Needham M., Cocks P., and F. G. *Investigating the Efficiency of the 3M Conix™ Reverse Cyclone Technology for DPI Drug Delivery*. N/D.
163. Coates, M., et al., *Influence of Air Flow on the Performance of a Dry Powder Inhaler Using Computational and Experimental Analyses.* Pharmaceutical research, 2005. **22**(9): p. 1445-1453.
164. Shur, J., et al., *Effect of device design on the in vitro performance and comparability for capsule-based dry powder inhalers.* The AAPS Journal, 2012. **14**(4): p. 667-676.
165. Coates, M.S., et al., *Effect of design on the performance of a dry powder inhaler using computational fluid dynamics. Part 2: Air inlet size.* Journal of Pharmaceutical Sciences, 2006. **95**(6): p. 1382-1392.
166. Zhou, Q., et al., *Effect of Device Design on the Aerosolization of a Carrier-Based Dry Powder Inhaler—a Case Study on Aerolizer® Foradile®.* The AAPS Journal, 2013. **15**(2): p. 511-522.
167. Tong, Z., et al., *Numerical study of the effects of particle size and polydispersity on the agglomerate dispersion in a cyclonic flow.* Chemical Engineering Journal, 2010. **164**(2): p. 432-441.
168. Donovan, M.J., et al., *Dry powder inhaler device influence on carrier particle performance.* Journal of Pharmaceutical Sciences, 2012.
169. Bisgaard, H., S. Pedersen, and K. Nikander, *Use of budesonide Turbuhaler® in young-children suspected of asthma.* European Respiratory Journal, 1994. **7**(4): p. 740-742.
170. Taki, M., et al., *The 'stage-by-stage' deposition of drugs from commercial single-active and combination dry powder inhaler formulations.* European Journal of Pharmaceutical Sciences, 2011. **43**(4): p. 225-235.
171. Terzano, C., *Pressurized Metered Dose Inhalers and Add-on Devices.* Pulmonary Pharmacology & Therapeutics, 2001. **14**(5): p. 351-366.
172. Newman, S.P. and M.T. Newhouse, *Effect of add-on devices for aerosol drug delivery: deposition studies and clinical aspects.* Journal of aerosol medicine, 1996. **9**(1): p. 55-70.
173. Matida, E.A., et al., *A new add-on spacer design concept for dry-powder inhalers.* Journal of Aerosol Science, 2004. **35**(7): p. 823-833.

174. Ehtezazi, T., et al., *Investigating improving powder deagglomeration via dry powder inhalers at a low inspiratory flow rate by employing add-on spacers.* Journal of Pharmaceutical Sciences, 2008. **97**(12): p. 5212-5221.
175. Coates, M.S., et al., *The role of capsule on the performance of a dry powder inhaler using computational and experimental analyses.* Pharmaceutical Research, 2005. **22**(6): p. 923-932.
176. Barry, P.W. and C. Ocallaghan, *In vitro comparison of the amount of salbutamol available for inhalation from different formulations used with different spacer devices.* European Respiratory Journal, 1997. **10**(6): p. 1345-1348.
177. Everard, M.L., S.G. Devadason, and P.N. Le Souef, *Particle size selection device for use with the Turbohaler.* Thorax, 1996. **51**(5): p. 537-539.
178. Pilcer, G., F. Vanderbist, and K. Amighi, *Correlations between cascade impactor analysis and laser diffraction techniques for the determination of the particle size of aerosolised powder formulations.* International journal of pharmaceutics, 2008. **358**(1): p. 75-81.
179. Borgström, L., B. Olsson, and L. Thorsson, *Degree of throat deposition can explain the variability in lung deposition of inhaled drugs.* Journal of aerosol medicine, 2006. **19**(4): p. 473-483.
180. Thorsson, L., et al., *Pharmacokinetics and systemic activity of fluticasone via Diskus® and pMDI, and of budesonide via Turbuhaler®.* British Journal of Clinical Pharmacology, 2001. **52**(5): p. 529-538.
181. Newman, S., et al., *Scintigraphic comparison of budesonide deposition from two dry powder inhalers.* European Respiratory Journal, 2000. **16**(1): p. 178-183.
182. Aileen Gibbons, et al., *In Vivo Lung Deposition Feasibility Study Comparing the Respira™ DPI to The Handihaler® in Human Subjects*, in *Respiratory Drug Delivery*2012: Phoenix, Arizona.
183. Golshahi, L., M. Noga, and W. Finlay, *Deposition of inhaled micrometer-sized particles in oropharyngeal airway replicas of children at constant flow rates.* Journal of Aerosol Science, 2012. **49**: p. 21-31.
184. Inthavong, K., et al., *Micron particle deposition in a tracheobronchial airway model under different breathing conditions.* Medical engineering & physics, 2010. **32**(10): p. 1198-1212.
185. Zhang, Y., K. Gilbertson, and W.H. Finlay, *In vivo-in vitro comparison of deposition in three mouth-throat models with Qvar® and Turbuhaler® inhalers.* Journal of aerosol medicine, 2007. **20**(3): p. 227-235.
186. Zhou, Y., J. Sun, and Y.-S. Cheng, *Comparison of deposition in the USP and physical mouth–throat models with solid and liquid particles.* Journal of aerosol medicine and pulmonary drug delivery, 2011. **24**(6): p. 277-284.
187. Srichana, T., G. Martin, and C. Marriott, *A Human Oral-throat Cast Integrated with a Twin-stage Impinger for Evaluation of Dry Powder Inhalers.* Journal of pharmacy and pharmacology, 2000. **52**(7): p. 771-778.
188. DeHaan, W. and W. Finlay, *Predicting extrathoracic deposition from dry powder inhalers.* Journal of aerosol science, 2004. **35**(3): p. 309-331.
189. Lin, T.-C., et al., *Mouthpiece diameter affects deposition efficiency in cast models of the human oral airways.* Journal of Aerosol Medicine, 2001. **14**(3): p. 335-341.
190. Verbanck, S., et al., *Aerosol profile extracted from spacers as a determinant of actual dose.* Pharmaceutical Research, 2004. **21**(12): p. 2213-2218.
191. Tarsin, W., K. Assi, and H. Chrystyn, *In-vitro intra-and inter-inhaler flow rate-dependent dosage emission from a combination of budesonide and eformoterol in a dry powder inhaler.* Journal of Aerosol Medicine, 2004. **17**(1): p. 25-32.
192. Thiel, C.G., *Cascade impactor data and the lognormal distribution: Nonlinear regression for a better fit.* Journal of aerosol medicine, 2002. **15**(4): p. 369-378.

193. Parisini, I., et al. *A Combined Computational Fluid Dynamic (CFD) and Compendial Testing Approach to Study Miniaturized Cyclone Spacers for Commercial Inhalers*. in *Respiratory Drug Delivery*. 2014. Fajardo, Puerto rico.
194. Begat, P., et al., *The cohesive-adhesive balances in dry powder inhaler formulations I: Direct quantification by atomic force microscopy.* Pharmaceutical Research, 2004. **21**(9): p. 1591-1597.
195. Thalberg, K., E. Berg, and M. Fransson, *Modeling dispersion of dry powders for inhalation. The concepts of total fines, cohesive energy and interaction parameters.* International Journal of Pharmaceutics, 2012. **427**(2): p. 224-233.
196. Calverley, P., et al., *Combined salmeterol and fluticasone in the treatment of chronic obstructive pulmonary disease: a randomised controlled trial.* The Lancet, 2003. **361**(9356): p. 449-456.
197. Kenyon, C., et al., *The effects of static charge in spacer devices on glucocorticosteroid aerosol deposition in asthmatic patients.* European Respiratory Journal, 1998. **11**(3): p. 606-610.
198. J.H. Wildhaber, et al., *Electrostatic charge on a plastic spacer device influences the delivery of salbutamol.* Eur Respir J, 1996. **9**: p. 1943–1946.
199. Wildhaber, J.H., et al., *Effect of electrostatic charge, flow, delay and multiple actuations on the in vitro delivery of salbutamol from different small volume spacers for infants.* Thorax, 1996. **51**(10): p. 985-988.
200. Kwok, P.C.L., R. Collins, and H.-K. Chan, *Effect of spacers on the electrostatic charge properties of metered dose inhaler aerosols.* Journal of aerosol science, 2006. **37**(12): p. 1671-1682.
201. Byron, P.R., J. Peart, and J.N. Staniforth, *Aerosol electrostatics I: properties of fine powders before and after aerosolization by dry powder inhalers.* Pharmaceutical Research, 1997. **14**(6): p. 698-705.
202. Le, V., E. Robins, and M. Flament, *Agglomerate behaviour of fluticasone propionate within dry powder inhaler formulations.* European Journal of Pharmaceutics and Biopharmaceutics, 2012. **80**(3): p. 596-603.
203. Jones, M.D., et al., *An investigation into the dispersion mechanisms of ternary dry powder inhaler formulations by the quantification of interparticulate forces.* Pharmaceutical Research, 2008. **25**(2): p. 337-348.
204. Tang, P., et al., *Does the United States Pharmacopeia throat introduce de-agglomeration of carrier-free powder from inhalers?* Pharmaceutical Research, 2012: p. 1-11.
205. Smyth, H., et al., *Spray pattern analysis for metered dose inhalers: effect of actuator design.* Pharmaceutical Research, 2006. **23**(7): p. 1591-1596.
206. Murphy, S., *Evaluation of Plume Geometry and Spray Pattern from a Dry Powder Devices using FDA Guidance*, in *Dru delivery to the Lung 24*2013: Edinburgh.
207. Hickey, A.J. and T.M. Crowder, *Next generation dry powder inhalation delivery systems.* Lung Biology in Health and Disease, 2007. **221**: p. 445.
208. M. Vidgren, et al., *Easyhaler® Multiple Dose Powder Inhaler—Practical and Effective Alternative to the Pressurized MDI.* Aerosol Science and Technology, 2007. **22**(4): p. 335-345.
209. Daniher, D.I. and J. Zhu, *Dry powder platform for pulmonary drug delivery.* Particuology, 2008. **6**(4): p. 225-238.
210. I Parisini, S.C., DD Symons, MB Brown, A Kostrzewski and D Murnane, *Assessment of a cyclone-type spacer device for use in dry powder inhalation*, in *Drug Delivery to the Lungs 22*2011: Edinburgh.
211. Martin, G.P., et al., *Characterisation of a carrier-free dry powder aerosol formulation using inertial impaction and laser diffraction.* Pharmaceutical Research, 2006. **23**(9): p. 2210-2219.
212. Begat, P., et al., *The role of force control agents in high-dose dry powder inhaler formulations.* Journal of Pharmaceutical Sciences, 2009. **98**(8): p. 2770-2783.

213. Jaffari, S., et al., *Rapid characterisation of the inherent dispersibility of respirable powders using dry dispersion laser diffraction.* International Journal of Pharmaceutics, 2013.
214. Jones, M.D., et al., *An investigation into the relationship between carrier-based dry powder inhalation performance and formulation cohesive-adhesive force balances.* European Journal of Pharmaceutics and Biopharmaceutics, 2008. **69**(2): p. 496-507.
215. Hooton, J.C., M.D. Jones, and R. Price, *Predicting the behavior of novel sugar carriers for dry powder inhaler formulations via the use of a cohesive–adhesive force balance approach.* Journal of Pharmaceutical Sciences, 2006. **95**(6): p. 1288-1297.
216. Tsukada, M., et al., *Adhesion force measurement of a DPI size pharmaceutical particle by colloid probe atomic force microscopy.* Powder technology, 2004. **141**(3): p. 262-269.
217. Kaialy, W., et al., *The influence of physical properties and morphology of crystallised lactose on delivery of salbutamol sulphate from dry powder inhalers.* Colloids and Surfaces B: Biointerfaces, 2012. **89**: p. 29-39.
218. Louey, M.D. and P.J. Stewart, *Particle interactions involved in aerosol dispersion of ternary interactive mixtures.* Pharmaceutical Research, 2002. **19**(10): p. 1524-1531.
219. Young, P.M., et al., *The use of colloid probe microscopy to predict aerosolization performance in dry powder inhalers: AFM and in vitro correlation.* Journal of Pharmaceutical Sciences, 2006. **95**(8): p. 1800-1809.
220. Behara, S.R.B., et al., *An approach to characterising the cohesive behaviour of powders using a flow titration aerosolisation based methodology.* Chemical Engineering Science, 2011. **66**(8): p. 1640-1648.
221. Xu, Z., et al., *Dry powder aerosols generated by standardized entrainment tubes from drug blends with lactose monohydrate: 1. Albuterol sulfate and disodium cromoglycate.* Journal of pharmaceutical sciences, 2010. **99**(8): p. 3398-3414.
222. Behara, S.R.B., et al., *The kinetics of cohesive powder de-agglomeration from three inhaler devices.* International journal of pharmaceutics, 2011. **421**(1): p. 72-81.
223. IIDA, K., et al., *Evaluation of Flow Properties of Dry Powder Inhalation of Salbutamol Sulfate with Lactose Carrier.* Chemical and pharmaceutical bulletin, 2001. **49**(10): p. 1326-1330.
224. Islam, N., et al., *Lactose surface modification by decantation: are drug-fine lactose ratios the key to better dispersion of salmeterol xinafoate from lactose-interactive mixtures?* Pharmaceutical Research, 2004. **21**(3): p. 492-499.
225. Islam, N., et al., *Effect of carrier size on the dispersion of salmeterol xinafoate from interactive mixtures.* Journal of Pharmaceutical Sciences, 2004. **93**(4): p. 1030-1038.
226. McNitt-Gray, M.F., et al., *Development and testing of image-processing methods for the quantitative assessment of airway hyperresponsiveness from high-resolution CT images.* Journal of Computer Assisted Tomography, 1997. **21**(6): p. 939-947.
227. Zanen, P., L.T. Go, and J.-W.J. Lammers, *The optimal particle size for parasympathicolytic aerosols in mild asthmatics.* International Journal of Pharmaceutics, 1995. **114**(1): p. 111-115.
228. Xu, Z., et al., *Dry powder aerosols generated by standardized entrainment tubes from drug blends with lactose monohydrate: 2. Ipratropium bromide monohydrate and fluticasone propionate.* Journal of pharmaceutical sciences, 2010. **99**(8): p. 3415-3429.
229. Buckton, G., *Characterisation of small changes in the physical properties of powders of significance for dry powder inhaler formulations.* Advanced drug delivery reviews, 1997. **26**(1): p. 17-27.
230. Lucas, P., et al., *Enhancement of small particle size dry powder aerosol formulations using an ultra low density additive.* Pharmaceutical Research, 1999. **16**(10): p. 1643-1647.
231. Nguyen, T.T., et al., *A centrifuge method to measure particle cohesion forces to substrate surfaces: The use of a force distribution concept for data interpretation.* International Journal of Pharmaceutics, 2010. **393**(1): p. 89-96.

232. Zeng, X.M., et al., *Effects of particle size and adding sequence of fine lactose on the deposition of salbutamol sulphate from a dry powder formulation.* International Journal of Pharmaceutics, 1999. **182**(2): p. 133-144.
233. Zhang, H. and J.F. Banfield, *Kinetics of crystallization and crystal growth of nanocrystalline anatase in nanometer-sized amorphous titania.* Chemistry of materials, 2002. **14**(10): p. 4145-4154.
234. Sprott, J.C., *Simple chaotic systems and circuits.* American Journal of Physics, 2000. **68**(8): p. 758-763.
235. Wright, D., et al., *Retrieval of aerosol properties from moments of the particle size distribution for kernels involving the step function: Cloud droplet activation.* Journal of aerosol science, 2002. **33**(2): p. 319-337.
236. Sarinas, P.S., et al., *Inspiratory flow rate and dynamic lung function in cystic fibrosis and chronic obstructive lung diseases.* CHEST Journal, 1998. **114**(4): p. 988-992.
237. Janssens, W., et al., *Inspiratory flow rates at different levels of resistance in elderly COPD patients.* European Respiratory Journal, 2008. **31**(1): p. 78-83.
238. Dewar, M., et al., *Peak inspiratory flow through turbuhaler< sup>®</sup> in chronic obstructive airways disease.* Respiratory Medicine, 1999. **93**(5): p. 342-344.
239. Byron P.R, et al., *Breath Profiles for Testing New DPI Devices in Development*, in *Respiratory Drug Delivery 2014*2014: Puerto Rico, USA. p. 295-302.
240. Casaro D, et al., *In vitro aerosol performances of NEXThaler® using representative inhalation profiles from asthmatic patients*, in *Respiratory Drug Delivery 2014*2014: Puerto rico, USA. p. 375-380.
241. Chapman, K.R., et al., *Delivery characteristics and patients' handling of two single-dose dry-powder inhalers used in COPD.* International Journal of Chronic Obstructive Pulmonary Disease, 2011. **6**: p. 353.
242. Bisgaard, H., et al., *Fine particle mass from the Diskus inhaler and Turbuhaler inhaler in children with asthma.* European Respiratory Journal, 1998. **11**(5): p. 1111-1115.
243. Chavan, V. and R. Dalby, *Effect of rise in simulated inspiratory flow rate and carrier particle size on powder emptying from dry powder inhalers.* AAPS PharmSci, 2000. **2**(2): p. 1-7.
244. Burnell, P., et al., *Design, validation and initial testing of the Electronic LungTM device.* Journal of Aerosol Science, 1998. **29**(8): p. 1011-1025.
245. Broeders, M.E.A.C., et al., *Peak inspiratory flow rate and slope of the inhalation profiles in dry powder inhalers.* European Respiratory Journal, 2001. **18**(5): p. 780-783.
246. Burnell, P., et al., *Ex-vivo product performance of DiskusTMand TurbuhalerTMinhalers using inhalation profiles from patients with severe chronic obstructive pulmonary disease.* Respiratory medicine, 2001. **95**(5): p. 324-330.
247. Finlay, W. and M. Gehmlich, *Inertial sizing of aerosol inhaled from two dry powder inhalers with realistic breath patterns versus constant flow rates.* International Journal of Pharmaceutics, 2000. **210**(1): p. 83-95.
248. Zhang, Y. and W.H. Finlay, *Experimental measurements of particle deposition in three proximal lung bifurcation models with an idealized mouth-throat.* Journal of Aerosol Medicine, 2005. **18**(4): p. 460-473.
249. Delvadia, R., et al., *In vitro tests for aerosol deposition II: IVIVCs for different dry powder inhalers in normal adults.* Journal of aerosol medicine and pulmonary drug delivery, 2013. **26**(3): p. 138-144.
250. Delvadia, R.R., P.W. Longest, and P.R. Byron, *In vitro tests for aerosol deposition. I: scaling a physical model of the upper airways to predict drug deposition variation in normal humans.* Journal of aerosol medicine and pulmonary drug delivery, 2012. **25**(1): p. 32-40.
251. Bland, M., *An Introduction to Medical Statistics*. Third ed2000, Oxford, United Kingdom: Oxford University Press.

252. Whitley, E. and J. Ball, *Statistics review 4: Sample size calculations.* Critical Care, 2002. **6**(4): p. 335-341.
253. Cohen, J., *A power primer.* Psychological Bulletin, 1992. **112**(1): p. 155.
254. Tarsin, W.Y., et al., *Emitted dose estimates from Seretide Diskus and Symbicort Turbuhaler following inhalation by severe asthmatics.* International Journal of Pharmaceutics, 2006. **316**(1-2): p. 131.
255. Bisgaard, H., *Automatic actuation of a dry powder inhaler into a nonelectrostatic spacer.* American journal of respiratory and critical care medicine, 1998. **157**(2): p. 518-521.
256. Broeders, M., et al., *Peak inspiratory flow rate and slope of the inhalation profiles in dry powder inhalers.* European Respiratory Journal, 2001. **18**(5): p. 780-783.
257. Elkins, M.R., et al., *Inspiratory Flows and Volumes in Subjects with Cystic Fibrosis Using a New Dry Powder Inhaler Device.* The open respiratory medicine journal, 2014. **8**: p. 1.
258. De Boer, A., H. Winter, and C. Lerk, *Inhalation characteristics and their effects on in vitro drug delivery from dry powder inhalers Part 1. Inhalation characteristics, work of breathing and volunteers' preference in dependence of the inhaler resistance.* International Journal of Pharmaceutics, 1996. **130**(2): p. 231-244.
259. Persson, G., B. Olsson, and S. Soliman, *The impact of inspiratory effort on inspiratory flow through Turbuhaler in asthmatic patients.* European Respiratory Journal, 1997. **10**(3): p. 681-684.
260. Bronsky, E.A., et al., *Inspiratory flow rates and volumes with the Aerolizer dry powder inhaler in asthmatic children and adults.* Current Medical Research and Opinion®, 2004. **20**(2): p. 131-137.
261. Tarsin, W.Y., et al., *Emitted dose estimates from Seretide(R) Diskus(R) and Symbicort(R) Turbuhaler(R) following inhalation by severe asthmatics.* International Journal of Pharmaceutics, 2006. **316**(1-2): p. 131-137.
262. Kamin, W.E.S., et al., *The inhalation manager: A new computer-based device to assess inhalation technique and drug delivery to the patient.* Journal of Aerosol Medicine-Deposition Clearance and Effects in the Lung, 2003. **16**(1): p. 21-29.
263. Ammari, W.G. and H. Chrystyn, *Optimizing the inhalation flow and technique through metered dose inhalers of asthmatic adults and children attending a community pharmacy.* Journal of Asthma, 2013. **50**(5): p. 505-513.
264. WHO. *http://www.who.int/respiratory/copd/en/*.